

FORMATION OF CaC_2 FROM CaO
AND "NASCENT" CARBON SPECIES IN
A ROTATING-ARC REACTOR

by

Chi Sang Kim

S.B., Massachusetts Institute of Technology
(January, 1974)

S.M., Massachusetts Institute of Technology
(January, 1974)

Submitted in Partial Fulfillment
of the Requirements for the
Degree of Doctor of Science

at the

MASSACHUSETTS INSTITUTE OF TECHNOLOGY

May, 1977

Signature of Author

Department of Chemical Engineering,
May 17, 1977

Certified by

~~Raymond F. Baddour, Thesis Supervisor~~

~~Jack B. Howard, Thesis Supervisor~~

~~Herman P. Meissner, Thesis Supervisor~~

Accepted by

G.C. Williams, Chairman
Departmental Committee on Graduate
Theses

Archives



ABSTRACT

FORMATION OF CaC_2 FROM CaO AND "NASCENT" CARBON SPECIES IN A ROTATING-ARC REACTOR

by Chi Sang Kim

Submitted to the Department of Chemical Engineering in May, 1977, in partial fulfillment of the requirements for the degree of Doctor of Science.

A novel method of manufacturing CaC_2 , whose main industrial use is to yield C_2H_2 by hydrolysis, from the reaction of lime (CaO) with "nascent" carbon and hydrogen species of intense chemical activity has been developed. In the method, fine lime powder was carried in a stream of hydrocarbon gas and passed through the arc-zone of a rotating-arc reactor which consisted of a 1/4" dia. graphite cathode rod placed in the axis of a tubular anode (1/2" i.d.) constructed of graphite. The arc was rotated by an external magnetic field. A high volatile coal was also successfully used as the source of the "nascent" carbon species by carrying in a stream of hydrogen an intimate mixture of fine powders of coal and lime and passing through the arc-zone.

In order to delineate the overall reaction mechanism, extensive studies were made with methane as the carbon source. The results indicated that the rate limiting step is in the gas phase decomposition of methane when the energy input (per g atom C in the feed gas) is less than the overall activation energy for the decomposition of methane; however, when the energy input is increased above the value, the rate controlling step shifts to chemical reactions within the lime particles, at least for the three particle sizes investigated (-8 μ , -44 μ , and -74 μ). The highest conversion of CaO to CaC_2 attained was 85%. The highest conversion of carbon in methane to CaC_2 and CO was 95%, which was obtained by feeding lime in excess of the stoichiometric feed rate.

Ethylene was also used as the source of "nascent" carbon species; the result was a general increase in energy efficiency over methane as the source of carbon. This was attributed to the higher C/H ratio, positive heat of formation unlike methane which possesses negative heat of formation

and lower activation energy for the decomposition of ethylene.

With a high volatile coal as the carbon source, the highest conversion of CaO to CaC₂ achieved was 61%. The highest conversion of the carbon in the coal to CaC₂ and CO was 90%. This showed that a high volatile coal can be as effective a source of "nascent" carbon species of intense chemical activity as hydrocarbons.

The lowest energy consumption achieved with coal as the carbon source was 32.1 kwhr/lb C₂H₂. It was 16.3 kwhr/lb C₂H₂ with methane as the carbon source. The energy efficiency can be improved in scaled-up reactors as arc-gas heaters are generally more efficient at larger scales.

Thesis Supervisors: Raymond F. Baddour
 Professor of Chemical Engineering

 Jack B. Howard
 Professor of Chemical Engineering

 Herman P. Meissner
 Professor of Chemical Engineering

Department of Chemical Engineering
Massachusetts Institute of Technology
Cambridge, Massachusetts 02139


May, 1977

Professor Irving Kaplan
Secretary of the Faculty
Massachusetts Institute of Technology
Cambridge, Massachusetts 02139

Dear Professor Kaplan:

In accordance with the regulation of the Faculty, I herewith submit a thesis, entitled "Formation of CaC_2 from CaO and 'Nascent' Carbon Species in a Rotating-Arc Reactor," in partial fulfillment of the requirements for the degree of Doctor of Science in Chemical Engineering at the Massachusetts Institute of Technology.

Respectfully Submitted,

Chi Sang Kim 

Acknowledgments

I wish to express my sincere appreciation to each of my three supervisors for their invaluable support during the course of this thesis. Professor Jack B. Howard made this thesis possible by initially encouraging me to get familiar with various aspects of existing coal conversion technology and to develop, if possible, a novel coal conversion process which could be made commercially viable in the near future. Professor Raymond F. Baddour, who possesses highly respected research experience in the area of plasma chemical processing, critically examined the feasibility of the proposed reaction scheme and provided me with the necessary encouragement and confidence in undertaking this thesis. His enthusiasm and helpful suggestions throughout the course of this research are deeply appreciated. Professor Herman P. Meissner critically examined the data and helped to improve the understanding of the problem.

I am extremely grateful to Dr. Val Krukonis of A.D. Little Co., who was instrumental in developing the AVCO-Arc-Coal process while he was with AVCO, for having made his experience with the rotating-arc reactor available to me. Without his vital suggestions in the construction of the reactor, I would have taken far more tortuous, if not torturous, a path in accomplishing the objectives of this thesis. In addition, I gratefully acknowledge his interest and helpful discussions during the course of this research.

I wish to extend my appreciation to my friend and former colleague, Dr. Orn Adalsteisson, for many helpful discussions on the general course of this research. Thanks are extended to Dan Ludington for his experimental help. Stanley Mitchell is to be thanked for his superb drawings and especially for his many invaluable technical suggestions. Charles Foshey helped me in setting up the experimental equipment and generously rendered me much technical assistance. Arthur Clifford is also to be thanked for his technical assistance. Edward Gumpka of the machine shop at the Center for Materials Science and Engineering machined most parts of the reactor. His excellent workmanship is highly acknowledged.

Table of Contents

	<u>Page</u>
List of Tables	xi
List of Figures	xii
1. Summary	1
1.1 Introduction	1
1.1.1. Background	1
1.1.2. Objectives	6
1.2 Apparatus and Procedure	7
1.2.1. Selection of Apparatus	7
1.2.2. Description of Apparatus	8
1.2.3. Materials	17
1.2.4. Analytical Procedure of Products	18
1.3 Results	20
1.3.1. Results of Methane Series Runs	20
1.3.1.1. Characteristics of Methane Series Runs	20
1.3.1.2. Reproducibility of Data	22
1.3.1.3. Experimental Results	24
1.3.2. Results of Ethylene Series Runs	34
1.3.3. Results of Coal Series Runs	36
1.3.3.1. Operational Characteristics	36
1.3.3.2. Experimental Results	37
1.4 Product Morphology	42
1.5 Discussion of Results	49
1.5.1. Methane Series Runs	49
1.5.1.1. Decomposition of Methane	50
1.5.1.2. Heat and Mass Transfer Between Gas and Particles	52
1.5.1.3. CaC ₂ Formation	55
1.5.2. Ethylene Series Runs	60
1.5.3. Coal Series Runs	61
1.5.4. Economic Feasibility of the Reaction Scheme	62
1.6 Conclusions	66
1.7 Recommendations	68
2. Introduction	70
2.1 Status of Acetylene in the Chemical Market	70

Table of Contents (cont'd)

	<u>Page</u>
2.2 Acetylene Manufacturing Processes	73
2.2.1. Acetylene from Calcium Carbide	73
2.2.1.1. Chemistry of Calcium Carbide Manufacture	74
2.2.2. Acetylene from the Pyrolysis of Hydro- carbons	78
2.2.2.1. Chemistry of Acetylene Forma- tion from Hydrocarbons	78
2.2.2.2. Industrial Processes of Acetylene Manufacture from Hydrocarbons	79
2.3 Novel Methods of Acetylene Manufacture	83
2.3.1. Direct Production of Acetylene from Coal	83
2.3.2. Direct Synthesis of Acetylene from Carbon-Hydrogen Systems at High Tem- peratures (above 2500°K)	86
2.4 Motivation	87
2.5 Chemical Reactions-in-Arc-Plasma Jets	89
2.5.1. Plasmas for High Temperature Chemistry	90
2.5.2. Review of Gas-Solid Metallurgical Type Reactions in Arc-Plasma Jets	93
2.6 Objectives	100
3. Apparatus and Procedure	102
3.1 Selection of Apparatus	102
3.2 Description of Apparatus	103
3.2.1. Details of the Rotating-Arc Reactor	103
3.2.1.1. The Head Assembly of the Rotating-Arc Reactor	103
3.2.1.2. Magnetic Coils	111
3.2.1.3. Reactor Shell: Cooling Chamber	113
3.2.1.4. Quench Probes and Sample Collecting System	115
3.2.2. Powder Feeding Device	117
3.2.3. Power Supply and Auxiliary Equipment	121
3.2.4. Layout of the Experimental Apparatus	123
3.3 Procedure of Reactor Operation	126

Table of Contents (cont'd)

	<u>Page</u>
3.3.1. Preparation of Reactor	126
3.3.2. Operation of Reactor	130
3.4 Materials	132
3.5 Analytical Procedure of Products	133
3.5.1. Analysis of Solid Product	133
3.5.2. Analysis of Gas Product	136
4. Results	137
4.1 Results of Methane Series Runs	137
4.1.1. Characteristics of Methane Series Runs	137
4.1.1.1. Arc Characteristics	137
4.1.1.1.1. Theoretical Con- sideration of Arc Charac- teristics	138
4.1.1.1.2. Observation of Arc Characteristics	140
4.1.1.2. Erosion of Graphite Elec- trodes	142
4.1.2. Reproducibility of Data	144
4.1.3. Experimental Results	146
4.1.3.1. Effect of Lime Feed Rates	148
4.1.3.2. Particle Size Effect	150
4.1.3.3. Effect of Quench Distances	150
4.1.3.4. Effect of Residence Time	151
4.1.3.5. Effects of Power Input and Methane Flow Rates	153
4.1.3.6. Gaseous Product Composition	156
4.2 Results of Ethylene Series Runs	159
4.2.1. Operational Characteristics	159
4.2.2. Experimental Results	160
4.3 Results of Coal Series Runs	162
4.3.1. Operational Characteristics	162
4.3.2. Experimental Results	163
4.4 Product Morphology	169
5. Discussion of Results	177
5.1 Methane Series Runs	177
5.1.1. Decomposition of Methane: Formation of Atoms and Free Radicals of Hydrogen and Carbon	178

Table of Contents (cont'd)

	<u>Page</u>
5.1.2. Heat and Mass Transfer Between Gas and Particles	185
5.1.3. CaC ₂ Formation	188
5.2 Ethylene Series Runs	195
5.3 Coal Series Runs	196
5.4 Economic Feasibility of the Reaction Scheme .	199
6. Conclusions	205
7. Recommendations	208
8. Appendix	210
8.1 Tabulation of Experimental Results	210
8.2 Supplementary Details of Analysis of Solid Product	211
Bibliography	221

List of Tables

	<u>Page</u>
Table 1.1 Timer Schedules for Reactor Operation . .	16
Table 1.2 Characteristics of Coal Used in the Present Study	19
Table 3.1 Timer Schedules for Reactor Operation . .	127
Table 3.2 Characteristics of Coal Used in the Present Study	134
Table 8-1 Methane Series Runs	214
Table 8-2 Methane Series Special Runs	218
Table 8-3 Ethylene Series Runs	219
Table 8-4 Coal Series Runs	220

List of Figures

		<u>Page</u>
Figure 1.1	Equilibrium Constant vs. Temperature for CaC ₂ Formation from CaO and C: CaO + 3C → CaC ₂ + CO	2
Figure 1.2a	Schematic of Rotating-Arc Reactor Head Assembly	9
Figure 1.2b	Schematic of Various Graphite Anodes .	10
Figure 1.2c	Schematic of Water-Cooled Copper Anode	10
Figure 1.2d	Simplified Overall View of the Reactor	12
Figure 1.2e	Schematic of Powder Feeder Box	13
Figure 1.2f	Layout of Experimental Apparatus	15
Figure 1.3	Arc Voltage-Current Characteristics of the Rotating-Arc in CH ₄ , with CaO Feeding .	21
Figure 1.4	CaO Conversion vs. Power Input at Various CH ₄ Flow Rates	25
Figure 1.5	CaO Conversion vs. Ratio of Actual to Stoichiometric Lime Feed Rates	27
Figure 1.6	CaO Conversion vs. Specific Gas Enthalpy; C ₂ H ₄ Runs are shown together with CH ₄ runs	31
Figure 1.7	CH ₄ Concentration vs. CaO Conversion in CH ₄ Series Runs	33
Figure 1.8	Variation of C ₂ H ₂ Concentration in Gas Product with Lime Feed Rates	35
Figure 1.9	CaO Conversion vs. Power Input, Coal Series Runs	38
Figure 1.10a	CaO Conversion as a Function of Energy Input per G Mole H ₂	40
Figure 1.10b	CaO Conversion vs. Energy per G Atom C in Coal	41

List of Figures (cont'd)

		<u>Page</u>
Figure 1.11	Reagent Grade CaO; -8 μ particles; SEM, x2000	44
Figure 1.12	Reagent grade lime at higher magnification; SEM, x5100	44
Figure 1.13	Natural calcite; -325 mesh particles; SEM, x950	44
Figure 1.14	Close-up of specimen on the left; SEM, x4800	44
Figure 1.15	Calcine of -325 mesh size calcite; shows spongy texture; SEM, x530	44
Figure 1.16	Close-up of specimen on the left; SEM, x2200	44
Figure 1.17	7.0% conversion, run no. M-79, -35 mesh calcine; x33000	45
Figure 1.18	21.7% conversion, run no. M-75; -325 mesh calcine; x33000	45
Figure 1.19	35.0% conversion, run no. M-64; reagent grade lime; x 33000	45
Figure 1.20	58.3% conversion, run no. M-74; -325 mesh calcine; x33000	45
Figure 1.21	64.0% conversion, run no. M-70, reagent grade lime; x33000	46
Figure 1.22	77.0% conversion, run no. M-76; -200 mesh calcine; x33000	46
Figure 1.23	79.5% conversion, run no. M-73; -325 mesh calcine; x33000	46
Figure 1.24	Methane black, run no. SM-1; no lime feeding; x33000	46
Figure 1.25	Coal series run #C-13, 22.9% conversion; reag. gr. lime; sample from reactor bottom; x33000	48
Figure 1.26	Coal series run #C-6, 38.2% conversion; reag. gr. lime; sample from reactor bottom; x33000	48

List of Figures (cont'd)

		<u>Page</u>
Figure 1.27	Coal series run #C-8, 49.8% conversion; reag. gr. lime; sample from quench probe; x33000	48
Figure 1.28	Coal series run #C-10, 53.0% conversion; reag. gr. lime; sample from quench probe; x33000	48
Figure 1.29	Equilibrium Composition for the Carbon- Hydrogen System in the Heterogeneous Region	53
Figure 1.30	Equilibrium Temperatures of the Carbon- Hydrogen System at Various Specific En- thalpies (Heterogeneous Region Only) .	54
Figure 1.31	Equilibrium Constant vs. Temperature for Various Reactions Related to CaC ₂ Formation	59
Figure 1.32	Thermodynamic Energy Required to Produce One lb C ₂ H ₂ via CaC ₂ from CaO and Hydro- carbons/or Coal & Hydrogen	63
Figure 2.1	Equilibrium Constant vs. Temperature for CaC ₂ Formation from CaO and C: CaO + 3C → CaC ₂ + CO	75
Figure 3.1	Schematic of Rotating-Arc Reaction Head Assembly	104
Figure 3.2a	Schematic of Various Graphite Anodes .	108
Figure 3.2b	Schematic of Water-Cooled Copper Anode	108
Figure 3.3	Simplified Overall View of the Reactor .	114
Figure 3.4	Schematic of Powder Feeder Box	118
Figure 3.5	Layout of Experimental Apparatus . . .	124
Figure 3.6	Photographs of Reactor Area and Control Panel	125
Figure 4.1	Arc Voltage-Current Characteristics of the Rotating-Arc in CH ₄ with CaO Feeding	141

List of Figures (cont'd)

		<u>Page</u>
Figure 4.2	CaO Conversion vs. Power Input at Various CH ₄ Flow Rates	147
Figure 4.3	CaO Conversion vs. Ratio of Actual to Stoichiometric Lime Feed Rates . . .	149
Figure 4.4	CaO Conversion vs. Specific Gas Enthalpy, CH ₄ Runs	155
Figure 4.5	CH ₄ Concentration vs. CaO Conversion in CH ₄ Series Runs	157
Figure 4.6	Variation of C ₂ H ₂ Concentration in Gas Product with Lime Feed Rates	158
Figure 4.7	CaO Conversion vs. Specific Gas Enthalpy; C ₂ H ₄ Runs are shown together with CH ₄ runs	161
Figure 4.8	CaO Conversion vs. Power Input, Coal Series Runs	165
Figure 4.9	CaO Conversion as a Function of Energy Input per G Mole H ₂	167
Figure 4.10	CaO Conversion vs. Energy per G Atom C in Coal	168
Figure 4.11	Reagent grade Ca; -8 μ particles; SEM, x2000	170
Figure 4.12	Reagent grade lime at higher magnification; SEM, x5100	170
Figure 4.13	Natural calcite; -325 mesh particles; SEM, x950	170
Figure 4.14	Close-up of specimen on the left; SEM, x4800	170
Figure 4.15	Calcine of -325 mesh size calcite; shows spongy texture; SEM, x530 . . .	170
Figure 4.16	Close-up of specimen on the left; SEM, x2200	170
Figure 4.17	7.0% conversion, run no. M-79; -35 mesh calcine; x33000	173

List of Figures (cont'd)

		<u>Page</u>
Figure 4.18	21.7% conversion, run no. M-75; -325 mesh calcine; x33000	173
Figure 4.19	35.0% conversion, run no. M-64; reagent grade lime; x33000	173
Figure 4.20	58.3% conversion, run no. M-74; -325 mesh calcine; x33000	173
Figure 4.21	64.0% conversion, run no. M-70; reagent grade lime; x33000	174
Figure 4.22	77.0% conversion, run no. M-76; -200 mesh calcine; x33000	174
Figure 4.23	79.5% conversion, run no. M-73; -325 mesh calcine; x33000	174
Figure 4.24	Methane black, run no. SM-1; no lime feeding; x33000	174
Figure 4.25	Coal series run #C-13, 22.9% conversion; reag. gr. lime; sample from reactor bottom; x33000	176
Figure 4.26	Coal series run #C-6, 38.2% conversion; reag. gr. lime; sample from reactor bottom; x33000	176
Figure 4.27	Coal series run #C-8, 49.8% conversion; reag. gr. lime; sample from quench probe; x33000	176
Figure 4.28	Coal series run #C-10, 53.0% conversion; reag. gr. lime; sample from quench probe; x33000	176
Figure 5.1	Equilibrium Composition for the Carbon-Hydrogen System in the Heterogeneous Region	182
Figure 5.2	Equilibrium Temperatures of the Carbon-Hydrogen System at Various Specific Enthalpies (Heterogeneous Region Only)	184
Figure 5.3	Equilibrium Constant vs. Temperature for Various Reactions Related to CaC ₂ Formation	194

List of Figures (cont'd)

	<u>Page</u>	
Figure 5.4	Thermodynamic Energy Required to Produce One lb C ₂ H ₂ via CaC ₂ from CaO and Hydrocarbons/or Coal & Hydrogen .	200
Figure 8.1	Oxidation of Product CaC ₂ in a Gas-Tight Flask Initially Filled with Air . . .	213

1. Summary

1.1. Introduction

1.1.1. Background

Although acetylene is an invaluable building block for the chemical industry, it has suffered continuous erosion of its major chemical markets in recent years because of competition from less expensive raw materials. Acetylene production in the U.S. reached its peak in 1965 (at 1.149 billion pounds) and has been declining since. In 1974, acetylene production amounted to only 507 million pounds, of which 402 millions pounds were used for the manufacture of chemicals and the balance for industrial welding and metal cutting (2).

The erosion of the acetylene market can be traced to the inability of the current processes to produce acetylene at a competitive price. Presently acetylene is produced via calcium carbide and from the pyrolysis of hydrocarbons.

Calcium carbide is produced commercially from lime and coke at 1800-2100°C and at atmospheric pressure in an electrothermal furnace (48);



Figure 1.1 shows the temperature dependence of the equilibrium constant of the above reaction. The molten product is tapped from the furnace intermittently and allowed to cool at ambient temperature before crushing and shipping for the

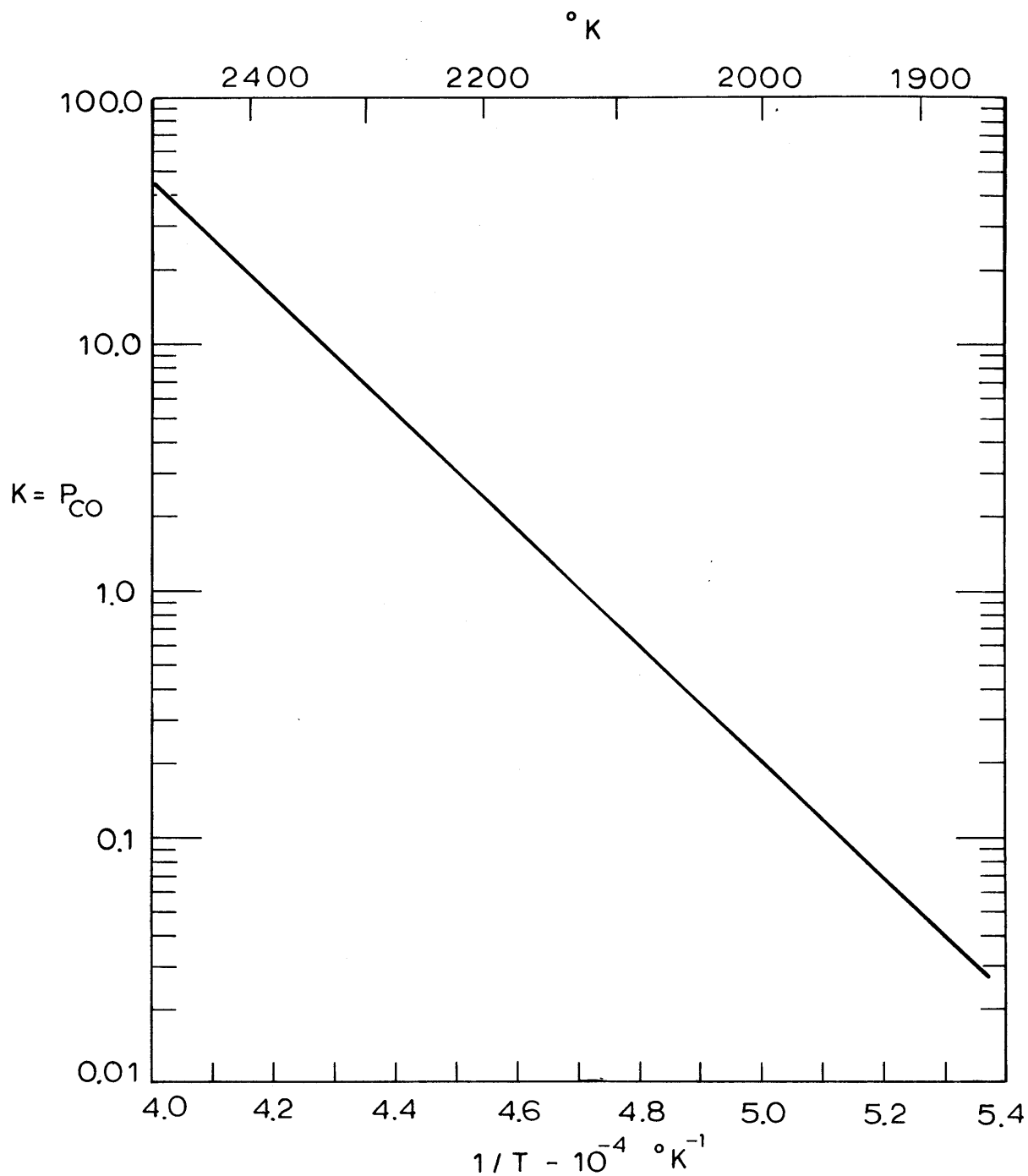
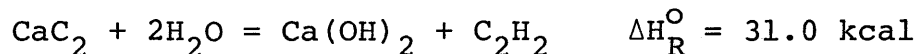


Fig. 1.1 Equilibrium Constant vs. Temperature for CaC_2 Formation from CaO and C : $\text{CaO} + 3\text{C} \rightarrow \text{CaC}_2 + \text{CO}$.

subsequent generation of acetylene by hydrolysis:



Acetylene thus produced is 99-99.8% pure on a dry basis and can be directly used for the synthesis of chemicals.

There are three general methods used commercially to manufacture acetylene from hydrocarbons. They are: (1) regenerative pyrolysis; (2) partial combustion; and (3) electrical discharge processes (48). However, none of the existing processes shows promise for reducing the acetylene price, while other hydrocarbon feedstocks have been decreasing in cost relative to acetylene in past years.

It has been well known in the area of coal gasification research that, if finely ground and well-dispersed coal is rapidly heated to a high temperature (preferably in a hydrogen environment), it can be gasified well in excess of what could be attained in a slow heating condition (6). The extent of gasification and the product gas composition are known to depend on the rate of heating and the final temperature under a given condition.

Especially if the final temperature is above approximately 1500°K, the main product will be acetylene because above that temperature it is thermodynamically more stable than most other hydrocarbon molecules. An electric arc is a convenient source of high temperature and has been widely used for the rapid heating of coal. Thus, Bond et al. (17, 18) were able to convert up to 20% of the initial carbon in a

high volatile coal to acetylene by injecting the fine powder of same into a d.c. argon plasma jet. When 10% hydrogen was added to the argon plasma, the conversion doubled to 40%. They were not able to add more than 10% H₂ to the plasma because of severe erosion of the electrodes and the ensuing arc instabilities. Similar experiments have been reported by Graves et al. (34), Kawana et al. (41), and Anderson et al. (1). Remarkably, Littlewood and co-workers (47, 57) of the University of Sheffield were able to convert up to 74% of the carbon in coal to acetylene by passing fine powder of a high volatile coal directly through the arc zone of a d.c. arc-gas heater operating in a 90% Ar/10% H₂ mixture. Nevertheless, the highest acetylene concentration was only on the order of 0.1% or less.

Krukonis et al. (28, 43) of AVCO Systems Division in Massachusetts have pursued the economic feasibility of producing acetylene directly from coal by passing the fine powder of same through a rotating arc with hydrogen as the carrier gas. Based on an average acetylene yield of about 20 wt % of coal fed with the acetylene concentration in the range of 8-10%, they concluded that the process can be commercially viable. In order to reduce the decomposition of acetylene, the reactor was operated at 0.3-0.5 atm absolute.

The main problem in manufacturing acetylene from hydrocarbons, as well as from coal, stems from the thermodynamic instability of acetylene, the very property which makes it attractive as a chemical raw material. In general, the

decomposition of acetylene can be minimized by quenching the reaction product very rapidly, which can be achieved only with a great deal of technical and operating difficulty in industrial processes. Acetylene decomposition can be further reduced by operating the process at low C_2H_2 partial pressure, which can result in high pumping and separation costs in addition to limited throughput of feed.

If the "nascent" carbon species concomitantly produced upon the pyrolysis of hydrocarbons or from the rapid heating of coal in hydrogen can react sufficiently quickly with lime (CaO), then one can produce CaC_2 instead of C_2H_2 as the main product in one-stage reaction. Unlike in the manufacture of acetylene, preserving the reaction product is not difficult because CaC_2 is thermodynamically stable relative to the elements in the range of temperatures of practical interest. Although there is no direct evidence that the reaction of lime and the "nascent" carbons can proceed fast enough to give an acceptable conversion of lime to CaC_2 , there exists some experimental evidence that the heterogeneous reaction may indeed go fast enough: in studies (66) involving injections of WO_3 and Ta_2O_5 powders suspended in a methane stream into a helium plasma jet, it was found that up to 94% of the WO_3 was converted to W , WC and W_2C , and up to 42% of the Ta_2O_5 to Ta , TaC and Ta_2C . The results generally demonstrate the intense chemical reactivity of carbon species in "nascent" stages and also indicate that the rather compli-

cated gas-solid reactions that involve several elementary steps can be carried out in good yields using a plasma jet.

1.1.2. Objectives

To investigate the feasibility of producing CaC_2 from the reaction of CaO with "nascent" carbons concomitantly produced upon the pyrolysis of hydrocarbons or from the rapid heating of a high volatile coal in hydrogen. Specifically, to perform the following:

Using methane as a carbon source, determine important process parameters and their quantitative effects on the formation of CaC_2 from the reaction of CaO with "nascent" carbon species; correlate them with the thermodynamics of the process and with the rather well-known mechanism of methane decomposition to construct a mechanistic picture of the overall process.

Use C_2H_4 in place of CH_4 and compare the results in view of differences in the C/H ratio and chemical and thermodynamic properties.

Use a high volatile coal in the reaction scheme and establish that coal can be as good a source of "nascent" carbon species as hydrocarbons for the formation of CaC_2 . Evaluate the commercial potential of the reaction scheme.

It is hoped that detailed knowledge of the process mechanism of the present reaction scheme will provide an added benefit of furthering the understanding of high-temperature gas-solid reactions that may rely on the extremely high reactivity of "nascent" chemical species for high conversions.

1.2. Apparatus and Procedure

1.2.1. Selection of Apparatus

The advantage of injecting reactants directly into the arc-zone rather than into the tail flame of an arc-heated auxiliary gas stream (alias a plasma jet) is obvious. Among several arc-discharge devices that allow direct passage of reactants through the arc zone (26, 28, 30, 62, 72), a d.c. rotating-arc reactor of the type used in the synthesis of acetylene from hydrocarbons by Du Pont (62) and from coal by AVCO (28) is chosen for the present study. It has rather well-established operational and mechanical characteristics that include high energy efficiency, arc stability, mechanical simplicity, ease of operation, and a comparatively large cross-sectional area of the interelectrode region which permits high throughput of feed through the arc zone.

It was decided that the rotating-arc reactor needs to be operated only one to three minutes to obtain products of truly a steady-state operation since the intrinsic reaction time may be in a range of 10^{-5} to 10^{-2} sec. Thus, the reactor was designed accordingly. Both electrodes are constructed of graphite and designed such that worn-out parts due to evaporation can be easily and inexpensively replaced after each run. Both graphite electrodes are held in position by water-cooled electrode holders to prevent excessive heating of other parts of the reactor.

1.2.2. Description of Apparatus

Figure 1.2a shows a schematic of the head assembly of the rotating-arc reactor. The cathode was 1/4" dia. and 1" long graphite rod, one end of which was threaded over the length of 1/4" for easy and secure insertion into the water-cooled cathode holder. The anode assembly for most runs consisted of a graphite anode-insert which slid into a graphite anode which was in most cases a 3" long x 2-1/2" o.d. cylinder with a 3/4" dia. opening as the anode nozzle. The anode insert was 1/2" in i.d. in all cases. In some cases, residence time of the reactants in the anode nozzle was prolonged by using graphite anodes of longer anode nozzles. The schematic of various graphite anodes is shown in Figure 1.2b.

Although the graphite anodes worked amiably well in methane and ethylene series runs, they posed a major problem in coal series runs, i.e., in those runs the feed particles fused in the pre-interelectrode region of the anode before reaching the arc zone, resulting in substantial particle hold-up in the region which in some cases extended even to the feeding line.

In order to eliminate the hot surface on which coal particles fused, a water-cooled copper anode was constructed and operated with some degree of success for a number of coal runs, as well as a few methane series runs. Figure 1.2c shows the schematic of the water-cooled copper anode, which was built in overall dimensions exactly the same as the 3"

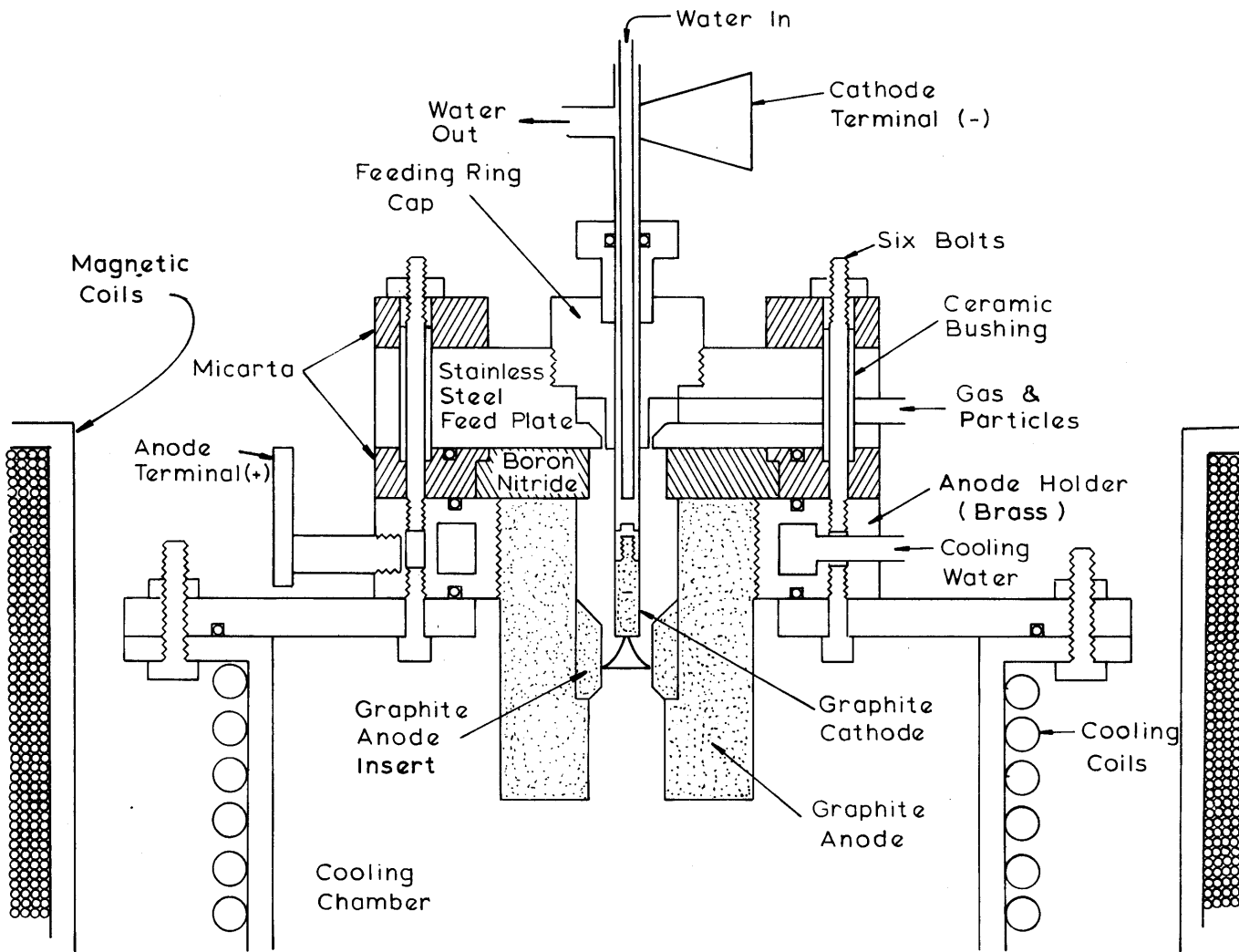


Fig. 1.2a Schematic of Rotating-Arc Reactor Head Assembly

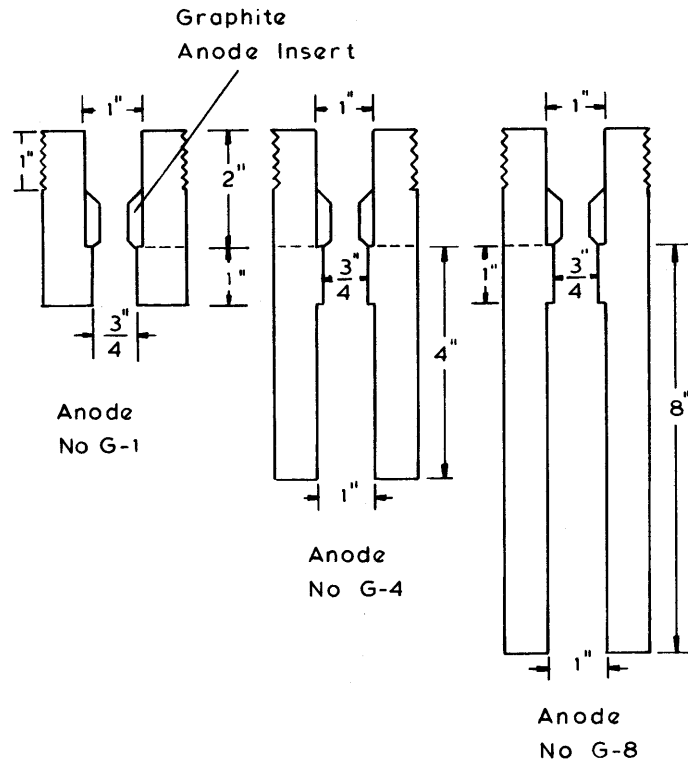


Fig. 1.2b Schematic of Various Graphite Anodes

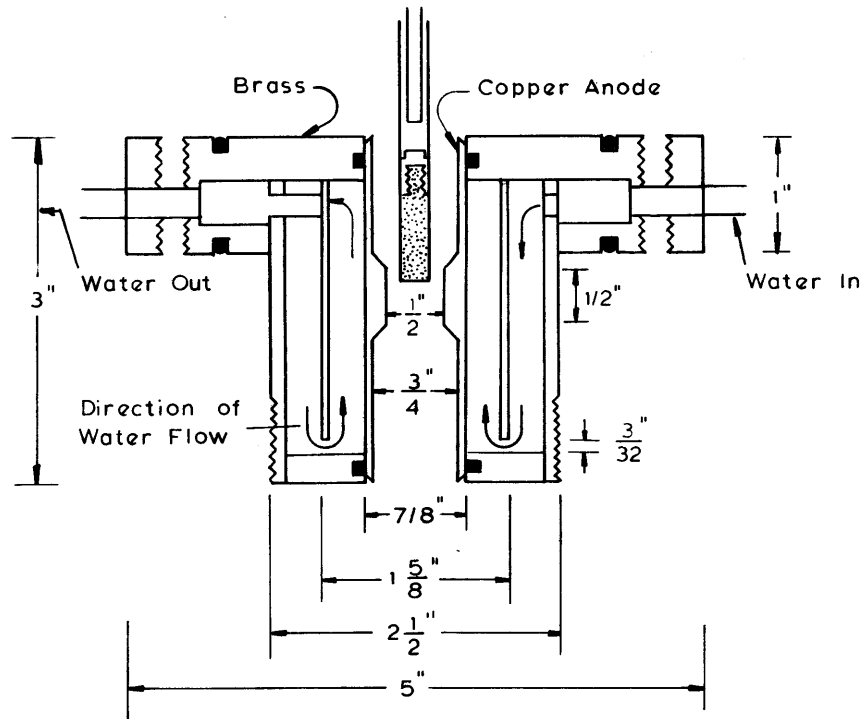


Fig. 1.2c Schematic of Water-Cooled Copper Anode

long graphite anode fitted in the brass anode holder. Unfortunately, it posed great experimental difficulty by burning out too frequently.

The reactants (gas and solid) were fed into the arc zone through a 1/32" wide annular slit in the bottom of the feed plate.

The arc column, which was sustained in the radial direction, was rotated very rapidly by an axial magnetic field provided by a solenoid placed concentrically outside the reactor shell near the arc-head assembly. The magnetic flux was measured to be about 120 gauss at the reactor axis.

Solid as well as gas products were collected by either one of two quench probes of different lengths, both of which consisted essentially of three concentric tubes. The innermost tube is a 1/4" o.d. copper tube. Figure 1.2d provides a simplified overall view of the reactor with one of the two quench probes placed in position. The solid product was collected in the solid sampling funnel which was equipped with a fritted disk filter. The gas product was sampled in an initially evacuated sampling can which was connected to the quench probe via a normally closed solenoid valve.

The powder feeding device (Figure 1.2e) consisted of a mechanically vibrated powder-hopper which unloads powder onto a conveyor-belt which in turn carries it to a powder-chute located at the opposite end of the hopper. The powder chute is the only outlet for the feed gas entering the

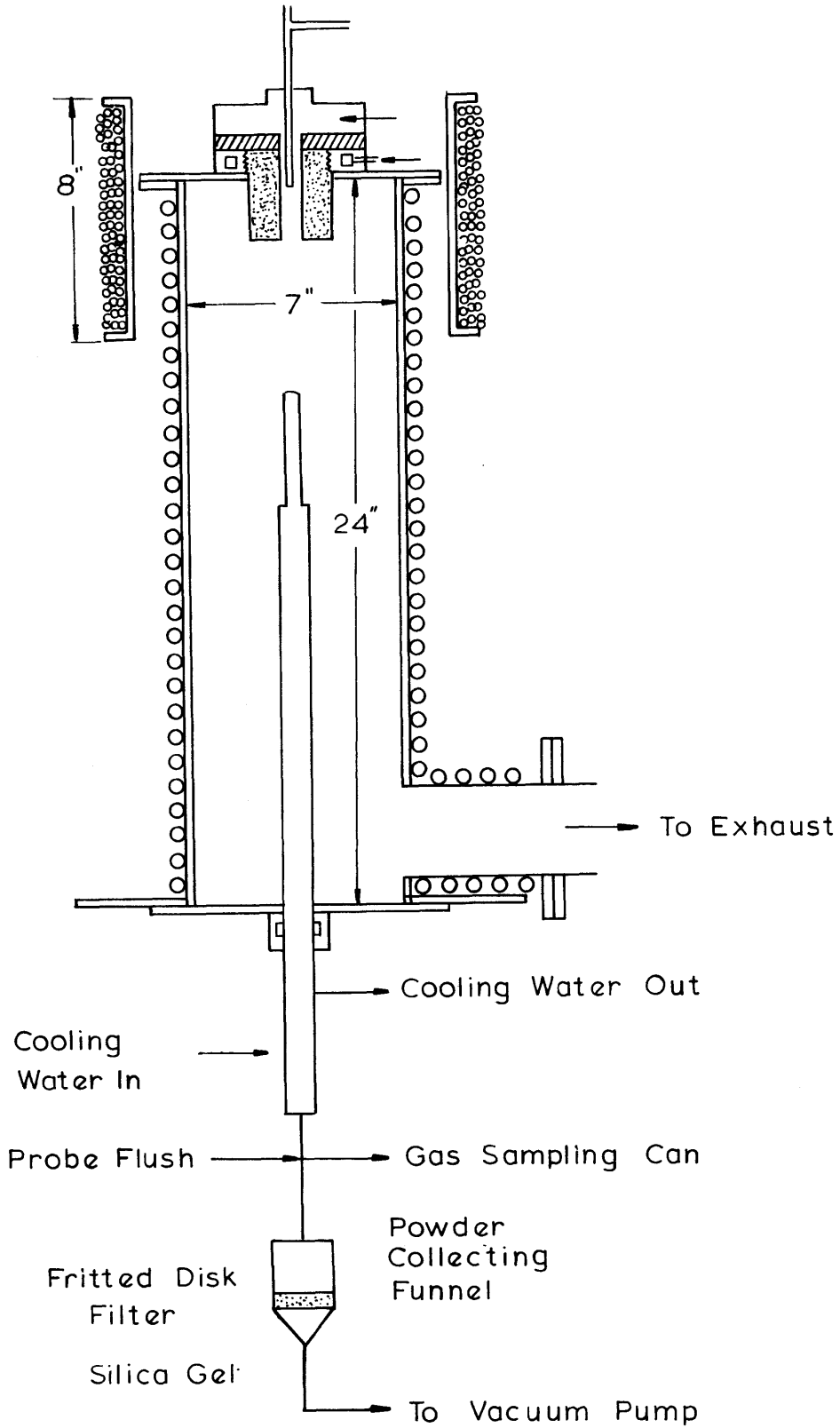


Fig. 1.2d Simplified Overall View of the Reactor

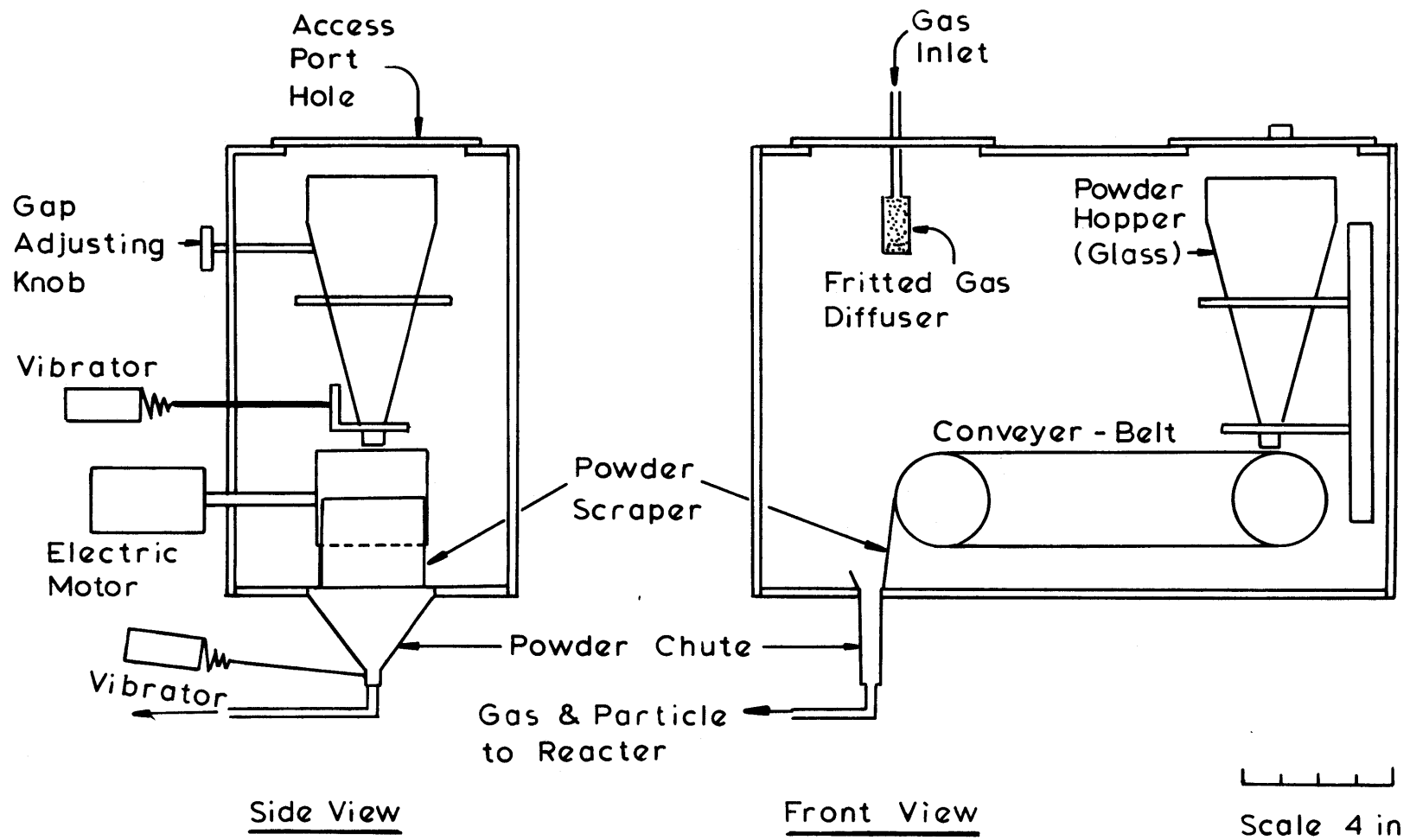


Fig. 1.2e Schematic of Powder Feeder Box

powder-feeder box, and subsequently the powder is carried by the gas into the rotating-arc reactor. Powder feed rate, which was calibrated by collecting the powder for a pre-determined period, was adjusted by manipulating the gap distance between the conveyor-belt and the bottom opening of the powder hopper. The powder feeder of this design performed very satisfactorily and provided essentially constant powder feed rates up to 50 gm/min.

Power to the arc was provided by a Miller welding power supply, model SR-1000B1, which had an open circuit voltage of 160 volts and was capable of delivering up to 40 kw to the electrodes. The power input to the arc was measured by a 200 volt voltmeter and a 500 amp ammeter. The arc was started and stabilized by using a Miller high frequency unit, model HF-15-1 (output 0.18 kw), which was placed in series with the power supply. The arc was always started by first establishing a high frequency discharge in argon and then switching the gas to the main arc gas of interest.

The layout of the experimental apparatus is shown in Figure 1.2f. In all experiments, the whole sequence of the reactor operation was automated by using a timer which could actuate up to 10 circuits individually. Two different timer schedules, one for the methane and ethylene series runs and another for the coal runs, were employed for reactor operation as shown in Table 1.1. In the coal series runs, powder feeding started 10 seconds from the initiation of the timer cycle instead of the usual 30 seconds for the methane

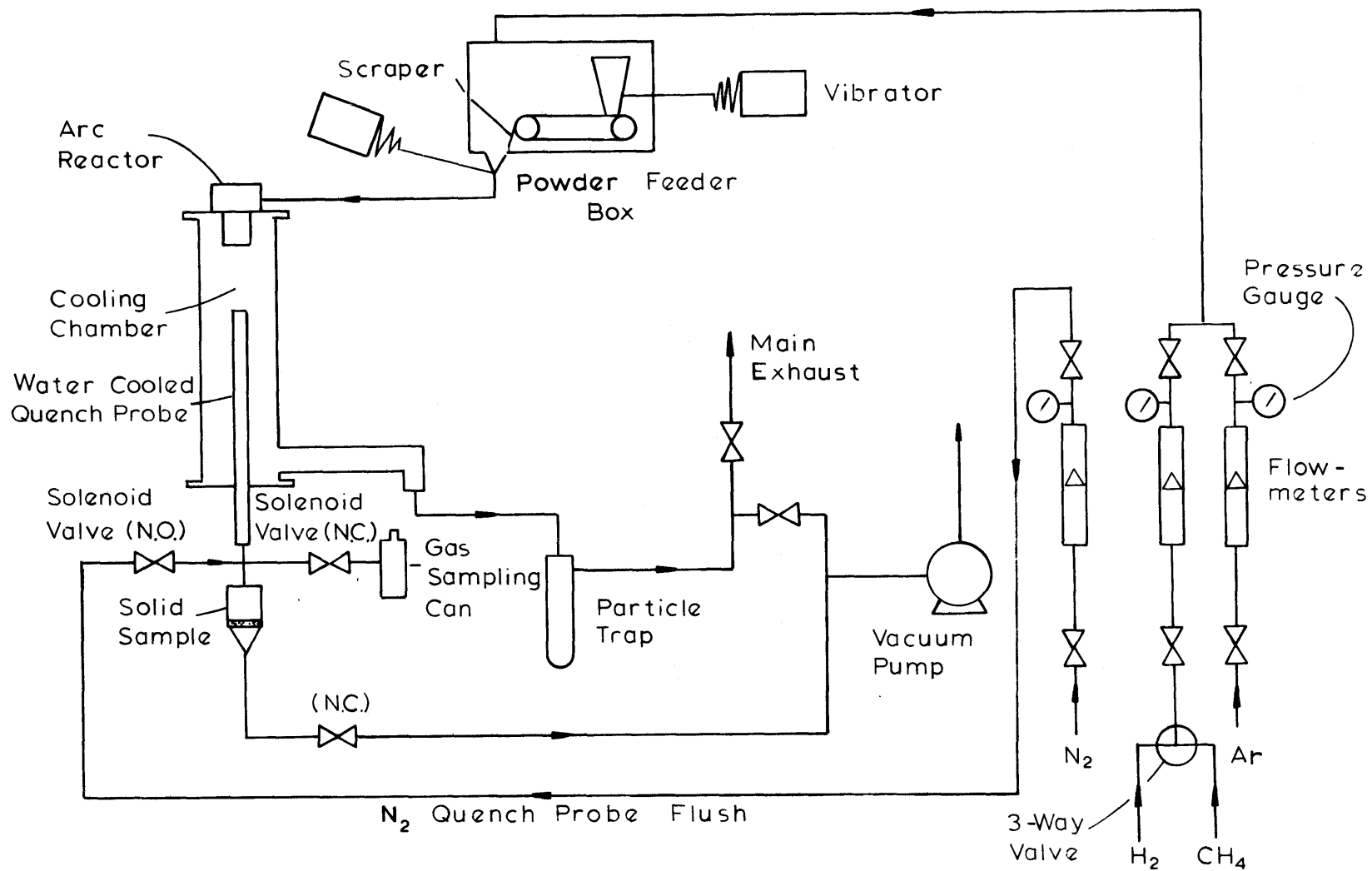
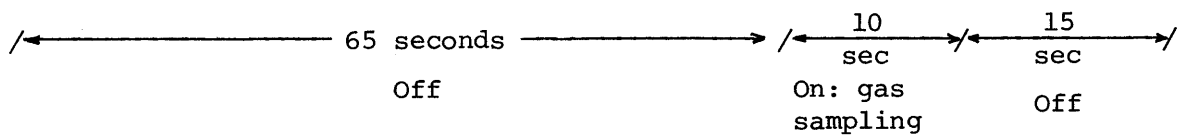
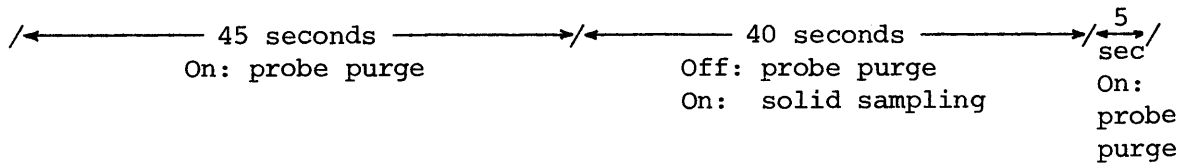
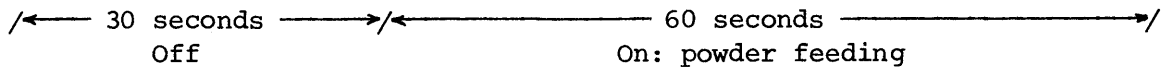
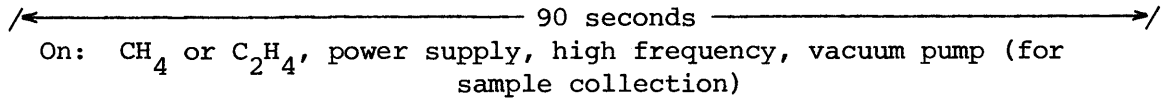


Fig. 1.2f Layout of Experimental Apparatus

Table 1.1

Timer Schedules for Reactor Operation

Timer Schedule I (for CH₄ or C₂H₄ series runs):



Timer Schedule II (for coal series runs)

Identical to Schedule I, except powder feeding, which starts 10 seconds after actuation of timer.

and ethylene series runs to prevent excessive evaporation of the graphite electrodes. In each reactor operation, the timer cycle was actuated after establishing the arc at a desired power level and then the arc voltage and amperage, both of which were fluctuating very rapidly over a very wide range when the arc was unstable as encountered in many cases, were recorded in 6-8 second intervals by reading off the voltmeter and ammeter. Both the arc voltage and amperage were read simultaneously in each reading in order to calculate the instantaneous power input, from which the average power input was calculated.

1.2.3. Materials

Two different types of CaO were used in the present study. One is reagent grade CaO manufactured by Mallin-krodt, Inc., whose particles are typically less than 8 μ in size as observed under an optical microscope. The other is a calcine of high purity natural calcite obtained through the courtesy of Pfizer, Inc. from its mine at Adams, Massachusetts. The chemical composition of the natural calcite was: 95% CaCO₃, 1.5% MgCO₃, 1.9% SiO₂, 0.4% Al₂O₃, 0.1% Fe₂O₃, and 0.2% moisture. Two different particle sizes of the calcine were obtained by calcining the natural calcites of -200 mesh (-74 μ) and -325 mesh (-44 μ) sizes at 1000°C for 10 hours or longer. The calcines revealed little change in particle size from the original limestones when viewed under either an optical or a scanning electron-microscope.

Commercial grade methane was obtained from Airco, Inc.; its hydrocarbon contents were 95.6% CH_4 , 1.8% C_2H_4 , and 0.3% C_3H_8 , as analyzed by a flame ionization detector. Ethylene was 99.9% pure.

The high volatile bituminous coal used in the present study was from the Ireland Mine (Consolidation Coal Company). Its characteristics are shown in Table 1.2.

1.2.4. Analytical Procedure of Products

The solid sample collected in the sampling funnel was analyzed for the CaC_2 content indirectly by measuring the acetylene evolved upon hydrolysis by using a flame ionization detector (Hewlett-Packard Series 700). The total calcium content in the hydrolyzed sample was then measured by first dissolving it in HCl, and then filtering and titrating the filtrate with EDTA at pH 12.5, following the method of complexometric titration outlined in (65). Since the calcium was entirely in the form of CaO before the reaction, the percentage of the total calcium in the form of CaC_2 in the sample also represented the percentage conversion of CaO to CaC_2 .

The hydrocarbons in the gas product were quantitatively determined by using the same flame ionizational detector. The hydrocarbons detected were mostly CH_4 , C_2H_2 , C_2H_4 , and in a few cases, C_2H_6 .

The analytical method outlined above for determining CaO conversion was fairly accurate and gave a deviation of

Table 1.2

Characteristics of Coal Used in the Present Study
(Pittsburgh Seam #8, hvA-b)

Proximate Analysis

<u>Characteristic</u>	<u>As Received</u>	<u>Dry</u>	<u>d.a.f.</u>
moisture	2.2	-	-
volatile matter	40.7	41.6	46.7
fixed carbon	46.3	47.3	53.3
ash	10.8	11.1	-

heating value: 14,377 BTU/lb d.a.f.

Ultimate Analysis

<u>Component</u>	<u>As Received, % by wt</u>
carbon	67.81
hydrogen	5.03
nitrogen	1.05
sulfur	4.83
oxygen	8.55 by difference

2% or less when the sample was handled in a glove bag filled with N_2 . When the sample was handled in the open air, the deviation was 6% or less even though the exposure of the product to the open air was kept as short as possible; however, the deviation was apt to be on the side of underestimating the true conversion because of the loss of CaC_2 by hydrolysis and oxidation.

1 3. Results

1.3.1. Results of Methane Series Runs

1.3.1.1. Characteristics of Methane Series Runs

The voltage-current characteristics of the rotating arc in CH_4 during CaO feeding are shown in Figure 1.3, which is prepared from average values of the voltages and currents read at regular intervals during each run. It clearly shows the falling voltage-rising current characteristic of a low to medium intensity arc. The effect of increasing the gas flow rate, from 16.0-17.3 l/min to 30.0-35.8 l/min and thus approximately by a factor of two, is seen to shift the arc characteristic curve upwards. It was due to increased convective cooling of the arc column at higher gas flow rates. Also, the arc voltage may have risen additionally due to elongation of the arc column since the latter was sustained in a cross flow of gas.

The relatively wide scattering of the data was mainly caused by the arc instabilities. The arc was mostly unstable when the gas flow rate was in a range of 30.0-35.8 l/min or higher. However, it was quite to moderately stable

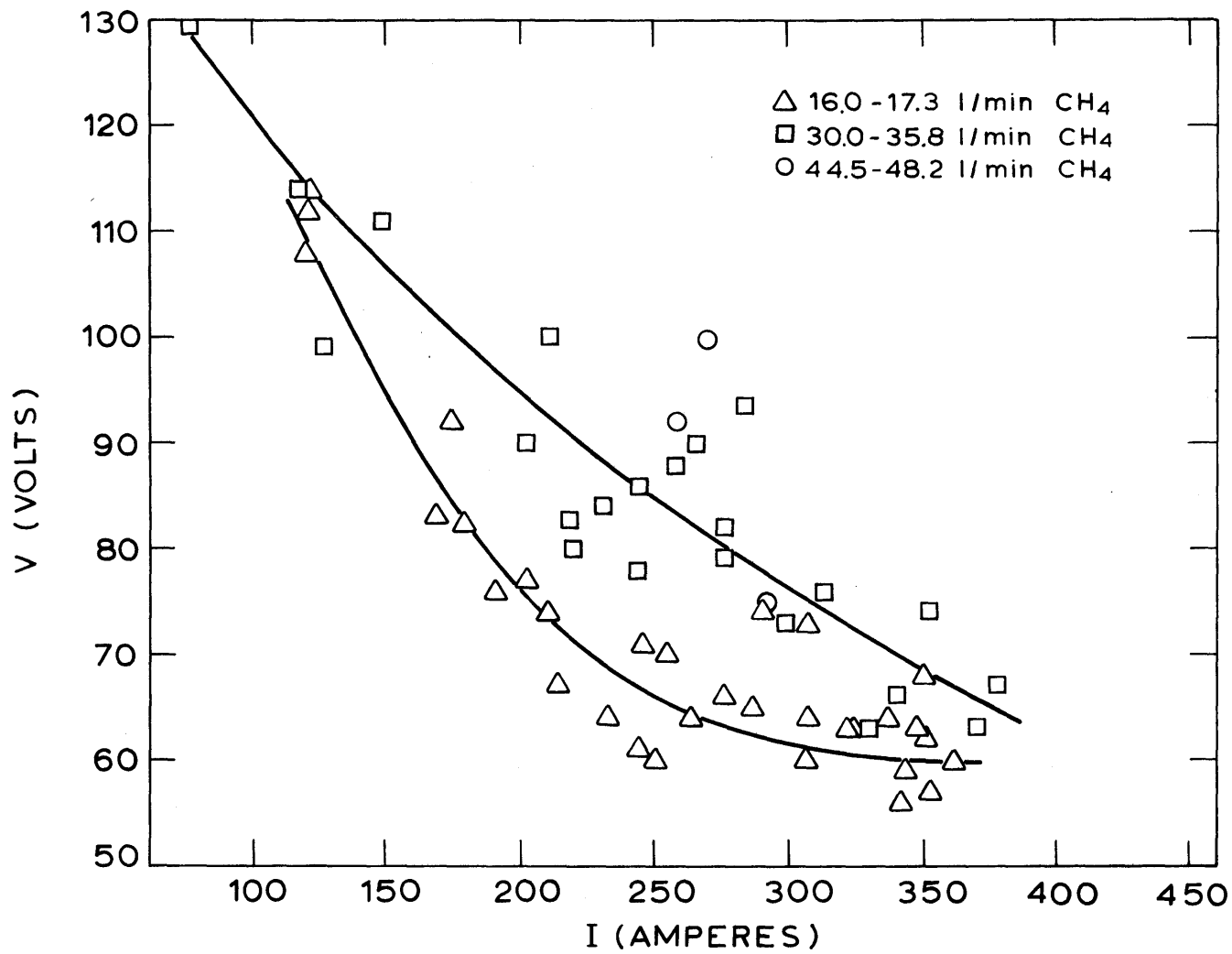


Fig. 1.3 Arc Voltage-Current Characteristics of the Rotating-Arc in CH_4 , with CaO Feeding

when the gas flow rate was in a range of 16.0-17.3 l/min and the arc voltage was lower than 75 volts; but it became fairly to very unstable when the voltage exceeded 80 volts. It was observed during actual runs that the voltage and current fluctuated in opposite directions in such a way that, in retrospect, the fluctuation seemed to have been tracing the arc characteristic curves.

The rate of carbon vaporization from the graphite cathode was typically around 0.2 g/min and rarely reached the maximum of 0.4 g/min when the methane flow rate was in a range of 16.0-17.3 l/min and the current was 300 amps or higher. Therefore the carbon vaporized from the electrode was typically around 2% and rarely exceeded the maximum of 5% of the carbon content of the methane flow. The percentage was even less at the higher methane flow rates due to increased carbon content in the gas flow and somewhat less severe erosion of the carbon electrode. The graphite anode used to show no noticeable weight loss after the run.

1.3.1.2. Reproducibility of Data

Power Input. The singular experimental factor which caused the relatively wide scattering of experimental results in the present study was the fluctuations of power input which proved so difficult to control as a result of the arc instabilities inherently encountered in many runs. Generally the fluctuations were rapid when the arc was unstable, their amplitudes becoming larger as the arcs became more unstable.

The arc, and hence the power input, was most stable when the methane flow rate was in a range of 16.0-17.3 l/min and the power input was 15.5 kw or higher, with a standard deviation of the power fluctuations in a range of 3-10% around the mean power input; however, below about 14 kw the deviation increased to anywhere from 10 to 30% of the mean. With the methane flow rate in a range of 30.0-35.8 l/min, the deviation of power fluctuations was in a range of 6-16% of the mean when the power input was 22 kw or higher; and below 22 kw it was typically on the order of 30% but occasionally reached up to the order of 60%.

Quantitative Analysis of Products. The accuracy of the analytical techniques is discussed in Section 1.2.4.

Spatial Distribution of Solid Product. Because of the fluctuations in the power input, the composition of the solid product collected in the sampling funnel may have been different from layer to layer, although the fluctuations were usually so rapid that the product distribution may not have been distinctive. Nevertheless, complete mixing of the layers was always ensured by stirring up the particles in the sampling funnel before taking portions of them for the subsequent analysis of CaC_2 .

The possibility of radial distribution of the solid product in the cooling chamber was examined by analyzing for CaC_2 the particles collected from the bottom and the side-walls of the chamber and comparing the results with those from the sampling funnel collected at a 15" quench distance.

The examination revealed that the % conversion of CaO to CaC₂ was lower by typically 2-3% and by as much as 7% for the samples collected from the bottom and the side-walls in comparison with those from the sampling funnel. This discrepancy was attributed to the hydrolysis of the CaC₂ product inside the cooling chamber by the moisture in the open air, which was let in during dismantling of the reactor. It used to take about three minutes to dismantle the reactor and collect the powders from the inside, which proved to be long enough to cause the hydrolysis noted above.

1.3.1.3. Experimental Results

Extensive experimental studies were carried out using CH₄ as the carbon source. The experimental parameters studied were: (1) power input, in a range of 10-26 kw; (2) methane flow rate, in three different levels -- 16.0-17.3 l/min, 30.0-35.8 l/min, and 44.5-48.2 l/min; (3) lime feed rate, in a range of 0.1-1.4 times the stoichiometric lime feed rate based on the carbon in the methane flow; (4) CaO particle size: -8 μ, -44 μ (i.e. -325 mesh size), and -74 μ (i.e. -200 mesh size) fractions; (5) residence time, varied up to an order of magnitude by varying anode nozzle length and diameter; and (6) quench distance, set at either 5" or 15".

The results from all the methane series runs are plotted in Figure 1.4 for the % CaO conversion (to CaC₂) vs. power input. In spite of the widely different ranges of the experi-

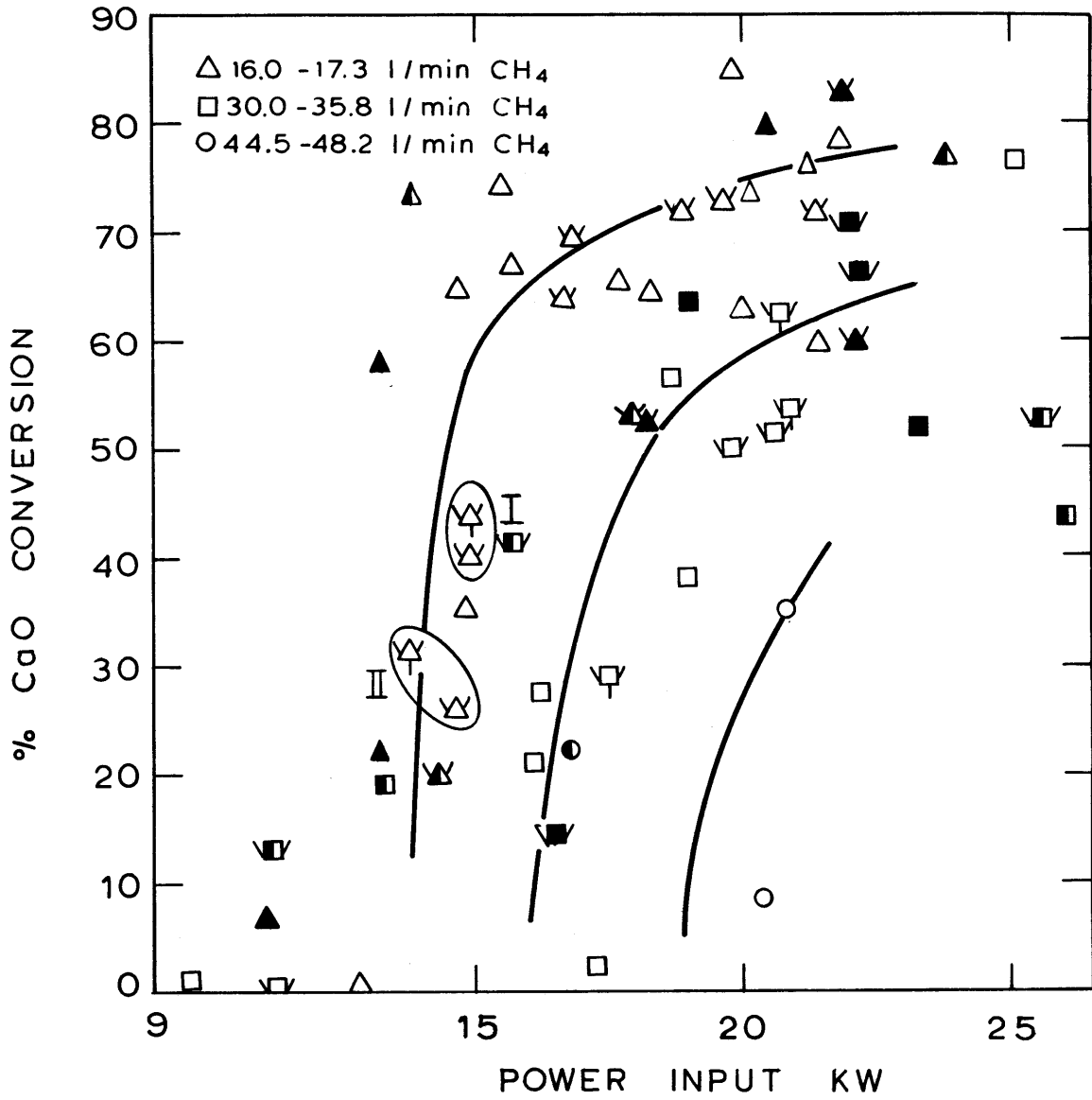


Fig. 1.4 CaO Conversion vs. Power Input at Various CH_4 Flow Rates

Particle Size; $\triangle, \square, \circ$, -8μ ; $\blacktriangle, \blacksquare, \bullet$, -44μ ; $\blacktriangle, \blacksquare, \bullet$, -74μ
 Quench Distance: 5 in. without & 15 in. with Arms.
 Residence Time: Regular (Anode No. G-1) without & Extended (G-4, G-8) with Tails.

mental parameters employed, the figure indicates that all the results can be correlated as a function of power input according only to the methane flow rates; thus, in the figure, three correlations can be found for each of the three levels of methane flow rates investigated. In general, the correlations are characterized by the presence of the rather narrow range of critical power input at each level of methane flow rates in which the % CaO conversion increases very rapidly with only slight increase of power input. Once over the critical power input region, the conversion attains more or less constant value and rises very slowly as the power input increases.

The existence of such correlations suggests that the single most important experimental parameter besides the power input is the gas flow rate. The scattering of the experimental data in the figure is relatively random and no systematic relations can be found for the other experimental parameters, at least within the ranges investigated. Rather, the relatively wide scattering of the data was mainly caused by the erratic power input, owing to arc instabilities inevitably encountered in many experiments.

The foregoing observations on the effect of the experimental parameters on the conversion of CaO to CaC₂ have very significant bearings on the mechanistic nature of the reaction of CaO with "nascent" carbonaceous species and are thus elaborated further in greater detail in the following.

Effect of Lime Feed Rates. In Figure 1.5 we see the

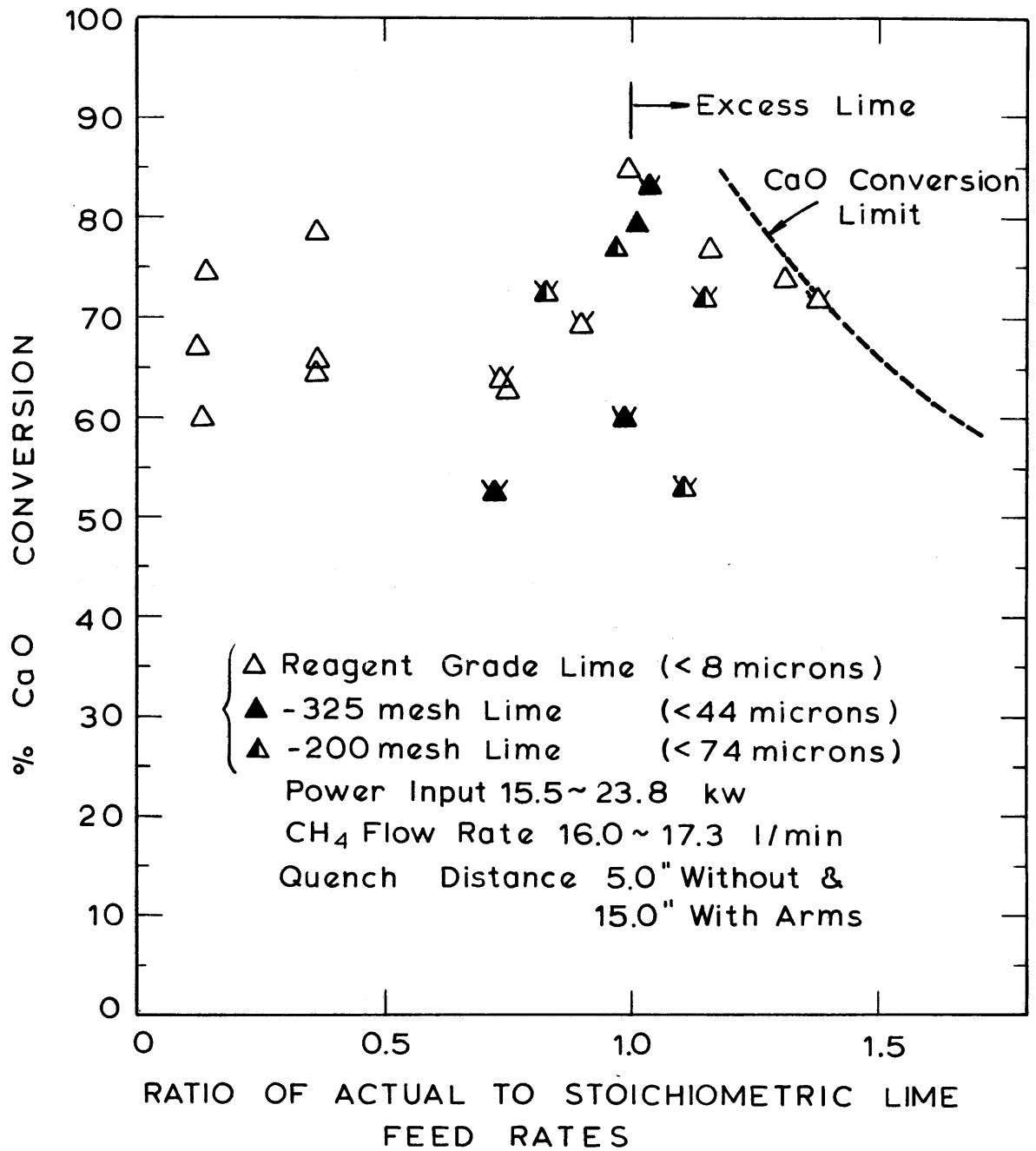


Fig. 1.5 CaO Conversion vs. Ratio of Actual to Stoichiometric Lime Feed Rates

effect of lime feed rates on the conversion of CaO to CaC₂ for methane flow rates in a range of 16.0-17.3 l/min with power inputs above 15.5 kw, thus above the threshold region in which it was seen that the conversion was sensitive to any slight change in power input. The figure shows that the conversion remained fairly constant around 70% even though the lime feed rates were varied from 0.12 to 1.38 times the stoichiometric feed rates based on the carbon content in the methane flows. The stoichiometric lime feed rates were in a range of 12.4-13.4 g/min for the methane flow rates in a range of 16.0-17.3 l/min.

The figure also indicates that the carbon in the methane can be reacted with CaO almost completely by feeding the latter in excess. The highest carbon conversion was obtained when the lime was fed 1.38 times the stoichiometric feed rate, which was 99.2% based on the methane flow alone and 95.1% inclusive of the carbon vaporized from the graphite electrodes.

Particle Size Effect. In order to delineate the effect of the particle sizes on the conversion of CaO to CaC₂, three particle sizes were used: -8 μ, -44 μ, and -74 μ. Both Figure 1.4 and Figure 1.5 indicate that the conversion was hardly affected by the lime particle sizes, although the -74 μ size fraction seemed to undergo slightly lower conversion than the other two. Nevertheless, the distinction is not very clear and thus it can be safely inferred that there was no particle size effect observed, at least with the par-

ticle sizes used in the experiments.

Effect of Quench Distances. In the present study the quench probe was set at either 5" or 15" from the anode nozzle exit. The quench probe often melted at the tip when it was placed at 1". As shown in both Figures 1.4 and 1.5, the effect of quench distance is not noticeable within the rather random scattering of the experimental data. This suggests that the solid product is thermally stable and little decomposition occurs during cooling. This is thermodynamically expected because the free energy of formation of CaC_2 is negative and thus thermodynamically stable relative to the elements from room temperature to its melting point at 2573°K. The free energy of formation is not known beyond the melting point, but extrapolation of the data indicates that it remains negative probably up to 3500°K.

Effect of Residence Time. The residence time of the reactants in the anode nozzle was normally in a range of 0.5-1.0 msec. In order to gain insight into the reaction mechanism, the residence time was sometimes increased by four- to slightly over thirteen-fold by using graphite anodes of different nozzle lengths and diameters. The various anodes are described and the schematic shown in Section 1.2.2.

Results from the runs with prolonged residence times are indicated in Figure 1.4 by the symbols affixed with the tails. In order to delineate the residence time effect clearly, the runs were intentionally made at the relatively

low conversion regions: e.g., if the reaction mechanism operative in and immediately beyond the arc zone was still effective over the entire length of the anode nozzle, then the conversion of CaO to CaC₂ would greatly increase with a several-fold increase in residence time. However, the results in general indicate that the conversion was not noticeably enhanced by the increased residence time. Specifically in each of the two groups marked I and II in the figure, in which the residence time of one run was increased by thirteen-fold over the other under otherwise similar reaction conditions, the conversion increased only by several percentage points despite the increased residence time by an order of magnitude.

Effects of Power Input and Methane Flow Rates: Specific Gas Energy. Thus far it has been shown that the conversion of CaO to CaC₂ was not affected by the variation in the experimental parameters such as lime feed rates, quench distance, residence time, and particle size, thus leaving the methane flow rate and the power input as the only two possible de facto experimental parameters affecting the overall reaction. The effect of the two parameters is presented in the following.

The data from Figure 1.4 are replotted in Figure 1.6 as a function of specific gas energy based on gross power inputs and methane flow rates. Also shown in the figure are the results of the ethylene series, which are discussed in the following section. The figure shows that the conversion

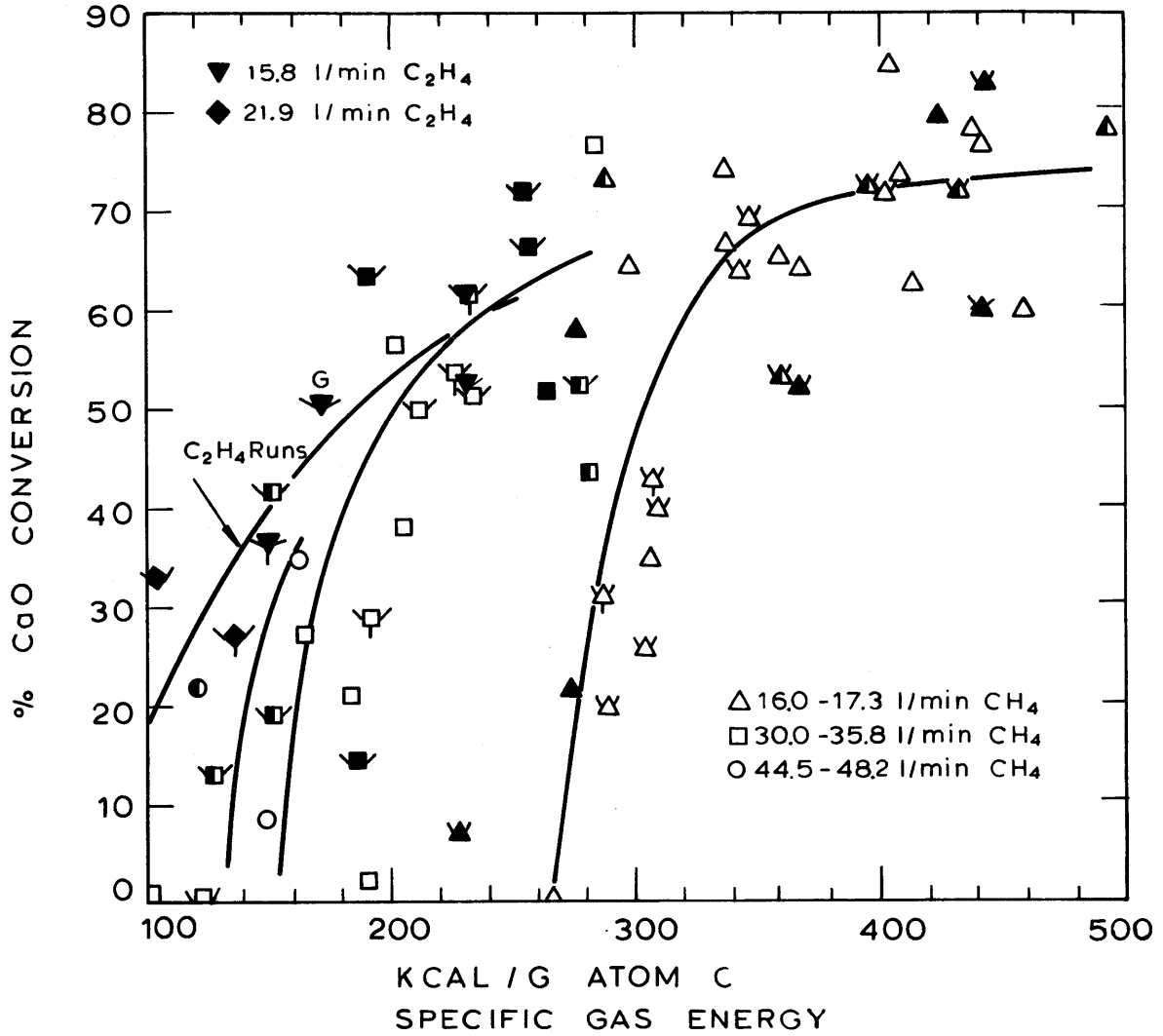


Fig. 1.6 CaO Conversion vs. Specific Gas Enthalpy; C₂H₄ Runs are shown together with CH₄ runs

Particle Size; △, □, ○, -8μ; ▲, ■, ●, -44μ; ▲, ■, ●, -74μ
 Quench Distance: 5 in. without & 15 in. with Arms.
 Residence Time: Regular (Anode No. G-1) without & Extended (G-4, G-8) with Tails.

of CaO to CaC₂ requires less specific gas energy at higher gas flow rates. The critical specific gas energies to effect the reaction seem to lie in a range of 280-310 kcal/g atom C in the case of 16.0-17.3 l/min CH₄, and in a range of 160-210 kcal/g atom C in the case of 30.0-35.8 l/min CH₄. Although sufficient data do not exist for the methane flow rates in a range of 44.5-48.2 l/min, the corresponding critical specific energy seems to lie in a range of 110-160 kcal/g atom C.

Gaseous Product Composition. The interdynamic relationship between the gaseous hydrocarbon products and the calcium carbide formation has been studied by collecting the gas products and analyzing them on a flame ionization detector. In most cases, the gaseous hydrocarbons detected above 0.01% in concentration were methane, ethylene, and acetylene, with occasional appearance of ethane at very low power input (e.g. 10 kw or less).

The methane concentration was usually lower than 1% when the conversion of CaO to CaC₂ was higher than 60%. Conversely, the CaO conversion was usually lower than 40% when the methane concentration was higher than 3%. The interdynamic relationship between the methane concentration and the % CaO conversion is shown in Figure 1.7, which contains all results from the experiments with 5" quench distance.

The ethylene concentration was typically below 0.1% and varied in similar fashion to the acetylene concentration,

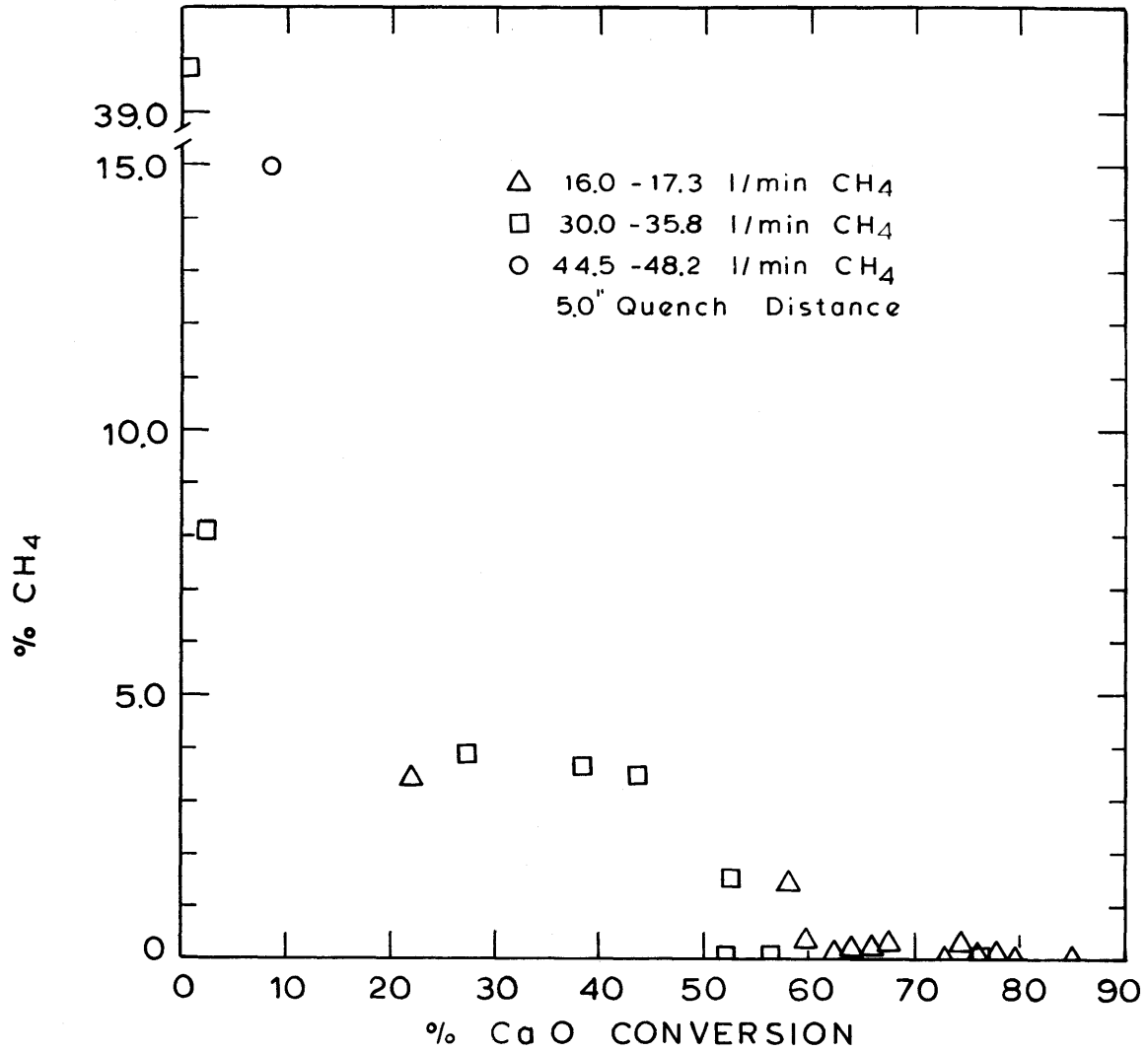


Fig. 1.7 CH₄ Concentration vs. CaO Conversion in CH₄ Series Runs

which is described below.

Variation of the acetylene concentration with lime feed rates is very remarkable and is shown in Figure 1.8. It contains all results from the experiments of 16.0-17.3 l/min CH_4 , 5" quench distance, and reagent grade CaO . Power inputs were beyond the critical region and in a range of 15.5-21.8 kw, in which it was previously shown that the % CaO conversion remained more or less constant around the 70% conversion level. Also included in the figure is the percentage of carbon in the methane reacted with CaO to produce CaC_2 and CO , which is calculated based on the % CaO conversion and the known lime feed rate. The figure thus prepared shows that the reduction of acetylene concentration was accelerated while the formation of CaC_2 and CO increased only linearly as the lime feed rate was raised.

1.3.2. Results of Ethylene Series Runs

Results of the ethylene series runs are plotted in Figure 1.6 for % CaO conversion vs. specific gas energy together with the results of the methane series runs. Of the six runs, only one (marked with G in the figure) was made with a graphite anode and the other five made with water-cooled copper anodes. In order to increase residence time, the water-cooled copper anode was sometimes affixed with a graphite cylinder of 1" i.d. x 3" o.d. and 5" long. In all cases, only -325 mesh lime particle size was used. The gas flow rate was either 15.8 l/min or 21.9 l/min, and lime feed

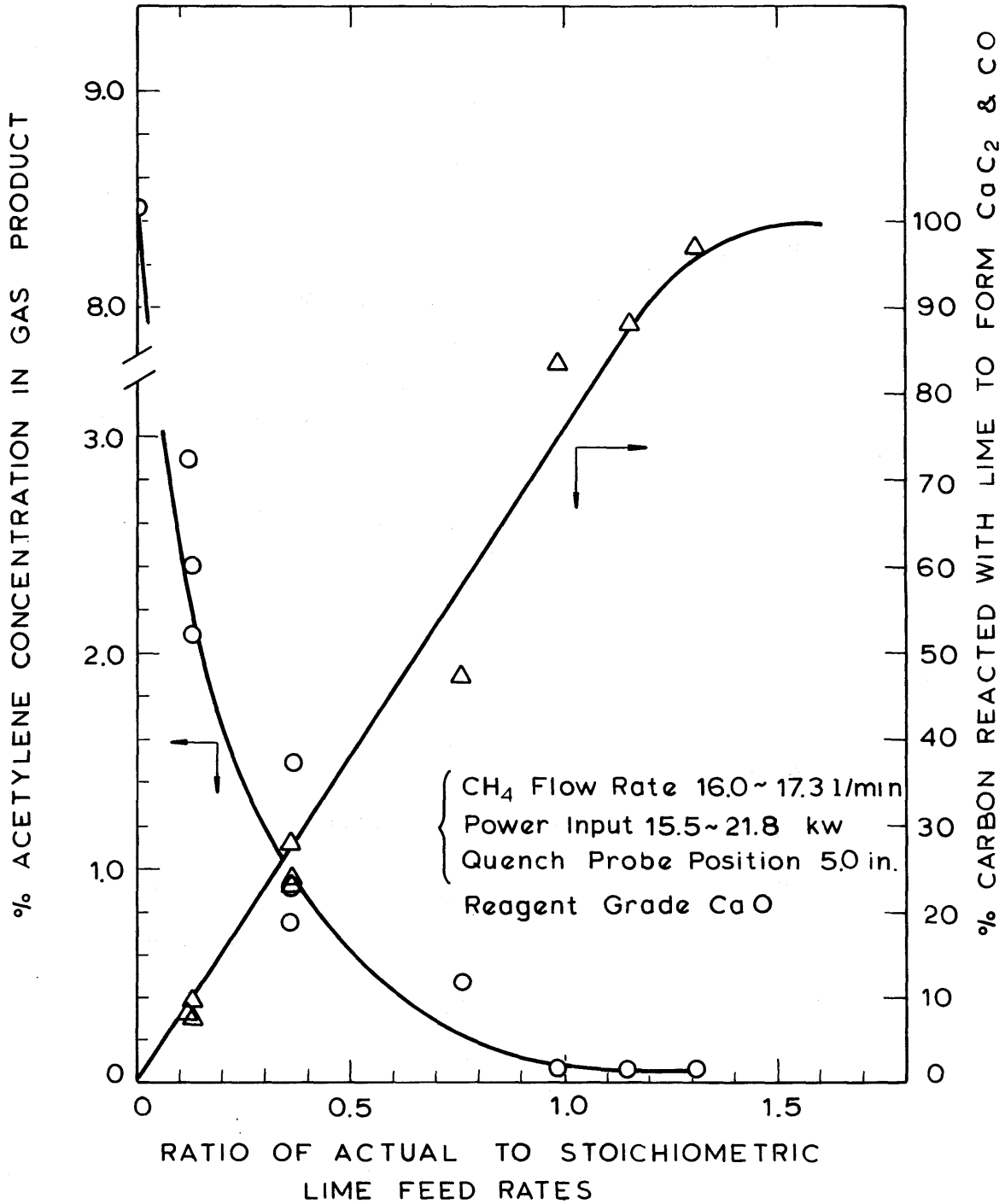


Fig. 1.8 Variation of C₂H₂ Concentration in Gas Product with Lime Feed Rates

rates were in a range of 0.95 to 1.20 times the stoichiometric feed rates. The quench probe was always positioned 15" from the anode nozzle.

As indicated in Figure 1.6, the % conversion of lime to CaC_2 increased with an increase in specific gas enthalpy as in the methane series runs, with a slight increase in energy efficiency at equivalent gas flow rates based on the carbon in the feed gas. Again, there was no noticeable effect of extended residence time on the CaO conversion as in the methane series runs.

1.3.3. Results of Coal Series Runs

1.3.3.1. Operational Characteristics

The greatest problem encountered in the coal series runs when the graphite anode was used was the fusion of the feed particles in the pre-interelectrode region of the anode before reaching the arc zone, resulting in substantial particle holdup in the region and in some instances even in the feeding line. Therefore, the powder feed rate reported in the study could be an overestimation of the true feed rate for several occasions; but there was no effective means of controlling this. Nevertheless, in order to ensure consistency of powder feeding, the feeding line was dismantled for visual inspection after each run, and the run was voided if there was any excessive powder holdup in the line.

In order to eliminate the hot surface on which the particles fused, a water-cooled copper anode was constructed

and operated with some degree of success for a number of coal runs. The details of the copper anode are presented in Section 1.2.2. Although the water-cooled copper anode completely eliminated the solid build-up in the pre-inter-electrode region of the anode, it posed great experimental difficulties by burning out too frequently. Therefore only five runs were made with the latter.

1.3.3.2. Experimental Results

In the coal series runs the powder feed was an intimate mixture of -170, +325 mesh coal and either a reagent grade lime of -8μ particle size or a calcine of -325 mesh (-44μ) limestone. In most experiments the powder feed contained 47.0 wt.% excess lime over the stoichiometric ratio, thus making 68.0% as the possible maximum conversion of CaO to CaC_2 ; this was in part to determine the maximum percentage of the carbon in the coal that could react with CaO to produce CaC_2 and CO . Only in three experiments was a mixture with 5.8% excess carbon by weight used. The powder feed rate ranged from 15.5 g/min to 51.0 g/min and the hydrogen flow rate was in a range of 14.6-48.4 l/min. The H/C ratio in the feed was in a range of 2.7 to 8.0 as calculated based on the hydrogen flow rate and both the hydrogen and the carbon contents of the coal. The quench distance was either 5" or 15".

All the experimental results of the coal series runs are presented in Figure 1.9 for the % conversion of CaO to

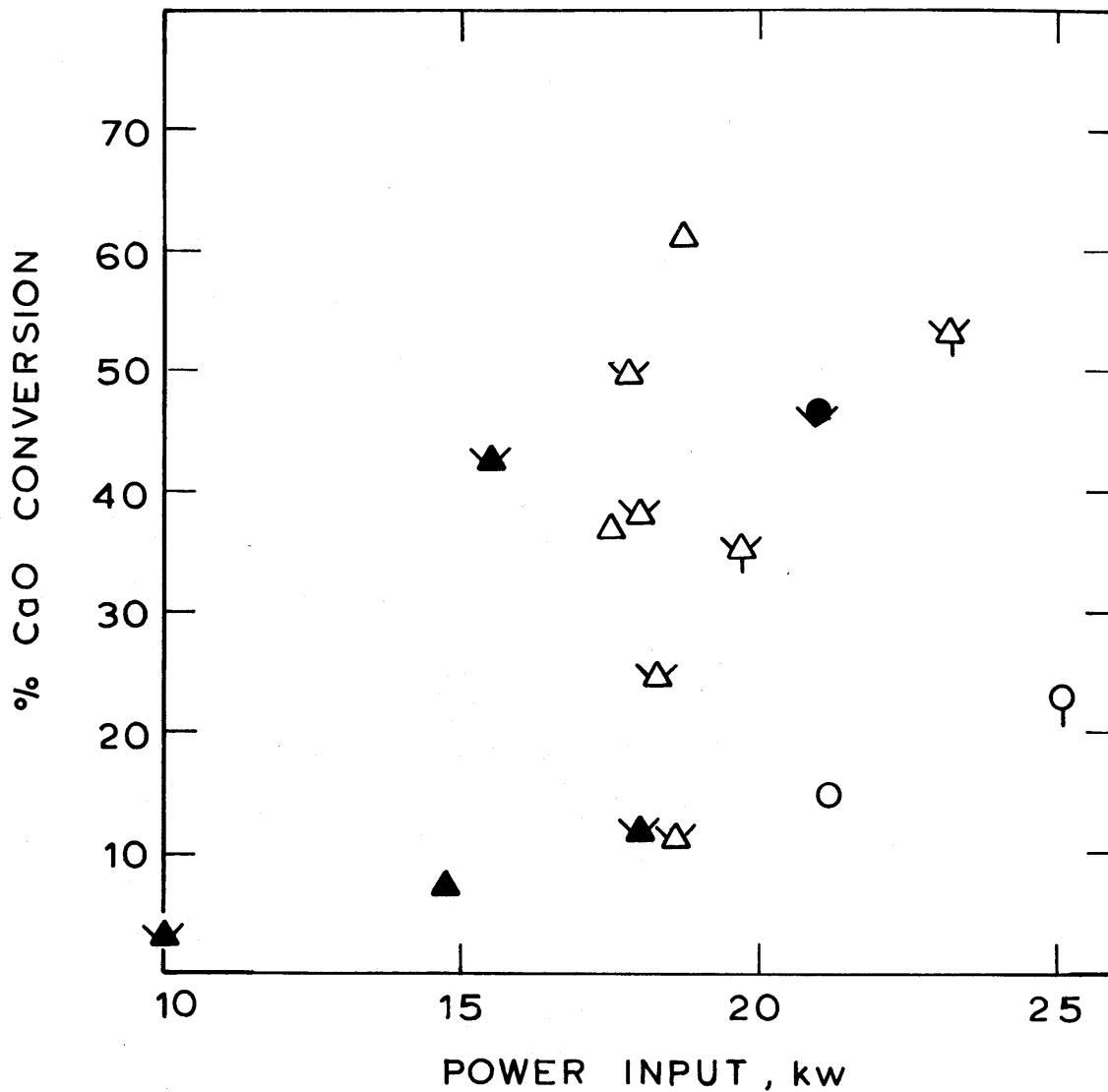


Fig. 1.9 CaO Conversion vs. Power Input, Coal Series Runs

Excess Lime (Molar CaO:C = 1.47:3.00); \triangle , \blacktriangle
Excess Carbon (Molar CaO:C = 1.00:3.06); \circ , \bullet

Graphite Anode; \triangle , \circ
Copper Anode; \blacktriangle , \bullet

Quench Distance; 5" without & 15" with Arms.
Residence Time; Regular without & Extended (G-4) with Tails.

CaC_2 as a function of power input. It fails to clearly show the effect of power on the CaO conversion, perhaps owing to the different experimental conditions employed for each data point. In this study no systematic attempt was made to delineate the various effects of hydrogen flow rate, powder feed rate, and coal-lime mixing ratio, as the study was exploratory in nature and also because it was so difficult to overcome the experimental difficulties encountered in many coal runs.

Nevertheless, the effects of the hydrogen flow rate and the powder feed rate combined with power input can be best seen in Figures 1.10a and 1.10b, which are plotted for % conversion vs. either gross energy input per unit volume of H_2 or gross energy input per gram atom of carbon in the solid feed. Despite the relatively wide scattering of the data, both figures suggest that the CaO conversion can be increased by increasing, as expected, either the specific gas enthalpy or the specific carbon enthalpy, or both. The highest % CaO conversion obtained in the study was 61.3%, whereas the possible maximum conversion in the particular run was 68.0% as the feed contained excess lime; therefore, in the same run it can be seen that 90.1% of the carbon in the coal reacted with CaO to form CaC_2 and CO. Since the carbon should have volatilized before reacting with the lime, it means that at least 90.1% of the carbon in the coal should have left the coal through volatilization. In most runs the hydrocarbons detected in the gas product used to be less than

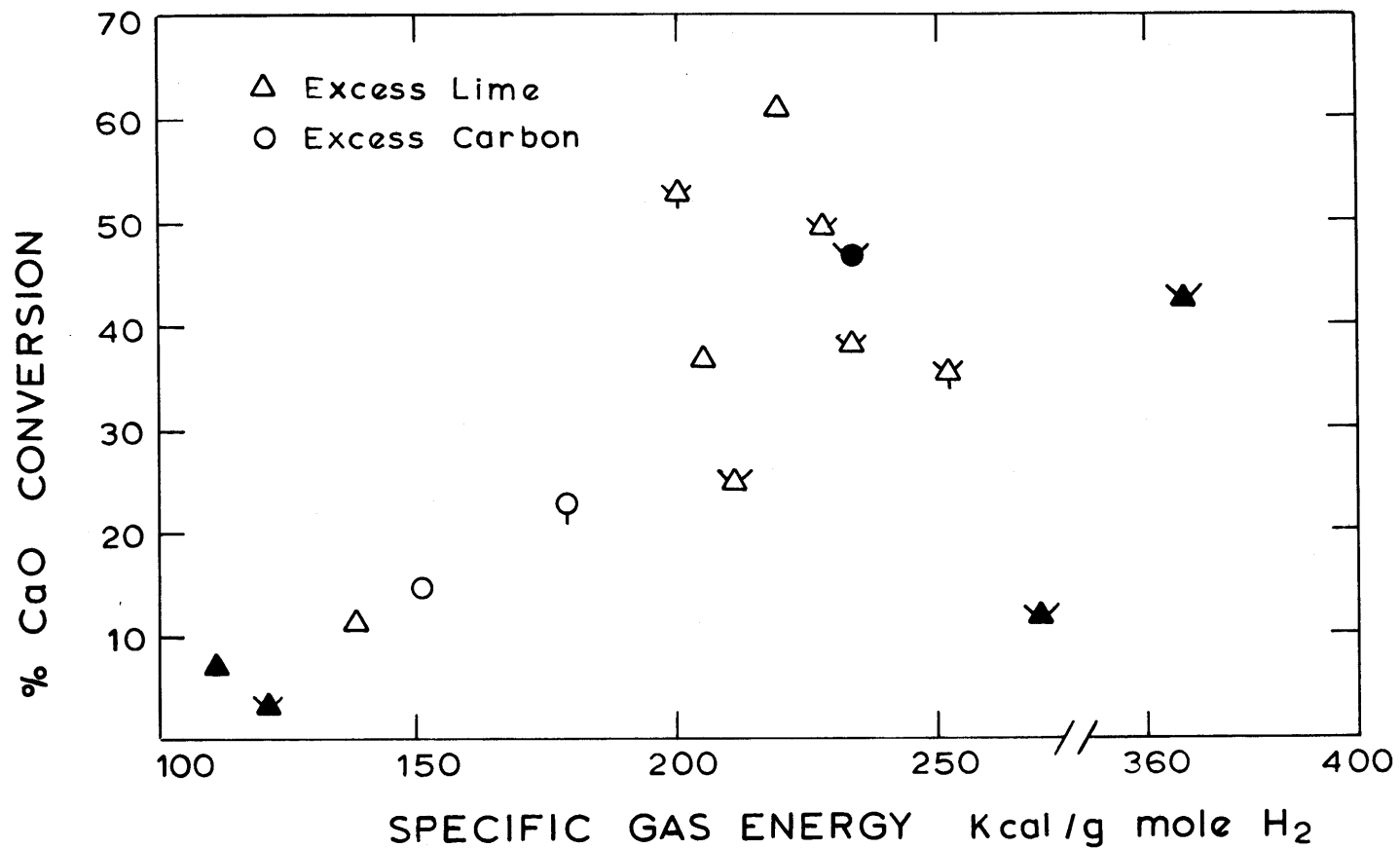


Fig. 1.10a CaO Conversion as a Function of Energy Input per G Mole H₂

Excess Lime (Molar CaO:C = 1.47:3.00); \triangle , \blacktriangle
 Excess Carbon (Molar CaO:C = 1.00:3.06); \circ , \bullet

Graphite Anode; \triangle , \circ
 Copper Anode; \blacktriangle , \bullet

Quench Distance; 5" without & 15" with Arms.
 Residence Time; Regular without & Extended (G-4) with Tails.

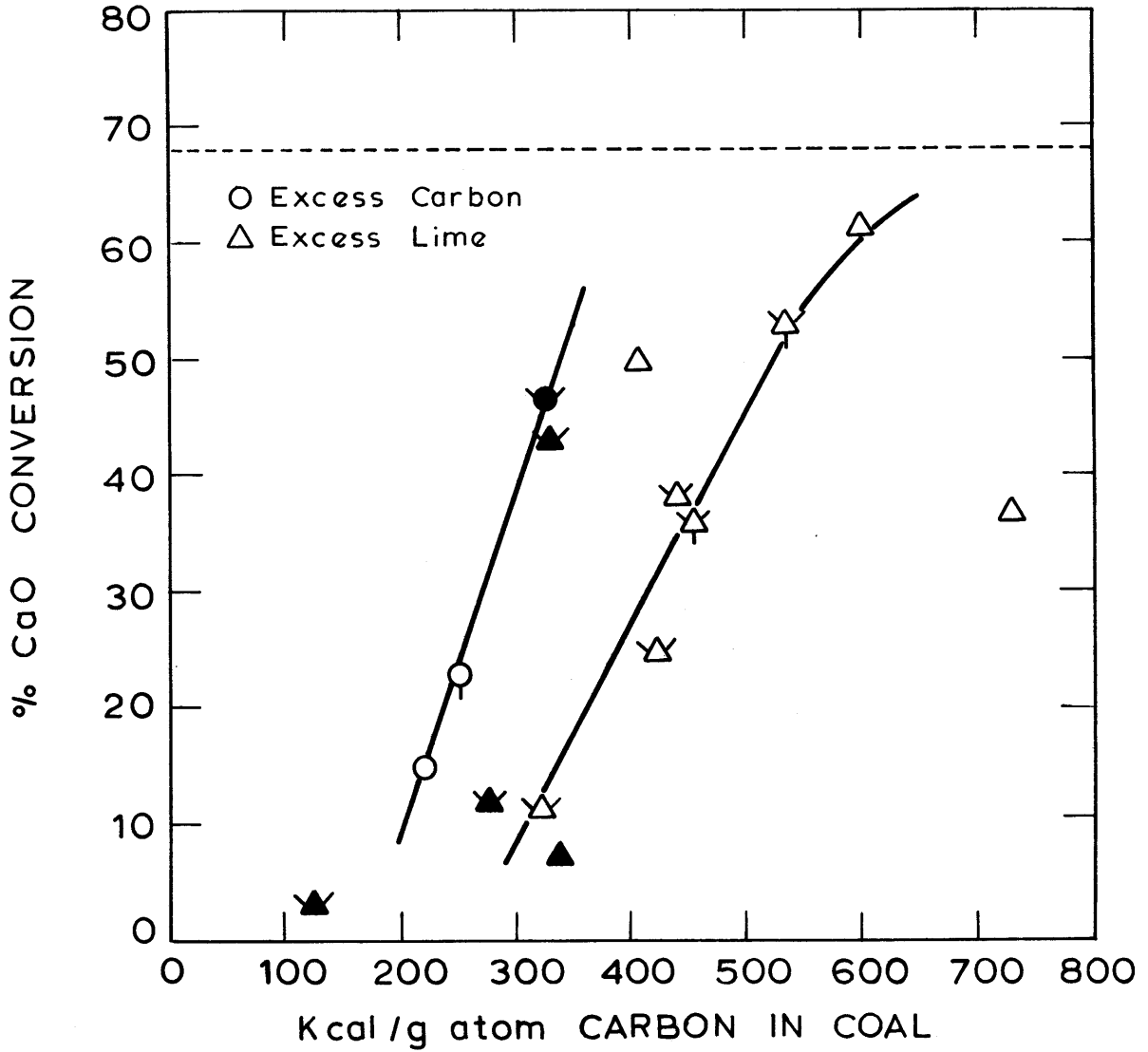


Fig. 1.10b CaO Conversion vs. Energy per G Atom C in Coal

Excess Lime (Molar CaO:C = 1.47:3.00); △, ▲
Excess Carbon (Molar CaO:C = 1.00:3.06); ○, ●

Graphite Anode; △, ○
Copper Anode; ▲, ●

Quench Distance; 5" without & 15" with Arms.
Residence Time; Regular without & Extended (G-4) with Tails.

0.5% in total concentration.

The effect of residence time was studied in three runs by using a graphite anode with extended anode nozzle (Anode No. G-4). Although the G-4 anode provided slightly over six times longer residence time than the regular anode (i.e. G-1), it seemed to show little effect on the conversion of CaO to CaC₂. Interestingly, in a few attempted but futile runs of the longer graphite anode and the water-cooled copper anode affixed with 5" long graphite cylinder or 1" i.d. x 3" o.d., the solid product completely melted during flight and condensed as large blobs on the top of the sample probe, thus preventing sample collection. The extensive melting was prevented to some extent by increasing either hydrogen flow rate or powder feed rate or both at a given power input. Such an extensive melting was not observed in the runs of the regular graphite anode (G-1), in which the solid product was produced as agglomerates of fine particles.

The energy efficiency, for which the reactor was not designed, was somewhat lower than either CH₄ or C₂H₄ runs, the lowest being 32.1 kwhr/lb C₂H₂.

1.4. Product Morphology

The external appearances of the reagent grade lime, precipitated CaCO₃, and both the -200 mesh and -325 mesh limestones and their calcined samples were examined under a scanning electron microscope. The SEM study did not show any consistent or significant differences between the two

grades of either the limestones or their calcined materials.

The reagent grade lime (Figure 1.11) typically showed the rhombic shape of the precipitated CaCO_3 but the edges were somewhat rounded. The lime particle size was mainly in a range of 0.5 to 3 μ but particles as large as 8 μ were occasionally observed. Examination at higher magnification (Figure 1.12) revealed that the lime was non-porous and resembled the precipitated CaCO_3 in texture.

The natural calcite had a rhombohedral shape with smooth surfaces (Figures 1.13 and 1.14). Few cleavage steps could be observed on the surfaces of the rhombs, which the SEM revealed as very coarsely grained and essentially free of intracrystalline voids.

Calcines of the natural calcite (Figures 1.15 and 1.16) retained the rhombic shape and size of their predecessor; however, unlike the calcite, most of the lime particles consisted of rounded grains that were partly fused together and as a result showed spongy texture and high porosity. The grains of the lime particles were mainly in the range of 0.5 to 1.0 μ in diameter.

Solid products at various stages of conversion from the methane- as well as the coal-series runs were microscopically examined in order to gain insight into the conversion process. Figures 1.17 through 1.23 show the electron micrographs of the products from the methane series runs with the conversions ranging from 7.0% to 79.5%. Remarkably, all the products were seen as agglomerates of extremely fine

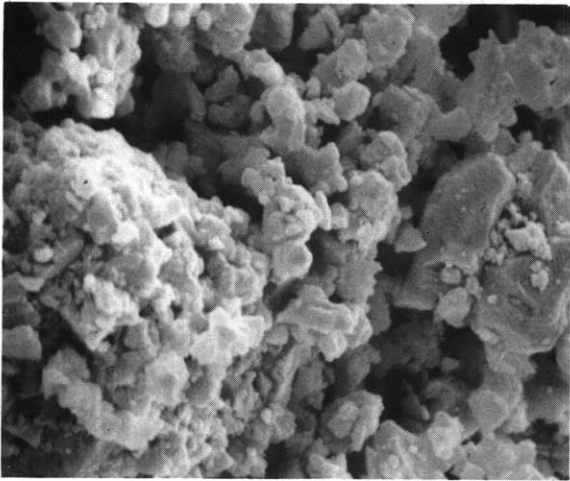


Fig. 1.11 Reagent grade CaO; -8μ particles; SEM, x2000

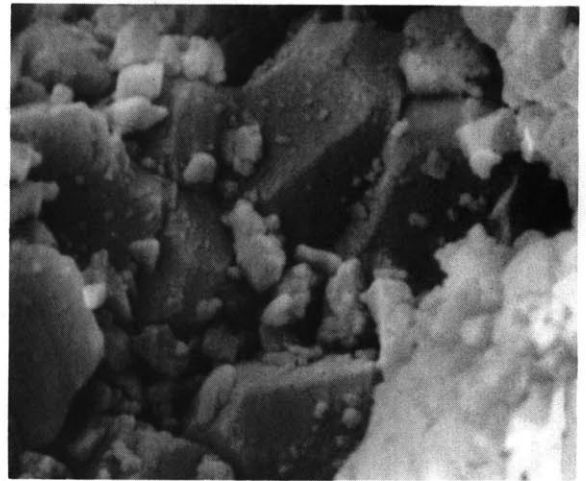


Fig. 1.12 Reagent grade lime at higher magnification; SEM, x5100

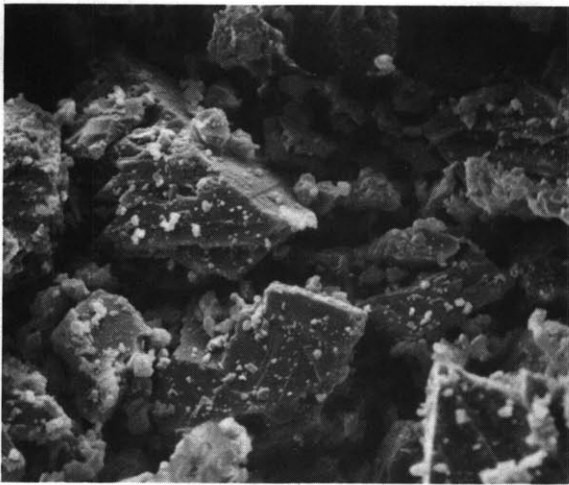


Fig. 1.13 Natural calcite; -325 mesh particles; SEM, x950

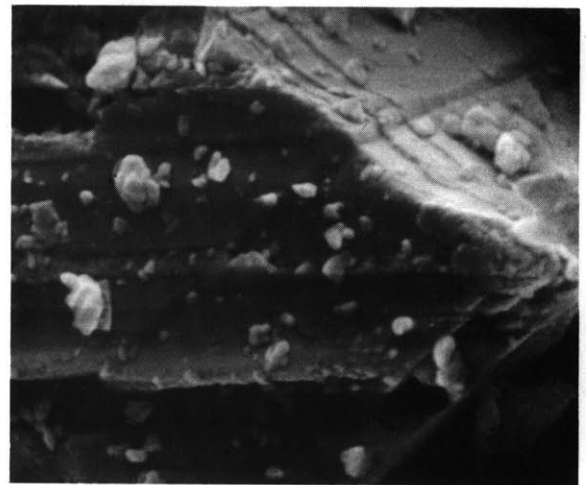


Fig. 1.14 Close-up of specimen on the left; SEM, x4800

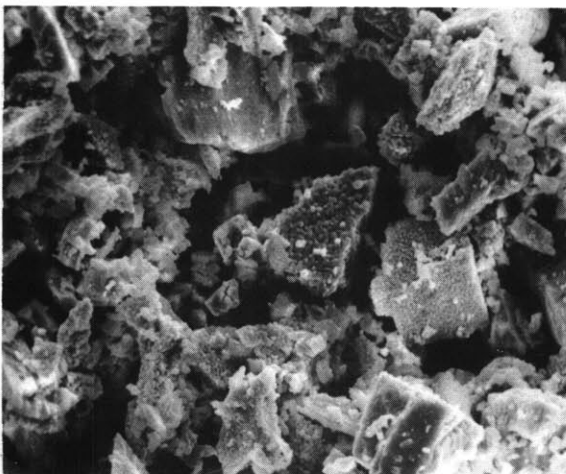


Fig. 1.15 Calcine of -325 mesh size calcite; shows spongy texture; SEM, x530

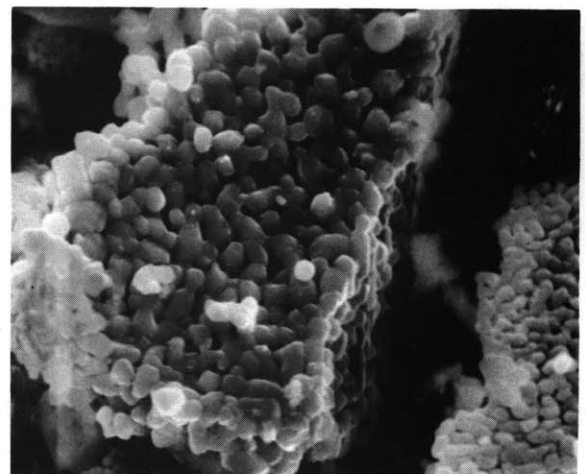


Fig. 1.16 Close-up of specimen on the left; SEM, x2200

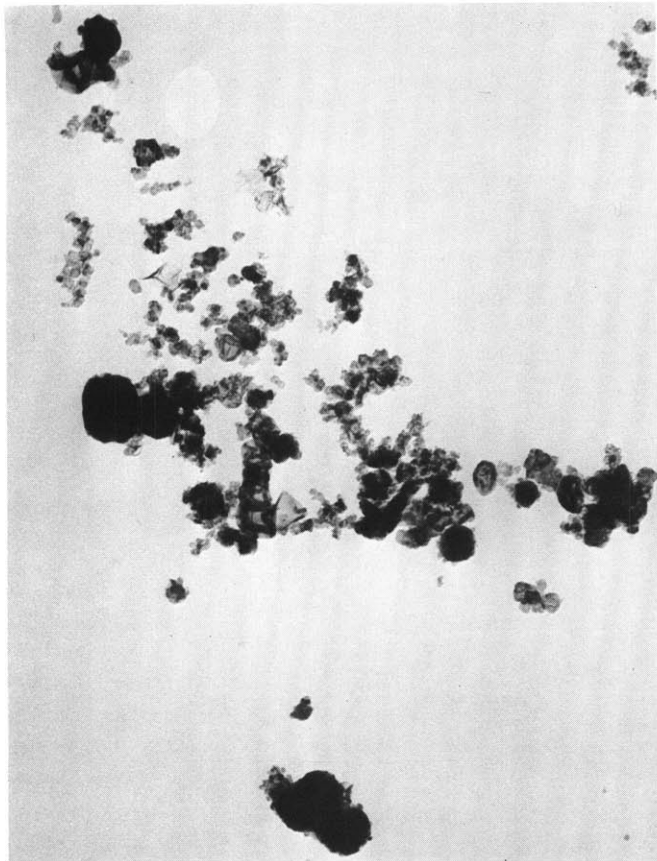


Fig. 1.17 7.0% conversion, run no. M-79; -325 mesh calcine; x33000

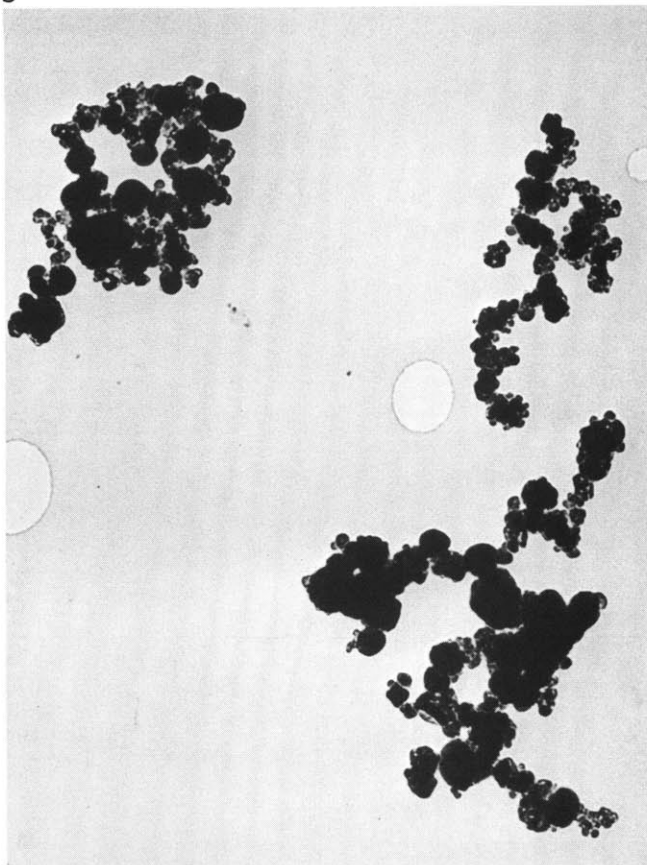


Fig. 1.18 21.7% conversion, run no. M-75; -325 mesh calcine; x33000

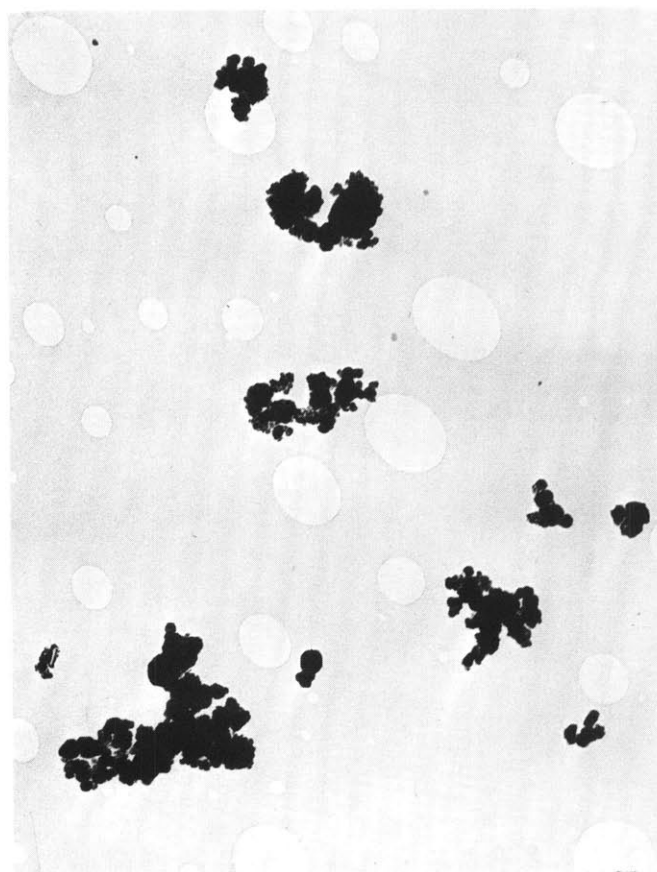


Fig. 1.19 35.0% conversion, run no. M-64; reagent grade lime; x33000

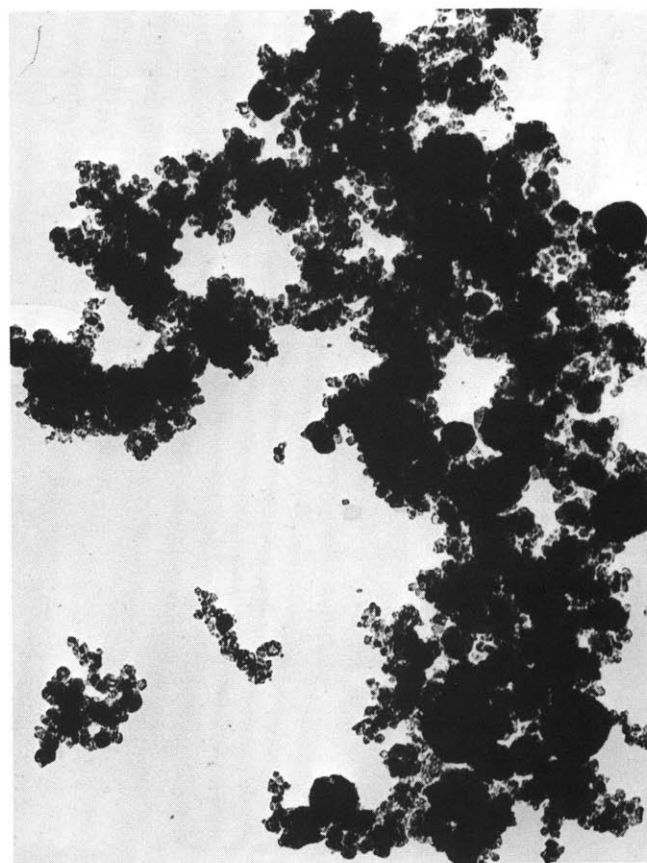


Fig. 1.20 58.3% conversion, run no. M-74; -325 mesh calcine; x33000

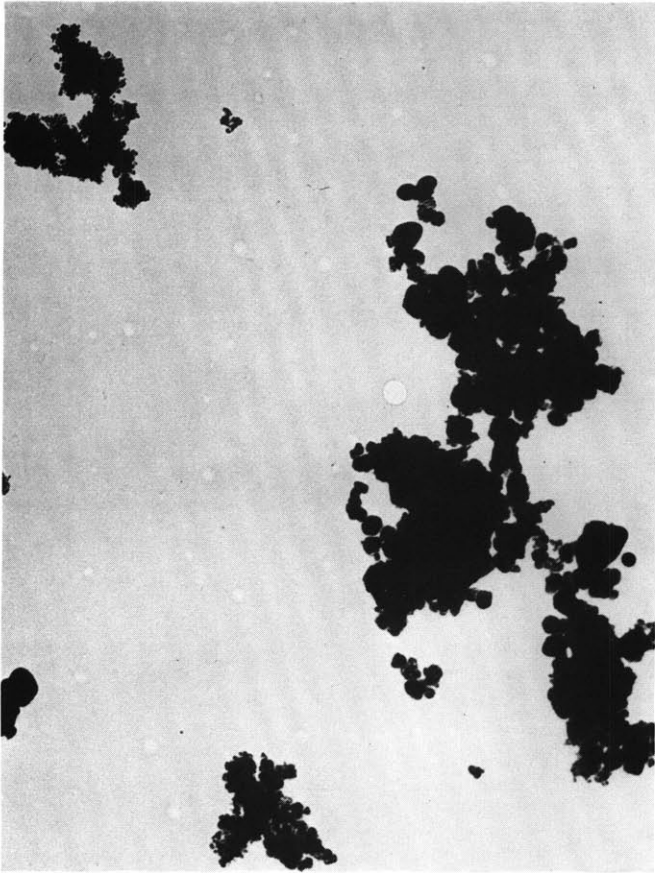


Fig. 1.21 64.0% conversion, run no. M-70; reagent grade lime; x33000

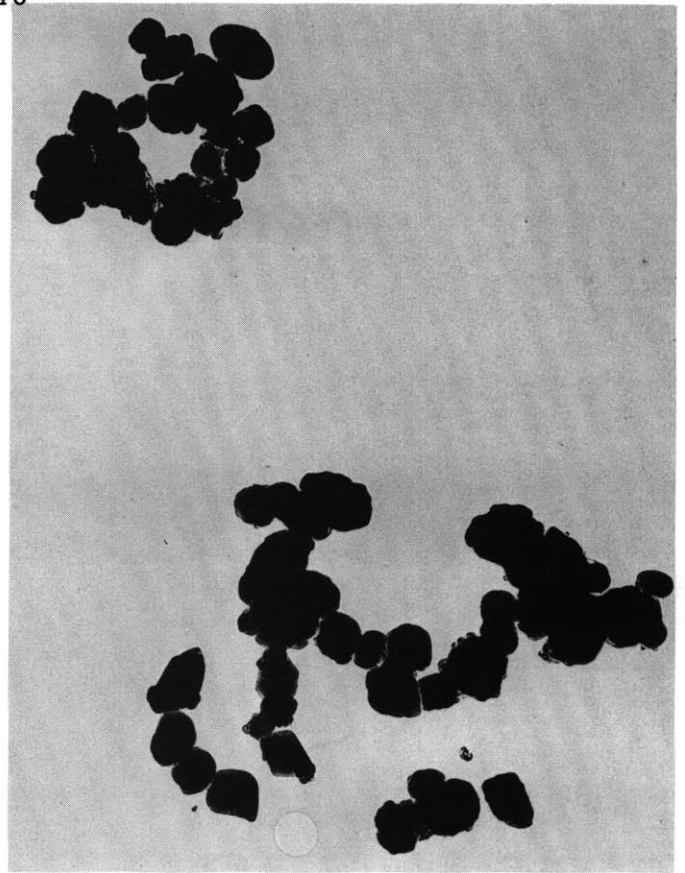


Fig. 1.22 77.0% conversion, run no. M-76; -200 mesh calcine; x33000

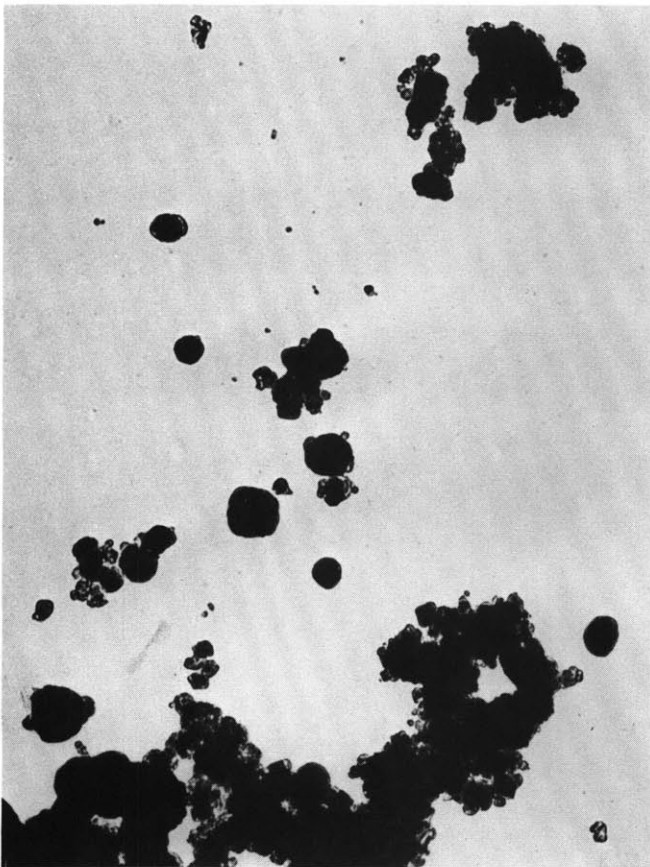


Fig. 1.23 79.5% conversion, run no. M-73; -325 mesh calcine; x33000

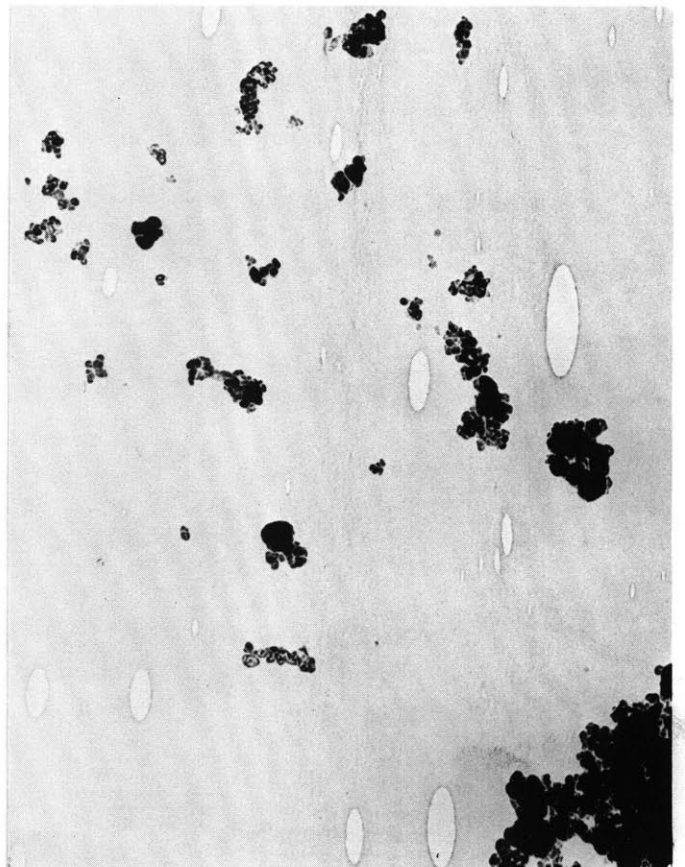


Fig. 1.24 Methane black, run no. SM-1; no lime feeding; x33000

particles which were mostly in the range of 200 \AA to 0.3μ , regardless of the degree of conversion and the original lime particle size. The constituent particles were of spherical shapes in all cases except at 7.0% conversion, in which angular granules on the order of 0.1μ in size were occasionally observed among the predominantly spherical particles of diameters from about 200 \AA to 0.3μ . It is very likely that the angular granules may have formed by mechanical breaking up of the original lime particles.

Pyrolysis of the methane used in the study yielded chain-like agglomerates of very fine carbon spheres ranging from 200 \AA to 400 \AA in diameter (Figure 1.24). Interestingly, most carbide products examined under the electron microscope were relatively devoid of the particles in the particle size range even when there should have existed copious amounts of free carbons which had failed to react with CaO to form CaC_2 and CO; and even if there were, the individual particles did not agglomerate together but clustered around the conspicuously larger particles. This indicates that methane decomposes heterogeneously in the presence of lime in the reactor.

As seen by the electron microscope, the products of the coal series runs were also agglomerates of fine spherical particles, as in the methane series runs (Figures 1.25 through 1.28). However, in the coal series runs the particle size distributions were much broader, and particles on the order of a micron or larger were often seen along with the

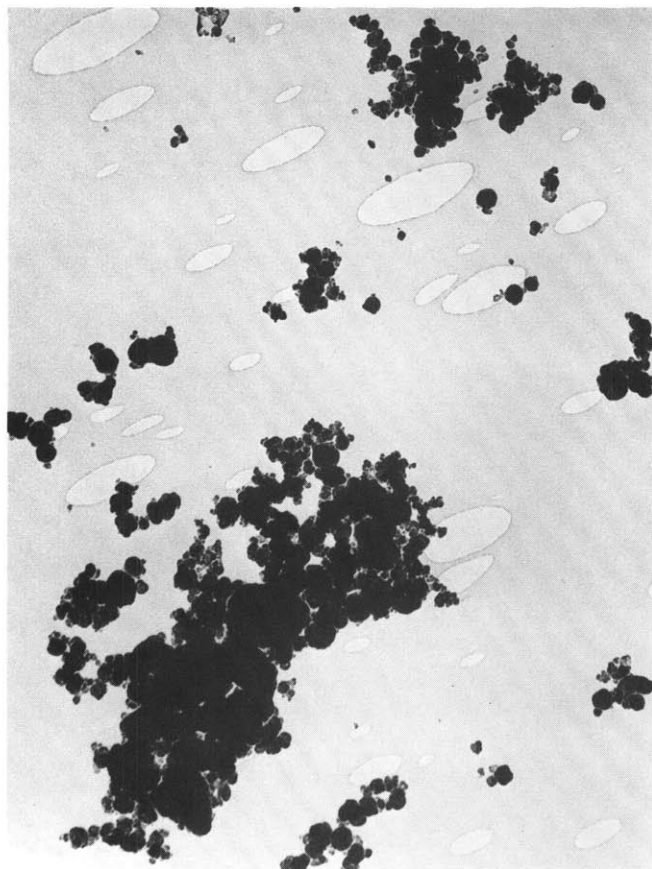


Fig. 1.25 Coal series run #C-13, 22.9% conversion; reag. gr. lime; sample from reactor bottom; x33000

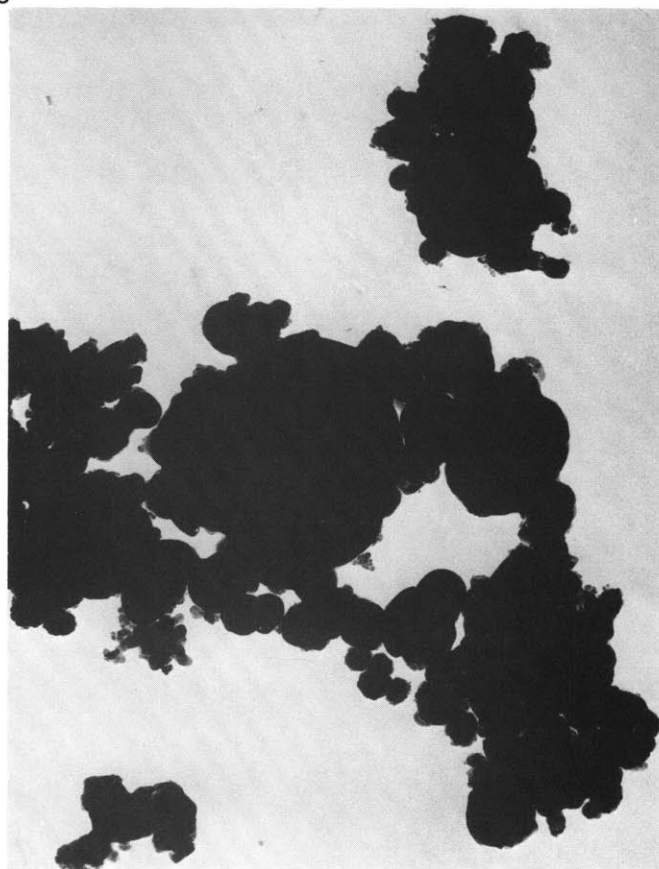


Fig. 1.26 Coal series run #C-6, 38.2% conversion; reag. gr. lime; sample from reactor bottom; x33000

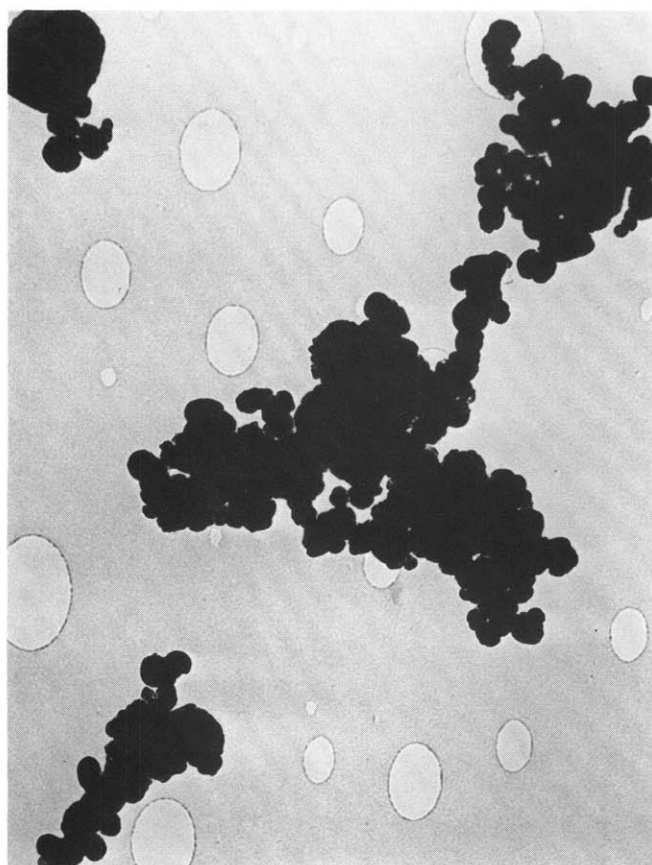


Fig. 1.27 Coal series run #C-8, 49.8% conversion; reag. gr. lime; sample from quench probe; x33000

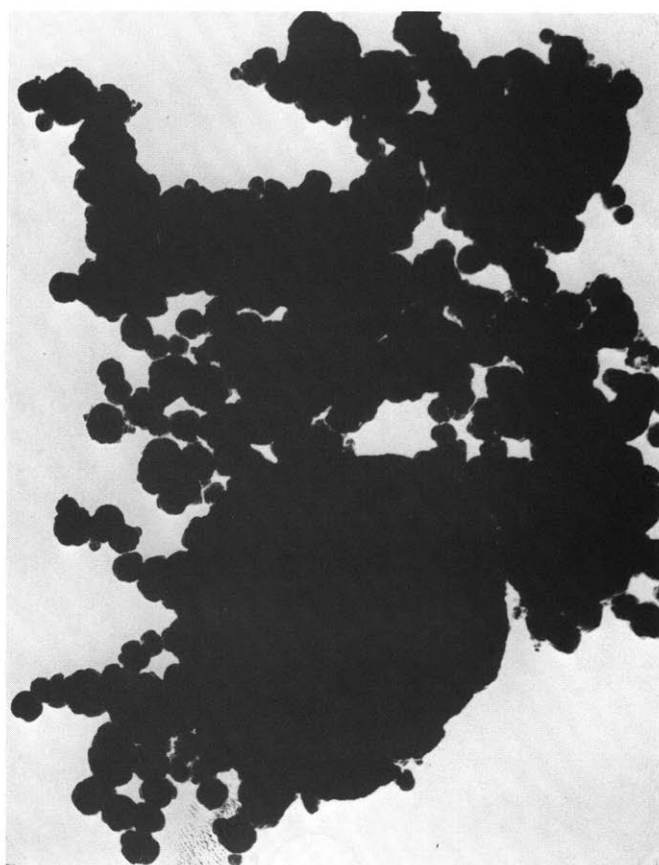


Fig. 1.28 Coal series run #C-10, 53.0% conversion; reag. gr. lime; sample from quench probe; x33000

particles in sizes comparable to those from the methane series runs. It is postulated that the particles larger than 0.3μ in diameter are mostly of coal char or ashes in origin.

1.5. Discussion of Results

1.5.1. Methane Series Runs

Needless to say, the formation of CaC_2 from the reaction of CaO with methane in the present reaction scheme is an extremely complicated physico-chemical phenomenon that involves the problems of chemical kinetics and heat and mass transfer in and between the gas and solid phases. Nevertheless, a certain generalization can be made regarding the mechanistic process of the overall reaction in that the electric energy is dissipated through the electric arc discharge mainly into the gas phase to almost instantaneously heat the methane to a high temperature, which then decomposes to produce an "outburst" of atoms and free radicals of carbon and hydrogen; these high enthalpy but thermally unstable species then diffuse to the particles to form more stable species by recombination or decomposition reactions or to directly react with CaO to participate in the reaction of CaC_2 formation. Such chemical reactions on the particle surfaces can greatly enhance heat and mass transfer between the gas and solid phases as the diffusing atoms and free radicals are consumed away at the particle surfaces and thus promote the overall chemical reaction as observed in the present study. There-

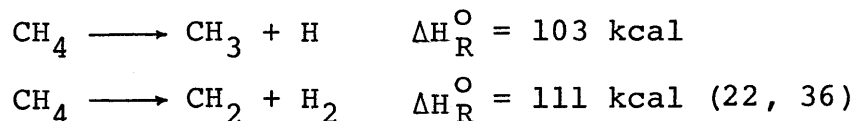
fore, according to the simplified mechanistic view of the overall process, this section is divided into: (1) decomposition of methane; (2) heat and mass transfer between gas and particles; and (3) formation of CaC_2 .

1.5.1.1. Decomposition of Methane

As discussed in Section 1.3.2., the conversion of CaO to CaC_2 in the present reaction scheme is characterized by the presence of a rather narrow range of critical specific gas energy for each of the three levels of methane flow rates investigated. The effect of increasing the gas flow rate is to diminish the critical specific energy, thus resulting in an increase in the overall energy efficiency of the reactor. For a methane flow in the range of 44.5-48.2 l/min, the specific gas energy seems to lie in the range of 110-160 kcal/g atom C.

The presence of the critical specific gas energy suggests that the initiation step of the overall reaction is an "outburst" of atoms and free radicals of carbon and hydrogen from the decomposition of methane.

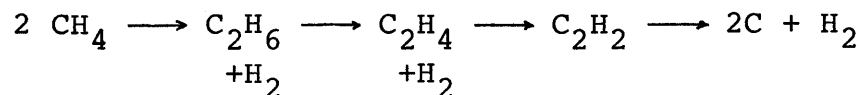
The initiation step of methane decomposition is generally believed to involve either or both of the following two reactions:



Although the first reaction is more favored now as the initi-

ation step (22), the second reaction may be also important, especially at high temperature.

The overall methane decomposition is generally accepted as a first order reaction which leads to formation of acetylene and of ultimate products by following a path (42, 51):



At temperatures above about 1500°K, the overall reaction is very rapid. In the reaction path, the acetylene selectivity decreases with increasing pressure because the decomposition of acetylene is a bimolecular process (8, 51), whereas its formation from methane is essentially unimolecular. Chen, Back and Back (22) have calculated the overall activation energy for the decomposition of methane in the pressure-independent region as 107.6 kcal/g mole, assuming that the initiation step is the formation of CH₃ and H and showed that most experimental values previously reported by other investigators, which ranged from 83 kcal to 103 kcal (42), were lower than the calculated value as the initial dissociation was in its pressure-dependent region.

If the reaction mixture is allowed to reach thermodynamic equilibrium at temperatures below about 2500°K, it will of course almost completely decompose to C and H₂; however, from about 2500°K acetylene and hydrocarbon radicals begin to exist in thermodynamic equilibrium in measurable amounts.

Figure 1.29 (16) shows the equilibrium composition of the carbon-hydrogen system in the heterogeneous region, i.e., solid carbon always present in the system. It was calculated by the method of Bauer and Duff (15). The gas temperature at the anode nozzle exit at a given specific gas energy can be estimated based on the equilibrium diagram, if one assumes that the carbon-hydrogen mixture fed at room temperature reaches thermodynamic equilibrium before reaching the nozzle exit. This is done for CH_3 , C_2H_4 , and $\text{C}_s\text{-H}_2$ mixtures at various C/H ratios in the heterogeneous region and shown in Figure 1.30.

With CH_4 as the carbon source, the formation of CaC_2 in the present reaction scheme apparently required an energy input at a minimum on the order of the activation energy for the decomposition of methane. The corresponding gas temperature is about 3000°K . In the present experiments, the specific gas energies based on gross power input, ranged from about 100 kcal to about 550 kcal/g atom C, and hence the corresponding gas temperatures may have been higher than 3000°K but lower than 4000°K . In this temperature range, the gas temperature of a carbon-hydrogen system of $\text{H/C} = 4$ is relatively insensitive to variation in power input because of the extensive formation of free radicals and hydrogen and gaseous carbon atoms.

1.5.1.2. Heat and Mass Transfer Between Gas and Particles

The H atoms and hydrocarbon radicals produced from the

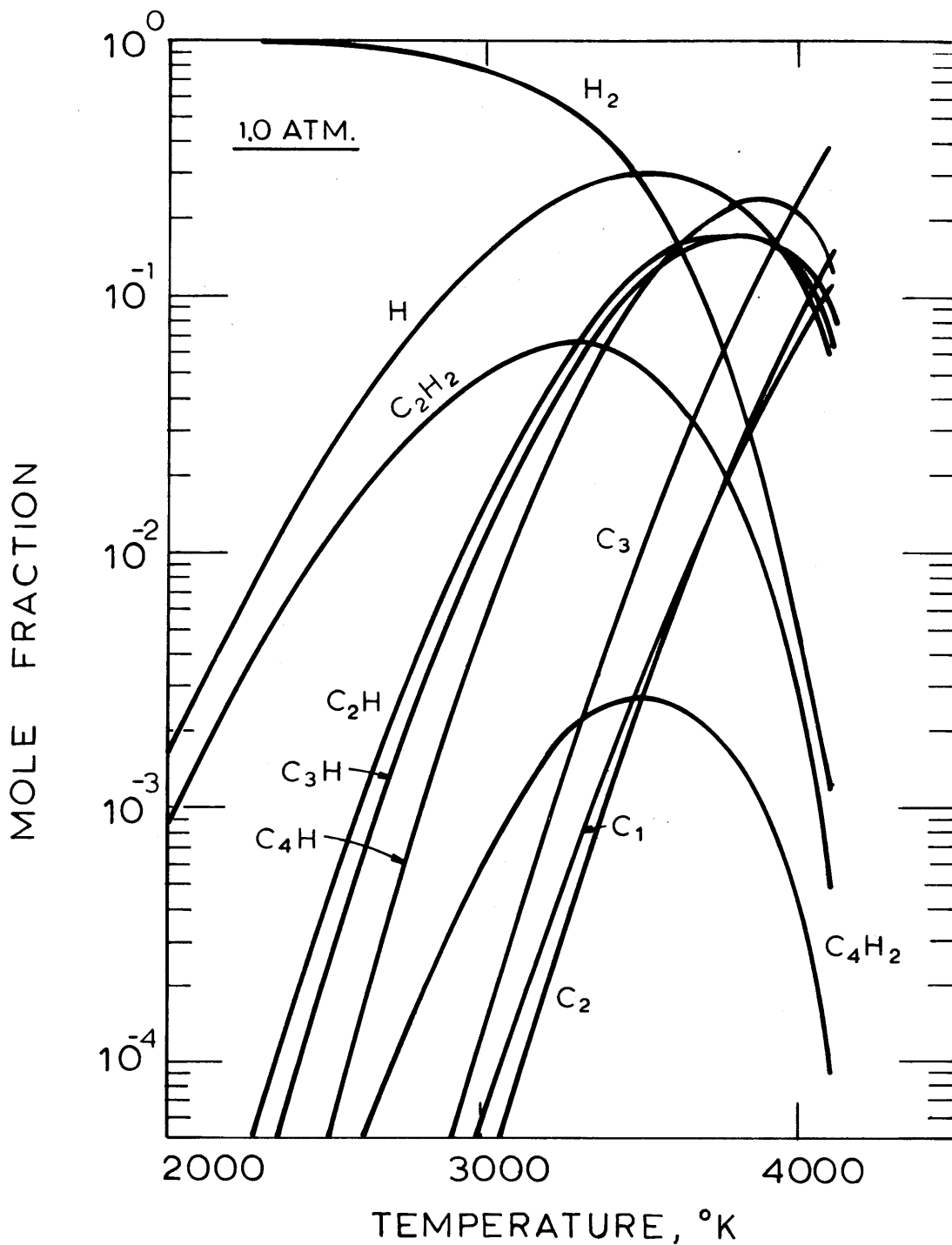


Fig. 1.29 Equilibrium Composition for the Carbon-Hydrogen System in the Heterogeneous Region

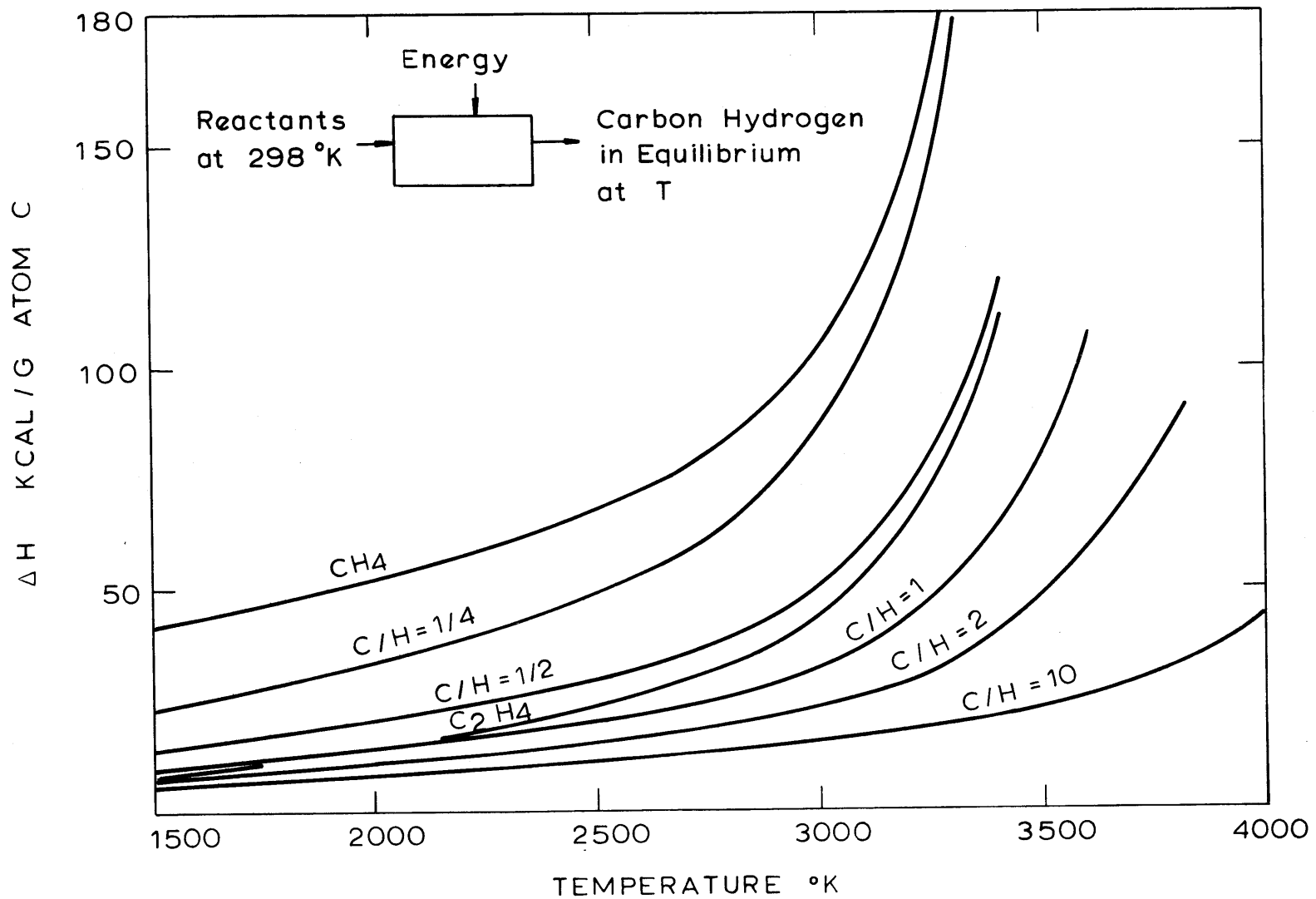


Fig. 1.30 Equilibrium Temperatures of the Carbon-Hydrogen System at Various Specific Enthalpies (Heterogeneous Region Only)

initiation stages of methane decomposition may begin to diffuse to the CaO particles as soon as they become "nascent." In such a system containing chemical species that are thermodynamically highly unstable, energy will be transported not only by conduction but also by diffusion currents carrying both thermal and chemical enthalpy, the latter being released when the diffusing but thermodynamically unstable chemical species turn to more stable species by recombination or spontaneous decomposition in the stream or on the cold particles. In addition, the gas phase reactions on the solid surface can be catalyzed to a varying degree depending on the composition of the solid material, thereby increasing the heat transfer even further. For the recombination of dissociated oxygen and nitrogen (33), a condition that accompanies hypersonic flights, pyrex is practically noncatalytic and metal oxides are moderately catalytic, while metals seem to be highly catalytic.

In the present experiments the diffusing chemical species that carry both thermal and chemical enthalpy to a particle can directly react with the chemical components of the particle. Heat, as well as mass transfer to such a chemically reacting surface can be even greater than to a catalytic but nonreactive surface.

1.5.1.3. CaC₂ Formation

In the methane series experiments, there was not noticeable effect of lime feed rates on the conversion of CaO to

CaC_2 even though they were varied from about 0.1 to 1.4 times the stoichiometric feed rates (Figure 1.5). The absence of the effect of lime feed rates on CaO conversion shows that the overall CaC_2 formation is a localized phenomenon around individual particles, not affected by the presence of each other.

The importance of the "nascent" chemical species in the formation of CaC_2 was experimentally confirmed in the experiments of prolonged residence time, in which it was shown that increasing the residence time of the reactants in the anode nozzle by an order of magnitude (from about 1 msec to 10 msec) increased the conversion only by a few percentage points. If the reaction mechanism operative in and immediately beyond the arc zone were still effective over the entire length of the anode nozzle, then the conversion should substantially increase with the increase in residence time; since this was not the case, one can conclude that the conversion of CaO to CaC_2 takes place only in the presence of the "nascent" chemical species which have a very short life span and hence may not exist far beyond the arc zone.

The formation of submicron-sized particles even at very low conversion (Figure 1.17) indicates that they are produced directly from CaO in the early stages of the overall reaction. The fine particles may have formed as a result of vaporization of CaO and its subsequent condensation, but it cannot be a dominant factor because the boiling point of CaO is known to be 3773°K (14), while in the methane series

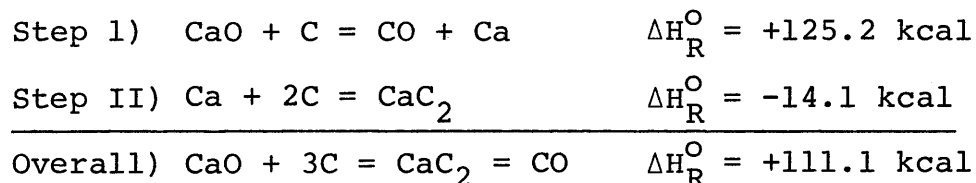
experiments the average gas temperature was most likely in the range of 3000°-4000°K. Instead, they may have formed predominantly from melting (m.p. 2888°K) and mechanical breaking-up of the CaO particles as a result of thermal stress while passing through the arc zone which is at substantially higher temperature than the average gas temperature. This postulation is substantiated by the presence of the submicron-sized grains that are angular in shape in the product of low conversion.

The absence of particle size effect on CaO conversion (Figures 1.4 and 1.5) apparently indicates that the overall CaC₂ formation is controlled by the chemical reaction within the CaO particles once an "outburst" of H atoms and other thermodynamically unstable species of intense chemical reactivity takes place in the initial stages of methane decomposition. It is also conceivable that the absence of particle size effect may have been caused by the mechanical breaking-up of original CaO particles into submicron-sized particles in the early stages of the overall conversion. Even if so, however, the conversion may have been still chemical-reaction-controlled because the broken-up particles were so small in particle size that diffusion may not have been the rate-limiting factor.

Increasing the specific gas energy beyond the critical value, which may be on the order of 100 kcal/g mole in the case of methane, may not significantly further CaO conversion because the CaC₂ formation is controlled by the chemical

reactions within the CaO particles.

Formation of CaC_2 in the present reaction scheme may still involve essentially the two elementary reaction steps of CaC_2 formation (50) from CaO and C(s):



However, the carbon reacting in the present reaction is "nascent" in nature and thus far more reactive than the carbon derived from C(s). In addition, H atoms and H_2 molecules produced in the present reaction scheme may actively participate in the reduction of CaO to Ca and CO in Step I. Although the polyatomic hydrocarbon radicals may directly react with CaO or Ca to form CaC_2 , it is more likely that they first decompose to the elements H and C and then react with either CaO or Ca.

In order to elucidate the reaction mechanism in the present experiments, the thermodynamics of various reactions related to CaC_2 formation involving both carbon and hydrogen are considered (Figure 1.31). In general, the thermodynamic consideration indicates the rate limiting step in the formation of CaC_2 is Step I, i.e., the reduction of CaO to Ca and CO, since the equilibrium constant for Step II is highly favored for the formation of CaC_2 and several orders of magnitude higher than Step I. Therefore, once Ca is formed, it will immediately proceed to form CaC_2 so long as enough carbon

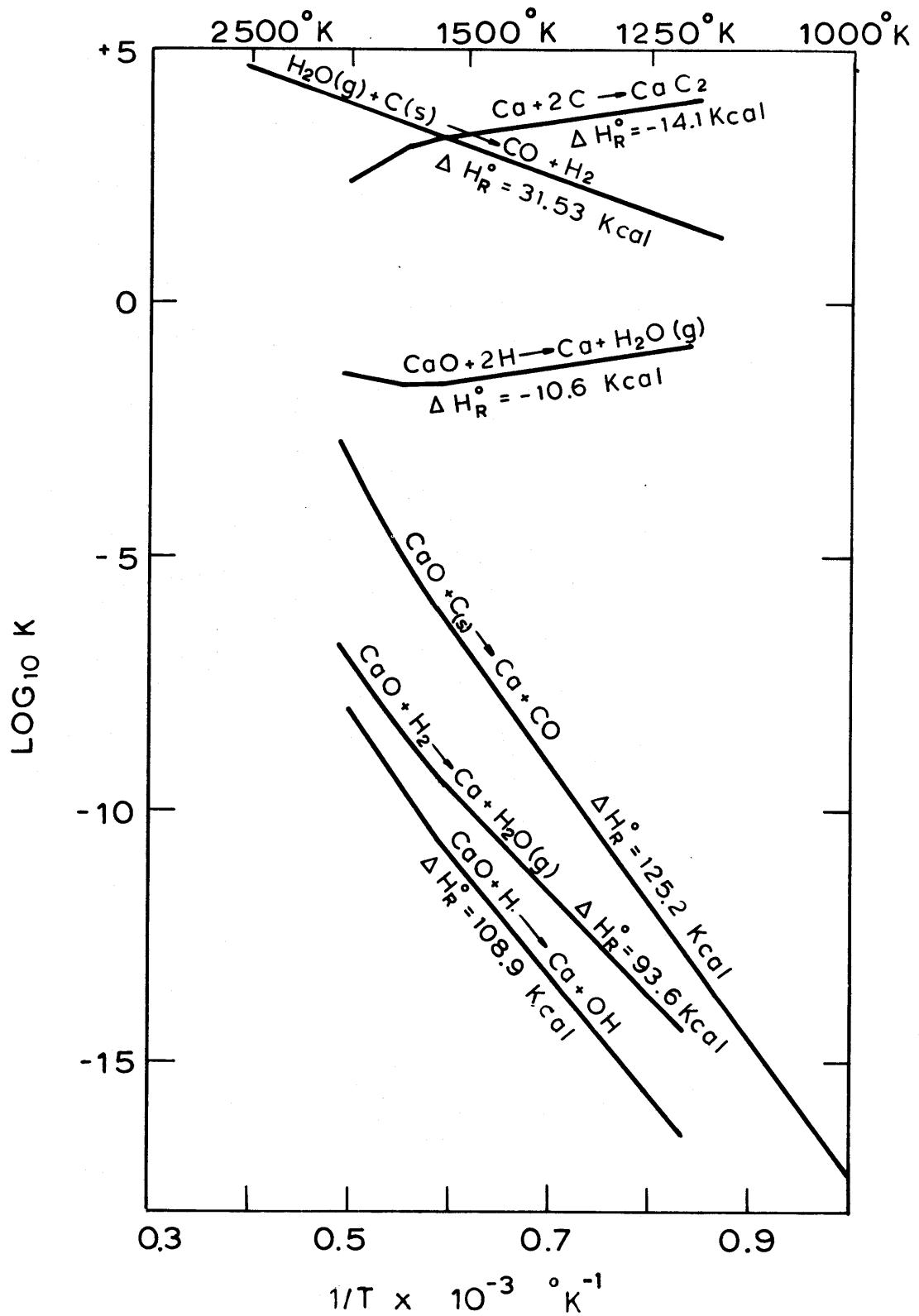
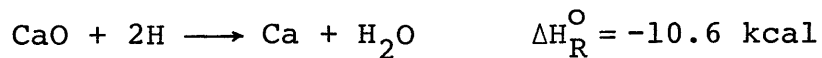


Fig. 1.31 Equilibrium Constant vs. Temperature for Various Reactions Related to CaC_2 Formation

is available for the reaction.

Reduction of CaO to form Ca can be greatly enhanced by H atoms in the initial stages of CaC₂ formation:



The H₂O produced will immediately react with "nascent" carbon species, and hence the reduction of CaO by H atoms can be greatly facilitated. The reaction of H₂O with carbon is highly favored in the direction of forming more CO and H₂ with increasing temperature. Nevertheless, the reduction of CaO by C may still be important, especially above about 2500°K, because of intense chemical activity of "nascent" carbon species.

Dissociation of the product CaC₂ in the intermediate range of temperatures during cooling is not likely to occur because the reaction $\text{Ca} + 2\text{C} = \text{CaC}_2$, which is thermodynamically favored for the formation of CaC₂ probably up to 3500°K as can be seen from the extrapolation of the existing data, is increasingly more favored toward the right as the temperature decreases.

1.5.2. Ethylene Series Runs

Ethylene requires less energy per g atom C to reach a given temperature than methane because it has a higher C/H ratio and, unlike methane which has a negative heat of formation, a positive heat of formation which makes the overall decomposition exothermic. In addition, the overall activa-

tion energy is of the order of 50 cal/mole, or 25 kcal/g atom C, for the decomposition of ethylene (9, 64). Therefore, one can expect the critical energy input required for the conversion of CaO to CaC₂ to be less for ethylene than methane as the carbon source. Nevertheless, the critical energy input will not be of the order of the overall activation energy for the decomposition of ethylene because the radicals produced in the initial stages of decomposition, which may be C₂H₃, C₂H₅, and others, may not be energetic enough.

The experimental results generally confirmed the considerations discussed above; the conversion of CaO to CaC₂ began to commence at lower energy input with ethylene as the carbon source than with methane at an equivalent carbon flow (Figure 1.6) and, as a result, the overall energy efficiency was generally higher.

1.5.3. Coal Series Runs

The overall mechanistic process of CaC₂ formation from the reaction of CaO and the "nascent" carbon species will be essentially the same regardless of whether the "nascent" species are derived from the pyrolysis of hydrocarbons or from the hydrogasification of coal. In the methane series experiments it was possible to make almost all the carbon of methane fed react with CaO to form CaC₂ and CO by feeding excess lime. Therefore, since it may be possible in view of the previous discussion to almost completely gasify a high

volatile coal in the present reaction scheme, one can expect the conversion of the carbon in coal to CaC_2 and CO to be very high under certain operating conditions. In the present experiments, the highest conversion of the carbon in coal was 90.1%, which was obtained by feeding a coal/lime mixture containing 47.0% wt.% excess lime over the stoichiometric mixing ratio.

Although it was firmly established in the present experiments that a high volatile coal can be an effective source of "nascent" carbon species of intense chemical activity, the specific energy requirement for the formation of CaC_2 was relatively high. The lowest SER even achieved with coal as the carbon source was 32.1 kwhr/lb C_2H_2 equivalent. The rather high energy requirement is undoubtedly due to the preliminary nature of the experiments.

1.5.4. Economic Feasibility of the Reaction Scheme

In Figure 1.32 we see the thermodynamic energy requirement as a function of temperature for producing enough CaC_2 at 1 atm to subsequently yield one lb C_2H_2 from the stoichiometric mixture of CaO and various carbon sources fed at 298°K. The thermodynamic effect of the presence of hydrogen in the feed is to increase the energy requirement for the overall CaC_2 formation because of the additional sensible energy required for heating the hydrogen to the reaction temperature. In addition, if the carbon source possesses a negative heat of formation, as does CH_4 , then the overall

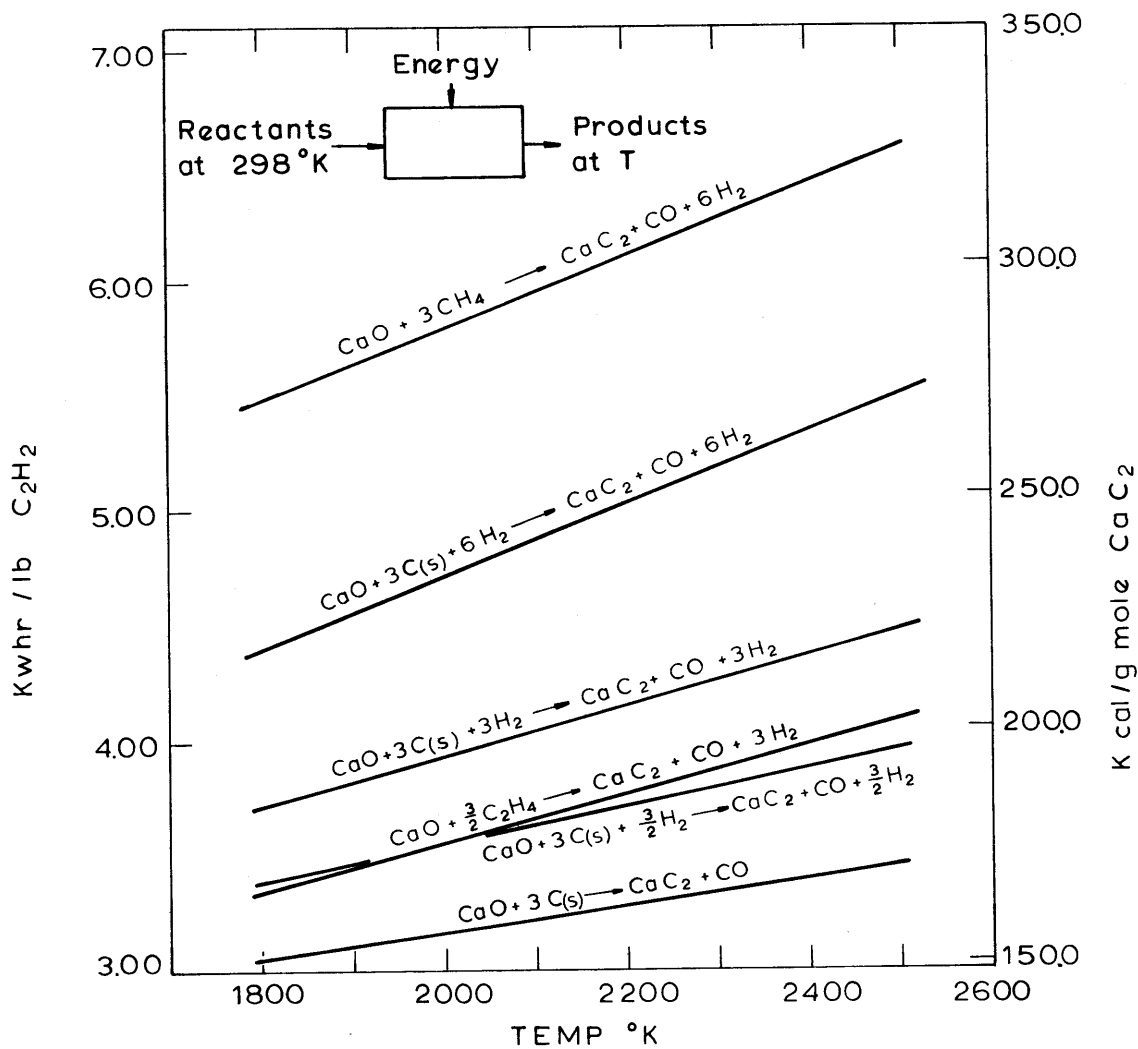


Fig. 1.32 Thermodynamic Energy Required to Produce One lb C₂H₂ via CaC₂ from CaO and Hydrocarbons/or Coal & Hydrogen

energy requirement will further increase due to the additional thermal energy required for decomposing it to C and H₂. Contrarily, a carbon source with a positive heat of formation will lower the energy requirement, as is the case with ethylene. In general the energy requirement increases with product temperature, and hence it is desirable to keep the latter as low as possible. The lower bound of the product temperature is uniquely determined by the equilibrium partial pressure of CO (see Figure 1.1). For the stoichiometric CaO-CH₄ mixture, the minimum energy requirement is 5.8 kwhr/lb C₂H₂ and occurs at 1980°K; for the CaO-C₂H₄ mixture it is 3.6 kwhr/lb C₂H₂ and occurs at 2020°K. As a reference, the CaO-C(s) mixture requires a minimum energy input of 3.2 kwhr/lb C₂H₂, which occurs at 2130°K.

For simplicity, coal is represented in the figure as β-graphite (i.e., $\Delta H_{f, \text{coal}}^{\circ} = 0$). In reality, coal may possess a positive heat of formation, which may be of the order of 10 kcal/g atom C (45, 53). If this is true, then the thermodynamic energy requirement for producing CaC₂ from the CaO-H₂-coal mixture will be lower by about 30 kcal/g mole CaC₂ (equivalent to 0.6 kwhr/lb C₂H₂) than as indicated in the figure. In the case of using coal as the carbon source, the minimum thermodynamic energy requirements are 4.7 kwhr/lb C₂H₂ (1980°K) and 4.0 kwhr/lb C₂H₂ (2020°K) for C/H ratios of, respectively, 1/4 and 1/2, assuming that the coal has a zero heat of formation. However, if coal does

possess a positive heat of formation of the order of 10 kcal/g atom C, as discussed above, then the thermodynamic energy requirement can be as low as 3.4 kwhr/lb C_2H_2 when the C/H ratio is 1/2.

The advantages of the present process over the AVCO Arc-Coal process (28), which was considered commercially viable at an SER of 4.0 kwhr/lb C_2H_2 , are several-fold in that it does not require the rather expensive C_2H_2 separation and purification step, it can be operated at the atmospheric pressure unlike the AVCO process (which was operated at 0.3-0.5 atm), and the thermal energy in the product stream can be recovered since the quenching requirement of the product in the present process is not as severe as the AVCO process. In the AVCO process, the energy required for separating and purifying C_2H_2 may be on the order of 1.3 kwhr/lb C_2H_2 , which is the value cited for the Huels Flaming Arc Process (52). Therefore, the present process can be competitive with the AVCO process if the energy consumption is in the range of 5.0-5.5 kwhr/lb C_2H_2 . At this range, it is also strongly competitive with the former method of manufacturing CaC_2 which requires an energy input of about 5.0 kwhr/lb C_2H_2 . It is so because: (1) capital cost is much lower as the reactor size is much smaller; (2) coal instead of coke is used as a raw material; and (3) operating cost is lower as it is essentially a continuous operation, whereas the former process is basically a semi-continuous operation in that the molten product is manually tapped from the furnaces intermit-

tently.

In the coal series experiments, the lowest energy consumption was 32.1 kwhr/lb C_2H_2 . In the methane series experiments it was 16.3 kwhr/lb C_2H_2 . The rather high energy requirement is undoubtedly due to the preliminary nature of the experiments and can be improved further in scaled-up reactors specifically designed for the energy efficiency. Thermodynamic consideration indicates that natural gas alone cannot be an economic source of carbon for the present process, unless the C/H ratio is increased by mixing heavier hydrocarbons. On a commercial scale the specific energy requirement should be in the range of 5.0-5.5 kwhr/lb C_2H_2 or less, which may be achieved in scaled-up reactors.

1.6 Conclusions

(1) A novel method of manufacturing CaC_2 from the reaction of CaO with "nascent" carbon and hydrogen species is developed in the present study; the "nascent" chemical species can be produced from the decomposition of hydrocarbons or from the hydrogasification of high volatile coals in a rotating-arc reactor.

(2) Extensive studies were made with methane as the source of carbon in order to delineate the overall reaction mechanism. The results from the methane series runs indicated the following:

- (a) The conversion of CaO to CaC_2 is a localized phenomenon around individual CaO particles.

- (b) There probably is a critical energy input on the order of the overall activation energy for the decomposition of methane in order for the CaO conversion to commence. This shows the importance of the role of the "nascent" chemical species in the CaO conversion or any endothermic reactions of heterogeneous type.
- (c) Once over the critical energy region, the conversion rises only slowly with an increase in energy input. This implies that the rate controlling step shifts from the gas phase to and around individual CaO particles as the energy input increases beyond the critical region.
- (d) No substantial particle size effect on the CaO conversion indicates that the overall conversion is probably chemical reaction-controlled.
- (e) The speed of quenching is not of importance in preserving the solid product CaC₂. Dissociation of CaC₂ in the intermediate range of temperatures during cooling is not thermodynamically favored.
- (f) Extending the residence time of the reactants in the anode nozzle downstream of the arc zone does not noticeably increase the conversion of CaO to CaC₂; this indicates that the conversion is driven by the "nascent" chemical species which are abundant only in and immediately beyond the arc zone.
- (g) Thermodynamic considerations indicate that the conversion of CaO to CaC₂ in the present process can be enhanced by H atoms which may directly reduce CaO to Ca and H₂O. The backward reaction is prevented by the reaction of nascent carbon species with H₂O to produce CO and H₂.

(3) Ethylene was also tried as the source of carbon; the result was a general increase in energy efficiency over methane as the source of carbon. This was attributed to the higher C/H ratio and the positive heat of formation of ethylene.

(4) A high volatile bituminous coal was also successfully used as a source of carbon for the conversion of CaO to

CaC₂ by carrying an intimate mixture of fine powders of the coal and CaO by hydrogen through a rotating arc. The highest CaO conversion achieved was 61%. The highest conversion of the carbon in coal to CaC₂ and CO was 90%, which was obtained when excess lime was present in the feed mixture.

1.7. Recommendations

(1) Scale up the present reactor to a minimum of 40 kw power level to increase the energy efficiency of the reaction scheme. This will also increase the arc stability. Results from the scaled-up studies together with the present experimental results will indicate the economic feasibility of the process at a much larger commercial scale operation (e.g. one megawatt or larger).

(2) In the case of using coal as the carbon source, determine the distribution of sulfur and nitrogen from the original coal in both gas and solid products. Sulfur in coal may end up as CaS which will yield H₂S upon hydrolysis. The desulfurized and possibly denitronized char from the present process can be a valuable "clean" fuel which can be used for other purposes.

(3) Investigate the feasibility of applying the present reaction scheme to other processes. So far, most studies involving an arc discharge were conducted by injecting the reactants into a high enthalpy jet downstream of the arc

zone. As a result the conversions were often low and the energy efficiencies were generally poor. The following reactions are suggested for future investigation:

- (a) Carry on the reduction of iron oxides by conveying an intimate mixture of fine powders of a high volatile coal and iron oxides by hydrogen through the arc zone. The gaseous byproducts H_2 and CO which are at high temperatures can be directly used for other chemical synthesis and thus can make the process economically more attractive.
- (b) Study the feasibility of producing various metals and metallic carbides from their respective oxides or halides.
- (c) Study the feasibility of producing various nitrides from their metals, metal oxides or halides. In this case N_2 , NH_3 and other nitrogen containing compounds can be used as the source of nitrogen.

2. Introduction

The present thesis concerns a novel scheme of producing CaC_2 whose main industrial use is to generate acetylene by hydrolysis, which in return can be used as an invaluable building block for the chemical industry. Therefore, in this section, the status of C_2H_2 in the chemical market is reviewed first, followed by the review of chemistries and both industrial and novel methods of acetylene manufacture and problems associated with them. Next, the advantages of the present reaction scheme as an acetylene manufacturing process are discussed. It is followed by a review of high-temperature chemical reactions in plasmas, as they are directly related to the present thesis work. Finally, objectives are presented at the end.

2.1 Status of Acetylene in the Chemical Market

Although acetylene is an invaluable building block for the chemical industry, it has suffered continuous erosion of its major chemical markets in recent years because of competition from less expensive raw materials. Acetylene production in the U.S. reached its peak in 1965 (at 1.149 billion pounds) and has been declining since. In 1974, acetylene production amounted to only 507 million pounds, of which 402 million pounds were used for the manufacture of chemicals and the balance for industrial welding and metal cutting (2).

The decline in chemical use of acetylene in spite of

the rapid growth, in recent years, of plastics and chemicals that can be derived from acetylene can be attributed mainly to the competition from ethylene as the feedstock for the manufacture of vinyl chloride, vinyl acetate, and other derivatives. Propylene has also totally replaced acetylene as the raw material for the manufacture of acrylonitrile, which consumed 174 million pounds (15% of total production) of acetylene in 1966. Furthermore, acetylene has been displaced by butadiene as the raw material for neoprene manufacture.

The non-chemical use of acetylene is directed mainly at metal cutting and welding. Consumption in this area amounted to approximately 100 million pounds in 1965, and 105 million pounds in 1974. Even in this area, acetylene is suffering from competition (e.g., electric-arc welding has replaced oxyacetylene welding to some extent and other gases such as LPG have replaced acetylene for some metal cutting applications).

The erosion of the acetylene market can be traced to the inability of the current processes to produce acetylene at a competitive price. Presently acetylene is produced via calcium carbide and from the pyrolysis of hydrocarbons. Calcium carbide, which is produced from the reaction of lime and coke in an electrothermal furnace at around 2000°C, was the only source of acetylene in the U.S. prior to 1951. Its production in the U.S. had grown very modestly from 700,000 tons in the early 1950s to about 1.1 million tons (equivalent to 630 million pounds of acetylene) in 1965, and in fact

experienced a reversal thereafter. In 1974, calcium carbide accounted for only 30% of the acetylene produced. The sharp decline in calcium carbide production in recent years reflects the inability of the process to reduce the price of calcium carbide-derived acetylene in order to be competitive with other hydrocarbon feedstocks for the manufacture of chemicals. Since calcium carbide is made from coke, which is derived from abundant coal, it may not be unthinkable that calcium carbide-derived acetylene could again become an invaluable building block for the chemical industry if petroleum becomes more scarce and nuclear fission or fusion power generation makes electricity more readily available. Nonetheless, if the current trend continues, calcium carbide-derived acetylene may cease to be used for the manufacture of chemicals in the not-so-distant future.

The future of hydrocarbon-derived acetylene, which is produced from regenerative, partial combustion, and electrical discharge processes, is also unpromising. This is the case because none of the existing processes show promise for reducing the acetylene price, while other hydrocarbon feedstocks (such as ethylene) have been decreasing in cost relative to acetylene in past years. In addition to the competition from other hydrocarbon feedstocks, it has been reported that partial oxidation processes and the Wulff process (a regenerative process), which once showed promise for reducing the acetylene price, have been plagued with operating and technical difficulties (4), thus preventing further expansion

of acetylene production from hydrocarbons. Neither do the electric-arc processes hold promise of lowering the acetylene price as they primarily depend on costly electricity for the endothermic formation of acetylene from hydrocarbons.

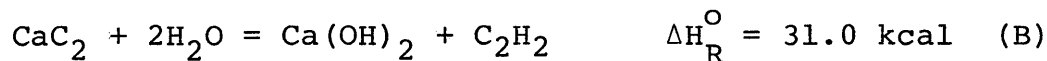
2.2. Acetylene Manufacturing Processes

2.2.1. Acetylene from Calcium Carbide

Calcium carbide is produced commercially from lime and coke at 1800-2100°C and at atmospheric pressure in an electro-thermal furnace (48):



The molten product is tapped from the furnace intermittently and allowed to cool at ambient temperature before crushing and shipping for the subsequent generation of acetylene by hydrolysis:



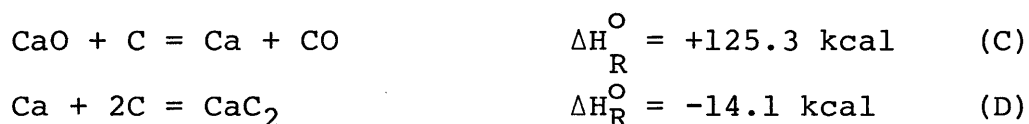
Acetylene thus produced is 99-99.8% pure on a dry basis and can be directly used for the synthesis of chemicals. Calcium carbide is a convenient form of transporting acetylene long distances in spite of the additional weight of the calcium; acetylene is difficult to ship long distances economically since it could undergo explosive decomposition reactions if compressed above about 1.5 atm.

2.2.1.1. Chemistry of Calcium Carbide Manufacture

Figure 2.1 shows the temperature dependence of the equilibrium constant in Reaction (A). Since CO is the only gaseous product from the reaction, the "threshold" temperature above which the reaction proceeds to the right to completion can be lowered by lowering the CO partial pressure of the system. When P_{CO} is one atm, the threshold temperature is 2130°K.

The melting point of a CaC_2 -CaO mixture varies with composition. All (49) found two eutectics melting at 2023° and 2073°K, containing 69.4% and 36.3% CaC_2 , respectively. The m.p. and b.p. of CaO are 2888° and 3773°K, respectively, and the m.p. of pure CaC_2 is 2573°K (14).

The reaction of CaO and C to form CaC_2 is generally believed to involve the following two elementary steps (50):



Both reactions are reversible.

Studies (54, 70) on reaction (C) below 1400°C in vacuo to avoid the subsequent formation of CaC_2 show that the weight decrease due to the evolution of CO and Ca vapor is approximately linear with time. The reaction velocity is doubled at every 32-34°C rise in temperature (54). The activation energy depends on the nature of lime and carbon. Tagawa et al. (70) report that the activation energy is 91.7, 135.5, and 146.6 kcal/mole for lime prepared at 900, 1100, and 1300°C,

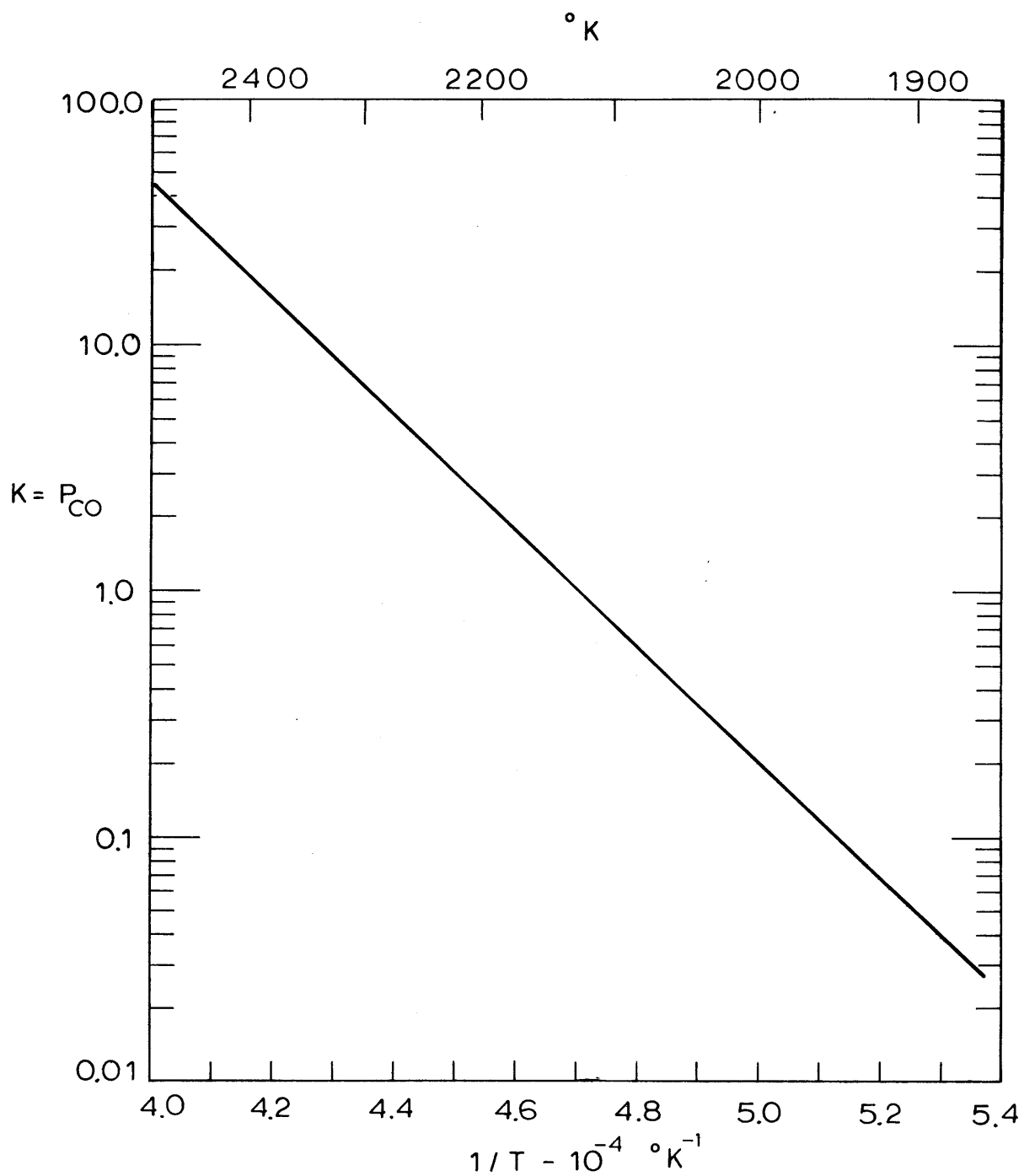


Fig. 1.1 Equilibrium Constant vs. Temperature for CaC_2 Formation from CaO and C : $CaO + 3C \rightarrow CaC_2 + CO$.

respectively, the reactivity of lime decreasing abruptly at the burning temperature region from 1000°C to 1100°C. The difference in the reactivity was attributed to the structural defects in lime as determined by the studies of x-ray diffraction pattern and of changes of lattice constant and surface area. Mukaibo and Yamanaka (54, 55) report that the activation energy for anthracite is 110.8-118.0; coke 124.8; pitchcoke 142.2; and charcoal 78.7 kcal/mole. They found that the reaction velocity increases proportionally to the area of contact between lime and carbon (56).

Reaction (D), which is the second stage of carbide formation, is controlled by the diffusion velocity of calcium vapor through the layers of CaC_2 formed on the surface of the carbon. The reaction is reversible; the decomposition of CaC_2 into its elements increases with temperature, and is rapid at 2200°C (50).

Tagawa and Sugawara (69) studied, as a solid-state reaction, the overall kinetics of CaC_2 formation from compressed cylindrical pellets (2 cm diameter x 3 cm height) of lime and carbon in the stoichiometric ratio at temperatures between 1600° and 1800°C, and at various reduced carbon monoxide pressures. They found it to follow an isothermal diffusion control model at the microscopic level and a homogeneous system at the macroscopic level. The reaction velocity depended strongly on the pressure of CO with an apparent activation energy of 143 kcal/g mole at 50 mm Hg P_{CO} and over 200 kcal/g mole at 100 mm Hg P_{CO} . Consequently,

they concluded that the reaction rate is governed by the diffusion process of CO through the product layer, as well as by diffusion of solids.

Recently, however, Brookes et al. (20) repeated the work of Tagawa and Sugawara and concluded that a reacting pellet of lime and carbon could not be considered as homogenous at the macroscopic level and that the overall reaction rate was predominantly governed by macroscopic heat transfer across the reacting pellet. Nonetheless, the postulation by Tagawa and Sugawara of the diffusion controlled formation of CaC_2 in the solid-solid reaction of lime and carbon may still remain valid if the dimension of the pellet is reduced such that homogeneity at the microscopic level can be maintained; in addition, it is also possible that the overall reaction rate is controlled not by diffusion but by intrinsic chemical reaction at the microscopic level if individual lime and carbon particles are small enough. These points need to be resolved in the future.

Torikai et al. (71) studied the formation of CaC_2 by the reaction of lime (10-20 mesh) and carbon (14-16 mesh) at 2000°C in an argon stream using a vertical electric furnace. Calcium carbide formed initially in a solid-state reaction, and then changed to a violent molten-state reaction. The reactivity of various carbonaceous materials was tested by using artificial graphite, carbide coke, petroleum coke, and anthracite. In the solid state, they showed little difference in reactivity, but in the molten state, anthracite

was the least reactive.

2.2.2. Acetylene from the Pyrolysis of Hydrocarbons

2.2.2.1. Chemistry of Acetylene Formation from Hydrocarbons

Acetylene is thermodynamically unstable relative to the elements C and H₂ and to most other hydrocarbons at lower temperatures. The free energy of formation of acetylene, however, decreases with increasing temperature, whereas that of most hydrocarbons shows the opposite trend; as a result, acetylene becomes more stable than most other hydrocarbons at temperatures above about 1500°K. Nonetheless, acetylene is still unstable with respect to its elements and does not exist in measurable quantities in thermodynamic equilibrium until the temperature reaches 2500°K or higher. Consequently, production of acetylene from the pyrolysis of hydrocarbons requires that the feedstock be heated quickly to a cracking temperature (usually below about 2000°C), and then quenched rapidly in order to avoid reaching the true thermodynamic equilibrium. In addition, the decomposition of acetylene can be further reduced by keeping its partial pressure low, either by operating at a reduced total pressure, or by the presence of diluents, or both (51). In the pyrolysis of hydrocarbons, the acetylene selectivity generally decreases with increasing pressure because the decomposition of acetylene is a bimolecular process, whereas its formation from hydrocarbons is typically unimolecular (51).

2.2.2.2. Industrial Processes of Acetylene Manufacture from Hydrocarbons

There are three general methods commercially used to manufacture acetylene from hydrocarbons. They are: (1) regenerative pyrolysis; (2) partial combustion; and (3) electrical discharge. A brief review of the three general methods is presented in the following. For a very comprehensive review, the readers are referred to Miller (48).

In the regenerative type of processes the gas to be cracked is placed in contact with a previously heated solid so that its temperature is raised to around 1300°C for methane feedstock, or 1100°C for other hydrocarbons, for a fraction of a second, followed by rapid quenching of the pyrolyzed gas. Among a number of processes based on the regenerative pyrolysis, only the Wulff process has been developed to full-scale operation. The Wulff process operates at a total pressure of 0.5 atm.

In the partial combustion type process, the feedstock is raised to high temperatures by burning part of it with a limited supply of oxygen or by feeding it into the flame of the complete combustion of some other fuel. To obtain a workable concentration of acetylene in the product gas, oxygen (90-98% pure) is usually used, and it is necessary to preheat the feedstock and oxygen prior to combustion. There are a number of processes based on the principles of partial combustion, which differ from each other only slightly in burning design, operating pressure, method of quench-

ing, and acetylene recovery. All partial combustion processes yield a raw gas containing relatively little (8-10%) C_2H_2 . As the partial combustion processes are relatively simple in operation, most acetylene today is produced from these processes in spite of the need of costly oxygen supply.

In the electric discharge processes, the energy required for the conversion of hydrocarbons to acetylene is supplied by means of electric discharges, which may be in the form of sparks, arcs, glow or high frequency discharges (52). Of these, only arcs are of practical importance because the other types of electric discharge have relatively low power efficiencies. To date, only two processes, both of which are utilizing a d.c. arc, have been adapted to commercial production of acetylene; they are (1) the Huels flaming arc process, and (2) the Du Pont process.

In the original Huels flaming arc process (30, 52), a hydrocarbon feed gas was brought into a central vortex section in a swirling pattern to aid in rotating a direct current arc sustained between a water-cooled hollow cathode and a water-cooled annular anode which is coaxially positioned underneath the former. A heavy hydrocarbon was also injected downstream of the anode as the initial quench. In a later modification of the original process, Huels developed and operated a hydrogen plasma jet furnace similar in geometry, but with the hydrocarbon feedstock injected totally downstream of the arc (30); as a result, the carbon formation in the furnace is prevented, which previously formed a hard

graphite deposit on the electrodes and thereby affected the stability of the arc. The arc reactor operates at 1 atm, and the product gas typically contains 15.9% C_2H_2 . The SER (Specific Energy Requirement) is about 6.0 kwhr/lb C_2H_2 , inclusive of 1.3 kwhr required for the separation processes from the cracked gas (52).

In the Du Pont process (62), which is not presently in use (5), hydrocarbons diluted with hydrogen were forced to flow through the interelectrode region of a d.c. rotating-arc reactor, which consisted of a pointed graphite cathode of rod shape positioned at the center of a water-cooled annular copper anode. The arc, which was maintained in the radial direction between the electrodes, was made to rotate at about 8000 r.p.m. with an axial magnetic field externally provided by magnetic coils concentrically surrounding the reactor. The rotating-arc reactor had arc characteristics of 3100 amp and 3500 volts, and operated at 400 mm Hg absolute to minimize the carbon formation. The SER seemed to be in the range of 3.5-4.5 kwhr/lb C_2H_2 in the cracked gas without allowing for isolation; thus the overall energy efficiency was not much better than the Huels process, especially when the energy required for pumping was considered.

Alternating current arcs can also be operated. They can be economically more attractive in large scale acetylene production than d.c. arcs because they do not require rectification equipment. Nonetheless, they have special requirements for stabilization since the arc can be extinguished

between cycles, which may have been the reason for their lagging behind d.c. arcs in being utilized in commercial scale production of acetylene. As in d.c. arc processes, a.c. arcs can also be operated in the hydrocarbon feed gas itself (38), or in an auxiliary gas (hydrogen), which is later mixed with the hydrocarbon to be converted (3).

Westinghouse Electric Corporation (38) has developed a multi-megawatt scale a.c. arc heater which consists of two hollow electrodes of equal diameter coaxially aligned with each other and separated by a narrow annular gap through which the arc gas can be introduced radially. A secondary feedstock can be admitted axially through the arc discharge. The arc is magnetically rotated. Operation of the reactor in pure methane at 1 atm yielded acetylene at about 4.0 kwhr/lb C_2H_2 ; however, at higher pressures the SER's were higher due to the increased decomposition of the acetylene already formed (38). In the Hoechst AC system (3), hydrogen is heated by a three-phase high current arc (1400 volts, 4200 amp) maintained between the tips of three consumable graphite electrodes and mixed in downstream with hydrocarbons to be pyrolyzed. It has economies similar to those of the Huels system.

In addition to the arc processes described above, there have been numerous studies involving other methods of transferring electrical energy into the hydrocarbon to be converted, which are comprehensively reviewed by Miller (52).

2.3. Novel Methods of Acetylene Manufacture

2.3.1. Direct Production of Acetylene from Coal

It has been well known in the area of coal gasification research that, if finely ground and well-dispersed coal is rapidly heated to a high temperature (preferably in a hydrogen environment), it can be gasified well in excess of what could be attained in a slow heating condition (6). The extent of gasification and the product gas composition are known to depend on the rate of heating and the final temperature under a given condition.

Especially if the final temperature is above approximately 1500°K, the main product will be acetylene because above that temperature it is thermodynamically stabler than most other hydrocarbon molecules. An electric arc is a convenient source of high temperature and has been widely used for the rapid heating of coal. In the following we review the studies of rapid heating of coal in electric arc devices.

Bond and co-workers (17, 18) studied the reactions of coal in an argon plasma jet heated by a d.c. arc heater which consisted of a pointed tungsten cathode positioned at the center of a water-cooled copper tube anode. The input power varied from 4.5 kw to 13.5 kw. The arc gas was passed through the electrode space at flow rates varying between 5 and 21 l/min. The coal was suspended in a stream of argon and fed through a hole in the anode nozzle. Injection of the coal particles through the interelectrode region was not possible because of severe erosion of the electrodes. The

hot product streams were quenched in a water-cooled tube fitted to the underside of the jet assembly. The gas product was composed of hydrogen, acetylene, and carbon monoxide. The extent of the reactions depended strongly on the rank and particle size of the coal. High volatile coals of particle diameter of less than 50 μ reacted most clearly; and an anthracite showed negligible reaction. For a coal of 36% volatile matter, fed at 0.3 g/min into an argon plasma, 20% of the initial carbon in the coal was converted to acetylene. When 10% hydrogen was added to the argon plasma, the conversion doubled to 40%. Hydrogen could not be added by more than 10% to the plasma because of severe erosion of the electrodes and the ensuing arc instabilities. Similar experiments have been reported by Graves et al. (34), Kawana et al. (41), and Anderson et al. (1).

Littlewood and co-workers (47, 57) of the University of Sheffield have also studied the reactions of coal in a plasma jet using an experimental device similar to the one used by Bond et al. However, they were able to pass up to 0.1 gm/min of coal directly through the interelectrode region by injecting it through holes drilled in a hollow cathode holder, which resulted in significant improvement in the acetylene yield. Especially when a 90% argon/10% hydrogen mixture was used as the principal arc-gas, the acetylene yields improved significantly; thus, the highest acetylene yield attained with the coal of volatile matter content of 36% by weight (d.a.f.) was 74% of the initial carbon in the

coal. Including CH_4 , C_2H_4 , and C_2H_6 , which are also reported to have been produced along with C_2H_2 , one can see that as high as 93% of the carbon in the coal has been gasified. Formation of CO was negligible. As in the other studies, H_2 could not be added by more than 10% due to the severe electrode erosion and arc instabilities. In the study, the decomposition of the acetylene and other hydrocarbon gas products was negligible because their partial pressures (concentrations) were always kept low. The highest acetylene concentration was only on the order of 0.1% or less.

Krukonis et al. (28, 43) of AVCO Systems Division in Lowell, Massachusetts, have pursued the economic feasibility of producing acetylene directly from coal. In their study a number of reaction schemes have evolved logically, starting from a scheme of using coal as the consumable anode for a d.c. arc discharge and finalizing around a rotating-arc reactor which allowed direct passage of finely pulverized coal through the arc-zone with hydrogen as the carrier gas. The rotating-arc reactor is very similar in principle to the Du Pont reactor (62), which was once used for producing acetylene. The AVCO experimental reactor operated at 100 kw power level and under reduced pressure (0.3-0.5 atm absolute) to minimize the decomposition of acetylene. The product stream contained acetylene typically in the range of 8-10%. The yield of acetylene averaged about 20 lbs per 100 lbs of coal fed and increased up to 35 lbs when more coal was fed downstream of the anode as a quench medium. However, material

balances using the ash in char as a tracer, i.e., assuming that the ash in coal does remain inert during reaction, indicated that probably 50-70 wt% of the coal may have been gasified, but that a substantial portion of it was lost as soot through decomposition. The power consumption was as low as 4 kwhr/lb C_2H_2 . Based on the results, AVCO concluded that the process can be commercially viable and has been preparing to proceed into the next phase with the construction and operation of a 1 megawatt pilot plant.

2.3.2. Direct Synthesis of Acetylene from Carbon-Hydrogen Systems at High Temperatures (above 2500°K)

From about 2500°K the carbon-hydrogen system in thermodynamic equilibrium begins to contain acetylene, hydrocarbon radicals, and hydrogen atoms in measurable quantities. In an optimal quenching condition of the equilibrium mixture, C_2H radicals can combine with H to form additional C_2H_2 (16, 40, 60). Thus, Blanchet (16) was able to obtain a maximum concentration of 26% C_2H_2 by reacting H_2 with carbon vapor produced from a consumable graphite anode in a high-intensity arc reactor. However, this process cannot be commercially viable because the energy required for the carbon-hydrogen system to reach above 2500°K is too high to be practical. Nevertheless, the carbon-hydrogen system at high temperature is further discussed in the "Discussion" section as it relates to the present thesis.

2.4 Motivation

As described previously, acetylene can be produced not only from the pyrolysis of hydrocarbons, but also from coal by the rapid heating of same, preferably in the presence of hydrogen, to 1500°K or higher, and immediate quenching of the reaction product to minimize the decomposition of acetylene. The process of manufacturing acetylene directly from coal can be economically feasible as shown by the AVCO Arc-Coal process. In the U.S., coal represents approximately 70% of the recoverable fossil fuel resources (7) and may eventually become the principal source of hydrocarbons and feedstocks. Therefore, the economics of chemicals-from-coal via acetylene become increasingly more attractive as the world's petroleum and natural gas reserves dwindle while its insatiable need to consume energy increases at an ever-accelerating rate.

Acetylene has been steadily losing in competitiveness as a feedstock in the chemical market, due to the inability of the existing processes to reduce the acetylene price relative to other raw materials. The main problem in manufacturing acetylene from hydrocarbons, as well as from coal, is in preserving the acetylene, which can be achieved to some extent by rapidly quenching the reaction product and by operating at low C_2H_2 partial pressure by diluting with other gases, or by reducing the total pressure, or by combining both these measures. The rapid quenching requirement, however, introduces a great deal of technical and operating difficulty to

the acetylene manufacturing processes. In addition, it also makes it difficult to recover the valuable sensible heat in the pyrolyzed gas. In some industrial processes the sensible heat is partially recovered by injecting additional hydrocarbons into the hot product stream to produce more acetylene, while cooling the product simultaneously. However, the processes are still burdened by the necessity of recycling the quench hydrocarbons to reduce the raw material costs, which is not an easy task, due to the presence of finely suspended carbon particles in the quenched stream and the degradation of the hydrocarbons by side-reactions. Operating at low C_2H_2 partial pressure can also result in high separation and pumping costs, as well as limited throughput of feed.

If the "nascent" carbons concomitantly produced upon the pyrolysis of hydrocarbons or from the rapid heating of coal in hydrogen can react sufficiently quickly with lime (CaO), then one can produce CaC_2 instead of C_2H_2 as the main product in one-stage reaction. This will eliminate the problems associated with preserving C_2H_2 . Therefore, unlike the AVCO Arc-Coal process or some hydrocarbon-acetylene processes which have to operate at reduced pressures, this process can be run at atmospheric pressure with substantial savings in pumping costs. As the dissociation of CaC_2 is much slower than that of C_2H_2 , it is also less difficult to recover a substantial amount of sensible heat from the hot product stream. The other major advantage of producing CaC_2 instead

of C_2H_2 is that the relatively expensive step of C_2H_2 separation and purification is not required. CaC_2 is also a convenient form of transporting acetylene over long distances since the latter cannot be compressed more than two atm because of explosion hazards.

The contemplated reaction scheme can also be superior over the industrial method of producing CaC_2 in electrothermal furnaces, because it requires as the source of carbon relatively cheap coal or other hydrocarbons instead of the rather expensive coke. Equipment size can be greatly reduced because of the extremely high rate of the process. In addition, the process can be coupled with other chemical processes which can utilize the high enthalpy gas products consisting mostly of H_2 and CO .

2.5. Chemical Reactions-in Arc-Plasma Jets

The proposed reaction scheme of producing CaC_2 requires that the reactants be heated rapidly to and supplied with the reaction energy at temperatures above about $2000^\circ K$, as dictated by the thermodynamics of the reaction. Such high-grade heat, i.e., highly concentrated specific energy, can be effectively supplied by means of electrical discharges which can be operated in the reactant gas itself or in an auxiliary gas which is later mixed with the reactants. Very often the success of high temperature chemical processes effected by means of electrical discharges depends greatly on the particular experimental approach to the problem,

especially when the reaction requires active participation of atoms and free radicals of intense chemical activity. Therefore, high temperature chemical processing by means of electrical discharges is reviewed in this section, with emphasis on gas-solid metallurgical type reactions in particular.

2.5.1. Plasmas for High Temperature Chemistry

The gas heated by means of electric discharge is often loosely called a plasma, even though the energy content of the gas may not be high enough to maintain a reasonable degree of ionization beyond the discharge point. A plasma can be used to achieve high temperatures in a chemical reaction, or as a reactant in the reaction itself. One of the main functions of the high temperature in plasma chemical reactions is to produce the precursors, e.g., atomic species and free radicals, which can actively participate in the reaction to yield the desired product. In general, intrinsic reaction times of plasma chemical processes are extremely short, and may range from 10^{-5} to 10^{-2} sec (74), resulting in extraordinarily high rates of processes.

The application of plasmas to chemical processing was attempted since the discovery of electric arcs in the early nineteenth century and appeared economically feasible, especially in the fixation of nitrogen, around the turn of the century when the advent of hydroelectric power made electricity readily available at very low cost. Soon afterwards,

however, accelerating demand for electricity and sharply increased supply of oil made electricity relatively expensive compared with fossil fuels as a source of energy for chemical reactions; hence the application of plasmas to chemical processing was largely ignored by science after the turn of the century (61) and was not firmly established in the chemical industry except in the synthesis of acetylene from hydrocarbons (27).

By 1960 renewed interest in the field of high temperature and advances in equipment for plasma generation had rekindled interest in the application of plasmas to chemical processing (27). The interest had been further spurred by the anticipation of lower priced electricity from the projected large-scale nuclear generators. Plasmas can be generated in d.c. and a.c. arc plasma generators with the line frequency (with efficiency of up to 95%) (74), high frequency and microwave generators, as well as in glow and corona discharges, in adiabatical piston compressors and shock tubes, in combustion flames, and by means of powerful lasers. To date, d.c. and a.c. arc plasma generators and their variants have been of particular industrial interest because of the high energy efficiency, relative ease of operation and maintenance, and operational versatility.

The list of chemical reactions that have been investigated in the newly developed plasma generators is, with some exaggeration, almost endless, but one can acquire a wide-ranging view in the area by combining, in his reading, the

following review articles (27, 61, 73, 74, 75). In general, chemical reactions suitable for industrial plasma processing may possess the following characteristics: (1) equilibrium is shifted to high temperatures; (2) reaction rates are sharply increased with a temperature increase; (3) high yields are obtained under substantially non-equilibrium conditions (74).

Plasma chemical processes can be grouped into two classes, depending on whether the plasma is "thermal" (i.e., $T_{\text{electron}} \approx T_{\text{ion}} \approx T_{\text{gas}}$) or "cold" (i.e., $T_{\text{electron}} > T_{\text{ion}} \approx T_{\text{gas}}$) (63). The cold plasma is less of industrial interest in the manufacture of bulk chemicals than the thermal plasma because the former has to be operated at pressures which are too low (probably below 50 mm Hg) to be economical (12). Therefore, in this review, the cold plasma type chemical processes are not included.

Chemical reactions in thermal plasmas can be in turn classified into two groups, depending on whether end products are intermediate or final products of a chemical process (74). The first type includes mostly gaseous reactions, the most notable example being a conversion of methane into acetylene. The second type includes mostly gas-solid metallurgical type reactions, although it may include a few homogeneous reactions such as the fixation of nitrogen from air.

The following section provides a comprehensive review of heterogeneous reactions of the second type in arc-plasma jets, as the contemplated reaction scheme belongs to this group.

2.5.2. Review of Gas-Solid Metallurgical Type Reactions in Arc-Plasma Jets

The characteristic of reactions of the second type is that the end products are final at high temperatures and thermodynamically allowed under equilibrium conditions. Obviously, in such reactions, a complete conversion can be invariably attained by prolonging the reaction time in a suitably designed plasma device, e.g., plasma jet directed to a stationary bed of solids to be processed or to a fluidized bed of solid particles in the upward flow of a plasma jet. The latter was once used by the Battelle Development Corporation (32) for the pilot-plant scale production of CaC_2 (150 tons/day) from lime and carbon with CO as the plasma gas. The process unit consisted of a 13 megawatt plasma generator coupled directly below a 10 ft dia. fluidized bed. The unit does not seem any more advantageous than the conventional electrothermal carbide furnace in terms of either equipment size or ease of operation. If, however, hydrocarbon or high volatile coal was mixed with lime and injected into a plasma jet containing H_2 in such a reactor configuration, then, as contemplated in the present thesis, the formation of extremely reactive "nascent" carbon species can greatly reduce the equipment size requirement and hence make simpler the operation of the fluidized bed. If the reaction is rapid enough, the need of the fluidized bed can be eliminated altogether.

A high conversion can also be expected in the high-intensity arc by using consumable anode of reagent materials (e.g.,

oxides, metals, etc.) pressed with carbon powder (27). However, energy efficiency of such a device is usually poor because it is necessary to vaporize the anode materials at temperatures probably well above the threshold reaction temperature of thermodynamic equilibrium.

Both methods of achieving a high conversion in the high-temperature gas-solid metallurgical type reaction is not of as much interest scientifically, because it is both thermodynamically and kinetically expected. Furthermore, as is the second method, the first method is relatively energy-inefficient, because the energy loss through the reactor walls per unit mass processed can be high due to the increased retention time and also because it may be necessary to maintain a high ratio of gas to solid flow rates; thus valuable electrical energy is wasted more as the sensible heat of the off-gas. In addition, throughput is rather limited in both methods.

Extraordinarily high throughput and energy efficiency can be achieved in one-stage reactions by injecting solid particles into a plasma jet, provided that such heterogeneous reactions can take place in plasma jets with sufficient velocity (typical reaction times = 10^{-5} to 10^{-2} sec). Literature surveys indicate that gas-solid metallurgical type reactions have been getting far less attention by science than gaseous reactions, which is understandable because one tends to rightfully suspect that such heterogeneous reactions may inherently proceed too slowly for such short residence time

devices. Investigation of gas-solid reactions in plasma jets has been further impeded because the experimental involvement is far more complicated than for gaseous reactions. This investigation has been performed mostly as exploratory experimentation directed at evaluating feasibility, which is understandable in view of the enormous complexity of chemistry and physics of such high-temperature gas-solid reactions in the plasma jet.

Stokes and co-workers (66, 67, 68) made feasibility studies on the reduction of metal oxides and synthesis of nitrides and carbides of a number of metals by pneumatically conveying solid particles to a d.c. plasma jet. Solid products were collected on a copper cold finger and quantitatively analyzed by x-ray diffraction. In order to study the effect of quenching speed on product decomposition, they placed the cold finger either 1/2" or 5" below the solid feeding point. Generally, products quenched at a 1/2" distance showed higher conversions than at a 5" quench distance, which fact they took as an indication that the products either decompose or undergo backward reactions in slow cooling conditions. However, it seems unlikely that the solid products which are thermodynamically allowed at high temperatures undergo decomposition or backward reactions noticeably because of so minor a delay in quenching. Rather, it is more likely that at the 1/2" quench distance the cold finger was too close to the anode nozzle of the plasma torch, so that the products collected on it were still undergoing further conversions as

they were exposed to much hotter gases than at a 5" quench distance. Gilles and Clump (29), who studied the reduction of iron ore in a similar system, experimentally observed additional reactions taking place on a cold finger type quenching device (their work is described below). At a 5" quench distance, such additional reactions are far less likely to take place because of turbulent mixing of the hot stream with cold gases in the water-cooled quenching chamber. Therefore, only the results of a 5" quench distance are presented in the following for the works of Stokes et al.

In the study of metal oxide reduction, they conveyed up to 5 gm/min of fine powder (mostly of 325 mesh) of various metal oxides into a helium plasma jet. In all cases, the particle conveying gas was H_2 , flowing at 13.6 l/min, which was also used as the reactant gas itself. The helium plasma jet was produced by passing 34 l/min He through a d.c. arc maintained at power inputs of 9-16 kw. Both WO_3 and ferric oxide underwent almost complete conversion. Both products were submicron-sized and of a highly pyrophoric nature. The highest reduction of Ta_2O_5 to Ta was 15.8%. TiO_2 , ZrO_2 , and Al_2O_3 were not reduced at all. They also prepared titanium nitride (100% conversion), tungsten nitride (25% conversion), and magnesium nitride (40% conversion) by conveying, by N_2 , their respective metal powders into a nitrogen plasma operating at 6-15 kw with nitrogen flow at 5 l/min (2.5 l/min for the conversion of magnesium). The titanium nitride ranged from 0.75 to 7.5 microns in particle size,

larger particles being easily broken down into smaller particles. The quench distance is reported only for the preparation of WN, which was only 1/4" from the feeding point. The results should be considered tentative, because the quench distance was either not given or too close to the plasma generator. TiO_2 did not react at all when introduced into a nitrogen plasma jet under similar reaction conditions.

Stokes and co-workers were also able to synthesize carbides of tungsten and tantalum by conveying the powdered metals or metal oxides by methane flowing at 6.5 l/min into a helium plasma jet operating at 9-17 kw with helium flow at 34 l/min. Carbon was always present in excess. The highest total conversion achieved with W as the starting material was 49.4%, of which 38.5% was W_2C and 10.9% WC. There was practically no difference in overall conversion between micron size and -325 mesh (-44 microns) tungsten particles. The highest conversion achieved for Ta powder (325 mesh size) was 43.3%, of which 30.0% was TaC and 13.3% Ta_2C . With WO_3 powder (325 mesh size), the three products of the reaction, W (43-81% conversion), WC (4-11% conversion), and W_2C (9-35% conversion) were formed in a total conversion of from 81-94%. Ta_2O_5 was converted to Ta (8-18% conversion), TaC (7-20% conversion), and Ta_2C (3-17% conversion), with the total conversion ranging from 18 to 42%. Al_2O_3 showed little conversion under similar reaction conditions with CH_4 as the carbon source.

Gilles and Clump (29) studied the reduction of iron ore

with hydrogen in a plasma jet using a reaction scheme similar to that of Stokes and co-workers. Reduction increased with increasing power input and by changing the ore size from the -200, +325 mesh to the -270, +325 mesh fraction. Reduction ranged from 33 to 69% with hydrogen plasma gas and from 6 to 42% with 25% H₂/75% Ar plasma gas. As evidenced by microscopic observation of the product, the conversion started at low reduction on the outside of the ore particles and penetrated deeper as the plasma energy increased. At high reduction, the product appeared as an agglomerate of very fine particles as small as 100 Å, which they attributed to mechanical breaking-up of the particles rather than vaporization and recondensation.

Gold et al. (31) of Bethlehem Steel Corporation, studied the feasibility of reducing iron oxide in an arc-heated gas mixture of hydrogen and natural gas at 100 kw and one megawatt levels. Pure molten iron was produced in the single-stage process with the net energy consumption as low as 1.2 kwhr/lb iron while the thermodynamic energy requirement was about 1.0 kwhr. Specific energy requirement was generally decreased by reactor scale-up from 100 kw to one megawatt, the use of finer ore particle size, and an increase in the natural gas/hydrogen ratio. The lowest gross energy consumption was 1.5 kwhr/lb iron which was achieved with the hydrogen/natural gas ratio of 2 at one megawatt level.

Bosch and de Vynck (19) report of preparing BN by injecting fine broken powder into a nitrogen or ammonia plasma

jet. They also produced B_4C by conveying powdered boron suspended in a propane-butane mixture into a hydrogen-argon plasma jet.

Wickens (76) reports of exploratory experiments for preparing B_4C by injecting into a plasma jet powdered B_2O_3 or $Na_2B_4O_7$ suspended in CH_4 and/or H_2 mixture. The attempts were futile and no reaction occurred.

Krzemu (44) explored the formation of silicone nitride from Si by injecting the metal powder into a nitrogen jet. Silicone nitrides of Si_xN_y type were formed with a total conversion ranging from 38-53%.

Westinghouse Electric Corporation (26) has developed an a.c. arc-heater, whose schematic is described briefly in Section 2.2.2. as it was used in the synthesis of acetylene from hydrocarbons, which allowed direct passage of powdered ore through the arc-zone for single-stage reductions of certain oxides, including iron, chromium, manganese, vanadium, and titanium. They reported that introduction of hydrocarbons to the arc-heater enhanced the reduction of ore.

* * * * *

The foregoing review indicates that many gas-solid metallurgical type reactions can take place in arc plasma jets with satisfactory yields. Refractory materials can react with gases in plasma jets to yield other desired refractory products, as shown in the preparation by Stokes et al. of carbides of tungsten and tantalum from the metals (W - m.p. 3370° , b.p. $5900^\circ C$; Ta - m.p. 2850° , b.p. $4100^\circ C$). Further-

more, the preparation of TaC from Ta₂O₅ and methane shows that the more complicated metallurgical type reactions that involve several steps can be carried out in good yields using a plasma jet.

2.6. Objectives

To investigate the feasibility of producing CaC₂ from the reaction of CaO with "nascent" carbons concomitantly produced upon the pyrolysis of hydrocarbons or from the rapid heating of a high volatile coal in hydrogen. Specifically, to perform the following:

Using methane as a carbon source, determine important process parameters and their quantitative effects on the formation of CaC₂ from the reaction of CaO with "nascent" carbon species; correlate them with the thermodynamics of the process and with the rather well-known mechanism of methane decomposition to construct a mechanistic picture of the overall process.

Use C₂H₄ in place of CH₄ and compare the results in view of differences in the C/H ratio and chemical and thermodynamic properties.

Use a high volatile coal in the reaction scheme and establish that coal can be as good a source of "nascent" carbon species as hydrocarbons for the formation of CaC₂. Evaluate the commercial potential of the reaction scheme.

It is hoped that detailed knowledge of the process mechanism of the present reaction scheme will provide an added bene-

fit of furthering the understanding of high-temperature gas-solid reactions that may rely on the extremely high reactivity of "nascent" chemical species for high conversions.

3. Apparatus and Procedure

3.1. Selection of Apparatus

The advantage of injecting reactants directly into the arc-zone rather than into the tail flame of an arc-heated auxiliary gas stream (alias a plasma jet) is obvious. Among several arc-discharge devices that allow direct passage of reactants through the arc zone (26, 28, 30, 62, 72), a d.c. rotating-arc reactor of the type used in the synthesis of acetylene from hydrocarbons by Du Pont and from coal by AVCO is chosen for the present study. It has rather well-established operational and mechanical characteristics that include high energy efficiency, arc stability, mechanical simplicity, ease of operation, and a comparatively large cross-sectional area of the interelectrode region which permits high throughput of feed through the arc zone.

It was decided that the rotating-arc reactor needs to be operated only one to three minutes to obtain products of truly a steady-state operation since the intrinsic reaction time may be in a range of 10^{-5} to 10^{-2} sec. Thus, the reactor is designed accordingly. Both electrodes are constructed of graphite and designed such that worn-out parts due to evaporation can be easily and inexpensively replaced after each run. Both graphite electrodes are held in position by water-cooled electrode holders to prevent excessive heating of other parts of the reactor.

The powder feeding device consists of a mechanically

vibrated powder-hopper which unloads powder onto a conveyor-belt which in turn carries it to a powder-chute located at the opposite end of the hopper. The powder-chute is the only outlet for the feed gas entering the powder-feeder box, and subsequently the powder is carried by the gas into the rotating-arc reactor. Powder feed rate is adjusted by manipulating the gap distance between the conveyor-belt and the bottom opening of the powder hopper. Solid as well as gas products are collected by a water-cooled quench probe comprising three concentric tubes. The innermost tube is a 1/4" o.d. copper tube.

3.2. Description of Apparatus

3.2.1. Details of the Rotating-Arc Reactor

3.2.1.1. The Head Assembly of the Rotating-Arc Reactor

Figure 3.1 shows the head assembly of the rotating-arc reactor which allowed passage of the reactants directly through the inter-electrode region. The cathode was 1/4" dia. and 1" long graphite rod, one end of which was threaded over the length of 1/4" for easy and secure insertion into the water-cooled cathode holder. The cathode holder consisted of a 1/4" o.d. and 5" long copper tube, one end of which was bonded by hard solder to a 1/4" dia. and 5/16" long copper rod, which was bored and threaded for adaptation of the threaded graphite cathode. An 1/8" o.d. stainless steel tube placed concentrically inside the cathode-holder divided

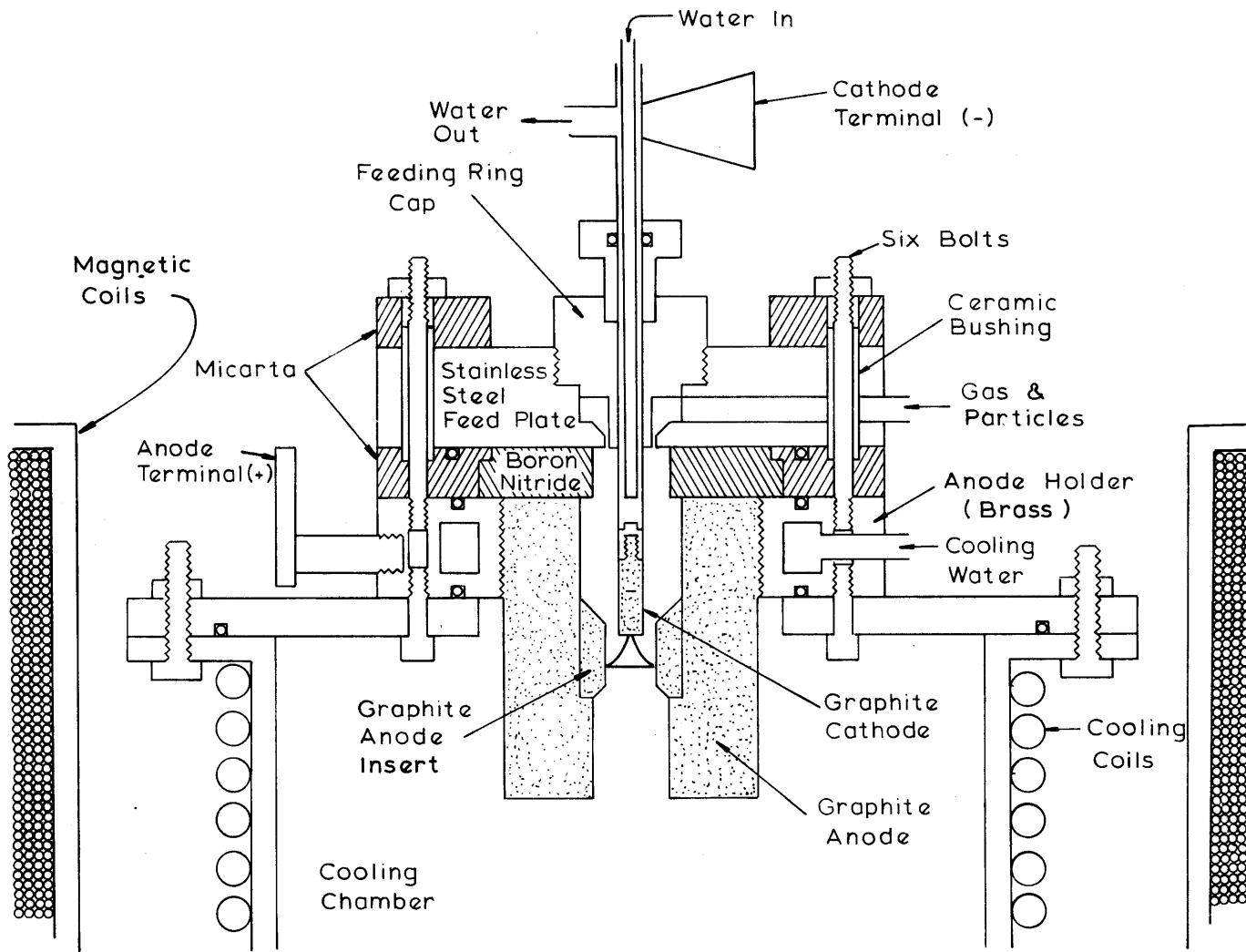


Fig. 3.1. Schematic of Rotating-Arc Reactor Head Assembly

the water flow which was normally flowing at 0.8 gal/min. The cathode assembly was inserted in the reactor through a 1/4" dia. hole located in the center of the stainless steel feeding-ring cap which contained a rubber O-ring for a gas tight seal while allowing easy sliding of the cathode holder.

The anode assembly for most runs consisted of a graphite anode-insert which slid into a graphite anode, which was in turn screwed into the water-cooled brass anode holder. The graphite anode-insert, which was discarded after each run, was 1" o.d. by 1/2" i.d. and 1" long. In order to streamline the gas flow, the upper portion of the insert was tapered off at 45° toward the axis. The lower portion of the inner 1/2" dia. opening was also conically expanded at 45°, starting 1/8" from the bottom; since the insert had a wall thickness of 1/4", this allowed 1/8" wide flat annular surface (1" o.d. by 3/4" i.d.) at the bottom to rest on the shoulder inside the graphite anode.

The graphite anode was in most cases a 3" long cylinder with 2-1/2" o.d. and 1" i.d., which extended 2" deep from the top and then narrowed to 3/4" i.d. to the bottom to hold the anode insert. The lower part of the graphite anode, which was the region immediately below the anode-insert, to be called the anode nozzle hereafter, served to insulate the high enthalpy stream emerging from the anode-insert from the cold ambient gas in the cooling chamber. In the case of a 3" long graphite anode, the anode nozzle was 1" long. In some cases longer residence times were provided for the high

enthalpy jet by using longer graphite anodes with extended anode nozzles. In all the cases the graphite anodes were constructed such that the anode-inserts were located at the same distances from the top. The schematic of various graphite anodes is shown in Figure 3.2a. Initially the insulation zone of all graphite anodes had a uniform diameter of 3/4". Later, in order to minimize the effect of solid deposits on the walls of the insulation zone and to provide a longer residence time for a given anode length, the 3/4" diameter insulation zones of the graphite anodes longer than 3" in overall lengths were enlarged to 1" in diameter, starting 1" from the bottom of the anode-insert to the end. In most cases, the solid deposits on the walls of the insulation zones ranged from 1/32" to 1/16" in thickness after 90 seconds of reactor operation. Usually the solid deposits seemed to have fused and formed a hard crust but came off the wall fairly easily. However, in a few cases of coal runs melting of the solid deposits were so extensive as to actually drip down.

The graphite anode was screwed into a brass water-cooled anode holder which was 1" long and 5" o.d. by 2-1/2" i.d. Water was circulated through the latter at 2.5 gal/min. It was in turn mounted in the middle of an annular stainless steel plate which was 10" o.d. by 3" i.d. and 1/4" thick, and which doubled as the top cover for the cooling chamber.

The graphite anodes were quite simple and inexpensive to construct, and were sturdy enough to withstand the ex-

tremely severe thermal, as well as chemical, conditions necessarily imposed by the nature of the experimental requirements, at least for the duration of a run which used to last no longer than two minutes. They also proved to be very versatile in arriving by trial-and-error at the present anode-throat diameter of 1/2"; any throat diameter larger than 1/2" required too high an arc voltage for the power supply and hence gave poorer arc stability.

Although the graphite anodes worked amiably well in methane and ethylene series runs, they posed a major problem in coal series runs, i.e., in those runs the feed particles fused in the pre-interelectrode region of the anode before reaching the arc zone, resulting in substantial particle hold-up in the region and in some instances even to the feeding line.

In order to eliminate the hot surface on which the particles fused, a water-cooled copper anode was constructed and operated with some degree of success for a number of coal runs, as well as a few methane and ethylene series runs. Figure 3.2b shows the schematic of the water-cooled copper anode, which was built in overall dimension exactly the same as the 3" long graphite anode fitted in the brass anode-holder. Water was circulated through the anode at 3 gal/min. All the parts except the copper anode itself were made of brass. The copper anode was made from a 7/8" dia. by 3" long copper rod, which was bored to 3/4" dia. throughout except at the throat, which was 1/2" both in diameter and

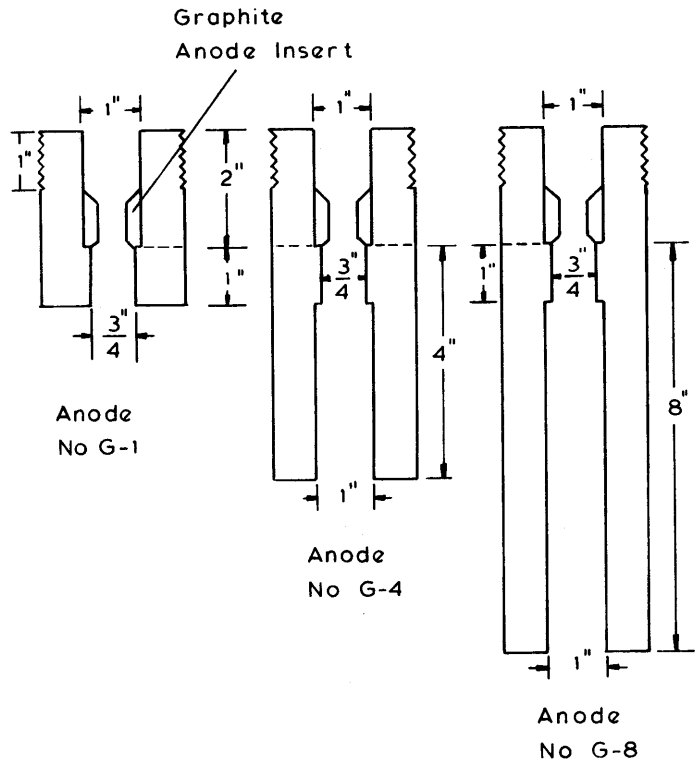


Fig. 3.2a Schematic of Various Graphite Anodes

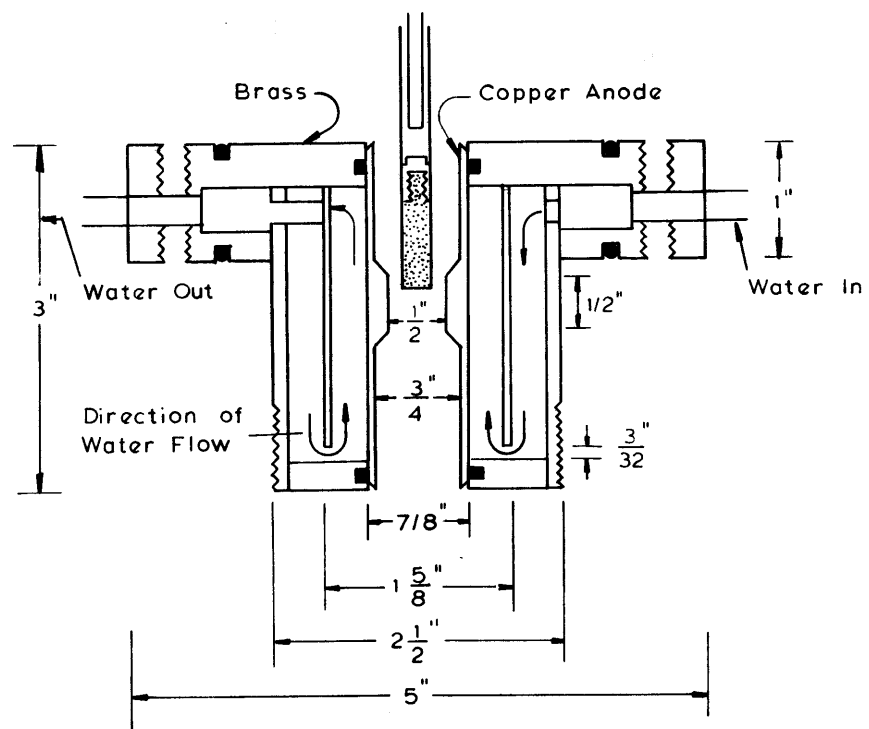


Fig. 3.2b Schematic of Water-Cooled Copper Anode

length; by placing the cathode tip 1/8" deep into the 1/2" dia. throat, it was possible to establish an arc only between the two and prevent arcing at the cathode holder, which would have melted it. Water tight seals for the copper anode were provided by the two O-rings at both ends of the anode sleeve. In order to provide longer residence times in some runs, the bottom part of the outer shell of the anode assembly was threaded so as to adapt graphite cylinders of different lengths with 2-1/2" o.d. by 1" i.d.

The water-cooled copper anode completely eliminated the solid build-up in the pre-interelectrode region of the anode; nevertheless, it posed great experimental difficulties by burning out too frequently. The burn-outs frequently occurred at the bottom extreme. In some cases the arc was found to have attached to a point beyond the anode-throat and burned a hole there.

The reactants (gas and solid) were fed into the arc zone through a 1/32" wide annular slit (1/2" o.d. by 7/16" i.d.) in the bottom of the feeding ring which was 1/4" deep and 1" o.d. by 7/16" i.d. The feed line, which was a 1/4" i.d. hole bored through the stainless steel feed plate, entered the feeding ring tangentially in the counter-clockwise direction; therefore, the reactants consequently entered the arc zone swirling more or less in the same direction. The stainless feed plate, which housed the feed line and the feeding ring, was 5" o.d. and 1" high. The inside of the feeding ring could be visually inspected for any powder

hold-up by unscrewing the feeding ring cap, which constituted the top and inner walls of the former; this feature also allowed easy access to and visual inspection of the cathode assembly, which consisted of the graphite cathode screwed into the water-cooled cathode holder, after each run, because it was held in position through the center of the feeding ring cap and hence came right out of the arc head assembly upon unscrewing. Without this feature the arc head assembly would have to be dismantled after each run for access to the graphite cathode, for during a run, it invariably grew radially by carbon deposition on the side and could not be pulled out of the feeding ring cap without breaking it.

The anode assembly was electrically separated from the stainless steel feed plate, and hence from the cathode assembly, by the 1/2" thick insulator ring which consisted of a boron nitride ring of 3" o.d. by 3/4" i.d. fitted inside a micarta ring of 5" o.d. by 3" i.d. The insulator of this design provided a good electric insulation while withstanding the high temperature of the graphite anode and the exposure to the severe operating conditions of the interelectrode region.

Both the insulator ring and the stainless steel feed plate were clamped to the brass anode-holder by six bolts. Since the bolts were directly screwed into the anode-holder, they had to be insulated from the feed plate with ceramic bushings. The annular seat of micarta for the nuts on the top of the feed plate further provided the necessary insula-

tion for the bolts.

3.2.1.2 Magnetic Coils

The arc column was rotated very rapidly by an axial magnetic field provided by a solenoid placed concentrically outside the reactor shell near the arc-head assembly. Such high speed rotation was possible because the axial magnetic field interacted with the arc column which was in radial direction to produce a force perpendicular to the plane of the field and arc; and thus the force induced the rotation of the arc. The magnitude and direction of the force acting on the arc column is given by the relation

$$\vec{F} = \vec{I} \times \vec{B}$$

where \vec{I} is the arc current and \vec{B} is the magnetic field vector.

The magnetic field strength required to make the arc rotate was estimated from the above formula by applying Newton's second law to equate the centrifugal force to the force generated in the magnetic force (see, for example, 35). This gives the following relation:

$$B = \frac{1.35}{r} \sqrt{V}$$

where B is the required field strength in gauss, r corresponds to the gap spacing in inches between the electrodes, and V is the arc voltage. Blanchet (16) also made a similar calculation to estimate the required field strength for his

high intensity arc reactor. For an arc operating at atmospheric pressure, the actual r.p.m. is of course much lower than the value that can be estimated from the above equations due to the collisions of electrons with gas molecules and the aerodynamic drag of the arc column (13).

The rotating-arc reactor had a gap space of 1/8" between the electrodes and operated in H₂ and CH₄ with an arc voltage typically in the range of 60-120 volts. Therefore, according to the above formula, the magnetic field strength should be in the range of 80-120 gauss.

The field strength of B of a solenoid can be calculated from the equation

$$B = \mu_0 i_0 n$$

where μ_0 is the permeability constant in Ampère's law, i_0 is the current in the solenoid, and n is the number of turns per unit length. Although the equation was derived for an infinitely long ideal solenoid, it holds quite well for actual solenoids for internal points near the center of the solenoid. For an actual solenoid,

$$B = 1.26 i_0 N/l$$

where N is the total number of turns, and l is the solenoid length in cm.

The solenoid was initially made of a total of 126 turns of No. 15 enameled copper wire wound in two layers over a length of 8" along a 12" o.d. x 11-1/2" i.d. plexiglass

cylinder. The total resistance of the solenoid was 3 ohms. The measured field strength of the solenoid at its axis was 56 gauss at a current of 7 amp. with an accompanying voltage drop of 21 volts, which agreed very well with the calculated value of 55 gauss.

In order to increase the magnetic field strength two more layers of the magnetic coil were wound on the existing solenoid and connected in parallel to the former. Thus the field strength exactly doubled while the potential drop across the solenoid remained the same as before. In all reactor operations the current in the solenoid was set at 13 amp. with the accompanying voltage drop of 20 volts. The magnetic flux thus produced was calculated to be 102 gauss and measured to be about 120 gauss at the reactor axis. The higher than theoretical value was due to the presence of the reactor shell which was made of iron; the elementary atomic dipoles in the iron lined up with the applied field B, thereby setting up their own field of induction and thus enhancing the field strength.

3.2.1.3. Reactor Shell: Cooling Chamber

Figure 3.3 shows the overall schematic of the rotating-arc reactor assembly. In this reactor the high enthalpy jet emerging from the anode nozzle was quenched in the cooling chamber which consisted of a carbon steel pipe of 7" i.d. and 24" long wrapped by four 3/8" o.d. copper coils which were soft-soldered onto it. The four coils were connected in

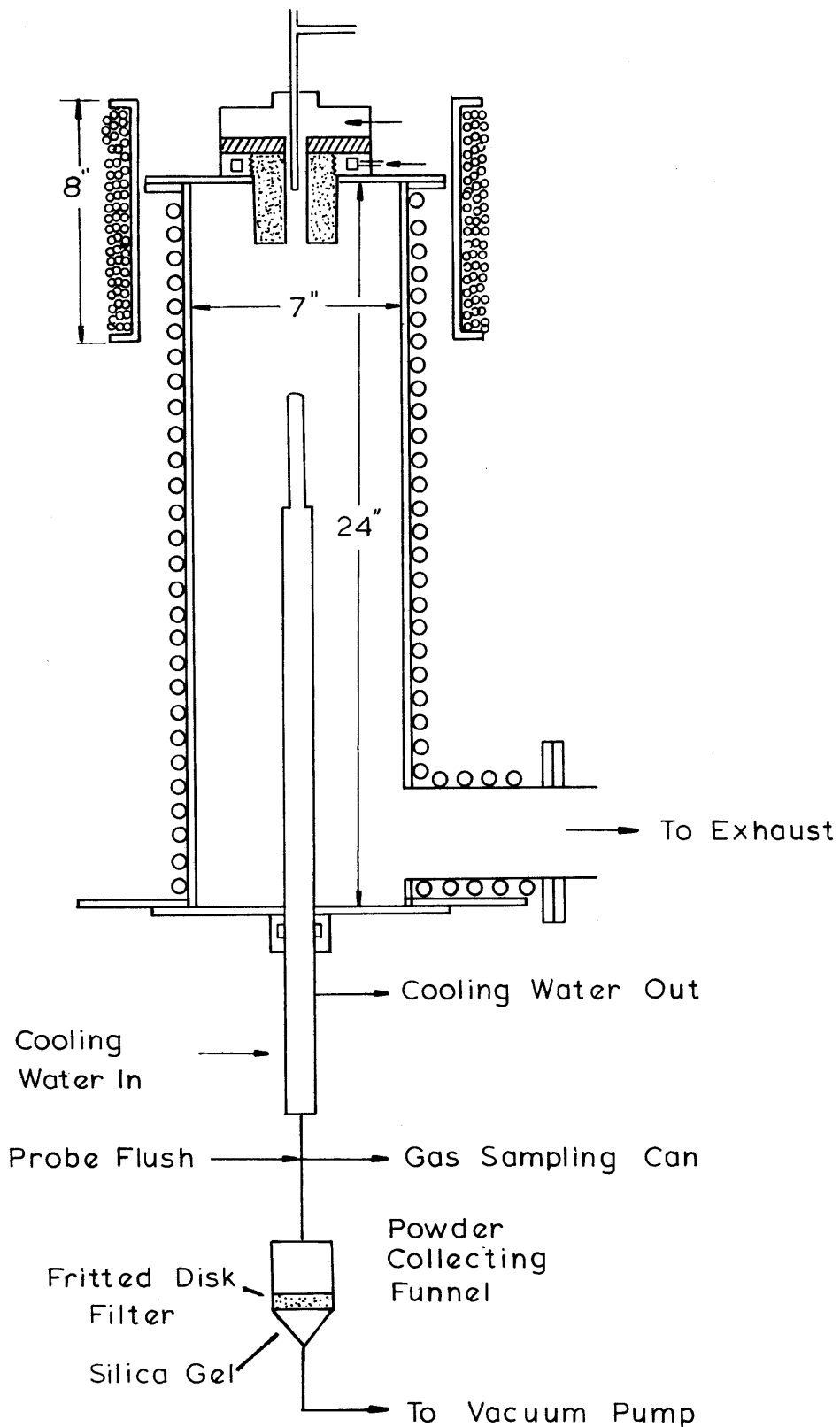


Fig. 3.3 Simplified Overall View of the Reactor

parallel to reduce the pressure drop across the lines and thus enable circulation of 12 gal/min directly from the city water line without the aid of a water pump.

The cooled exhaust gas from the reactor was removed of particulate matter before being piped to the exhaust duct for the ventilation hood installed above the reactor assembly. The exhaust duct directly led to the roof of the building.

3.2.1.4 Quench Probes and Sample Collecting System

Two quench probes of different lengths were used to quench and collect samples of both the gas and solid products. Essentially both probes consisted of 1/4" o.d. copper tubes jacketed by 1" o.d. copper tubes, with 5/8" o.d. tubes in the middle to divide the water flow. The longer probe was 27" long and the shorter 15". Both probes were inserted through the center-hole of the bottom cover of the cooling chamber and positioned to various distances from the anode nozzle.

In order not to block the gas flow when placed close to the anode nozzle, the inlet portion of the longer quench probe was fitted over the length of 3" with smaller outer (5/8" o.d.) and middle (7/16" o.d.) tubes. With this design it was possible to directly connect it to the city water line and still circulate 4 gal/min of cooling water, thus eliminating the need of a water pump; were the outer tubes 5/8" o.d all the way to the water inlet, the pressure drop would have

been so great that a water pump would have been needed to provide an adequate water flow. The end caps joining the outer and the inner tubes were made of copper and the connections were arc-welded, which performed well up to 2" from the anode nozzle; initially the end cap for the longer quench probe was made of brass, but it melted at a distance of 2-1/2" from the anode nozzle.

During a run the sample probe was kept purged all the time with 2 l/min of N_2 , except the sample collecting period itself, to ensure collecting samples representative of a steady state operation; this also prevented plugging of the probe before a sample was withdrawn. The solid product was collected in the solid sampling funnel which was equipped with a fritted disk filter. The funnel was dessicated all the time with silica gel placed in the space below the filter. A vacuum pump attached downstream of the funnel ensured a gas flow equivalent to 20 l/min of H_2 through the quench probe during the sample collection period.

The gas product was sampled in an initially evaluated sampling can which was connected to the quench probe via a normally closed solenoid valve. The gas entering the sampling can was freed of particulate matter with loosely packed glass wool placed in the line between the quench probe and the solenoid valve. The sampling can was 322 ml in total volume and was equipped with a septum port through which the gas sample could be withdrawn by a gas syringe. The gas products were analyzed only for hydrocarbons with a

Hewlett-Packard flame ionization detector unit, model 700.

3.2.2. Powder Feeding Device

Figure 3.4 shows the schematic of the powder feeder box which was successfully used throughout the experiments. The device essentially consisted of a motor-driven loop of 3" wide belt which conveyed powders loaded onto it from a 350 ml glass powder funnel into the powder feeding line. Two 2-1/2" dia. aluminum rollers separated by 9" from center to center supported the belt-loop. A metal plate placed underneath the belt between the rollers prevented it from sagging in the middle. The belt-loop was driven by an electric motor (torque: 7 lb-in) connected to the shaft of one of the two rollers. The motor rotated at 9.6 r.p.m.

The powder funnel was rebuilt from a commercially available glass powder funnel of 200 ml capacity by fusing 1" long glass cylinder on top of it for added capacity. The slope angle of the powder funnel was 15°, and the bottom opening was 5/8" in diameter. It was secured to a rack and pinion type gear to adjust the gap between the belt and the bottom opening of the funnel. To prevent channeling and aid the flow of powders, the funnel was vibrated with an electric vibrator. Although the powder feed rate could also be varied by varying the intensity of vibration as well as by changing the belt speed, it was satisfactorily accomplished in most cases simply by adjusting the gap height of the bottom of the funnel above the belt conveyor.

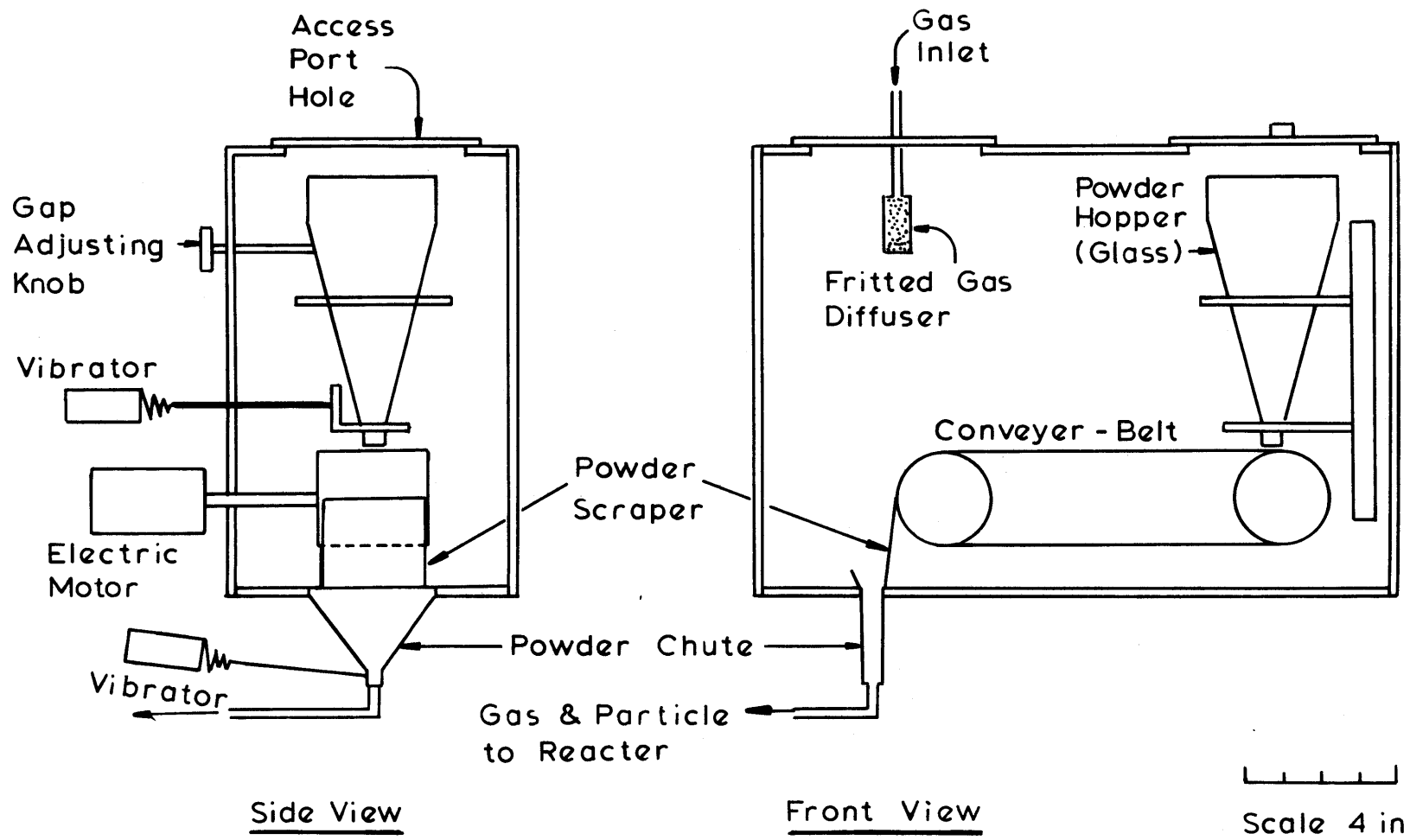


Fig. 3.4 Schematic of Powder Feeder Box

The belt-conveyor system and the powder funnel assembly were encased in a box which was constructed of 1/4" thick brass plates. The box was 17" side, 12" high, and 7-1/2" deep. In order to observe consistency of the powder feeding, one side (17" x 12") was covered with a 1/2" thick plate of plexiglass. The motor, the vibrator, and the knob for adjusting the funnel height were all placed outside the box by making necessary connections through O-rings. Two 4-1/2" dia. ports on the top of the box allowed easy access to the inside for cleaning and replenishing of the powder funnel. The covers for both ports were equipped with O-rings for a gas tight seal. The cover on the top of the powder funnel was equipped with a special 3/8" o.d. tube fitting to allow a limited access to it. The other cover contained a 1/4" o.d. tube fitting on the outside and a fritted gas diffuser on the inside through which gases were introduced into the box without blowing off particles.

The powders carried on the belt conveyor were dropped off into the powder chute located at the foot of the roller which was on the opposite side of the powder funnel. The powder chute was 3-1/2" across and 1/2" wide at the mouth, and was triangular in shape when viewed from the front of the belt conveyor and rectangular from the side. The powders were scraped off from the belt and directed into the chute by a thin metal plate leaning against the roller from below. The apex in the bottom of the powder chute was equipped with a fitting for the 3/8" o.d. powder line; since it was also

the only outlet for the gas which entered the box, the powders were pneumatically conveyed through the powder line to the reactor. The powder chute was vibrated with a vibrator to prevent sticking of particles on the inside walls.

Replenishing of the powder feeder box was accomplished by first filling the powder hopper with the highly hygroscopic solids inside a moisture-free isolation box, followed by sealing of its top and bottom openings with plastic films before transferring it into the powder feeder box. Once seated inside the box, the hopper was removed of the plastic film from its bottom and the cover was quickly closed. In the meantime about 5 l/min of argon flow was maintained into the box to drive out any moisture-laden air. (Note: Since the box, which now was completely closed except at the gas inlet, was made of plexiglass on one side and hence could not withstand too high a pressure, the inlet pressure of argon was always kept below 5 psig.). Finally, in order to equalize the pressure inside the powder hopper with that of the box, the plastic film covering the top of the former was punctuated with a rigid wire through the special fitting in the cover, located right above the hopper.

Calibration of the powder feeding was accomplished by presetting the gap height of the bottom of the funnel above the belt conveyor and then collecting the powders for one minute (or one-half minute at high feed rates, i.e., 20 gm/min or higher) in a 250 ml flask attached to the powder chute. In order to facilitate the powder flow into the flask

while keeping moisture-laden air out, 5 l/min of argon was introduced into the powder feeding box and thence to the flask during the calibration; the gas entering the latter was vented to the atmosphere through a fritted gas diffuser to prevent any incidental loss of particles by entrainment. The whole procedure was repeated until the desired feed rate was attained.

The powder feeder of this design performed very satisfactorily in most cases and provided essentially constant powder feed rates up to 50 gm/min. Checking the powder feed rate after each run showed that it used to vary by no more than 8%. The singular factor which caused the most significant variation in powder feeding was the level of the powder in the funnel; when the volume of the powder left in the funnel was less than 1/4 of the total capacity, the powder feed rate occasionally changed by as much as 50% at high rates of powder feeding (20 gm/min or higher). In the experiments, all the runs with variations higher than 15% were discarded; if the variation was less than 15%, but higher than 5%, an average was used for the powder feed rate; if the variation was 5% or less, the first calibration result was used.

3.2.3. Power Supply and Auxiliary Equipment

Power to the arc was provided by a Miller welding power supply, model SR-1000B1, which had an open circuit voltage of 160 volts and was capable of delivering up to 40 kw to

the electrodes. The power supply had a falling voltage vs. amperage characteristic which allowed in principle some reasonable variations in arc length or arc voltage with relatively minor changes in arc current. Although the open circuit voltage of a power supply has little relationship with arc voltage which is largely determined by arc length under a given operating condition, it is desirable for the former to be at least twice the latter for the reason of arc stability. Therefore, the selection, or availability, of a power supply usually dictates the gap distance between the electrodes, even though it may have to be found by trial-and-error.

The output power of the power supply was controlled by the current control, which varied essentially the slope of the volt-ampere curve pivoted at the open circuit voltage; this made both the arc voltage and arc current change because of shift of the intersection of the power supply characteristic and the arc characteristic. During a reactor operation the power supply was operated from the control panel by using a remote current control and a remote contactor control switch which energized and de-energized the electrodes. The power input to the arc was measured by a 200 volt voltmeter and a 500 amp ammeter.

The arc was started and stabilized by using a Miller high frequency unit, model HF-15-1, which was placed in series with the power supply. The output power of the unit was only 180 watts, which amounted to less than 2% of the electrical

power into the arc. The unit was not powerful enough to establish a high frequency discharge in gases other than argon or helium in the present reactor design. Therefore, in order to start arc, the high frequency discharge was first established in argon. As soon as the h.f. discharge was established, the remote contactor control of the power supply was closed to deliver direct current to the electrodes and thus to initiate arc. Afterwards, argon was turned off and the main arc gas was turned on, and the normal reactor operation was assumed.

Power to the magnetic coils was furnished by a small d.c. power supply which was capable of delivering up to 15 amperes in the range of 0-25 volts. In reactor operation the direct current passing through the magnetic coils was set at 13 amperes with accompanying voltage drop of 20 volts. The magnetic flux thus produced was measured to be about 120 gauss at the reactor axis.

3.2.4. Layout of the Experimental Apparatus

Figure 3.5 shows the layout of the experimental apparatus, and Figure 3.6 exhibits photographs of the reactor area and the control panel.

In all cases, the whole sequence of the reactor operation was automated by using a timer (Eagle Signal model TM-10-A6-10-01), which could actuate up to 10 circuits individually, and which was connected with the power supply, high frequency unit, vacuum pump, powder feeding mechanism, and

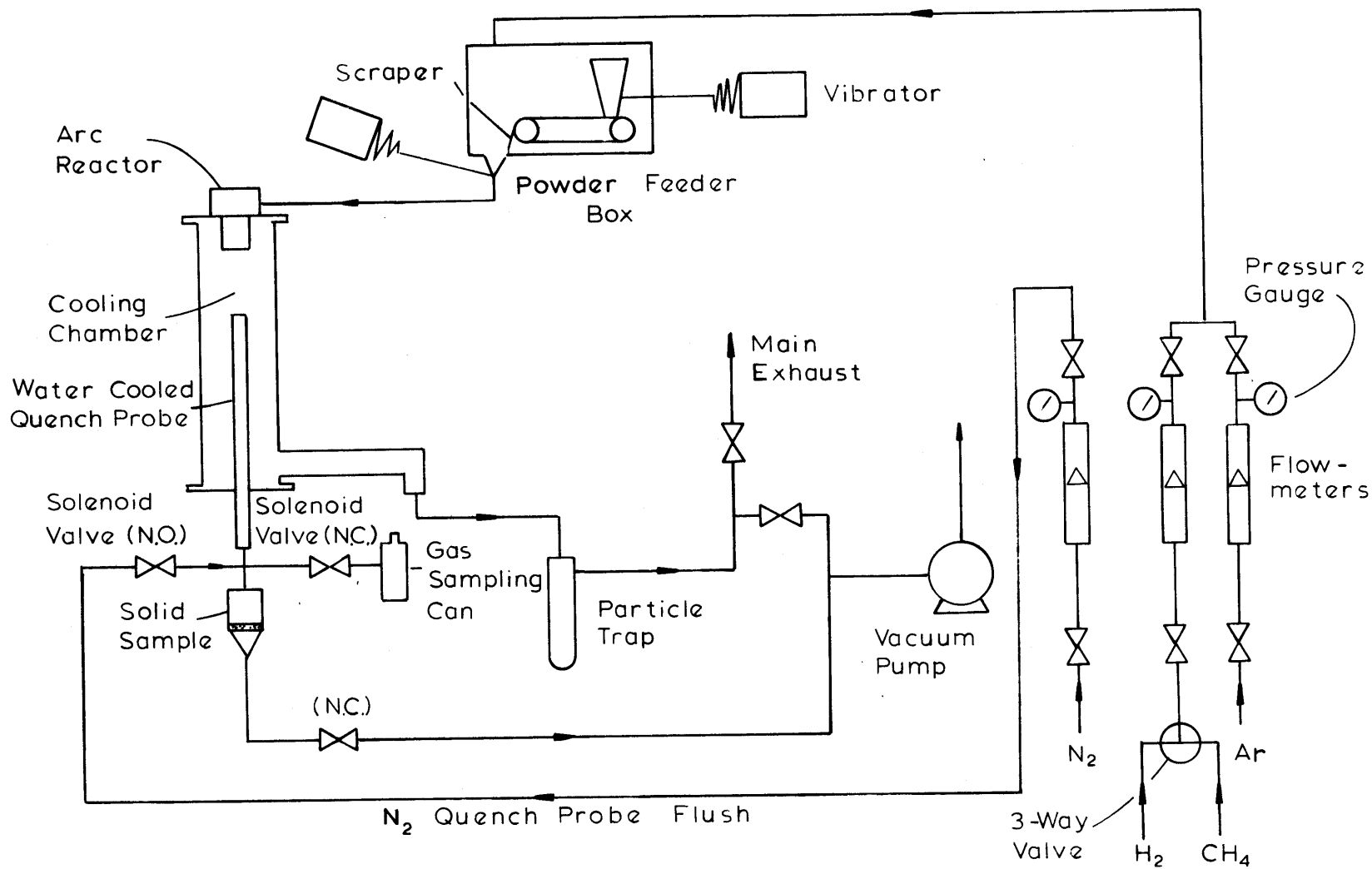
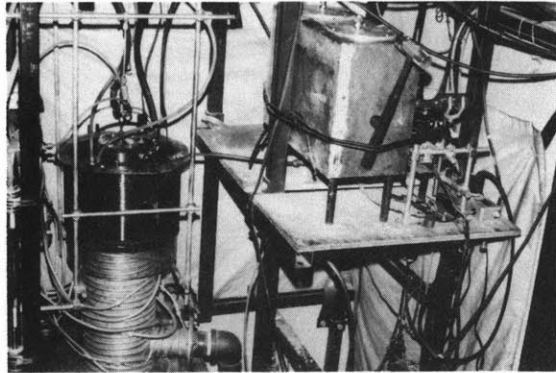
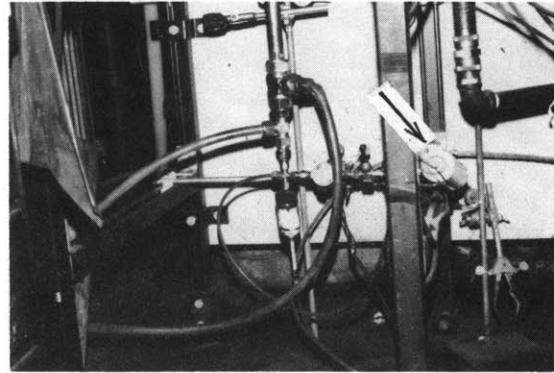


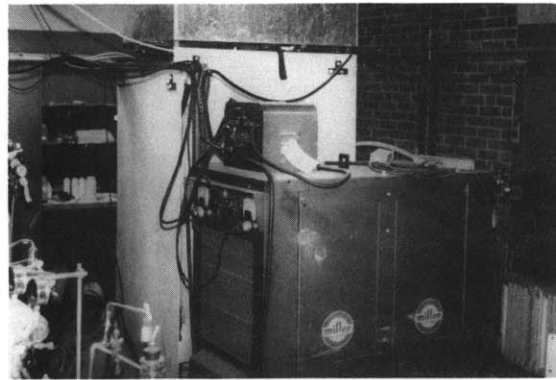
Fig. 3.5 Layout of Experimental Apparatus



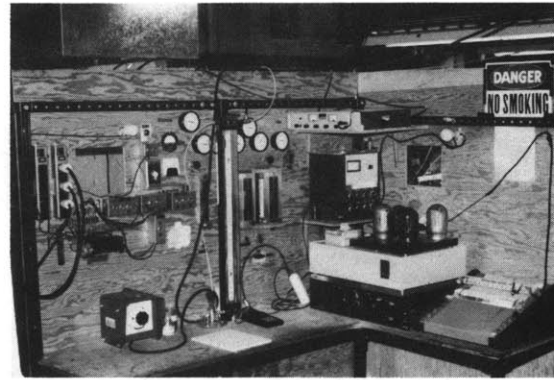
(a) View of the reactor area. At left, the rotating-arc reactor with arc-head assembly, magnetic coils, copper tube wrapped reactor shell, and main exhaust. At upper right, powder-feeder box.



(b) View of sample collection system at the reactor bottom. Solid sample collection funnel is attached to the end of the water-cooled quench probe along with probe purge gas line (on the left) and gas sampling system (on the right) consisting of a solenoid valve and an evacuated can (arrow).



(c) View of main power supply with high frequency unit placed on top. In rear, reactor area covered with explosion shields with ventilation hood above.



(d) View of control panel. At left, remote current control on the bench and, above it, a timer for process control. Gas chromatograph unit and d.c. power supply for magnetic coils are shown on the right.

Fig. 3.6 Photographs of Reactor Area and Control Panel

the various solenoid valves of the sample collection system. The reactor operation was usually limited to 90 seconds from the establishment of arc at desired power level, during which the operator could pay his entire attention to reading the somewhat fluctuating arc voltage and current as the other procedures were automated with the timer.

Because of explosion hazards, the reactor area was physically separated from the control area. The reactor assembly was placed in the corner of the room, and the two sides of the reactor area which were facing the open space of the room were barricaded by 1/4" thick free-swinging asbestos panels with bomb-blankets lining the insides for added protection. A ventilation hood was installed above the entire reactor assembly through which about 500 ft³/min of air was continuously removed for possible leakage of H₂ or other flammable gases.

3.3 Procedure of Reactor Operation

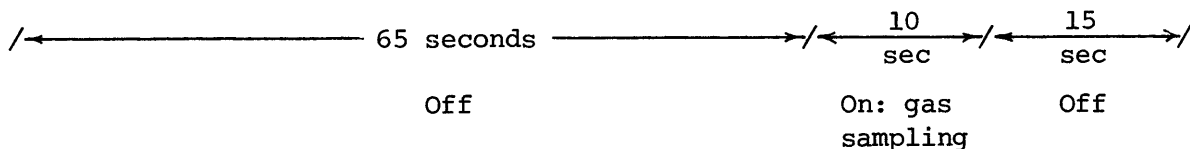
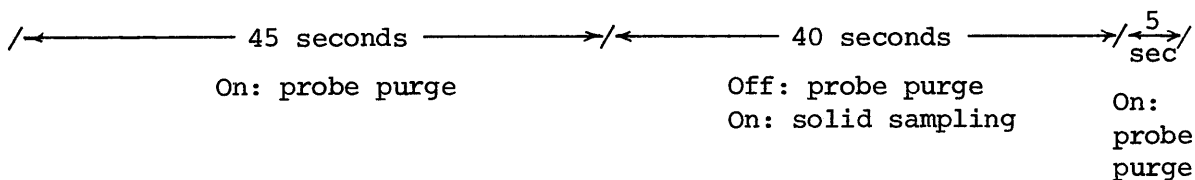
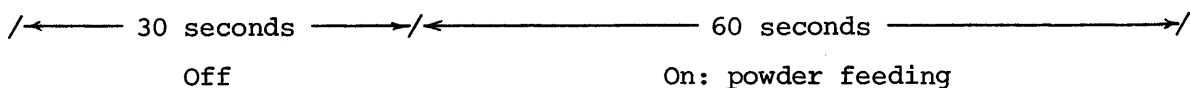
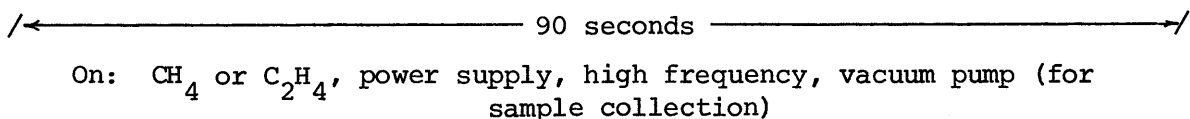
3.3.1. Preparation of Reactor

Preparation of an experiment always started with selecting one of the two timer schedules shown in Table 3.1, depending on whether the reactant gas was methane (or ethylene) or hydrogen. In the coal series runs powder feeding started 10 seconds from the initiation of the timer cycle instead of the usual 30 seconds for the methane or ethylene series runs; this prevented excessive erosion of the graphite electrodes owing to the suppressing effect of the volatilized carbon

Table 3.1

Timer Schedules for Reactor Operation

Timer Schedule I (for CH₄ or C₂H₄ series runs):



Timer Schedule II (for coal series runs)

Identical to Schedule I, except powder feeding which starts 10 seconds after actuation of timer.

from coal.

After the selection of a timer schedule the powder feeder box was serviced and adjusted for a desired powder feed rate, following the procedure outlined in the section Powder Feeding Device. To keep moisture-laden air out while servicing the box, it was always provided with a positive flow of argon by maintaining the inlet pressure at 3 psig. The volume of powder in the powder hopper was always kept above 1/3 of its total capacity to ensure a constant powder feed rate. The outlet of the powder feeder box was kept closed and was not connected to the reactor until the following procedures were taken.

The head assembly of the rotating-arc reactor was completed by positioning the tip of the graphite cathode 1/8" deep into the 1/2" dia. anode throat. The cathode and anode holders were always inspected for any sign of water leakage before they were assembled.

The product sampling system was prepared by positioning the quench probe through the center of the bottom plate at the desired quench distance from the anode nozzle exit and then making all the necessary connections, such as cooling water lines, quench probe purge line, and gas and solid sampling systems. The solid collecting funnel was dessicated all the time with the silica gel powders placed in the lower chamber below the fritted disk filter. The gas sampling can was under 29.5" Hg of vacuum or less. The line connecting the solenoid valve for the gas sampling can to the quench

probe was loosely packed with glass wool to filter particles out.

Circulation of cooling water for the cooling chamber, quench probe, cathode and anode holders, was then started and checked for any water leakage. The water circulation rates were: cooling chamber, 12 gal/min; quench probe, 4 gal/min; cathode holder, 0.8 gal/min; and anode holder, 2.5 gal/min.

Next, the reactor assembly was completed by connecting the powder feeder box to the powder feeding line of the reactor; prior to the connection the quench probe was started and purged with 3 l/min N_2 to keep any lime particles from depositing into the quench probe.

The last step of the reactor preparation consisted in setting the main gas (i.e., H_2 , CH_4 , or C_2H_4) at a desired flow rate, followed by shutting off all the gas flows to the reactor and closing the main exhaust line valve and then replacing the air in the reactor assembly with argon (and N_2) by alternating between 10" Hg vacuum and 3 psig. three times. The quench probe was always purged with N_2 whenever there was an argon flow into the reactor because of possible entrainment of lime particles in the gas which was passing through the powder feeder box. Afterwards, the main exhaust line valve was open, the quench probe purge was started, and the argon flow was adjusted to 15 l/min in preparation for the ignition of arc.

3.3.2 Operation of Reactor

Just before the reactor operation the gas sampling can was checked and evacuated again if necessary to keep the vacuum at 29.5" Hg or less. The timer was then reset, the d.c. power supply for the solenoid was turned on, and the remote current control of the welding power supply was turned down to the minimum setting to prevent excessive heating of the electrodes when the arc was initiated in argon.

The arc was started in argon by switching on the high frequency unit to establish a high frequency discharge between the electrodes and then closing the remote contactor control of the power supply to deliver d.c. power to the electrodes and thus to initiate arc. The arc voltage and amperage were usually 30-40 volts and 40-55 amperes at this stage. After establishing the arc, the main gas was turned on and the argon flow was turned off. As the main gas was replacing the argon in the powder feeder box, the arc voltage started rising and the arc current falling.

In order to prevent extinguishing of the arc during the transition period, the remote current control of the power supply was slowly turned up such as to keep the arc current above 50 but below 200 amperes to minimize erosion of the electrodes prior to assuming normal reactor operation. In general, an arc voltage randomly fluctuating between 70 and 150 volts marked complete replacement of the argon with the main gas in the powder feeder box, which occurred in most cases after two or three minutes from the switching of argon

with the main gas. The current control was then set to the predetermined setting in an attempt to provide a desired power input to the arc; nevertheless, it was often difficult to maintain the power input at a desired level because of arc instability encountered in many cases. Once the arc was established at a desired power level, the prescheduled reactor operation was started by starting the timer cycle.

Normally the arc voltage was in a range of 70-110 volts in methane, 65-100 volts in ethylene, and 80-130 volts in hydrogen when the arc current ranged from 80 to 300 amperes. Interestingly the arc voltage dropped upon commencement of powder feeding to a range of 60-85 volts in methane, 55-70 volts in ethylene, and 60-85 volts in hydrogen with commensurate increase of the arc current to a range of 130-360 amperes. These phenomena were obviously caused by the ionization of some calcium vapors present in the arc zone. Care was always taken to keep the arc current below 350 amperes; otherwise, the graphite cathode evaporated away very rapidly, resulting in melting of the water-cooled cathode holder before the end of the scheduled run.

After the timer cycle was started, the arc voltage and amperage, both of which were fluctuating very rapidly over a relatively wide range when the arc was unstable as encountered in many cases, were recorded in 6-8 second intervals by reading off the voltmeter and ammeter. Both the arc voltage and amperage were read simultaneously in each reading in order to calculate the instantaneous power input, from which the

average power input was calculated.

3.4. Materials

Two different types of CaO were used in the present study. One is reagent grade CaO manufactured by Mallinkrodt, Inc., whose particles were typically less than 8 μ in size as observed under an optical microscope. The other is a calcine of high purity natural calcite obtained through the courtesy of Pfizer, Inc. from its mine at Adams, Massachusetts. The chemical composition of the natural calcite was: 95% CaCO₃, 1.5% MgCO₃, 1.9% SiO₂, 0.4% Al₂O₃, 0.1% Fe₂O₃, and 0.2% moisture. Two different particle sizes of the calcine were obtained by calcining the natural calcites of -200 and -325 mesh sizes at 1000°C for 10 hours or longer. In the -200 mesh calcite, 16% by weight was above 325 mesh size; in the -325 mesh size, 76% by weight was above 7.5 μ in particle size. The calcines revealed little change in particle size from the original limestones when viewed under either an optical or a scanning electron-microscope.

Commercial grade methane (i.e., compressed natural gas) was obtained from Airco, Inc.; its hydrocarbon contents were 95.6% CH₄, 1.8% C₂H₄, and 0.3% C₃H₈, as analyzed by a flame ionization detector. Because of the presence of both C₂H₄ and C₃H₈, total carbon content of the natural gas was equivalent to that of almost pure methane. Ethylene was 99.9% pure and obtained from Matheson Gas Company.

The high volatile bituminous coal used in the present

study was from the Ireland Mine (Consolidation Coal Company). Its characteristics are shown in Table 3.2.

3.5. Analytical Procedure of Products

3.5.1. Analysis of Solid Product

The solid sample collected in the sampling funnel was analyzed for the CaC_2 content indirectly by measuring the acetylene evolved upon hydrolysis by using a flame ionization detector. The first step of the procedure consisted of transferring about 5-30mg of the solid sample from the sample collecting funnel to a 50 ml flask and closing it with a rubber stopper equipped with a special fitting containing a septum port. Initially it was done in the open air, trying to keep the exposure time at 15 seconds or less. Nevertheless, the solid product CaC_2 was in such a fine particulate form that it was found to deteriorate very rapidly by reacting with the moisture in the open air. It was also found to oxidize fairly rapidly at room temperature, to decompose to CaO and carbon in the presence of oxygen. Therefore in the later part of the study the samples were handled in a glove bag filled with N_2 .

The flask was then injected through the septum port of 1.0 cc C_2H_6 as an internal standard and then of 5.00 cc of distilled water as quickly and evenly as possible to avoid developing locally hot spots. In a few cases of high conversion, the sample incandesced even under N_2 and explosively so under air during the water injection. The gas inside the

Table 3.2

Characteristics of Coal Used in the Present Study
(Pittsburgh Seam #8, hvA-b)

Proximate Analysis

<u>Characteristic</u>	<u>As Received</u>	<u>Dry</u>	<u>d.a.f.</u>
moisture	2.2	-	-
volatile matter	40.7	41.6	46.7
fixed carbon	46.3	47.3	53.3
ash	10.8	11.1	-

heating value: 14,377 BTU/lb d.a.f.

Ultimate Analysis

<u>Component</u>	<u>As Received, % by wt</u>
carbon	67.81
hydrogen	5.03
nitrogen	1.05
sulfur	4.83
oxygen	8.55 by difference

flask was then quantitatively analyzed for C_2H_2 and C_2H_6 by using a flame ionization detector (Hewlett-Packard Series 700). The gas chromatograph column was 1/8" o.d. x 3 ft long and was packed with 80/100 mesh Poropak N. The column temperature was 40°C and the carrier gas was helium flowing at 40 ml/min. The calibration gas was prepared just prior to the analysis by blending in a gas tight 50 ml flask 1.0 ml C_2H_6 and between 1.0 ml and 5.0 ml C_2H_2 , depending on the anticipated C_2H_2 volume in the sample flask.

Next, the total calcium content in the hydrolyzed sample was determined by first dissolving it in HCl, and then filtering and titrating the filtrate with 0.02 M EDTA at pH 12.5, following the method of complexometric titration outlined in (65). The indicator used in the titration was hydroxynaphtol blue.

Since all the calcium in the product should have existed as CaO before the reaction, the percentage of the total calcium which existed as CaC_2 in the sample also represented the percentage conversion of CaO to CaC_2 , i.e.:

$$\% \text{ CaO Conversion} = \frac{N_{CaC_2}}{N_{Ca}^O} * 100$$

where N_{CaC_2} = number of moles of CaC_2 , $N_{CaC_2} = N_{C_2H_2}$

N_{Ca}^O = number of moles of Ca, equivalent to CaO before the reaction.

The analytical method outlined above for determining CaO conversion was fairly accurate and gave a deviation of 2% or

less when the sample was handled in a glove bag filled with N_2 . When the sample was handled in the open air, the deviation was 6% or less; however, the deviation was apt to be on the side of underestimating the true conversion because of the loss of CaC_2 by hydrolysis and oxidation.

Because of their relative importance, the analytical methods described above are further elaborated in the Appendices.

3.5.2. Analysis of Gas Product

The gaseous product collected in the sampling can was analyzed for hydrocarbons by using the same flame ionization detector that was used for the analysis of CaC_2 by hydrolysis. Gas samples were withdrawn from the sampling can through the septum port by using a gas tight syringe. The hydrocarbons detected in the gas product were mostly CH_4 , C_2H_2 , C_2H_4 , and in a few cases, C_2H_6 . Calibration gas was prepared by injecting 6.5 cc each of the four hydrocarbon gases into an empty can of 322 ml in volume which initially contained the air.

4. Results

The reaction of CaO with "nascent" carbonaceous species to produce CaC_2 in the rotating-arc reactor was studied by using mainly CH_4 , and in a few cases C_2H_4 , as the carbon source. In addition a high volatile bituminous coal was also used as the source of the "nascent" carbonaceous species in the reaction scheme. Accordingly, the experimental results are presented in three sections consisting of methane series runs, ethylene series runs, and coal series runs.

4.1. Results of Methane Series Runs

4.1.1. Characteristics of Methane Series Runs

4.1.1.1. Arc Characteristics

The most difficult problem encountered in the arc operation was maintaining the stability of arc in CH_4 or other molecular gases, even though it was no problem in helium or argon. This was probably because the power supply characteristics failed to satisfactorily meet the variation of the electric field of the molecular gases. The characteristics of the power supply, which had an open circuit voltage of 160 volts, are described in Section 3.2.3. It is always desirable for the reason of arc stability that the open circuit voltage of the power supply be at least twice the arc voltage. On many occasions in the methane series experiments the arc was quite to moderately stable when the voltage was lower than 75 volts but usually became unstable when it was over 80 volts.

4.1.1.1.1. Theoretical Consideration of Arc Characteristics

The longitudinal electric field of the arc column, which provides the main source of energy for the electrons to ionize and excite the gas, is generally greater for molecular gases than the atomic gases since molecular gases absorb more energy by dissociation and excitation of rotational and vibrational levels. The electric field of molecular gases can, of course, decrease in the presence of elements of low ionization potentials. Therefore, in the present experiments, the arc voltage invariably dropped by 5-35 volts upon commencement of CaO feeding due to the ionization of some calcium vapors in the arc zone.

Some very simple but useful functional relations have been found for a freely burning vertical arc by treating it as a vertical heated cylinder and applying dimensional analysis after some simplifying assumptions (see Refs. (23, 58) for details). The heat transfer from the arc was then shown as $Nu = f(Gr, Pr)$, where the symbols represent the Nusselt, Grasshof, and Prandtl numbers. From the relation, the functional dependency of electric field on arc current can be derived:

$$E = \text{const. } i^{-n}$$

For air, the experimental value of n is 0.6, which indicates that a relatively small change in E can sometimes induce an intolerable increase in arc current, or vice versa. The same observation also applies to other gases in principle. The

pressure dependency of E can also be derived from the dimensionless relation:

$$E = \text{const. } p^m$$

where the experimental values of m for N₂, H₂, He, and A are, respectively, 0.31, 0.32, 0.20, and 0.16.

Norman and Fells (58) have developed a similar relationship for the case of an arc in forced axial convection (i.e., in impressed gas flow in the direction of the arc column axis), which may be expressed in the form

$$\text{Nu} = \text{const. } \text{Re}^n$$

where Re is the Reynolds number. The experimentally found value of n for air is 0.5. This leads to an expression relating the power dissipation to the gas flow velocity:

$$E_i = \text{const. } (u_i)^a$$

For air, a = 0.44. Rearranging, we have

$$E = \text{const. } u_i^{a-1}$$

Thus, at a given arc current, increasing the gas flow velocity will result in an increase in E. In other words, the electric field increases as the gas flow velocity is raised in order to compensate for increased energy losses due to the increase in convective cooling of the arc column. All the above functional relations can provide simple but extremely useful guidelines in scaling up an arc-gas heater or operating it at dif-

ferent pressures.

4.1.1.1.2. Observation of Arc Characteristics

The voltage-current characteristics of the rotating-arc in CH_4 during CaO feeding are shown in Figure 4.1, which is prepared from average values of the voltages and currents read at regular intervals during each run. It clearly shows the falling voltage-rising current characteristic of a low to medium intensity arc. The effect of increasing the gas flow rate, from 16.0-17.3 l/min to 30.0-35.8 l/min and thus approximately by a factor of two, is seen to shift the arc characteristic curve upwards. This was due, as explained above, to increased convective cooling of the arc column at higher gas flow rates. Also, the arc voltage may have risen additionally due to elongation of the arc column since the latter was sustained in a cross flow of gas.

The relatively wide scattering of the data was mainly caused by the arc instabilities. The arc was mostly unstable when the gas flow rate was in a range of 30.0-35.8 l/min or higher. However, it was quite to moderately stable when the gas flow rate was in a range of 16.0-17.3 l/min and the arc voltage was lower than 75 volts; but it became fairly to very unstable when the voltage exceeded 80 volts. It was observed during actual runs that the voltage and current fluctuated in opposite directions in such a way that, in retrospect, the fluctuation seemed to have been tracing the arc characteristic curves.

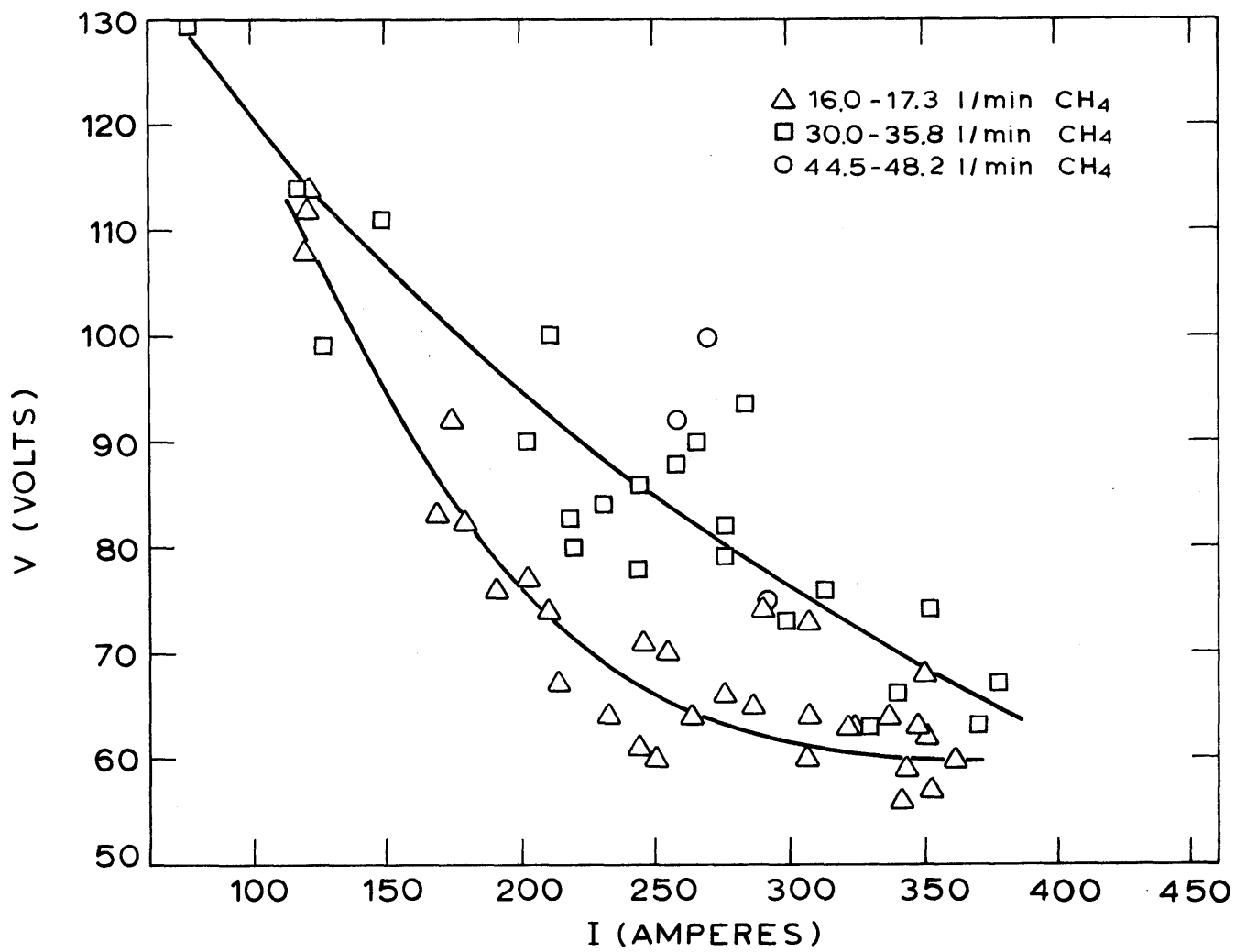


Fig. 4.1 Arc Voltage-Current Characteristics of the Rotating-Arc in CH₄, with CaO Feeding

4.1.1.2. Erosion of Graphite Electrodes

Erosion of the graphite electrodes was always more pronounced with the cathode than the anode because, in the reactor, the cathodic end of the arc was limited only to the tip of the cathode, whereas the anodic end was rapidly rotated over the annular surface of the anode. Therefore the cathode may have been heated more intensely than the anode, even though the temperature of the anodic spot itself may have been equal to or higher than that of the cathodic spot, owing to the effects of the heat of "vaporization" of electrons at the cathode and the heat of "condensation" of electrons at the anode.

The erosion of the graphite cathode was strongly affected by the type of gas, its flow rate and the current density at the cathode tip, among many other things. In general, the downward flow of gas restricted the cathodic end of the arc to the central portion of the cathode tip as evidenced by the crater-like bottom which was observed to have formed in every run.

In the methane series runs the graphite cathode always grew radially to harden due to the deposition and fusion of calcium compounds and carbon (from the decomposition of CH_4) on its cylindrical surface, the radial growth becoming more pronounced toward the bottom; simultaneously, it receded at the tip, leaving a crater-like bottom. As a result, the graphite cathode actually looked bell-shaped after a run in the hydrocarbon gas. However, the flared bottom of the

cathode rarely exceeded 5/16" in diameter in the methane series runs.

The rate of consumption of the graphite cathode strongly depended on the current density at the cathode tip and, of course, methane flow rate, the consumption rate becoming lower as the gas flow rate was increased at the same current density. The typical length of the 1/4" diameter graphite cathode consumed away after an actual run in methane flowing in a range of 16.0-17.3 l/min, which was scheduled in all cases to last 90 seconds (including the period of lime feeding), is as follows: 3/16"-1/2" for the cathode current density in a range of 950-1100 amperes/cm² (300-350 amperes), 1/16"-1/4" for 790-950 amp/cm² (250-300 amp), and 0-3/16" for 470-790 amp/cm² (150-250 amp). Below 470 amp/cm² there was no erosion but a slight elongation of the cathode at the skirts of the bottom.

The rate of carbon vaporization from the graphite cathode was typically around 0.2 g/min and rarely reached the maximum of 0.4 g/min when the methane flow rate was in a range of 16.0-17.3 l/min and the current was 300 amps or higher. Therefore the carbon vaporized from the electrode was typically around 2% and rarely exceeded the maximum of 5% of the carbon content of the methane flow. The percentage was even less at the higher methane flow rates due to increased carbon content in the gas flow and somewhat less severe erosion of the carbon electrode.

The erosion of the graphite anode insert was not as

severe as that of the cathode. Examination of used anode inserts revealed that the anodic end of the arc was moving upward along the inner surface as the cathode tip was receding away, thus keeping the arc length and hence the arc voltage more or less constant. Interestingly, the insert used to gain weight slightly after a run even when there was a distinctive sign of erosion around the tracks of the arc. This was undoubtedly due to the fusion of solids on the other parts of the insert.

4.1.2. Reproducibility of Data

Power Input. The singular experimental factor which caused the relatively wide scattering of experimental results in the present study was the fluctuations in power input which proved so difficult to control as a result of the arc instabilities inherently encountered in many runs. Generally the fluctuations were rapid when the arc was unstable, their amplitudes becoming larger as the arcs became more unstable.

The arc, and hence the power input, was most stable when the methane flow rate was in a range of 16.0-17.3 l/min and the power input was 15.5 kw or higher, with a standard deviation of the power fluctuations in a range of 3-10% around the mean power input; however, below about 14 kw the deviation increased to anywhere from 10 to 30% of the mean. With the methane flow rate in a range of 30.0-35.8 l/min, the deviation of power fluctuations was in a range of 6-16% of the mean when the power input was 22 kw or higher; and below 22 kw

it was typically on the order of 30% but occasionally reached up to the order of 60%.

Quantitative Analysis of Products. The accuracy of the analytical techniques is discussed in Section 3.5.

Spatial Distribution of Solid Product. Because of the fluctuations in the power input, the composition of the solid product collected in the sampling funnel may have been different from layer to layer, although the fluctuations were usually so rapid that the product distribution may not have been distinctive. Nevertheless, complete mixing of the layers was always ensured by stirring up the particles in the sampling funnel before taking portions of them for the subsequent analysis of CaC_2 .

The possibility of radial distribution of the solid product in the cooling chamber was examined by analyzing for CaC_2 the particles collected from the bottom and the side-walls of the chamber and comparing the results with those from the sampling funnel collected at a 15" quench distance. The examination revealed that the % conversion of CaO to CaC_2 was lower by typically 2-3% and by as much as 7% for the samples collected from the bottom and the side-walls in comparison with those from the sampling funnel. This discrepancy was attributed to the hydrolysis of the CaC_2 product inside the cooling chamber by the moisture in the open air, which was let in during dismantling of the reactor. It used to take about three minutes to dismantle the reactor and collect the powders from the inside, which proved to be long

enough to cause the hydrolysis noted above.

4.1.3. Experimental Results

Extensive experimental studies were carried out using CH_4 as the carbon source. The experimental parameters studied were: (1) power input, in a range of 10-26 kw; (2) methane flow rate, in three different levels -- 16.0-17.3 l/min, 30.0-35.8 l/min, and 44.5-48.2 l/min; (3) lime feed rate, in a range of 0.1-1.4 times the stoichiometric lime feed rate based on the carbon in the methane flow; (4) CaO particle size: -8μ , -44μ (i.e. -325 mesh size), and -74μ (i.e. -200 mesh size) fractions; (5) residence time, varied up to an order of magnitude by varying anode nozzle length and diameter; and (6) quench distance, set at either 5" or 15".

The results from all the methane series runs are plotted in Figure 4.2 for the % CaO conversion (to CaC_2) vs. power input. (Note: Complete tabulation of all the experimental data is presented in Appendix 8.1.) In spite of the widely different ranges of the experimental parameters employed, the figure indicates that all the results can be correlated as a function of power input according only to the methane flow rates; thus, in the figure, three correlations can be found for each of the three levels of methane flow rates investigated. In general, the correlations are characterized by the presence of the rather narrow range of critical power input at each level of methane flow rates in which the % CaO

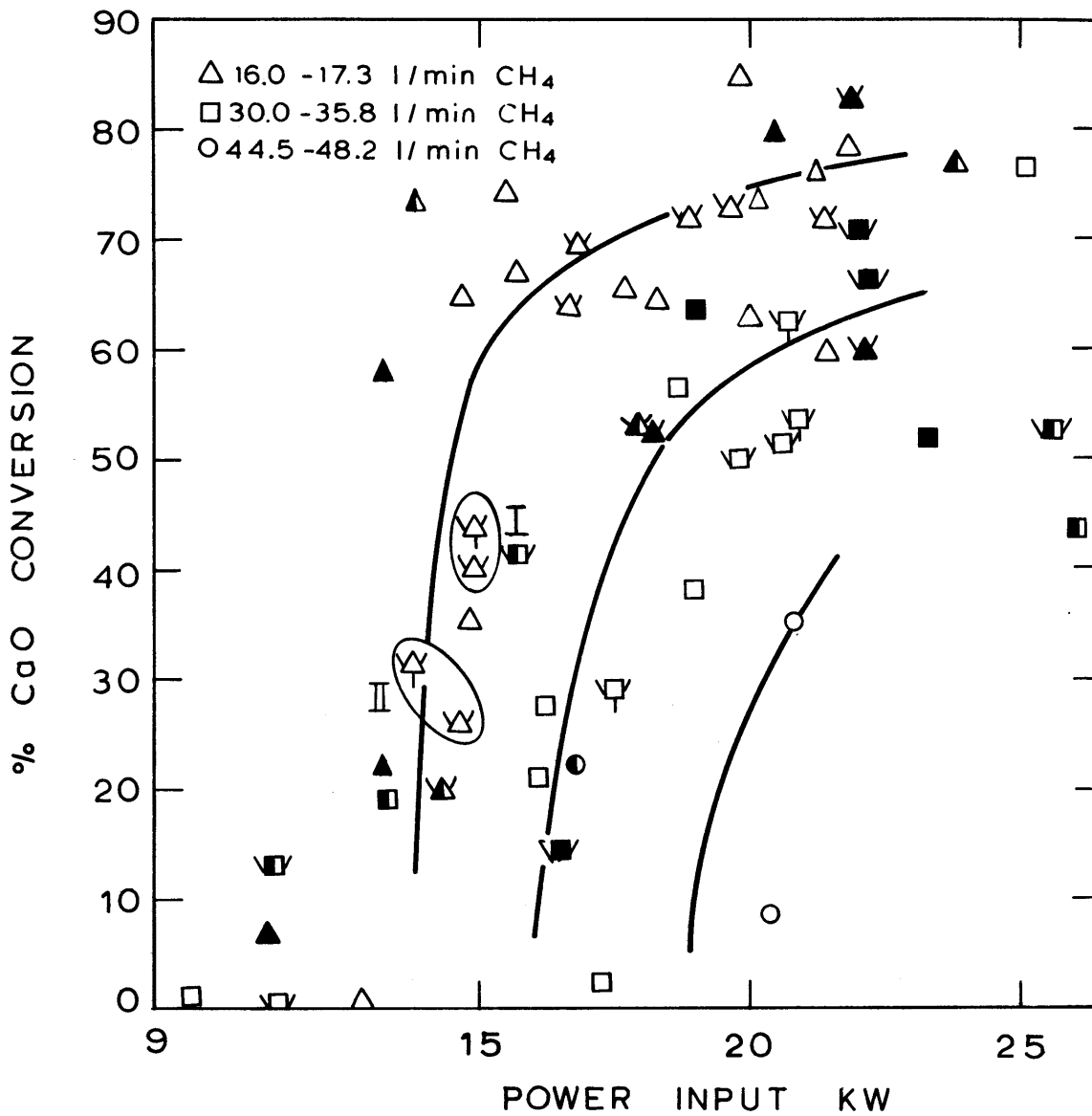


Fig. 4.2 Cao Conversion vs. Power Input at Various CH_4 Flow Rates

Particle Size; $\triangle, \square, \circ$, -8 μ ; $\blacktriangle, \blacksquare, \bullet$, -44 μ ; $\blacktriangle, \blacksquare, \bullet$, -74 μ
 Quench Distance: 5 in. without & 15 in. with Arms.
 Residence Time: Regular (Anode No. G-1) without & Extended (G-4, G-8) with Tails.

conversion increases very rapidly with only slight increase of power input. Once over the critical power input region, the conversion attains more or less constant value and rises very slowly as the power input increases.

The existence of such correlations suggests that the single most important experimental parameter besides the power input is the gas flow rate. The scattering of the experimental data in the figure is relatively random and no systematic relations can be found for the other experimental parameters, at least within the ranges investigated. Rather, the relatively wide scattering of the data was mainly caused by the erratic power input, owing to arc instabilities inevitably encountered in many experiments.

The foregoing observations on the effect of the experimental parameters on the conversion of CaO to CaC_2 have very significant bearings on the mechanistic nature of the reaction of CaO with "nascent" carbonaceous species and are thus elaborated further in greater detail in the following.

4.1.3.1. Effect of Lime Feed Rates

In Figure 4.3 we show the effect of lime feed rates on the conversion of CaO to CaC_2 for methane flow rates in a range of 16.0-17.3 l/min with power inputs above 15.5 kw, thus above the threshold region in which it was seen that the conversion was sensitive to any slight change in power input. The figure shows that the conversion remained fairly constant around 70% even though the lime feed rates were varied from

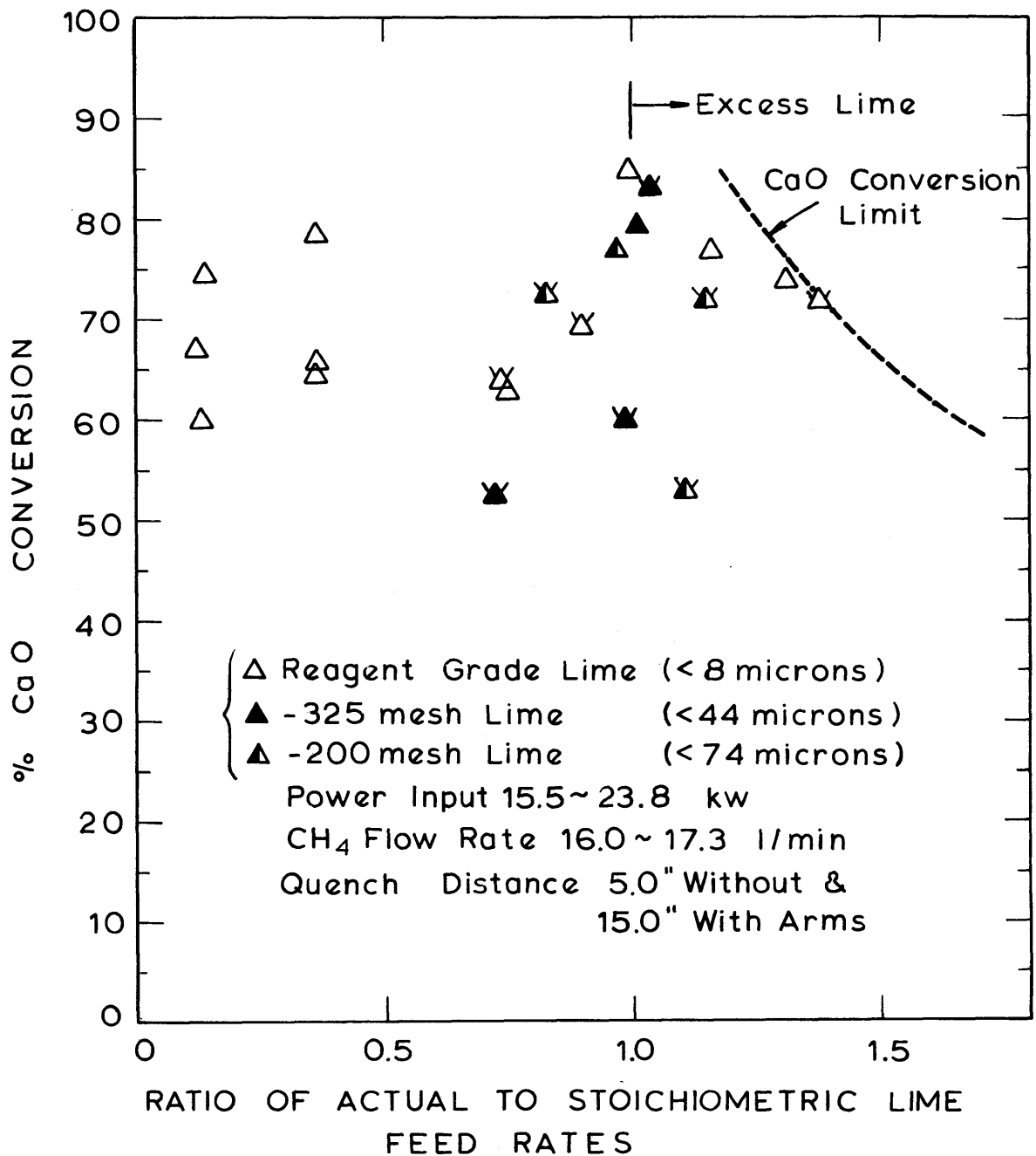


Fig. 4.3 CaO Conversion vs. Ratio of Actual to Stoichiometric Lime Feed Rates

0.12 to 1.38 times the stoichiometric feed rates based on the carbon content in the methane flows. The stoichiometric lime feedrates were in a range of 12.4-13.4 g/min for the methane flow rates in a range of 16.0-17.3 l/min.

The figure also indicates that the carbon in the methane can be reacted with CaO almost completely by feeding the latter in excess. The highest carbon conversion was obtained when the lime was fed 1.38 times the stoichiometric feed rate, which was 99.2% based on the methane flow alone and 95.1% inclusive of the carbon vaporized from the graphite electrodes.

4.1.3.2. Partice Size Effect

In order to delineate the effect of the particle sizes on the conversion of CaO to CaC_2 , three particle sizes were used: -8μ , -44μ , and -74μ . Both Figure 4.2 and Figure 4.3 indicate that the conversion was hardly affected by the lime particle sizes, although the -74μ size fraction seemed to undergo slightly lower conversion than the other two. Nevertheless, the distinction is not very clear and thus it can be safely inferred that there was no particle size effect observed, at least with the particle sizes used in the experiments.

4.1.3.3. Effect of Quench Distances

The effect of quenching speeds on overall product formation can yield valuable information on the stability of the

product. If the product is highly thermally unstable, then slow quenching will result in the decomposition of the product. For a thorough study of the effect of quenching speeds, it is always desirable to know the temperature history of the product during cooling. Unfortunately, however, temperature could not be measured in this study because thermocouples could not effectively operate in the present reactor system due to the carburizing condition of the product stream and the electric noise emitted by the high frequency unit which had to be kept on during reactor operation.

In the present study the quench probe was set at either 5" or 15" from the anode nozzle exit. The quench probe often melted at the tip when it was placed at 1". As shown in both Figures 4.2 and 4.3, the effect of quench distance is not noticeable within the rather random scattering of the experimental data. This suggests that the solid product is thermally stable and little decomposition occurs during cooling. This is thermodynamically expected because the free energy of formation of CaC_2 is negative and thus thermodynamically stable relative to the elements from room temperature to its melting point of 2573°K . The free energy of formation is not known beyond the melting point, but extrapolation of the data indicates that it remains negative probably up to 3500°K .

4.1.3.4. Effect of Residence Time

The residence time of the reactants in the anode nozzle

was normally in a range of 0.5-1.0 msec. In order to gain insight into the reaction mechanism, the residence time was sometimes increased by four- to slightly over thirteen-fold by using graphite anodes of different nozzle lengths and diameters. The various anodes are described and the schematic are shown in Section 3.2.1.1. The residence time can also be changed effectively by varying the gas flow rate and/or the power input. As an example, if the gas flow and the power input are both reduced by one-half, the residence time will be doubled while the energy input per unit volume of gas remains the same as before. Nevertheless, any direct study of the residence time effect in this way was very difficult due to the arc instabilities encountered in many arc operations and the rather narrow range of power input, which may have been imposed mainly by the power supply characteristics.

Results from the runs with prolonged residence times are indicated in Figure 4.2 by the symbols affixed with the tails. In order to delineate the residence time effect clearly, the runs were intentionally made at the relatively low conversion regions: e.g., if the reaction mechanism operative in and immediately beyond the arc zones were still effective over the entire length of the anode nozzle, then the conversion of CaO to CaC_2 would greatly increase with a several-fold increase in the residence time. However, the results in general indicate that the conversion was not noticeably enhanced by the increased residence time. Specifically in

each of the two groups marked I and II in the figure, in which the residence time of one run was increased by thirteen-fold over the other under otherwise similar reaction conditions, the conversion increased only by several percentage points despite the increased residence time by an order of magnitude.

4.1.3.5. Effects of Power Input and Methane Flow Rates

Thus far it has been shown that the conversion of CaO to CaC₂ was not affected by the variation in the experimental parameters such as lime feed rates, quench distance, residence time, and particle size, thus leaving the methane flow rate and the power input as the only two possible de facto experimental parameters affecting the overall reaction. The effect of the two parameters is presented in the following.

As shown in Figure 4.2, all results obtained at a given level of methane flow rate can be correlated with a single line, unaffected by the other experimental parameters. For each level of the three methane flow rates investigated, the effect of power input is characterized by the existence of the critical power input regions in which the % CaO conversion rises very rapidly with only slight increase in power input. Beyond the critical region the conversion attains more or less constant value and rises only slowly as the power input increases, and below which there seems to be no conversion of CaO to CaC₂ taking place. The critical power

input regions seem to lie in a range of 13-15 kw for 16.0-17.3 l/min CH_4 and 15-18 kw for 30.0-35.8 l/min CH_4 ; for 44.5-48.2 l/min CH_4 , there were insufficient data taken due to extreme arc instabilities.

The effect of increasing methane flow rate is characterized in Figure 4.2 by the shift of the CaO conversion correlation curve in the direction of higher power input. Therefore, at the methane flow rate of 30.0-35.8 l/min the power consumption was usually higher than at 16.0-17.3 l/min to effect the same level of CaO conversion, and at 44.5-48.2 l/min it was even higher. Nevertheless, the increase in power consumption used to be less than in proportion to the increase in the gas flow, thus resulting in improved energy efficiency of the reactor. This fact can be readily seen in Figure 4.4, in which the data from Figure 4.2 are re-plotted as a function of specific gas energy based on gross power inputs and methane flow rates. It shows that the conversion of CaO to CaC_2 requires less specific gas energy at higher gas flow rates. The critical specific gas energies to effect the reaction seem to lie in a range of 280-310 kcal/g atom C in the case of 16.0-17.3 l/min CH_4 , and in a range of 160-210 kcal/g atom C in the case of 30.0-35.8 l/min CH_4 . Although sufficient data do not exist for the methane flow rates in a range of 44.5-48.2 l/min, the corresponding critical specific energy seems to lie in a range of 110-160 kcal/g atom C.

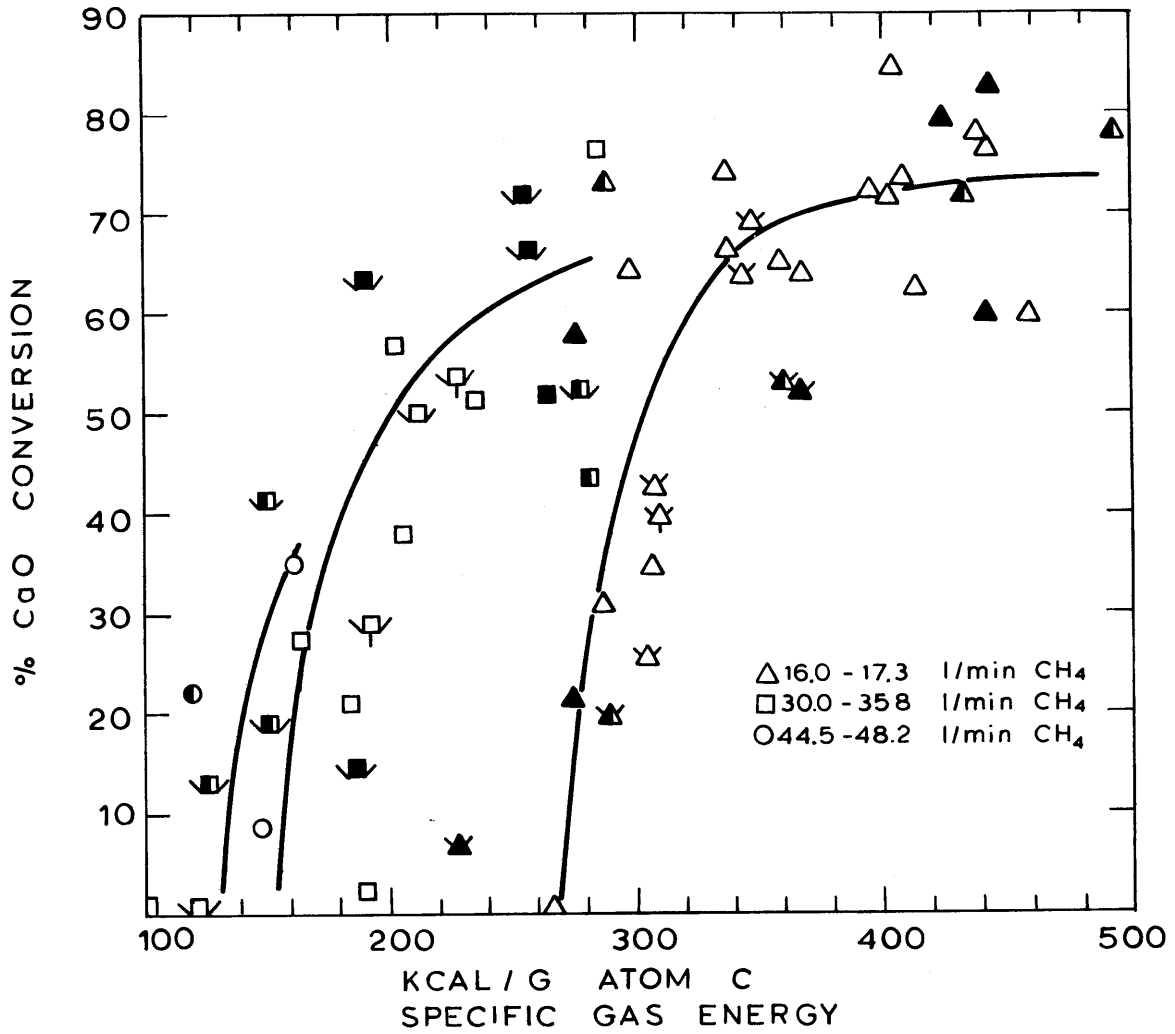


Fig. 4.4 CaO Conversion vs. Specific Gas Enthalpy, CH₄ Runs

Particle Size; Δ , \square , \circ , -8 μ ; \blacktriangle , \blacksquare , \bullet , -44 μ ; \blacktriangle , \blacksquare , \bullet , -74 μ
Quench Distance: 5 in. without & 15 in. with Arms.
Residence Time: Regular (Anode No. G-1) without & Extended (G-4, G-8) with Tails.

4.1.3.6. Gaseous Product Composition

The interdynamic relationship between the gaseous hydrocarbon products and the calcium carbide formation has been studied by collecting the gas products and analyzing them on a flame ionization detector. In most cases, the gaseous hydrocarbons detected above 0.01% in concentration were methane, ethylene, and acetylene, with occasional appearance of ethane at very low power input (e.g. 10 kw or less).

The methane concentration was usually lower than 1% when the conversion of CaO to CaC₂ was higher than 60%. Conversely, the CaO conversion was usually lower than 40% when the methane concentration was higher than 3%. The interdynamic relationship between the methane concentration and the % CaO conversion is shown in Figure 4.5, which contains all results from the experiments with 5" quench distance.

The ethylene concentration was typically below 0.1% and varied in similar fashion to the acetylene concentration, which is described below.

Variation of the acetylene concentration with lime feed rates is very remarkable and is shown in Figure 4.6. It contains all results from the experiments of 16.0-17.3 l/min CH₄, 5" quench distance, and reagent grade CaO. Power inputs were beyond the critical region and in a range of 15.5-21.8 kw, in which it was previously shown that the % CaO conversion remained more or less constant around the 70% conversion level. Also included in the figure is the per-

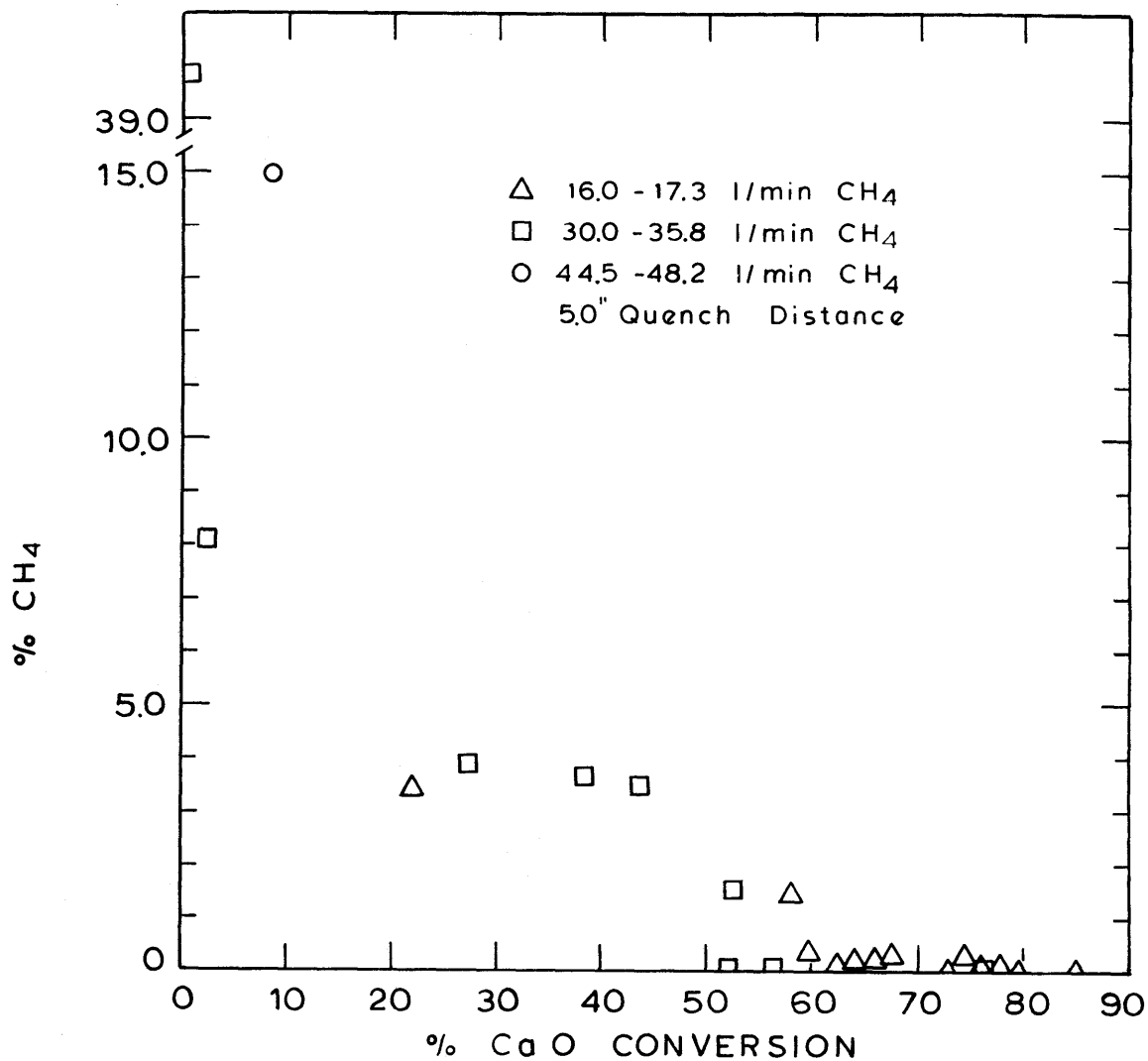


Fig. 4.5 CH_4 Concentration vs. CaO Conversion in CH_4 Series Runs

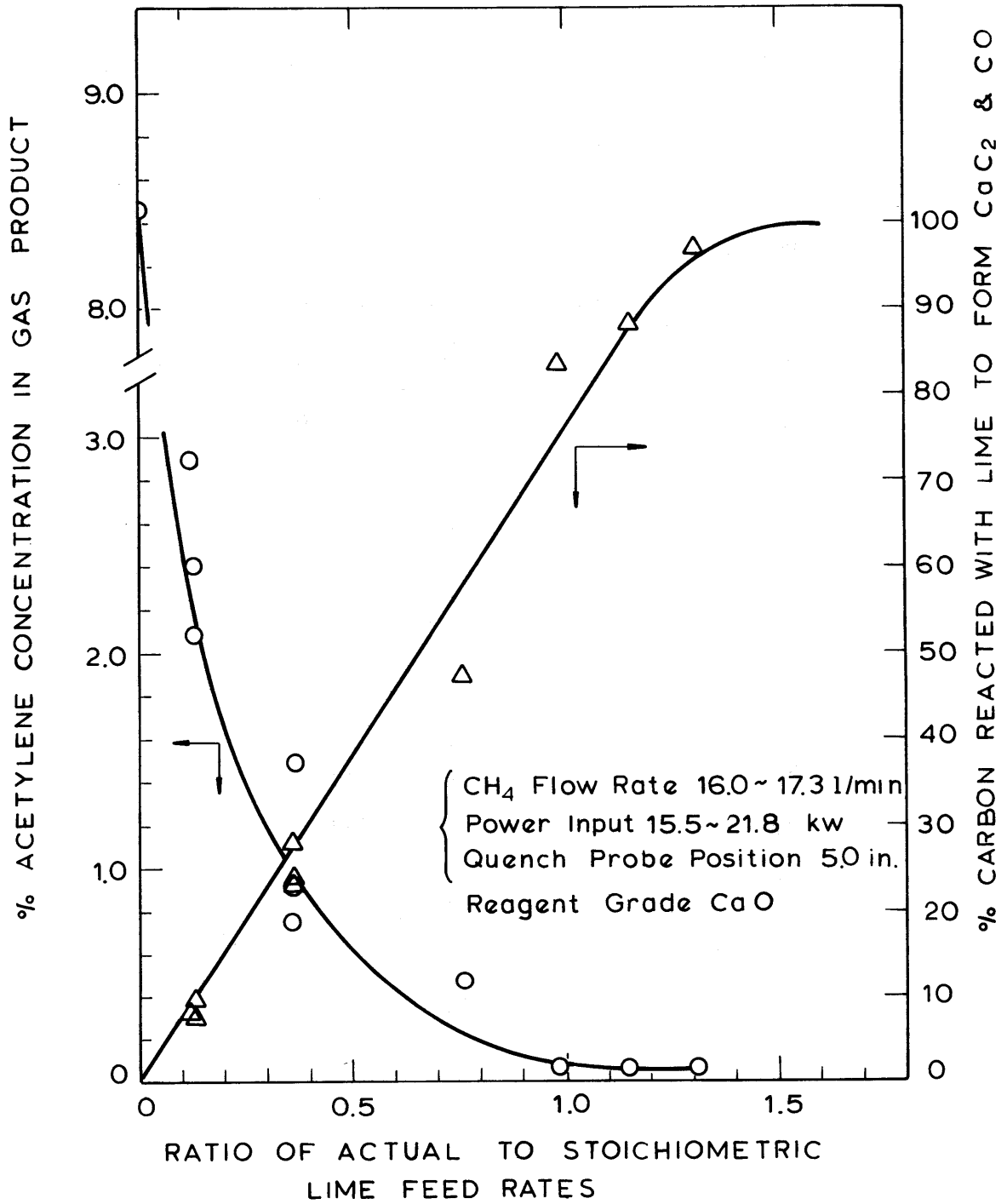


Fig. 4.6 Variation of C_2H_2 Concentration in Gas Product with Lime Feed Rates

centage of carbon in the methane reacted with CaO to produce CaC_2 and CO, which is calculated based on the % CaO conversion and the known lime feed rate. The figure thus prepared shows that the reduction of acetylene concentration was accelerated while the formation of CaC_2 and CO increased only linearly as the lime feed rate was raised.

4.2 Results of Ethylene Series Runs

4.2.1. Operational Characteristics

In ethylene series runs the radial growth of the graphite cathode was far more extensive than in the methane series runs, which was undoubtedly due to the relative ease of the decomposition of ethylene in comparison with methane. The activation energy of decomposition of ethylene is about 1/5 of methane per gram atom of carbon. The greatest radial growth usually occurred at about 1/8" from the cathode tip and typically reached to 7/16" in diameter. The erosion at the cathode tip used to be slightly less than in the corresponding methane runs with the same arc currents, but extensive enough to cause the cathode tip to recede out of the 1/2" diameter opening of the anode insert as in many methane series runs. The cathode tip was on all occasions placed 1/8" deep into the insert opening before starting an arc operation. In addition, the anode inserts used to show little sign of erosion; on the contrary, in a few cases the insert openings narrowed from 1/2" to 7/16" due to fusion of solids on the inner surfaces. As a result, the arc

voltage used to drop from 65-80 volts to as low as 20-30 volts toward the end of a run as the arc length shortened.

In order to reduce decomposition of ethylene in the pre-interelectrode region and also to prevent fusion of solids in the anode insert, the graphite anode was replaced with a water-cooled copper anode which is described in Section 3.2.1.1. Nevertheless, the latter did not prevent the voltage from dropping, although the fusion of solids in the anode throat was almost completely eliminated. This suggested that the dropping of arc voltage was mainly due to the rather extensive radial growth of the graphite cathode which still persisted in the water-cooled anode. Since the arc-voltage drop was always accompanied by the substantial increase in arc current, the current control of the power supply had to be lowered toward the end of each run in order to prevent the cathode from burning out.

4.2.2. Experimental Results

Results of the ethylene series runs are plotted in Figure 4.7 for % CaO conversion vs. specific gas energy together with the results of the methane series runs. Of the six runs, only one (marked with G in the figure) was made with a graphite anode and the other five were made with water-cooled copper anodes. In order to increase residence time, the water-cooled copper anode was sometimes affixed with a graphite cylinder of 1" i.d. x 3" o.d. and 5" long. In all cases, only -325 mesh lime particle size was used. The gas

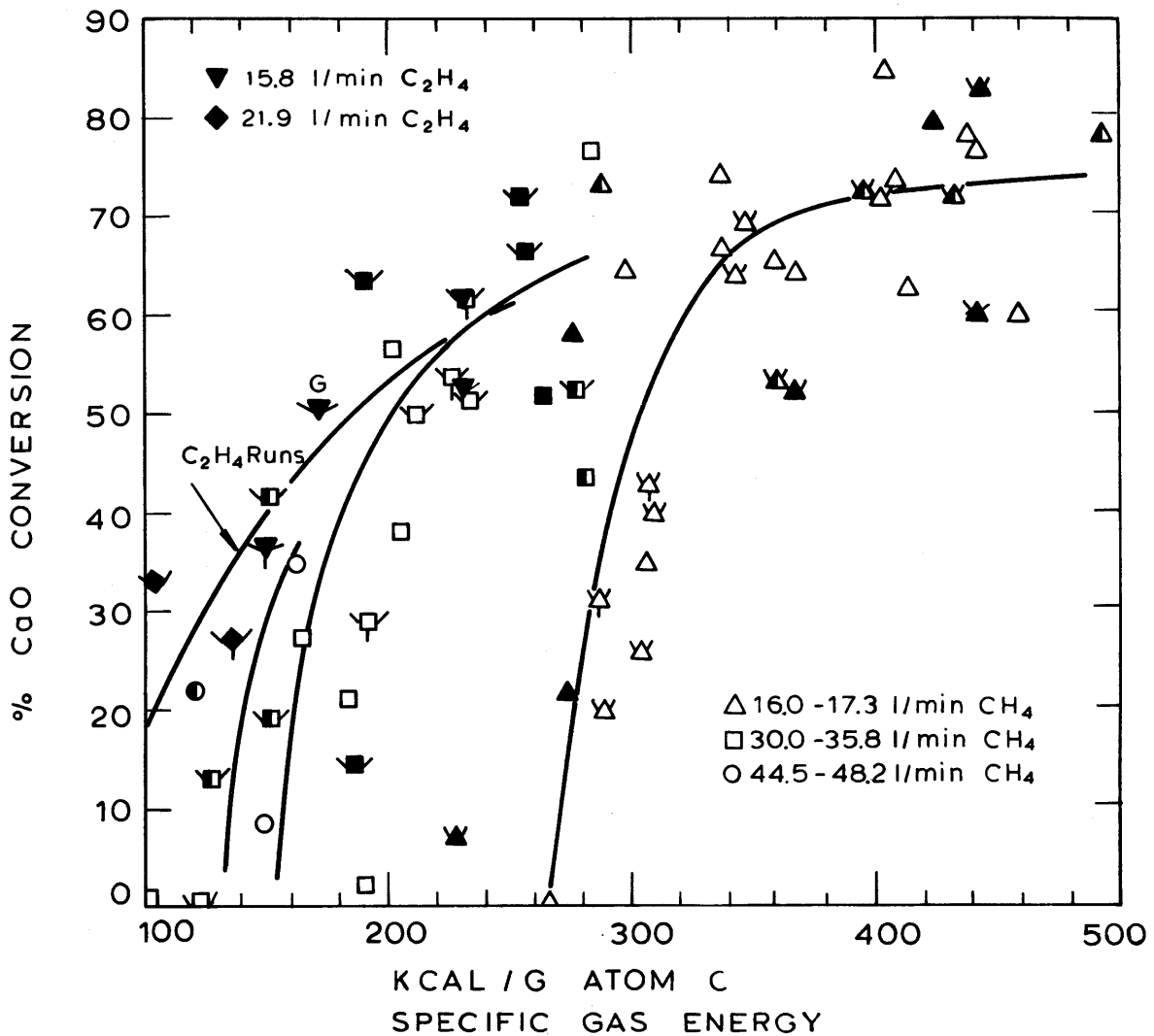


Fig. 4.7 CaO Conversion vs. Specific Gas Enthalpy; C₂H₄ Runs are shown together with CH₄ runs

Particle Size; Δ , \square , \circ , -8 μ ; \blacktriangle , \blacksquare , \bullet , -44 μ ; \blacktriangle , \blacksquare , \bullet , -74 μ
 Quench Distance: 5 in. without & 15 in. with Arms.
 Residence Time: Regular (Anode No. G-1) without & Extended (G-4, G-8) with Tails.

flow rate was either 15.8 l/min or 21.9 l/min, and lime feed rates were in a range of 0.95 to 1.20 times the stoichiometric feed rates. The quench probe was always positioned 15" from the anode nozzle.

As indicated in Figure 4.7, the % conversion of lime to CaC_2 increased with an increase in specific gas enthalpy as in the methane series runs, with a slight increase in energy efficiency at equivalent gas flow rates based on the carbon in the feed gas. Again, there was not noticeable effect of extended residence time on the CaO conversion as in the methane series runs.

4.3 Results of Coal Series Runs

4.3.1. Operational Characteristics

Because of the rapid vaporization of the graphite cathode when the arc was operated in hydrogen alone, feeding of the mixture of fine powders of lime and coal was always started only 10 seconds after the hydrogen arc was fully established at a desired power level instead of the usual 30 seconds as in CH_4 and C_2H_4 series runs. As a result, erosion of the graphite cathode was greatly reduced owing to the suppressing effect rendered by the volatilized carbon from the coal. The erosion of the graphite cathode was further reduced by increasing the gas flow rate; however, it used to have a detrimental effect on the stability of the arc. The arc voltage was initially in a range of 70-130 volts with the current in a range of 80-300 amperes, but it typically dropped

upon commencement of powder feeding to 60-85 volts with commensurate increase of the current to a range of 130-360 amperes.

The greatest problem encountered in the coal series runs when the graphite anode was used was the fusion of the feed particles in the pre-interelectrode region of the anode before reaching the arc zone, resulting in substantial particle holdup in the region and in some instances even in the feeding line. Therefore, the powder feed rate reported in the study could be an overestimation of the true feed rate for several occasions; but there was no effective means of controlling this. Nevertheless, in order to ensure consistency of powder feeding, the feeding line was dismantled for visual inspection after each run, and the run was voided if there was any excessive powder holdup in the line.

In order to eliminate the hot surface on which the particles fused, a water-cooled copper anode was constructed and operated with some degree of success for a number of coal runs. The details of the copper anode are presented in Section 3.2.1.1. Although the water-cooled copper anode completely eliminated the solid build-up in the pre-inter-electrode region of the anode, it posed great experimental difficulties by burning out too frequently. Therefore only five runs were made with the latter.

4.3.2. Experimental Results

In the coal series runs the powder feed was an intimate

mixture of -170, +325 mesh coal and either a reagent grade lime of -8μ particle size or a calcine of -325 mesh (-44μ) limestone. In most experiments the powder feed contained 47.0 wt.% excess lime over the stoichiometric ratio, thus making 68.0% as the possible maximum conversion of CaO to CaC₂; this was in part to determine the maximum percentage of the carbon in the coal that could react with CaO to produce CaC₂ and CO. Only in three experiments was a mixture with 5.8% excess carbon by weight used. The powder feed rate ranged from 15.5 g/min to 51.0 g/min and the hydrogen flow rate was in a range of 14.6-48.4 l/min. The H/C ratio in the feed was in a range of 2.7 to 8.0 as calculated based on the hydrogen flow rate and both the hydrogen and the carbon contents of the coal. The quench distance was either 5" or 15".

All the experimental results of the coal series runs are presented in Figure 4.8 for the % conversion of CaO to CaC₂ as a function of power input. It fails to clearly show the effect of power input on the CaO conversion, perhaps owing to the different experimental conditions employed for each data point. In this study no systematic attempt was made to delineate the various effects of hydrogen flow rate, powder feed rate, and coal-lime mixing ratio, as the study was exploratory in nature and also because it was so difficult to overcome the experimental difficulties encountered in many coal runs.

Nevertheless, the effects of the hydrogen flow rate and

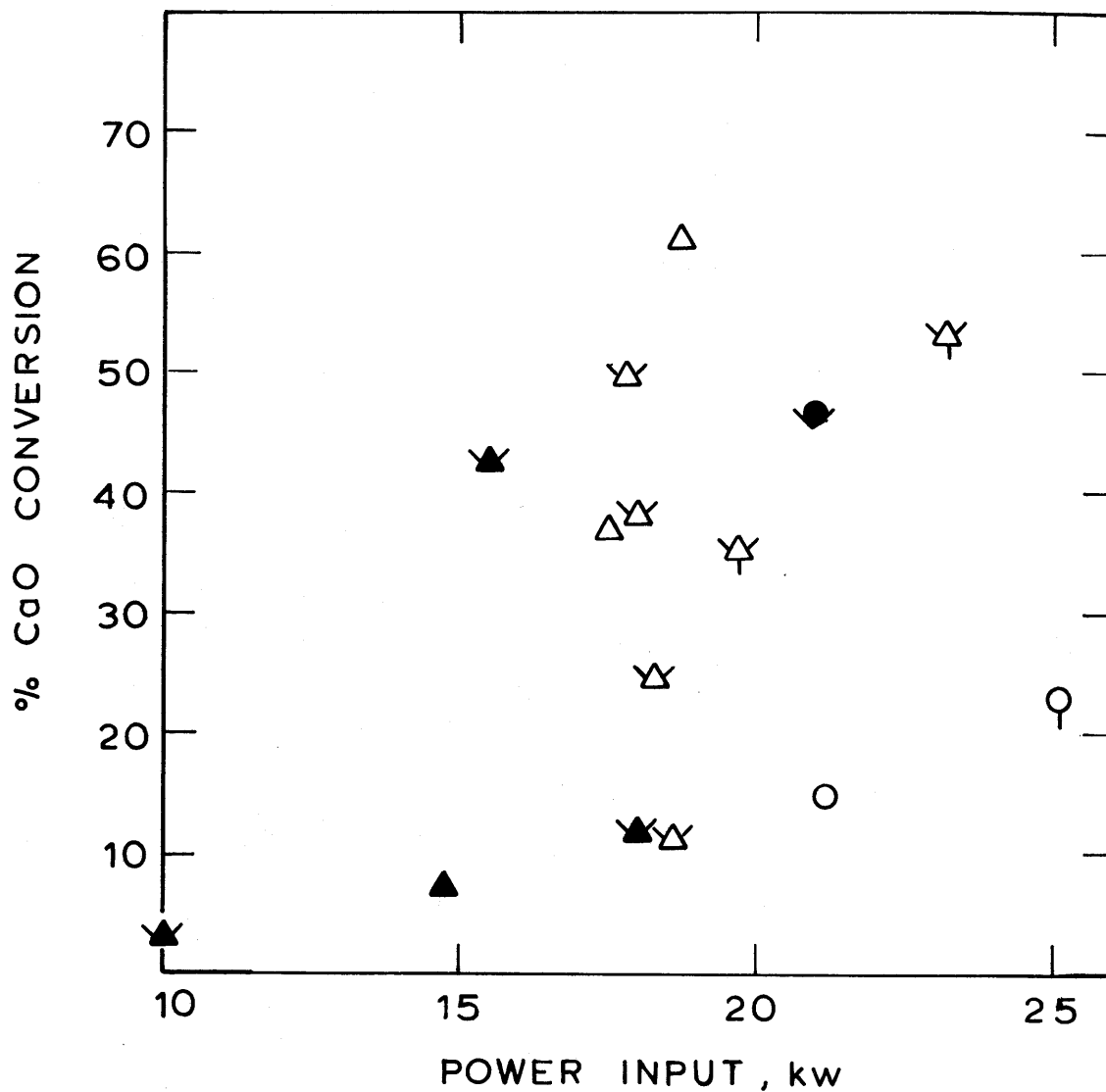


Fig. 4.8 CaO Conversion vs. Power Input, Coal Series Runs

Excess Lime (Molar CaO:C = 1.47:3.00); \triangle , \blacktriangle
 Excess Carbon (Molar CaO:C = 1.00:3.06); \circ , \bullet

Graphite Anode; \triangle , \circ
 Copper Anode; \blacktriangle , \bullet

Quench Distance; 5" without & 15" with Arms.

Residence Time; Regular without & Extended (G-4) with Tails.

the powder feed rate combined with power input can be best seen in Figures 4.9 and 4.10, which are plotted for % conversion vs. either gross energy input per unit volume of H_2 or gross energy input per gram atom of carbon in the solid feed. Despite the relatively wide scattering of the data, both figures suggest that the CaO conversion can be increased by increasing, as expected, either the specific gas enthalpy or the specific carbon enthalpy, or both. The highest % CaO conversion obtained in the study was 61.3%, whereas the possible maximum conversion in the particular run was 68.0% as the feed contained excess lime; therefore, in the same run it can be seen that 90.1% of the carbon in the coal reacted with CaO to form CaC_2 and CO. Since the carbon should have volatilized before reacting with the lime, it means that at least 90.1% of the carbon in the coal should have left the coal through volatilization. In most runs the hydrocarbons detected in the gas product used to be less than 0.5% in total concentration.

The effect of residence time was studied in three runs by using a graphite anode with extended anode nozzle (Anode No. G-4). Although the G-4 anode provided slightly over six times longer residence time than the regular anode (i.e. G-1), it seemed to show little effect on the conversion of CaO to CaC_2 . Interestingly, in a few attempted but futile runs of the longer graphite anode and the water-cooled copper anode affixed with 5" long graphite cylinder of 1" i.d. x 3" o.d., the solid product completely melted during flight

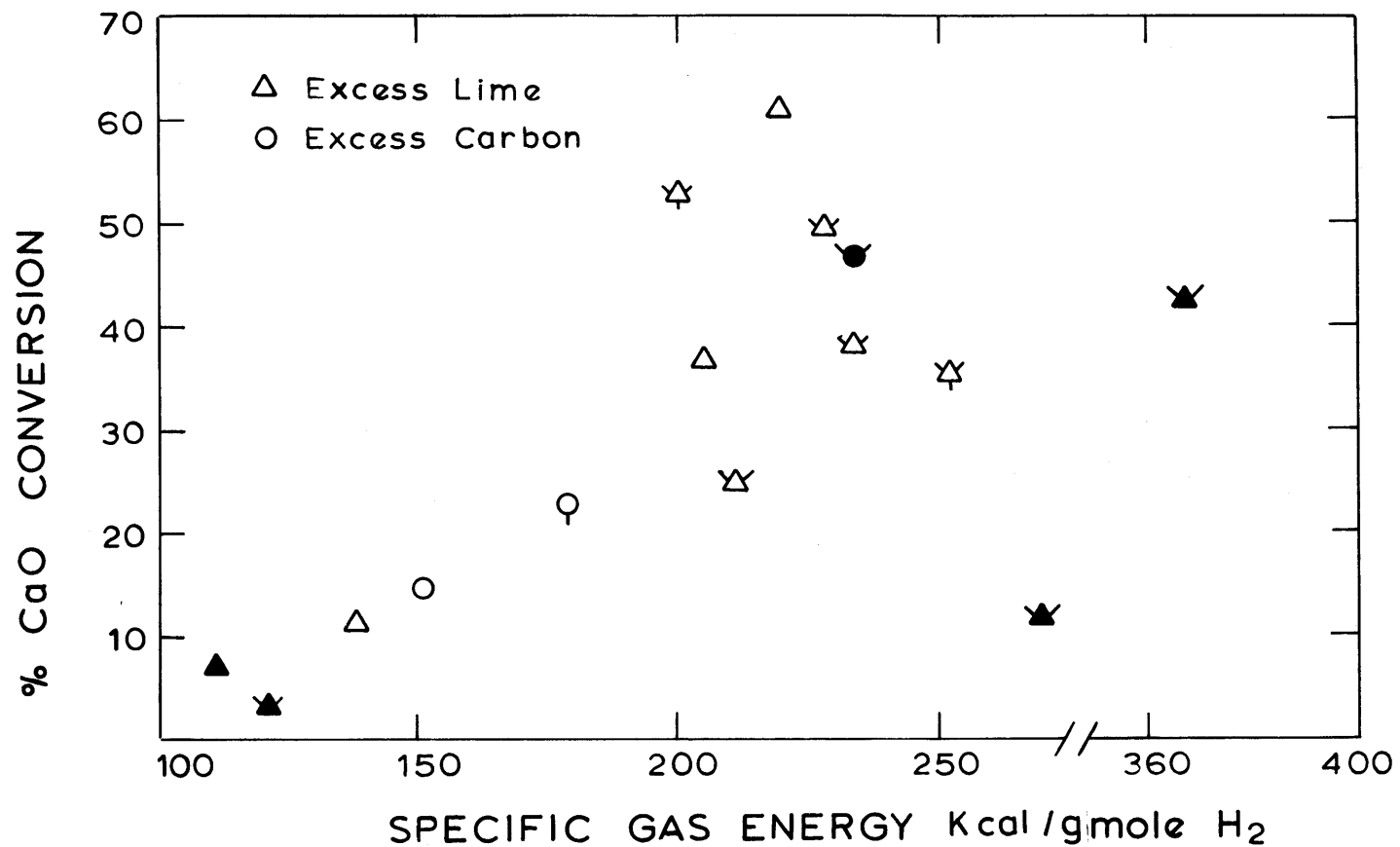


Fig. 4.9 CaO Conversion as a Function of Energy Input per G Mole H₂

Excess Lime (Molar CaO:C = 1.47:3.00); △, ▲
 Excess Carbon (Molar CaO:C = 1.00:3.06); ○, ●

Graphite Anode; △, ○
 Copper Anode; ▲, ●

Quench Distance; 5" without & 15" with Arms.
 Residence Time; Regular without & Extended (G-4) with Tails.

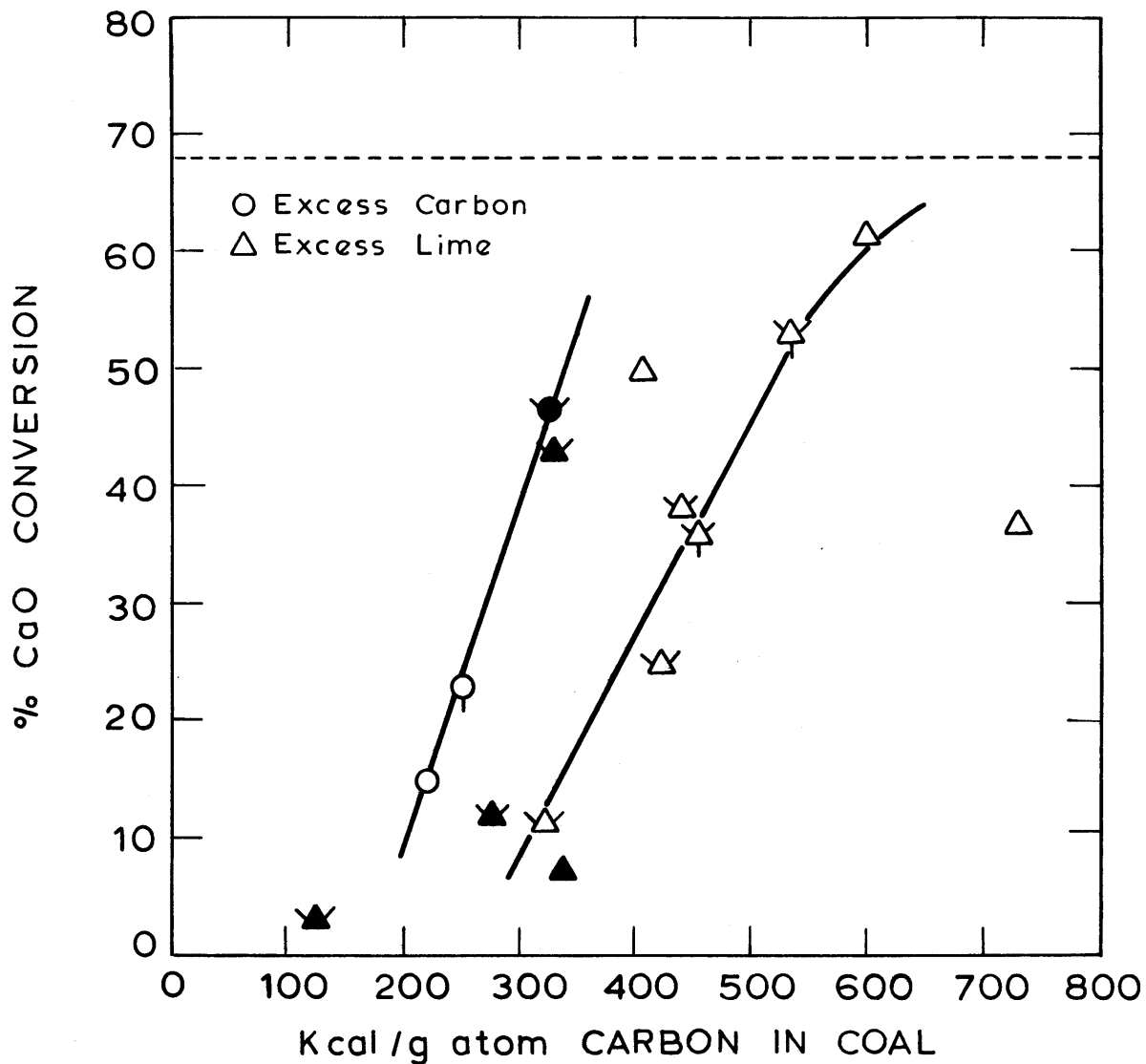


Fig. 4.10 CaO Conversion vs. Energy per G Atom C in Coal

Excess Lime (Molar CaO:C = 1.47:3.00); \triangle , \blacktriangle
 Excess Carbon (Molar CaO:C = 1.00:3.06); \circ , \bullet

Graphite Anode; \triangle , \circ
 Copper Anode; \blacktriangle , \bullet

Quench Distance; 5" without & 15" with Arms.

Residence Time; Regular without & Extended (G-4) with Tails.

and condensed as large blobs on the top of the sample probe, thus preventing sample collection. The extensive melting was prevented to some extent by increasing either hydrogen flow rate or powder feed rate or both at a given power input. Such an extensive melting was not observed in the runs of the regular graphite anode (G-1), in which the solid product was produced as agglomerates of fine particles.

The energy efficiency, for which the reactor was not designed, was somewhat lower than either CH_4 or C_2H_4 runs, the lowest being 32.2 kwhr/lb C_2H_2 .

4.4. Product Morphology

The various limes, limestones, and collected product were examined under an optical microscope and either a scanning- or a transmission electron microscope, and the pictures are selectively reproduced and discussed in the following.

The external appearances of the reagent grade lime, precipitated CaCO_3 , and both the -200 mesh and -325 mesh limestones and their calcined samples were examined under a scanning electron microscope. The SEM study did not show any consistent or significant differences between the two grades of either the limestones or their calcined materials.

The reagent grade lime (Figure 4.11) typically showed the rhombic shape of the precipitated CaCO_3 but the edges were somewhat rounded. The lime particle size was mainly in a range of 0.5 to 3 μ but particles as large as 8 μ were

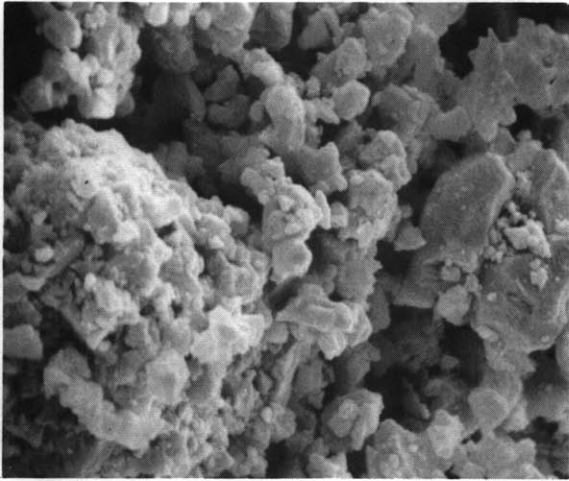


Fig. 4.11 Reagent grade CaO; -8μ particles; SEM, x2000

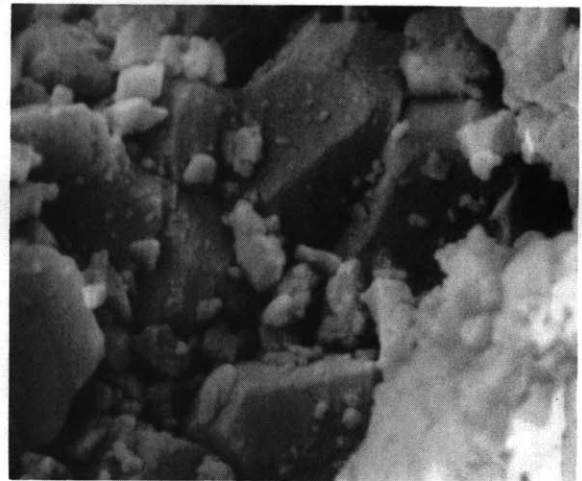


Fig. 4.12 Reagent grade lime at higher magnification; SEM, x5100

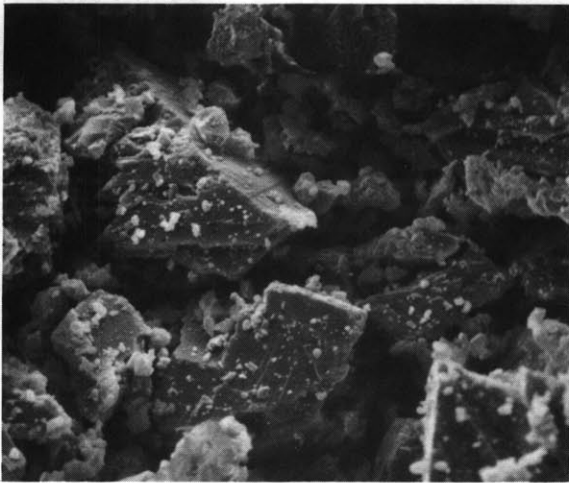


Fig. 4.13 Natural calcite; -325 mesh particles; SEM, x950

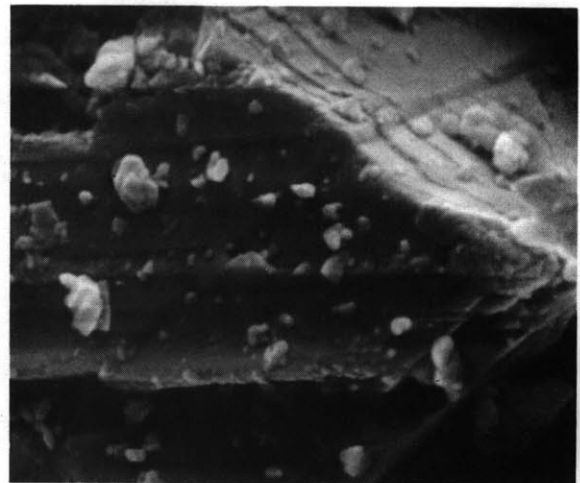


Fig. 4.14 Close-up of specimen on the left; SEM, x4800

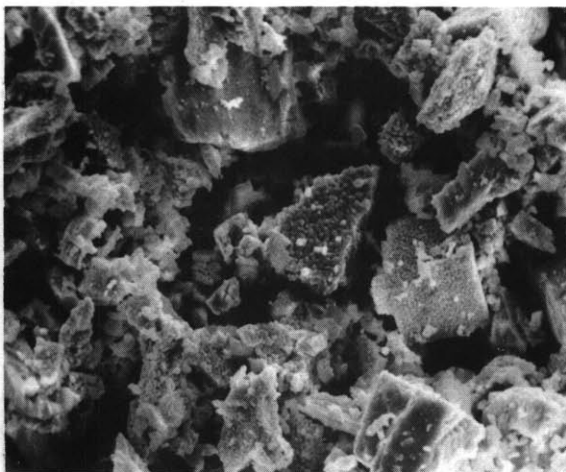


Fig. 4.15 Calcine of -325 mesh size calcite; shows spongy texture; SEM, x530

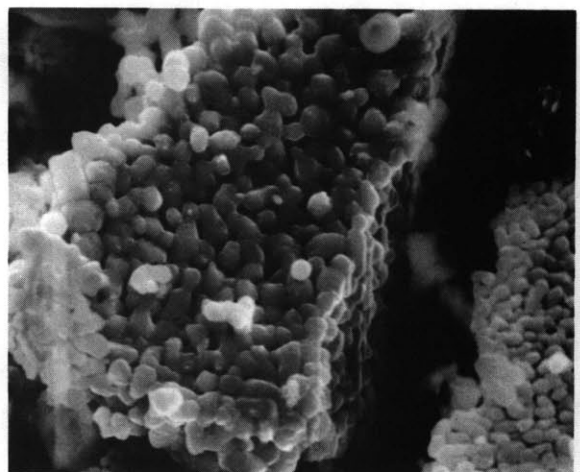


Fig. 4.16 Close-up of specimen on the left; SEM, x2200

occasionally observed. Examination at higher magnification (Figure 4.12) revealed that the lime was non-porous and resembled the precipitated CaCO_3 in texture.

The natural calcite had a rhombohedral shape with smooth surfaces (Figures 4.13 and 4.14). Few cleavage steps could be observed on the surfaces of the rhombs, which the SEM revealed as very coarsely grained and essentially free of intracrystalline voids.

Calcines of the natural calcite (Figures 4.15 and 4.16) retained the rhombic shape and size of their predecessor; however, unlike the calcite, most of the lime particles consisted of rounded grains that were partly fused together and as a result showed spongy texture and high porosity. The grains of the lime particles were mainly in the range of 0.5 to 1.0 μ in diameter. According to Harvey (37), calcines of high purity limestones show porosity increases, then decreases as the temperature of calcination is changed from 1700° to 2040°F. These porosity changes are reported to be accompanied by a series of changes in texture, starting from granular, altering to rounded granular, then to sponge, and finally to an interlocking granular texture with blocky grains of lime. In this study, all the calcination was done only at 1000°C in order to avoid ambiguities arising from different physical structures of the calcines.

Solid products at various stages of conversion from the methane- as well as the coal-series runs were microscopically examined in order to gain insight into the conversion process.

Under an optical microscope they were seen as agglomerates of very fine particles, in pieces about the same size or larger than the original lime particles. Since the constituent particles of the agglomerates were too small to be identified by the optical microscope, the solid product was placed on a grid and examined under a direct electron microscope. Figures 4.17 through 4.23 show the electron micrographs of the products from the methane series runs with the conversions ranging from 7.0% to 79.5%. Remarkably, all the products were seen as agglomerates of extremely fine particles which were mostly in the range of 200 \AA to 0.3μ , regardless of the degree of conversion and the original lime particle size. The constituent particles were of spherical shapes in all cases except at 7.0% conversion, in which angular granules on the order of 0.1μ in size were occasionally observed among the predominantly spherical particles of diameters from about 200 \AA to 0.3μ . It is very likely that the angular granules may have formed by mechanical breaking up of the original lime particles.

Pyrolysis of the methane used in the study yielded chain-like agglomerates of very fine carbon spheres ranging from 200 \AA to 400 \AA in diameter (Figure 4.24). Interestingly, most carbide products examined under the electron microscope were relatively devoid of the particles in the particle size range even when there should have existed copious amounts of free carbons which had failed to react with CaO to form CaC_2 and CO; and even if there were, the individual particles

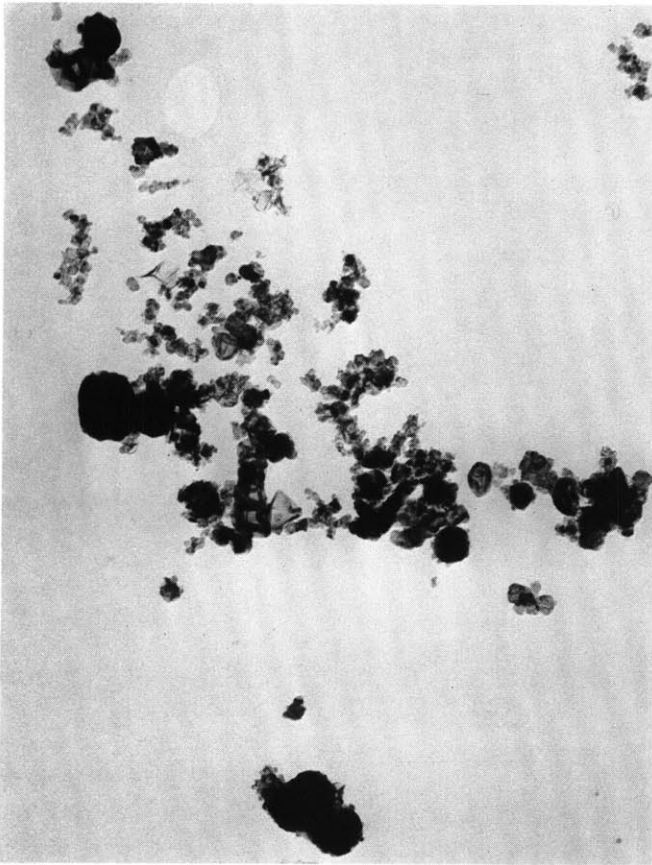


Fig. 4.17 7.0% conversion, run no. M-79; -325 mesh calcine; x33000

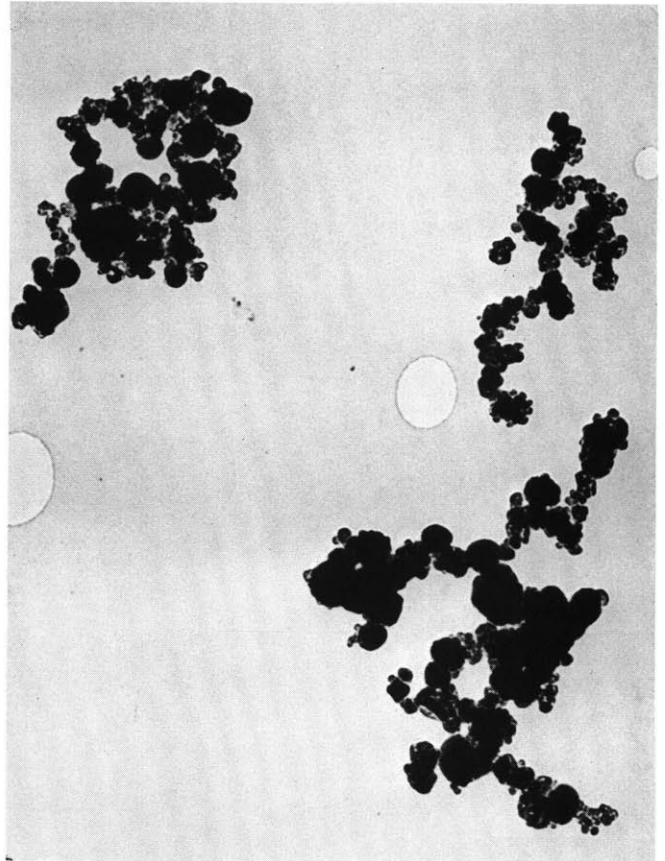


Fig. 4.18 21.7% conversion, run no. M-75; -325 mesh calcine; x33000

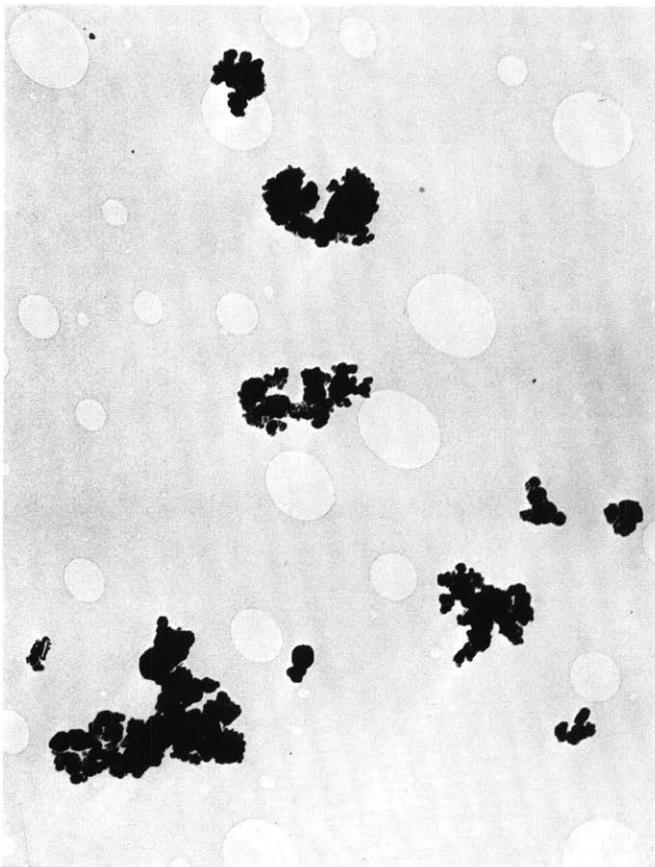


Fig. 4.19 35.0% conversion, run no. M-64; reagent grade lime; x33000

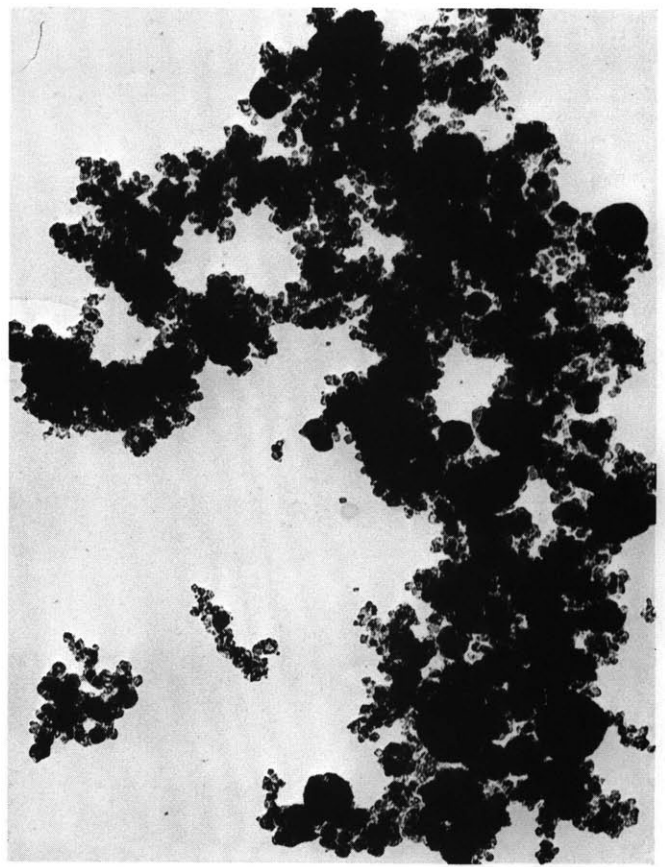


Fig. 4.20 58.3% conversion, run no. M-74; -325 mesh calcine; x33000

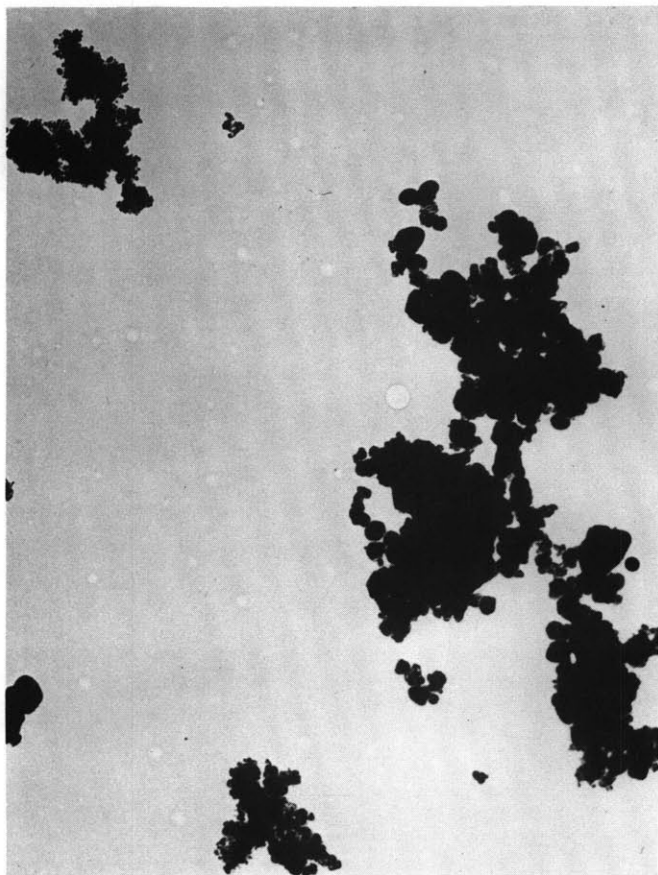


Fig. 4.21 64.0% conversion, run no. M-70; reagent grade lime; x33000

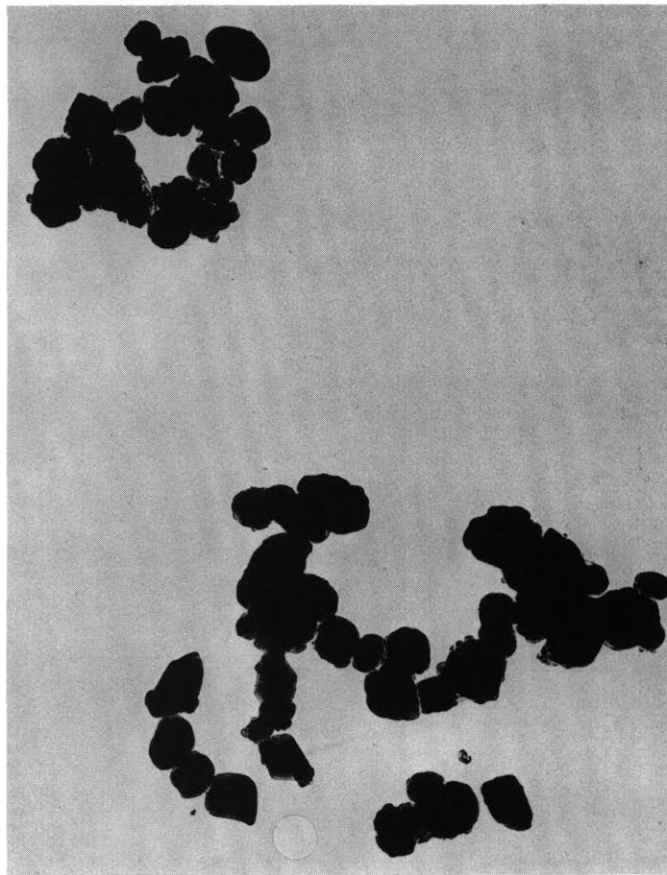


Fig. 4.22 77.0% conversion, run no. M-76; -200 mesh calcine; x33000

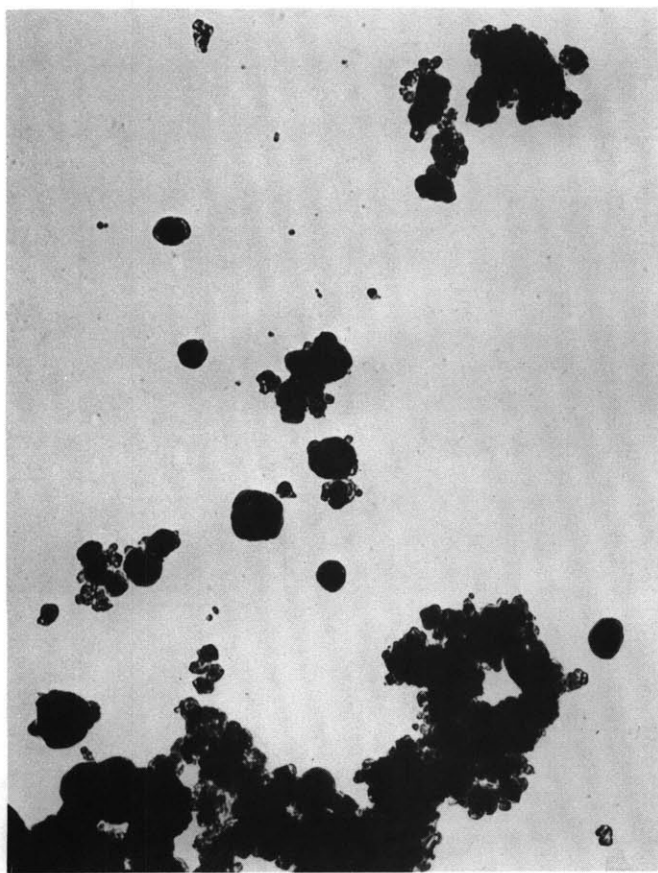


Fig. 4.23 79.5% conversion, run no. M-73; -325 mesh calcine; x33000

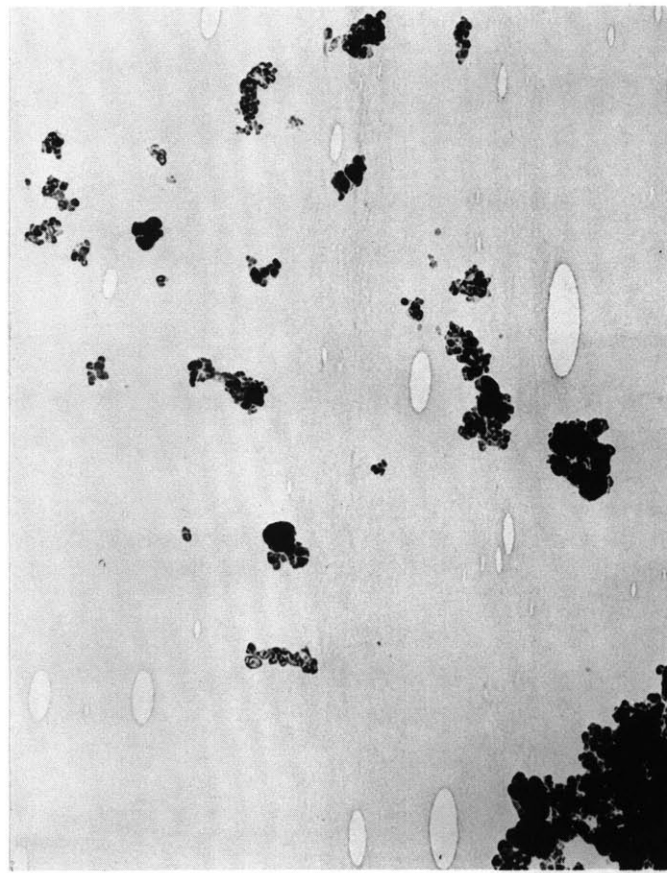


Fig. 4.24 Methane black, run no. SM-1; no lime feeding; x33000

did not agglomerate together but clustered around the conspicuously larger particles. This indicates that methane decomposes heterogeneously in the presence of lime in the reactor.

As seen by the electron microscope, the products of the coal series runs were also agglomerates of fine spherical particles, as in the methane series runs (Figures 4.25 through 4.28). However, in the coal series runs the particle size distributions were much broader, and particles on the order of a micron or larger were often seen along with the particles in sizes comparable to those from the methane series runs. It is postulated that the particles larger than 0.3μ in diameter are mostly of coal char or ashes in origin.

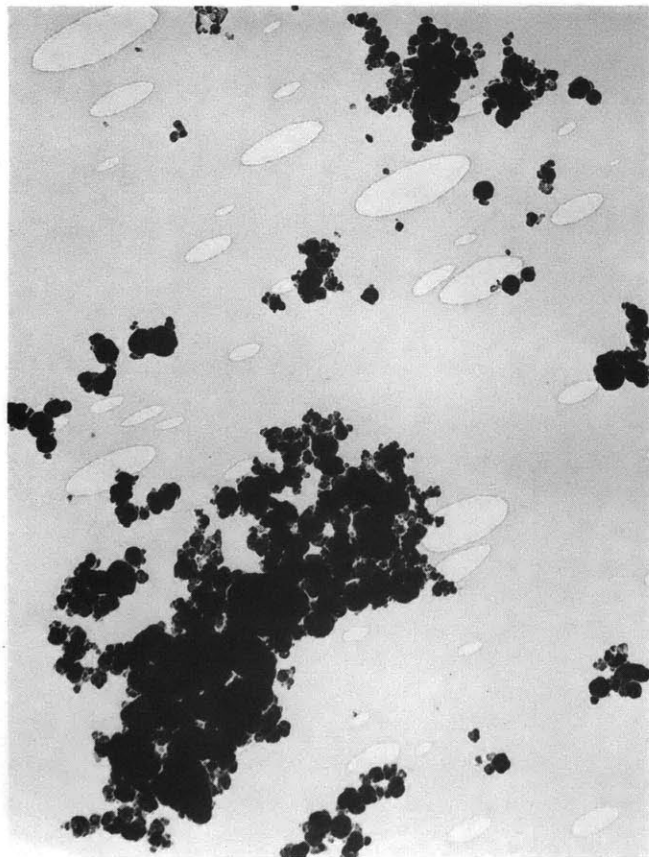


Fig. 4.25 Coal series run #C-13, 22.9% conversion; reag. gr. lime; sample from reactor bottom; x33000

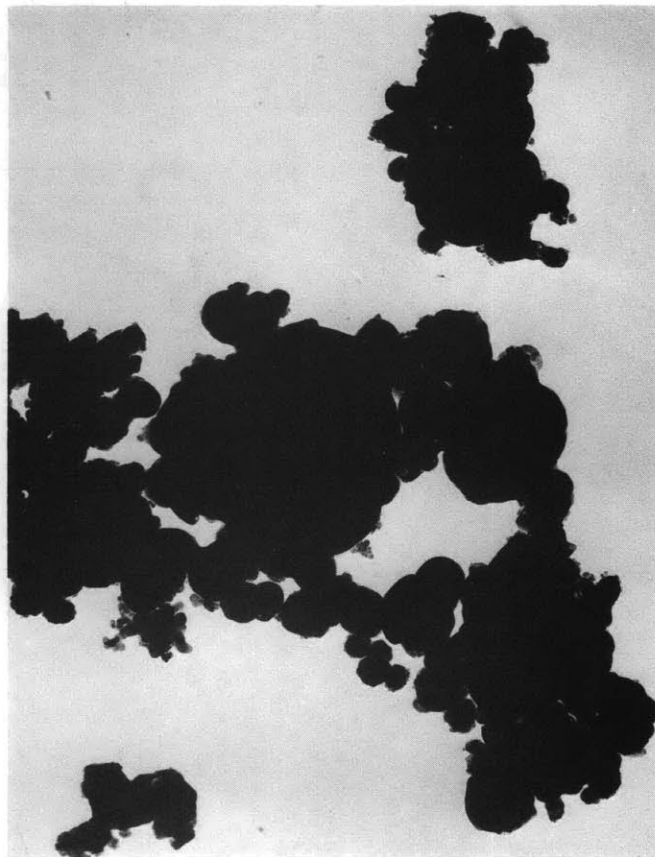


Fig. 4.26 Coal series run #C-6, 38.2% conversion; reag. gr. lime; sample from reactor bottom; x33000

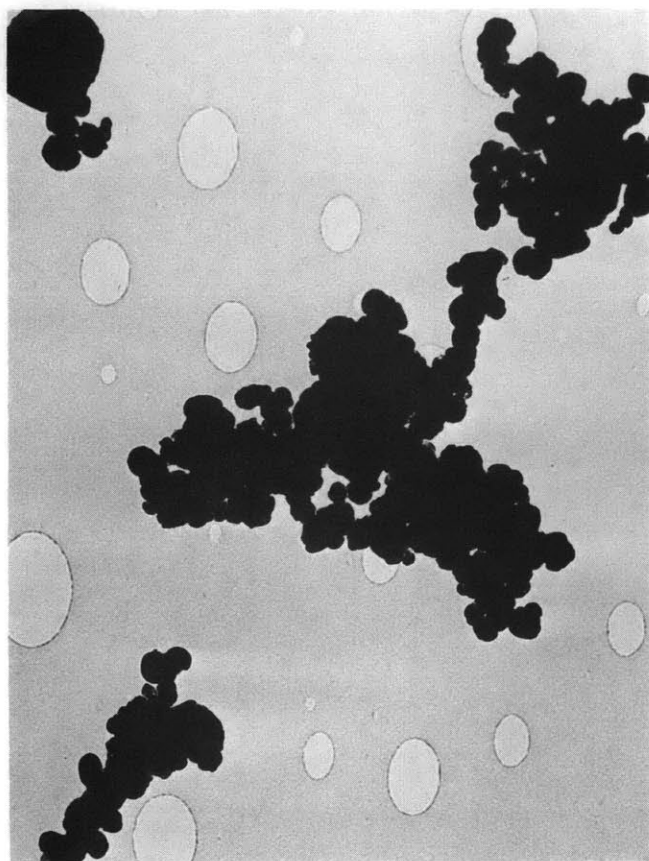


Fig. 4.27 Coal series run #C-8, 49.8% conversion; reag. gr. lime; sample from quench probe; x33000

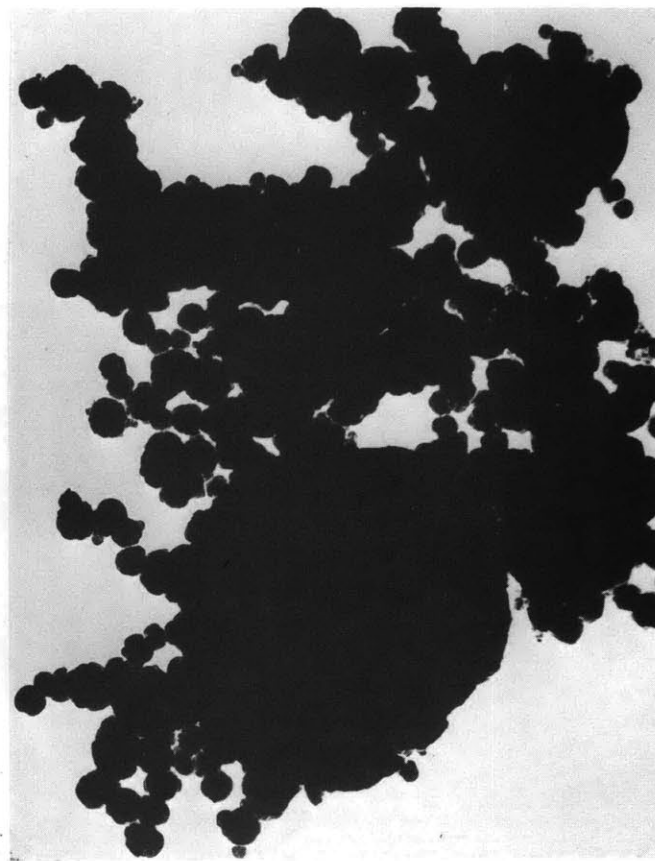


Fig. 4.28 Coal series run #C-10, 53.0% conversion; reag. gr. lime; sample from quench probe; x33000

5. Discussion of Results

5.1. Methane Series Runs

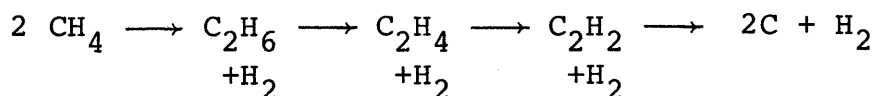
Needless to say, the formation of CaC_2 from the reaction of CaO with methane in the present reaction scheme is an extremely complicated physico-chemical phenomenon that involves the problems of chemical kinetics and heat and mass transfer in and between the gas and solid phases. Nevertheless, a certain generalization can be made regarding the mechanistic process of the overall reaction in that the electric energy is dissipated through the electric arc discharge mainly into the gas phase to almost instantaneously heat the methane to a high temperature, which then decomposes to produce an "outburst" of atoms and free radicals of carbon and hydrogen; these high enthalpy but thermally unstable species then diffuse to the particles to form more stable species by recombination or decomposition reactions or to directly react with CaO to participate in the reaction of CaC_2 formation. Such chemical reactions on the particle surfaces can greatly enhance heat and mass transfer between the gas and solid phases as the diffusing atoms and free radicals are consumed away at the particle surfaces and thus promote the overall chemical reaction as observed in the present study. Therefore, according to the simplified mechanistic view of the overall process, this section is divided into: (1) decomposition of methane, (2) heat and mass transfer between gas and particles, and (3) formation of CaC_2 .

5.1.1. Decomposition of Methane: Formation of Atoms and Free Radicals of Hydrogen and Carbon

It was seen in the section on the experimental results that the conversion of CaO to CaC₂ can be correlated as a function of power input with a single line at a given methane flow rate. In general, the correlation line is characterized by the presence of a rather narrow range of power input in which the conversion increases very rapidly with only slight increase of power input. Once over the critical power range the conversion attains more or less constant value and rises very slowly as the power increases. The specific gas energy corresponding to the critical power input region is in the range of 280-310 kcal/g atom C and 160-210 kcal/g atom C when the gas flow rate is in the range of 16.0-17.3 l/min and 30.0-35.8 l/min, respectively. Although there exist no sufficient data, the critical specific gas energy seems to lie in a range of 110-160 kcal/g atom C when the methane flow is in the range of 44.5-48.2 l/min. The reason that the critical specific gas energy diminishes as the methane flow increases may be that the energy efficiency of the reactor increases as the gas flow increases. Gilles and Clump (29), who used a hydrogen plasma to reduce iron ore, also noted that the efficiency of their plasma torch increased in proportion to the hydrogen flow. Therefore, in the present study, the specific gas energy at a higher methane flow may approximate the true value better than the one at a lower methane flow.

The presence of the critical specific gas energy suggests that the initiation step of the overall reaction is an "out-burst" of atoms and free radicals of carbon and hydrogen from the decomposition of methane.

The overall methane decomposition is generally believed to be a first order reaction which leads to formation of acetylene and of ultimate products by the following path (42, 51):

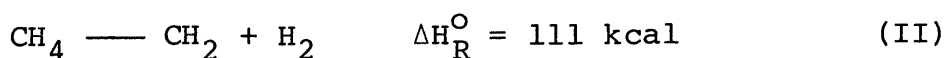
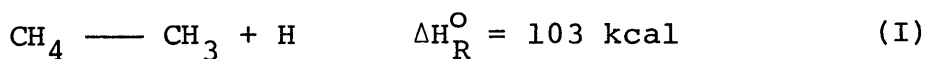


At temperatures above about 1500°K the overall reaction is very rapid. In the reaction path, the acetylene selectivity decreases with increasing pressure because the decomposition of acetylene is a bimolecular process (8, 51), whereas its formation from methane is essentially unimolecular.

The reported overall activation energies for the decomposition of methane ranged from about 83 kcal to 103 kcal, the variation stemming mainly from the different types of reactors used in the studies. In general, shock-tube studies gave a higher activation energy than non-shock-tube studies (42). The distribution of the overall activation energy was attributed to a radical chain mechanism (24), to an effect of heat transfer from reactor wall to gas in flow reactors (39), or to heterogeneous effects that may enter into the kinetics in non-shock-tube studies in general (22, 36). Recently, however, the initial stages of the decomposition were suspected

to be pressure-dependent and believed to have caused the distribution of the overall activation energy because most previous experimental results were made in the pressure-dependent region (22, 36). The overall activation energy in the pressure-independent region was calculated by unimolecular theory as 107.6 kcal/g mole assuming that the initiation step is the formation of CH_3 and H from CH_4 (22).

The initiation step of the methane decomposition is generally believed to involve either or both of the following two reactions:



The heat of reaction of Reaction (I) is well accepted as 103 kcal, but there still exist some uncertainties regarding the corresponding value for Reaction (II), which ranges from about 100 to about 111 kcal, depending on whose reported value one chooses to use for $\Delta H_{\text{f}}^{\circ}(\text{CH}_2)$ (36). However, the value for $\Delta H_{\text{f}}^{\circ}(\text{CH}_2)$ seems more likely to be about 93 kcal (22, 36), which makes the heat of reaction for (II) about 111 kcal.

Although Reaction (I) is more favored now as the initiation step (22), the second reaction may also be important, especially at high temperatures. The thermodynamic stability of the radicals formed in the initiation reactions increases strongly with temperature relative to elements C and H_2 ; therefore, during pyrolysis at high temperature as in the

present study, the concentration of these radicals can be substantially higher than at lower temperatures. Nevertheless, the radicals, i.e. CH_3 , CH_2 , etc., are truly transient species in that they are not thermodynamically stable enough to exist in thermodynamic equilibrium even at substantially high temperatures, e.g. 2500°K or higher. In general, they are considered to further react between each other and methane molecules to form C_2H_6 which may subsequently undergo dehydrogenation reactions to form C_2H_2 and, ultimately, C and H_2 if the reaction mixture is not quenched fast enough.

If the reaction mixture is allowed to reach thermodynamic equilibrium at temperatures below about 2500°K , it will of course almost completely decompose to C and H_2 ; however, from about 2500°K acetylene and hydrocarbon radicals begin to exist in thermodynamic equilibrium in measurable amounts.

In Figure 5.1 (16) we see the equilibrium composition of the carbon-hydrogen system in the heterogeneous region, i.e., solid carbon always present in the system. It was calculated by the method of Bauer and Duff (15). In an optimal quenching condition, the equilibrium mixture of the carbon-hydrogen system at 2500°K or above can yield acetylene in excess of the composition indicated by the equilibrium diagram because C_2H can combine with H to form additional C_2H_2 during cooling. The role of C_2H as precursor to C_2H_2 was theoretically considered and experimentally confirmed in the works of Plooster and Reed (60), Baddour and Iwasyk (11), and Baddour and Blanchet (10). Especially in the work of Baddour and

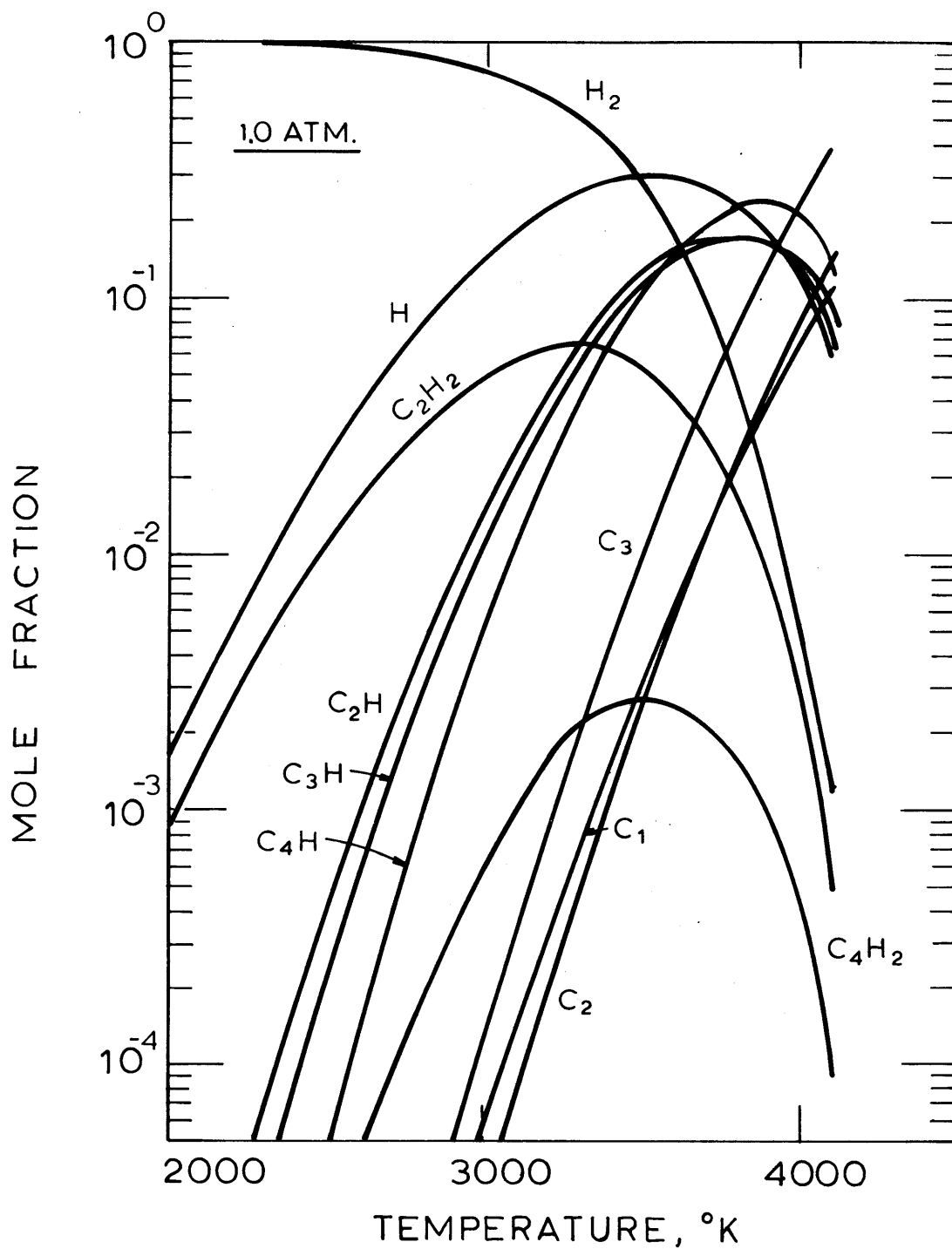


Fig. 5.1 Equilibrium Composition for the Carbon-Hydrogen System in the Heterogeneous Region

Blanchet (10), in which the carbon-hydrogen systems under thermodynamic equilibrium in both the heterogeneous and homogeneous regions were theoretically and experimentally studied for temperatures up to 5000°K, it was possible to obtain a maximum concentration of 52% C₂H₂ by reacting CH₄ with carbon vapor produced from a consumable graphite anode in a high-intensity arc reactor. However, according to their calculations, the maximum C₂H₂ concentration that can be obtained under optimum quenching conditions from an equilibrium system initially charged with CH₄ alone, i.e. no carbon vapor was added, is only slightly over 12%; this maximum occurs in the homogeneous region in the range of 3300°K-4100°K. The carbon sublimation temperature of the system is calculated at about 3200°K. Therefore, since there was no extra source of carbon vapor in the present reactor system, the maximum C₂H₂ concentration obtainable in the present experiments would have been only 12% if methane was allowed to reach thermodynamic equilibrium.

The gas temperature at the anode nozzle exit at a given specific gas energy can be estimated based on the equilibrium diagram (Figure 5.1) if one assumes that the carbon-hydrogen mixture fed at room temperature reaches thermodynamic equilibrium before reaching the nozzle exit. This is done for CH₄, C₂H₄, and C_s-H₂ mixtures at various C/H ratios in the heterogeneous region and shown in Figure 5.2.

With CH₄ as the carbon source, the formation of CaC₂ in the present reaction scheme apparently required an energy

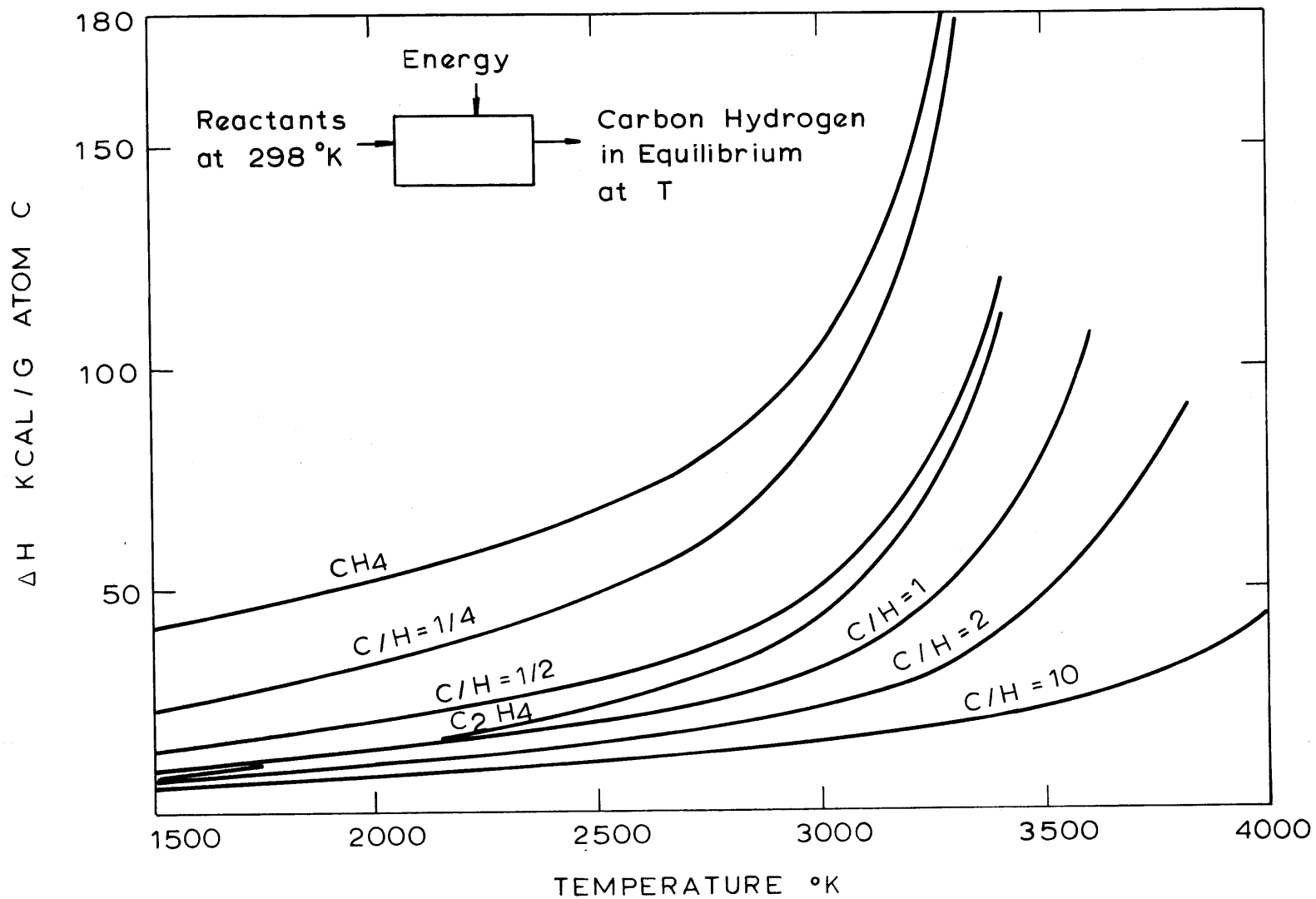


Fig. 5.2 Equilibrium Temperatures of the Carbon-Hydrogen System at Various Specific Enthalpies (Heterogeneous Region Only)

input at a minimum on the order of the activation energy for the decomposition of methane, which is about 100 kcal/g atom C. The corresponding gas temperature is about 3000°K. In the present experiments, the specific gas energies based on gross power input, ranged from about 100 kcal to about 550 kcal/g atom C, and hence the corresponding gas temperatures may have been higher than 3000°K but lower than 4000°K. In this temperature range, the gas temperature of a carbon-hydrogen system of H/C = 4 is relatively insensitive to variation in power input because of the extensive formation of free radicals and hydrogen and gaseous carbon atoms.

5.1.2. Heat and Mass Transfer Between Gas and Particles

The H atoms and hydrocarbon radicals produced from the initiation stages of methane decomposition may begin to diffuse to the CaO particles as soon as they become "nascent." In such a system containing chemical species that are thermodynamically highly unstable, energy will be transported not only by conduction but also by diffusion currents carrying both thermal and chemical enthalpy, the latter being released when the diffusing but thermodynamically unstable chemical species turn to more stabler species by recombination or spontaneous decomposition in the stream or on the cold particles.

A solution of the reactive boundary layer problem has been formulated by Lees (46) and Fay and Riddell (25) for the case of a dissociating air, a condition that accompanies

hypersonic flights, for two extreme regimes: the recombination rate is very fast relative to the characteristic diffusion time of the dissociated atoms (thermodynamic equilibrium boundary layer) or very slow (frozen boundary layer). In the latter case, recombination does not take place in the boundary layer but on the solid surface which may have a varying degree of catalytic effect on the reaction depending on the solid material. For the recombination of dissociated oxygen and nitrogen (33), pyrex is practically noncatalytic and metal oxides are moderately catalytic while metals seem to be highly catalytic. The catalytic efficiency of some materials has a strong positive temperature dependency; consequently, a higher surface temperature will increase the recombination heat release at the surface while the conducted heat is diminished as a result of the reduced temperature gradient. Therefore, composition of solid materials can greatly affect the rate of heat transfer in the case of a dissociating gas.

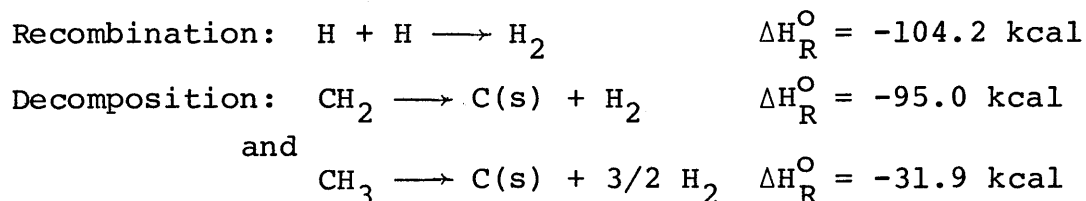
Heat transfer to the particles being heated by a thermal plasma can be greatly increased if the plasma contains a dissociating gas. According to the analysis by Capitelli et al. (21), heat transfer to $60 \mu \text{Al}_2\text{O}_3$ particles injected into a thermal plasma can be approximately 80% higher in an Ar+8% N_2 than in a pure argon plasma under otherwise identical conditions. Nevertheless, the result should be regarded only as tentative because of the oversimplifying assumptions they necessarily had to make to arrive at the conclusion.

In the present experiments the diffusing chemical species that carry both thermal and chemical enthalpy to a particle can directly react with the chemical components of the particle. Heat transfer to such a chemically reacting surface can be even greater than to a catalytic but nonreactive surface.

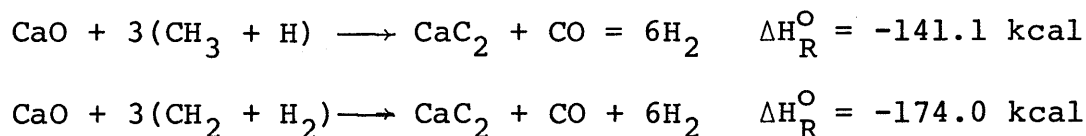
The catalytic effect of CaO on the overall decomposition of CH₄ leading to ultimate products C and H₂ is experimentally observed as evidenced by Figure 4.5, which shows that the C₂H₂ concentration in the gas product diminishes very sharply initially as the lime feed rate increases from zero while the conversion of carbon in methane to CaC₂ and CO increases only linearly with the lime feed rate until the carbon is almost completely converted at an excess lime feed rate. The catalytic effect of CaO on methane decomposition is also shown in the electron photomicrographs (Figures 4.17 through 4.23) of solid products, which indicate that CH₄ is heterogeneously decomposed in the presence of CaO.

The energy that can be released within the reactive boundary layer of a CaO particle by recombination and decomposition of the atoms and radicals of hydrogen and carbon that are produced upon the decomposition of methane can be high enough to heat the lime particle to a reaction temperature and supply the reaction energy for CaC₂ formation at the temperature. As an example, the recombination of H atoms and the decomposition of CH₂ and CH₃ radicals, all of which are the intermediates produced in the initial stages of methane

decomposition, are shown in the following:



The thermodynamic values are taken from (14). The overall energetics of CaC_2 formation are presented in the following for the case of CaO reacting with the "nascent" chemical species in the initial stages of methane decomposition:



Therefore CaC_2 formation can be highly exothermic when CaO reacts with H atoms and CH_2 and CH_3 radicals. This point is elaborated further in the following section.

5.1.3. CaC_2 Formation

The foregoing discussions concerned the formation of highly reactive "nascent" species in the initial stages of methane decomposition and the subsequent diffusion of the species to CaO particles across the reactive boundary layer carrying both thermal and chemical enthalpy. It was shown that heat and mass transfer to the particles can be greatly enhanced due to the chemical reactions taking place within the boundary layer. In this section the mechanism of CaC_2 formation is discussed.

In the methane series experiments, there was no noticeable effect of lime feed rates on the conversion of CaO to CaC₂ even though they were varied from about 0.1 to 1.4 times the stoichiometric feed rates (Figure 4.3). Therefore it was possible to convert almost all carbon in the methane fed into CaC₂ and CO by simply feeding excess lime at specific gas energies above the critical values. The absence of the effect of lime feed rates on CaO conversion shows that the overall CaC₂ formation is a localized phenomenon around individual particles, not affected by the presence of each other.

It was also observed that there was no substantial particle size effect on CaO conversion even though the original CaO particle size was varied by an order of magnitude. Electron photomicrographs (Figures 4.17 through 4.23) showed that the solid product is invariably an agglomerate of extremely fine spheres of diameters ranging from 200 Å to 0.3 μ regardless of original lime particle size and the level of CaO conversion; at 7.0% conversion (Figure 4.17), however, angular grains of the order of 0.1 μ in size were occasionally observed among the predominantly spherical particles of about 200 Å to 0.3 μ, as in the other cases.

The individual particles of calcines of the natural limestones used in the present experiments were seen to consist of submicron sized round grains that were fused together, giving a sponge-like texture to the calcines (Figures 4.15 and 4.16). The grains were mostly in the range of 0.5-1.0 μ

in diameter, which was substantially higher than the particle size range of the product. Therefore, the fine particles of the product cannot be attributed to breaking-up of the original lime particles into the individual grains; in addition, the reagent grade CaO, which did not have the sponge-like texture of the natural calcines, also produced agglomerates of fine particles in the particle size range.

The formation of submicron-sized particles even at very low conversion indicates that they are produced directly from CaO in the early stages of the overall reaction. The fine particles may have formed as a result of vaporization of CaO and its subsequent condensation, but it cannot be a dominant factor because the boiling point of CaO is known to be 3773°K (14), while in the methane series experiments the average gas temperature was most likely in the range of 3000°-4000°K. Instead, they may have formed predominantly from melting (m.p. 2888°K) and mechanical breaking-up of the CaO particles as a result of thermal stress while passing through the arc zone which is at substantially higher temperature than the average gas temperature. This postulation is substantiated by the presence of the submicron-sized grains that are angular in shape in the product of low conversion.

Formation of submicron-sized particles from gas-solid reactions in a "plasma" jet is also observed by Stokes et al. (66, 68) and Gilles and Clump (29): in the study on carrying -325 mesh WO₃ powder in a hydrogen stream into a helium "plasma" jet, Stokes et al. (66, 68) were able to reduce up

to 95% of the original WO_3 to W. They reported that the average particle size of the produce was from 0.5 to 1 micron. Gilles and Clump (29) injected iron ore of -74, +44 μ in particle size into a pure H_2 or 25% H_2 - 75% Ar plasma jet and were able to convert up to 70% of the ore into iron. At low reduction, they reported that the reduction started on the outside of the particles and penetrated deeper as the plasma energy increased. At high reduction, however, the product appeared as an agglomerate of very fine particles as small as 100 \AA , which they attributed to mechanical breaking-up of the product rather than by vaporization of iron.

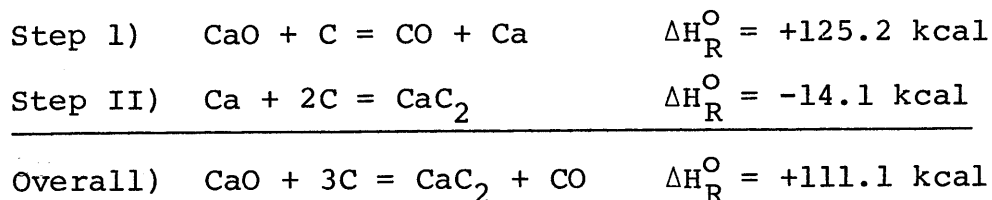
The absence of particle size effect on CaO conversion apparently indicates that the overall CaC_2 formation is controlled by the chemical reaction within the CaO particles once an "outburst" of H atoms and other high enthalpy but thermodynamically unstable species takes place in the initial stages of methane decomposition. It is also conceivable that the absence of particle size effect may have been caused by the mechanical breaking-up of original CaO particles into submicron-sized particles in the early stages of the overall conversion. Even if so, however, the conversion may have been still chemical-reaction-controlled because the broken-up particles were so small in particle size that diffusion may not have been the rate-limiting factor.

The role of the "nascent" chemical species in the formation of CaC_2 was experimentally confirmed in the experiments

of prolonged residence time, in which it was shown that increasing the residence time of the reactants in the anode nozzle by an order of magnitude (from about 1 msec to 10 msec) increased the conversion only by a few percentage points. If the reaction mechanism operative in and immediately beyond the arc zone were still effective over the entire length of the anode nozzle, then the conversion should substantially increase with the increase in residence time; since this was not the case, one can conclude that the conversion of CaO to CaC₂ takes place only in the presence of the "nascent" chemical species which have a very short life span and hence may not exist far beyond the arc zone.

Increasing the specific gas energy beyond the critical value, which may be on the order of 100 kcal/g mole in the case of methane, may not significantly further CaO conversion because the CaC₂ formation is controlled by the chemical reactions within the CaO particles.

Formation of CaC₂ in the present reaction scheme may still involve essentially the two elementary reaction steps of CaC₂ formation from CaO and C(s):

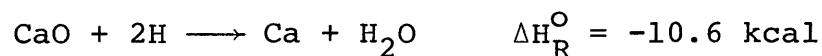


However, the carbon reacting in the present reaction is "nascent" in nature and thus far more reactive than the carbon derived from C(s). In addition, H atoms and H₂ molecules

produced in the present reaction scheme may actively participate in the reduction of CaO to Ca and CO in Step I. Although the polyatomic hydrocarbon radicals may directly react with CaO or Ca to form CaC₂, it is more likely that they first decompose to the elements H and C and then react with either CaO or Ca.

In order to elucidate the reaction mechanism in the present experiments, the thermodynamics of various reactions related to CaC₂ formation involving both carbon and hydrogen are considered (Figure 5.3). In general, the thermodynamic consideration indicates the rate limiting step in the formation of CaC₂ is Step I, i.e., the reduction of CaO to Ca and CO, since the equilibrium constant for Step II is highly favored for the formation of CaC₂ and several orders of magnitude higher than Step I. Therefore, once Ca is formed, it will immediately proceed to form CaC₂ so long as enough carbon is available for the reaction.

Reduction of CaO to form Ca can be greatly enhanced by H atoms in the initial stages of CaC₂ formation:



The H₂O produced will immediately react with "nascent" carbon species, and hence the reduction of CaO by H atoms can be greatly facilitated. The reaction of H₂O with carbon is highly favored in the direction of forming more CO and H₂ with increasing temperature. Nevertheless, the reduction of CaO

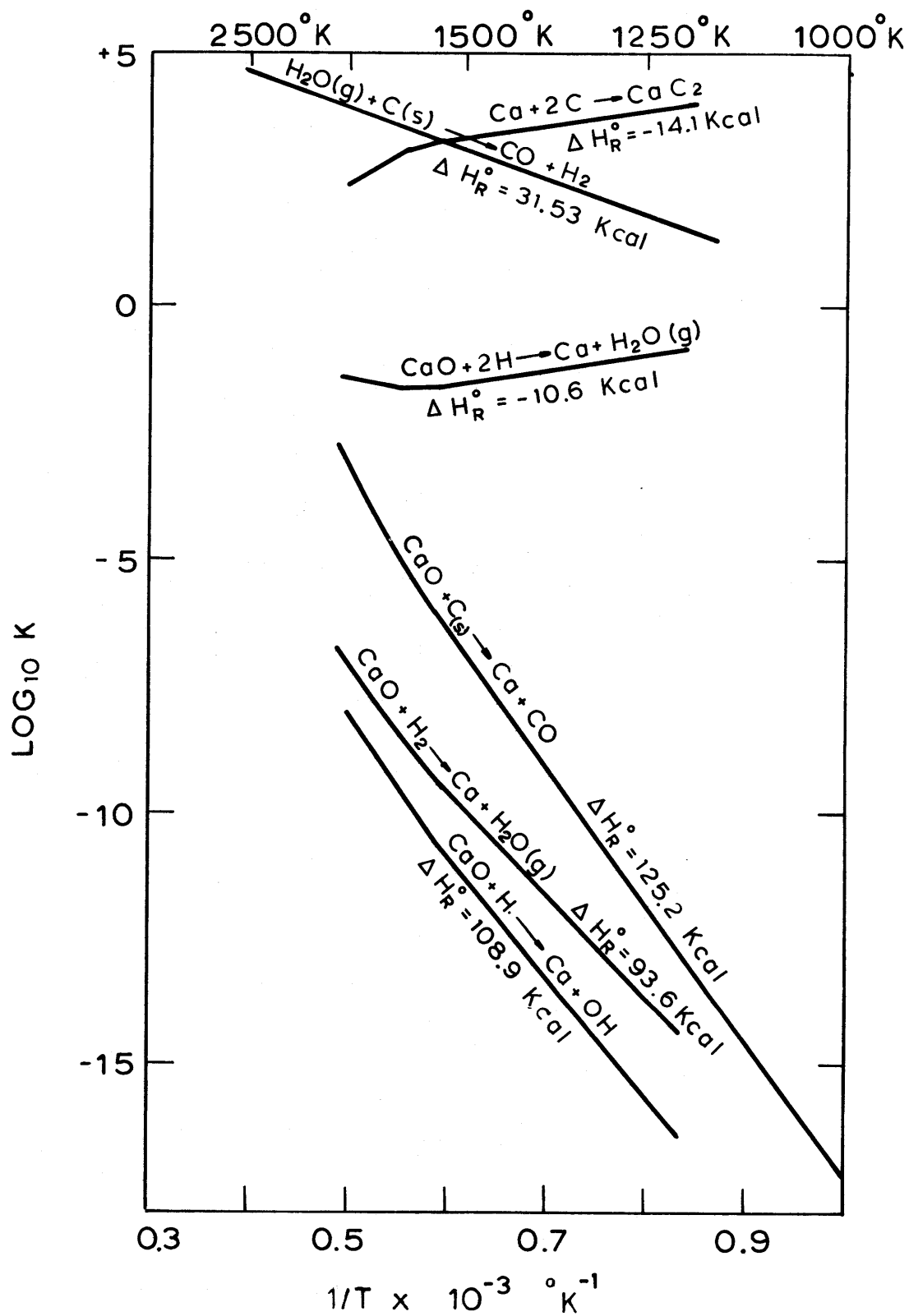


Fig. 5.3 Equilibrium Constant vs. Temperature for Various Reactions Related to CaC_2 Formation

by C may still be important, especially above about 2500°K, because of intense chemical activity of "nascent" carbon species.

In the present experiments, the overall formation of CaC_2 was seen to be limited by the chemical reactions within the CaO particles. In view of the thermodynamic considerations on the two elementary steps of CaC_2 formation, it seems the rate limiting step is the reduction of CaO to Ca. Once Ca is formed, it will immediately proceed to form CaC_2 . Dissociation of the product CaC_2 in the intermediate range of temperatures during cooling is not likely to occur because the reaction $\text{Ca} + 2\text{C} = \text{CaC}_2$, which is thermodynamically favored for the formation of CaC_2 probably up to 3500°K as can be seen from the extrapolation of the existing data, is increasingly more favored toward the right as the temperature decreases.

5.2. Ethylene Series Runs

Ethylene requires less energy per g atom C to reach a given temperature than methane because it has a higher C/H ratio and, unlike methane which has a negative heat of formation, a positive heat of formation which makes the overall decomposition exothermic. As an example, ethylene, per g atom C basis, requires less than one-half of the energy required for methane to reach 3000°K (Figure 5.2), which is slightly over 100 kcal/g atom C for the latter. In addition, the overall activation energy is of the order of 50 cal/mole,

or 25 kcal/g atom C, for the decomposition of ethylene (9, 64). Therefore, one can expect the critical energy input required for the conversion of CaO to CaC₂ to be less for ethylene than methane as the carbon source. Nevertheless, the critical energy input will not be of the order of the overall activation energy for the decomposition of ethylene because the radicals produced in the initial stages of decomposition, which may be C₂H₃, C₂H₅, and others, may not be energetic enough.

The experimental results generally confirmed the considerations discussed above; the conversion of CaO to CaC₂ began to commence at lower energy input with ethylene as the carbon source than with methane at an equivalent carbon flow (Figure 4.7) and, as a result, the overall energy efficiency was generally higher.

5.3. Coal Series Runs

In the present reaction scheme of producing CaC₂ from coal and lime, the carbon in coal has to volatilize first before reacting with lime. Volatilization of a high volatile coal can be far more extensive under flash heating conditions than slow heating conditions, especially in an H₂ atmosphere. In general, the extent of volatilization and the gas product composition depend on the rate of heating and the final temperature. However, if the final temperature is above about 1500°K, C₂H₂ can be produced as the main product because above the temperature it is thermodynamically stabler

than most other hydrocarbons. The overall formation of C_2H_2 from the hydrogasification of a high volatile coal is a transient phenomenon as in the high temperature pyrolysis of hydrocarbons in that the acetylene formed will decompose to ultimate products C and H_2 unless the reaction is immediately arrested by quenching.

The extent of coal volatilization can be very substantial in electric-arc discharge devices as previously described in the Introduction. It is discussed in the section that the volatilization of a high volatile coal can be almost complete if the fine powder of coal is directly passed through an electric-arc discharge sustained in a stream of hydrogen. However, substantial fractions of the volatilized product can be lost as C and H_2 due to its thermodynamic instability under the operating conditions of practical interest.

The overall mechanistic process of CaC_2 formation from the reaction of CaO and the "nascent" carbon species will be essentially the same regardless of whether the "nascent" species are derived from the pyrolysis of hydrocarbons or from the hydrogasification of coal. In the methane series experiments it was possible to make almost all the carbon of methane fed react with CaO to form CaC_2 and CO by feeding excess lime. Therefore, since it may be possible in view of the previous discussion to almost completely gasify a high volatile coal in the present reaction scheme, one can expect the conversion of the carbon in coal to CaC_2 and CO to be

very high under certain operating conditions. In the present experiments, the highest conversion of the carbon in coal was 90.1%, which was obtained by feeding a coal/lime mixture containing 47.0 wt.% excess lime over the stoichiometric mixing ratio.

As discussed in the Introduction section, Krukonis et al. (28, 43) used a rotating-arc reactor which was schematically similar to the one used in the present study to investigate the economic feasibility of producing C_2H_2 directly from coal. The overall process of the study was very similar to the present study in that a fine powder (-80 mesh) of a high volatile coal, volatile matter content of 38 wt.% (as received), was carried by hydrogen through the arc zone. In the study, the formation of soot was always substantial, indicating that the decomposition of the hydrocarbons (mainly C_2H_2) gasified from coal was fairly extensive in most runs. Applying the ash tracer technique to three runs, they estimated that between 57 and 68 wt.% of the coal fed might have been gasified. The specific gas energy of the runs analyzed was in a range of 25 to 52 kcal/g mole H_2 and the specific solid energy was in a range of 25 to 47 kcal/g atom C. The C/H ratio of the gas-solid feed mixture was in a range of 1/2.5 to 1/3.1 (H in the coal included). The power input was 60-100 kw with the reactor operating at 0.3-0.5 atm.

Although it was firmly established in the present experiments that a high volatile coal can be an effective source of "nascent" carbon species of intense chemical ac-

tivity, the specific energy requirement for the formation of CaC_2 was relatively high. The lowest SER ever achieved with coal as the carbon source was 32.1 kwhr/lb C_2H_2 equivalent. The rather high energy requirement is undoubtedly due to the preliminary nature of the experiments. As discussed above, the analysis by Krukonis et al. suggested that gasification of coal can be substantial at an energy input on the order of only 50 kcal/g atom C. For a Coal- H_2 -CaO system which contains carbon and CaO at the stoichiometric ratio, the energy required for a complete conversion of CaO to CaC_2 is generally somewhat higher than the 50 kcal/g atom rate. This indicates that a high conversion of CaO to CaC_2 can be achieved with the energy requirement approaching the thermodynamic minimum in scaled-up reactors of high energy efficiency.

5.4. Economic Feasibility of the Reaction Scheme

In Figure 5.4 we see the thermodynamic energy requirement as a function of temperature for producing enough CaC_2 at 1 atm to subsequently yield one lb C_2H_2 from the stoichiometric mixture of CaO and various carbon sources fed at 298°K. The thermodynamic effect of the presence of hydrogen in the feed is to increase the energy requirement for the overall CaC_2 formation because of the additional sensible energy required for heating the hydrogen to the reaction temperature. In addition if the carbon source possesses a negative heat of formation, as does CH_4 , then the overall

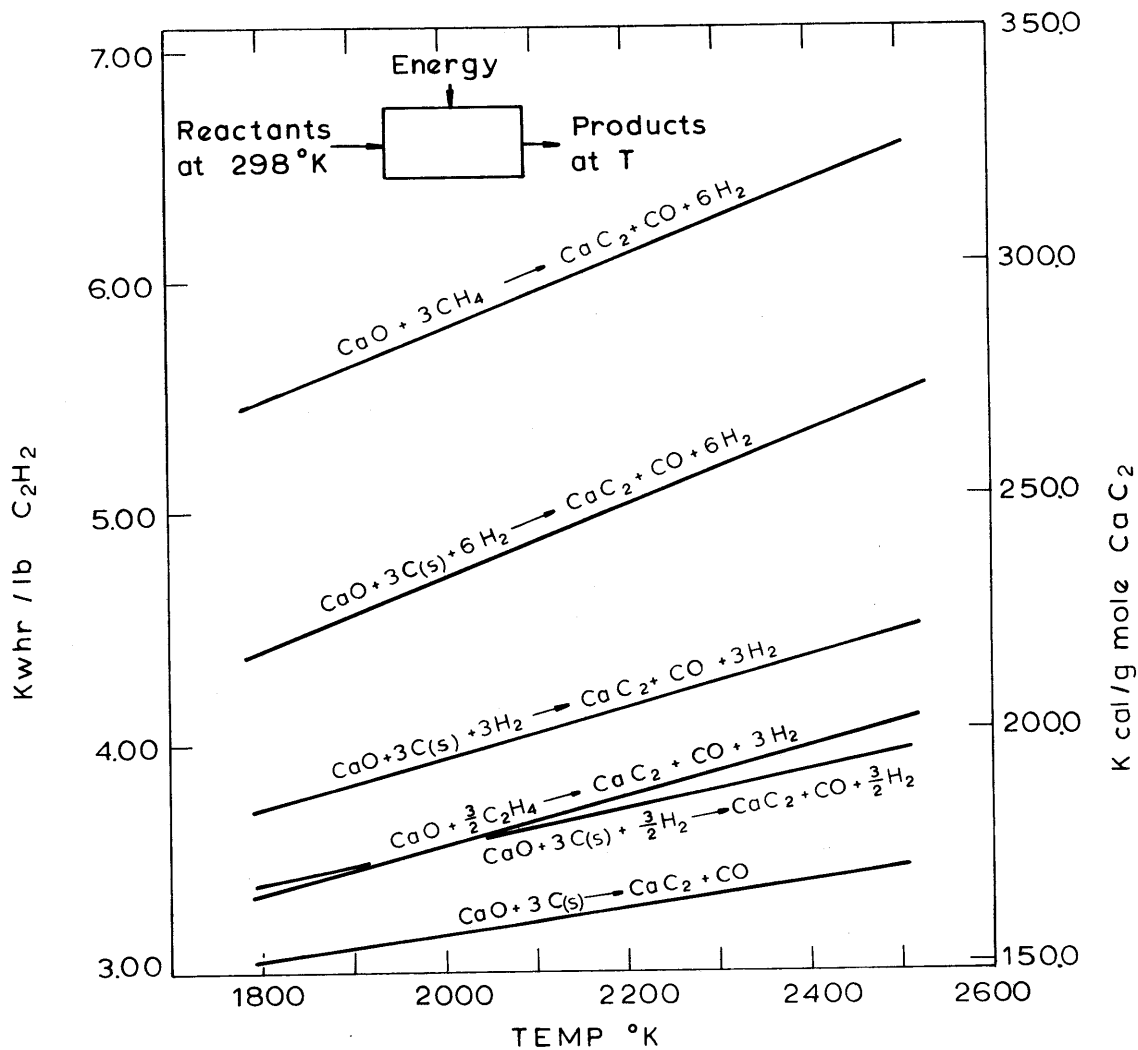


Fig. 5.4 Thermodynamic Energy Required to Produce One lb C₂H₂ from CaO and Hydrocarbons/or Coal & Hydrogen

energy requirement will further increase due to the additional thermal energy required for decomposing it to C and H₂. Contrarily, a carbon source with a positive heat of formation will lower the energy requirement, as is the case with ethylene. In general the energy requirement increases with product temperature, and hence it is desirable to keep the latter as low as possible. The lower bound of the product temperature is uniquely determined by the equilibrium partial pressure of CO (see Figure 2.1). For the stoichiometric CaO-CH₄ mixture, the minimum energy requirement is 5.8 kwhr/lb C₂H₂ and occurs at 1980°K; for the CaO-C₂H₄ mixture it is 3.6 kwhr/lb C₂H₂ and occurs at 2020°K. As a reference, the CaO-C(s) mixture requires a minimum energy input of 3.2 kwhr/lb C₂H₂, which occurs at 2130°K.

For simplicity, coal is represented in the figure as β-graphite (i.e., $\Delta H_{f, \text{coal}}^{\circ} = 0$). In reality, coal may possess a positive heat of formation, which may be of the order of 10 kcal/g atom C (45, 53). If this is true, then the thermodynamic energy requirement for producing CaC₂ from the CaO-H₂-Coal mixture will be lower by about 30 kcal/g mole CaC₂ (equivalent to 0.6 kwhr/lb C₂H₂) than as indicated in the figure. In the case of using coal as the carbon source, the minimum thermodynamic energy requirements are 4.7 kwhr/lb C₂H₂ (1980°K) and 4.0 kwhr/lb C₂H₂ (2020°K) for C/H ratios of, respectively, 1/4 and 1/2, assuming that the coal has a zero heat of formation. However, if coal does

possess a positive heat of formation of the order of 10 kcal/g atom C, as discussed above, then the thermodynamic energy requirement can be as low as 3.4 kwhr/lb C_2H_2 when the C/H ratio is 1/2.

In 1972, AVCO (28) concluded that C_2H_2 could be directly produced from coal in a rotating-arc reactor at a price low enough to be competitive with any of the current C_2H_2 manufacturing processes and even with ethylene as the feedstock for the polyvinyl chloride market. The conclusion was based on the following experimental results: yield of 35 lbs C_2H_2 /100 lbs coal, C_2H_2 concentration of 10%, and an energy requirement of 4.0 kwhr/lb C_2H_2 . Although the overall picture of the energy related area has drastically changed since then, it may still serve as a useful guide for the present process.

The advantages of the present process over the AVCO Arc-Coal process are several fold in that it does not require the rather expensive C_2H_2 separation and purification step, it can be operated at the atmospheric pressure unlike the AVCO process (which was operated at 0.3-0.5 atm), and the thermal energy in the product stream can be recovered since the quenching requirement of the product in the present process is not as severe as the AVCO process. In the AVCO process, the energy required for separating and purifying C_2H_2 may be on the order of 1.3 kwhr/lb C_2H_2 , which is the value cited for the Huels Flaming Arc Process (52). Therefore, the present process can be competitive with the AVCO

process if the energy consumption is in the range of 5.0-5.5 kwhr/lb C_2H_2 . At this range, it is also strongly competitive with the former method of manufacturing CaC_2 which requires an energy input of about 5.0 kwhr/lb C_2H_2 . It is so because: (1) capital cost is much lower as the reactor size is much smaller; (2) coal instead of coke is used as a raw material; and (3) operating cost is lower as it is essentially a continuous operation, whereas the former process is basically a semi-continuous operation in that the molten product is manually tapped from the furnaces intermittently.

The present process can also be regarded as a net producer of hydrogen since it does not consume H_2 but, on the contrary, may yield additional H_2 from hydrogen containing carbon sources. A high volatile coal typically has about 0.6-1.0 H atoms per atom C. Furthermore, since the gas product, which is at 2000°K or higher, will contain a high concentration of CO, additional H_2 can be produced from the water-gas shift reaction utilizing its own sensible energy for the reaction energy.

In the coal series experiments the lowest energy consumption was 32.1 kwhr/lb C_2H_2 . In the methane series experiments it was 16.3 kwhr/lb C_2H_2 . However, it could have been as low as 9.2 kwhr/lb C_2H_2 were the lime feed rate increased so as to achieve 100% conversion of the carbon in the methane fed to CaC_2 and CO; it was seen in the methane series experiments that lime feed rates did not affect the

overall CaO conversion so long as the conversion was not limited by the availability of carbon.

The energy efficiency of an endothermic reaction of heterogeneous type in an arc-discharge reactor can be high, as demonstrated by Bethlehem Steel Corporation in reducing iron oxides by an arc-heated gas mixture of hydrogen and natural gas at 100 kw and one megawatt levels (31); in the process pure molten iron was produced with the net energy consumption as low as 1.2 kwhr/lb iron, while the minimum thermodynamic energy requirement was about 1.0 kwhr/lb iron. The specific energy requirement was decreased by reactor scale-up from 100 kw to one megawatt, the use of finer ore particle size, and decrease in the hydrogen/natural gas ratio. The lowest gross energy consumption was 1.5 kwhr/lb iron which was achieved with the hydrogen/natural gas ratio of 2 at one megawatt level.

The results from the present experiments and from the reduction of iron oxides by Bethlehem Steel Corporation indicate that CaC_2 can be produced from the present reaction scheme at an energy efficiency close to the thermodynamic value; in the case of using a high volatile coal as a source of carbon, the thermodynamic energy requirement can be as low as 3.4 kwhr/lb C_2H_2 when the C/H ratio in the feed is 1/2. Hydrocarbons can also be used as the source of carbon for manufacturing CaC_2 in the present reaction scheme; however, natural gas may not become an economical source of carbon unless the C/H ratio is increased by mixing with other heavier hydrocarbons.

6. Conclusions

(1) A novel method of manufacturing CaC_2 from the reaction of CaO with "nascent" carbon and hydrogen species is developed in the present study; the "nascent" chemical species can be produced from the decomposition of hydrocarbons or from the hydrogasification of high volatile coals in a rotating-arc reactor.

(2) Extensive studies were made with methane as the source of carbon in order to delineate the overall reaction mechanism. The results from the methane series runs indicated the following:

- (a) Lime feed rates do not affect the conversion of CaO to CaC_2 so long as the conversion is not limited by the availability of carbon in the feed. This indicates that the conversion is a localized phenomenon around individual CaO particles. It also indicates that complete conversion of carbon in the feed to CaC_2 and CO can be achieved by simply increasing the lime feed rate; 95% was the highest conversion of C from the methane fed to CaC_2 and CO .
- (b) There probably is a critical energy input on the order of the overall activation energy for the decomposition of methane in order for the CaO conversion to commence. This shows the importance of the role of the "nascent" chemical species in the CaO conversion or any endothermic reactions of heterogeneous type.
- (c) Once over the critical energy region, the conversion rises only slowly with an increase in energy input. This implies that the rate controlling step shifts from the gas phase to and around individual CaO particles as the energy input increases beyond the critical region.
- (d) No substantial particle size effect on the CaO conversion with feeding of CaO particles of

-8 μ , -44 μ , and 74 μ in size indicates that the overall conversion is probably chemical reaction-controlled. Nevertheless, it is not clear whether the absence of particle size effect is the result of mechanical breaking up of CaO particles in the early stages of the overall reaction. Even if so, however, the overall CaO conversion may still be chemical reaction-controlled because the broken-up particles are extremely fine (less than 0.3 μ).

- (e) The speed of quenching is not of importance in preserving the solid product CaC₂. Dissociation of CaC₂ in the intermediate range of temperatures during cooling is not thermodynamically favored.
- (f) Extending the residence time of the reactants in the anode nozzle downstream of the arc zone does not noticeably increase the conversion of CaO to CaC₂; this indicates that the conversion is driven by the "nascent" chemical species which are abundant only in and immediately beyond the arc zone.
- (g) Thermodynamic considerations indicate that the conversion of CaO to CaC₂ in the present process can be enhanced by H atoms which may directly reduce CaO to Ca and H₂O. The backward reaction is prevented by the reaction of nascent carbon species with H₂O to produce CO and H₂.

(3). Ethylene was also tried as the source of carbon; the result was a general increase in energy efficiency over methane as the source of carbon. This was attributed to the higher C/H ratio and the positive heat of formation of ethylene. The lowest specific energy requirement was 16.0 kwhr/lb C₂H₂.

(4) A high volatile bituminous coal was also successfully used as a source of carbon for the conversion of CaO to CaC₂ by carrying an intimate mixture of fine powders of the coal and CaO by hydrogen through a rotating arc. The highest

CaO conversion achieved was 61%. The highest conversion of the carbon in coal to CaC_2 and CO was 90%, which was obtained when excess lime was present in the feed mixture.

(5) The energy efficiency of the present process can be improved in scaled-up reactors. Presently, the lowest energy consumption achieved with coal as the carbon source was 32.1 kwhr/lb C_2H_2 . It was 16.3 kwhr/lb C_2H_2 with methane as the source of carbon. Thermodynamic consideration indicates natural gas alone cannot be an economic source of carbon for the present process. On a commercial scale the specific energy requirement should be in the range of 5.0-5.5 kwhr/lb C_2H_2 , which may be achieved in scaled-up reactors.

7. Recommendations

- (1) Scale up the present reactor to a minimum of 40 kw power level to increase the energy efficiency of the reaction scheme. This will also increase the arc stability. Results from the scaled-up studies together with the present experimental results will indicate the economic feasibility of the process at a much larger commercial scale operation (e.g. one megawatt or larger).

- (2) Improve the design and operation of a water-cooled copper anode and conduct an expansive matrix study with coal as the carbon source to determine effects of various experimental parameters on CaO conversion.

- (3) Expand the analysis of the gas products to include non-hydrocarbon gases by using a thermal conductivity gas chromatograph; correlate CO concentration in the gas product with CaC₂ production rate. In the present study, only hydrocarbons were analyzed on a flame ionization detector.

- (4) In the case of using coal as the carbon source, determine the distribution of sulfur and nitrogen from the original coal in both gas and solid products. Sulfur in coal may end up as CaS which will yield H₂S upon hydrolysis. The desulfurized and possibly denitronized char from the present process can be a valuable "clean" fuel which can be used for other purposes.

(5) Investigate the feasibility of applying the present reaction scheme to other processes. So far, most studies involving an arc discharge were conducted by injecting the reactants into a high enthalpy jet downstream of the arc zone. As a result the conversions were often low and the energy efficiencies were generally poor. The following reactions are suggested for future investigation:

- (a) Carry on the reduction of iron oxides by conveying an intimate mixture of fine powders of a high volatile coal and iron oxides by hydrogen through the arc zone. The gaseous byproducts H_2 and CO which are at high temperatures can be directly used for other chemical synthesis and thus can make the process economically more attractive.
- (b) Study the feasibility of producing various metals and metallic carbides from their respective oxides or halides.
- (c) Study the feasibility of producing various nitrides from their metals, metal oxides or halides. In this case N_2 , NH_3 and other nitrogen containing compounds can be used as the source of nitrogen.

8. Appendix

8.1. Tabulation of Experimental Results

Complete tabulation of the experimental results from the methane series runs is presented in Table 8-1. All information contained in the table is self-evident in meaning and requires little explanation, except for the following: S.D. stands for standard deviation from an arithmetic mean. SER stands for Specific Energy Requirement which is defined as the energy consumed in producing enough CaC_2 to ultimately yield one lb C_2H_2 . The column ACTUAL/STOI. LIME stands for ratios of actual to stoichiometric lime feed rates based on the carbon content of the feed gas. Types of anode used in the experiments are given in the column REMARKS. The schematics of various anodes are shown in Figure 3-2a and 3-2b. The stability of arc in each run was more or less subjectively judged according to the following classes: very unstable, fairly unstable, fairly stable, and very stable.

The standard condition for all gas flow rates cited is at 70°F and 1 atm.

Table 8-2 contains the experimental results of a methane run without solid feeding and other runs of feeding either $\text{Ca}(\text{OH})_2$ or CaCO_3 instead of CaO . As expected SER's were substantially higher for producing CaC_2 from $\text{Ca}(\text{OH})_2$ or CaCO_3 than from CaO .

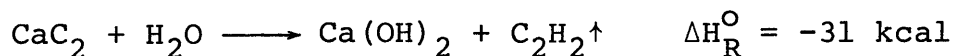
Table 8-3 contains the experimental results of the ethylene series runs. The water-cooled copper anode is denoted

as C-0, and C-5 if it is affixed with a 5" long graphite tube of 3" o.d. x 1" i.d. at the bottom.

The experimental results of the coal series runs are presented in Table 8-4, the format for which generally follows that of the other tables. The H/C ratio cited in the column REMARKS is based on C in coal and H in both coal and the feed gas, H₂.

8.2. Supplementary Details of Analysis of Solid Product

CaC₂ vigorously reacts with water according to the reaction:



The solid product CaC₂ manufactured in the rotating-arc reactor was in fine particulate form and deteriorated very rapidly by reacting with the moisture in the open air. It was also found to rapidly oxidize at room temperature to decompose to CaO and carbon in the presence of oxygen. In order to see how fast the CaC₂ can deteriorate in the presence of oxygen, particles collected in the sample collecting funnel from one run (original CaO conversion = 82.9%) were transferred in the open air into four 50 ml flasks and the contents were quantitatively analyzed for CaC₂ at different times over a period of five days. The initial CaC₂ content in each flask was such that there was always excess air present for the complete oxidation of the CaC₂. As a control case solid product from another run (CaO conversion = 63.5%) was divided into three flasks inside an N₂-filled glove bag

and also analyzed at different times. Figure 8.1 thus prepared shows that the product CaC_2 can fairly rapidly oxidize even at room temperature. In the present experiments the solids were mostly handled in an N_2 -filled glove bag, and if they were handled in the open air, they were analyzed within an hour to minimize the extent of oxidation.

Quantitative Analysis of Ca. The calcium content of the solid product was measured by first dissolving the calcium in dilute HCl and then volumetrically titrating the filtered solution by the method of complexometric titration (14). The method is based on the reaction of calcium with EDTA (Ethylenediaminetetraacetic acid) to form stable complexes. The analytical procedure is given in the following: add 5 ml of 10% hydroxylamine hydrochloride solution and 3 ml of triethanolamine to the solution. This is to complex interfering ions such as aluminum, magnesium, and iron. Adjust the pH of the solution to 12.5 by adding appropriate amounts of 5 N KOH. At the pH magnesium precipitates as the hydroxide. Place the solution on a magnetic stirrer. This is to prevent possible coprecipitation of calcium and adsorption of the indicator on the magnesium hydroxide which would make the end point difficult to determine. Now, add about 100 mg of hydroxynaphthol blue indicator and titrate the solution with 0.02 M EDTA to a permanent blue color.

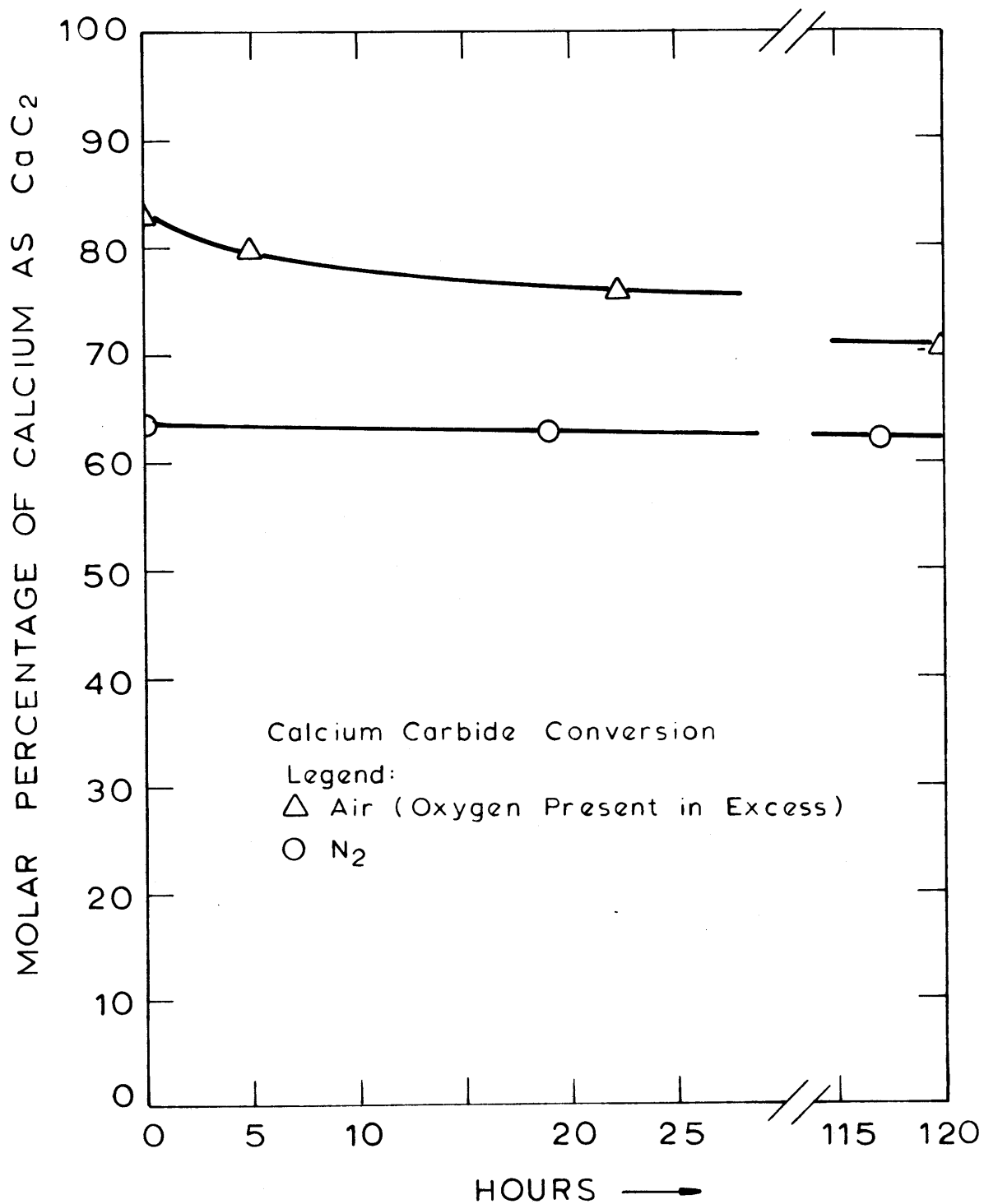


Fig. 8.1 Oxidation of Product CaC₂ in a Gas-Tight Sample Flask Initially Filled with Air

TABLE 8-1. METHANE SERIES RUNS

RUN NO.	METHANE FLOW RATE (L/MIN)	LIME FEED RATE (G/MIN)	ACTUAL/STOI. LIME	AVG P INPUT (KW)	(S.D.)	SOLID ENERGY (KCAL /G MOLE LIME)	GAS ENERGY (KCAL /G ATOM CARBON)	QUENCH DISTANCE (IN.)	CON-VERSION (%)	SER (KW-HR PER LB ACETYLENE)	GASEOUS PRODUCT (VOL.%)	REMARKS
M- 2	17.1	2.0 (AVG V=	0.151 82	14.7 S.D.=	0.52 2.9)	5900 (AVG I=	297 180	5.0 S.D.=	64.4 0.0)	185.5	MISSED	ANODE = G-1 REAG. GR. LIME ARC F. STABLE
M- 3	16.0	1.6 (AVG V=	0.129 77	15.5 S.D.=	0.42 5.8)	7793 (AVG I=	336 203	5.0 S.D.=	74.5 15.3)	211.9	CH4= 0.31 C2H4= 0.52 C2H2= 2.08	ANODE = G-1 REAG. GR. LIME ARC F. STABLE
M- 4	16.1	1.5 (AVG V=	0.120 74	15.7 S.D.=	0.91 3.5)	8402 (AVG I=	337 211	5.0 S.D.=	66.7 17.5)	255.2	CH4= 0.33 C2H4= 0.59 C2H2= 2.90	ANODE = G-1 REAG. GR. LIME ARC F. STABLE
M- 5	16.1	1.6 (AVG V=	0.128 74	21.4 S.D.=	1.57 4.9)	10731 (AVG I=	459 291	5.0 S.D.=	60.0 28.5)	362.3	CH4= 0.37 C2H4= 0.62 C2H2= 2.40	ANODE = G-1 REAG. GR. LIME ARC F. UNSTABLE
M- 6	17.1	4.8 (AVG V=	0.362 70	17.7 S.D.=	1.69 8.9)	2967 (AVG I=	359 255	5.0 S.D.=	65.7 23.5)	91.5	CH4= 0.21 C2H4= 0.27 C2H2= 1.49	ANODE = G-1 REAG. GR. LIME
M- 7	17.2	4.8 (AVG V=	0.360 65	18.3 S.D.=	1.44 7.5)	3061 (AVG I=	368 287	5.0 S.D.=	64.3 52.9)	96.4	CH4= 0.18 C2H4= 0.23 C2H2= 0.91	ANODE = G-1 REAG. GR. LIME
M- 8	17.2	4.8 (AVG V=	0.360 62	21.8 S.D.=	0.96 2.7)	3647 (AVG I=	438 351	5.0 S.D.=	78.3 20.4)	94.4	CH4= 0.15 C2H4= 0.17 C2H2= 0.75	ANODE = G-1 REAG. GR. LIME
M- 9	16.9	12.9 (AVG V=	0.986 63	19.8 S.D.=	1.65 10.6)	1229 (AVG I=	404 322	5.0 S.D.=	84.8 55.5)	29.4	CH4= 0.04 C2H4= 0.00 C2H2= 0.07	ANODE = G-1 REAG. GR. LIME
M-10	17.1	17.3 (AVG V=	1.307 59	20.2 S.D.=	1.56 5.3)	936 (AVG I=	408 344	5.0 S.D.=	73.8 39.1)	25.7	CH4= 0.03 C2H4= 0.00 C2H2= 0.06	ANODE = G-1 REAG. GR. LIME
M-13	31.5	12.4 (AVG V=	0.508 80	17.3 S.D.=	2.31 9.5)	1123 (AVG I=	190 220	5.0 S.D.=	2.1 41.5)	1083.0	CH4= 8.06 C2H4= 0.20 C2H2= 0.61	ANODE = G-1 REAG. GR. LIME ARC V. UNSTABLE
M-14	33.5	12.4 (AVG V=	0.478 129	9.7 S.D.=	1.47 2.5)	631 (AVG I=	101 76	5.0 S.D.=	1.0 12.7)	1278.1	CH4= 39.81 C2H4= 0.34 C2H2= 2.40	ANODE = G-1 REAG. GR. LIME ARC F. UNSTABLE
M-15	30.6	13.4 (AVG V=	0.565 67	25.1 S.D.=	2.22 6.7)	1504 (AVG I=	284 378	5.0 S.D.=	76.5 47.3)	39.8	CH4= 0.09 C2H4= 0.04 C2H2= 0.32	ANODE = G-1 REAG. GR. LIME ARC F. UNSTABLE
M-16	34.1	24.9 (AVG V=	0.943 90	16.2 S.D.=	8.16 22.4)	522 (AVG I=	164 203	5.0 S.D.=	27.3 121.9)	38.8	CH4= 2.01 C2H4= 0.05 C2H2= 0.31	ANODE = G-1 REAG. GR. LIME ARC V. UNSTABLE
M-17	30.2	22.0 (AVG V=	0.941 100	16.1 S.D.=	8.86 39.1)	586 (AVG I=	184 211	5.0 S.D.=	20.8 144.4)	57.1	CH4= 3.91 C2H4= 0.11 C2H2= 0.42	ANODE = G-1 REAG. GR. LIME ARC V. UNSTABLE

TABLE 8-1. METHANE SERIES RUNS (CONTINUED)

RUN NO.	METHANE FLOW RATE (L/MIN)	LIME FEED RATE (G/MIN)	ACTUAL/STOI. LIME	AVG P INPUT (KW)	(S.D.)	SOLID ENERGY (KCAL /G MOLE LIME)	GAS ENERGY (KCAL /G ATOM CARBON)	QUENCH DISTANCE (IN.)	CON-VERSION (%)	SER (KW-HR PER LB ACETYLENE)	GASEOUS PRODUCT (VOL.%)	REMARKS
M-18	16.2	17.3 (AVG V=	1.380 56	18.9 S.D.=	0.97 4.4)	876 (AVG I=	403 342	15.0 S.D.=	71.9 30.8)	24.7	CH4= 0.16 C2H4= 0.00 C2H2= 0.47	ANODE = G-1 REAG. GR. LIME ARC V. STABLE
M-19	30.4	23.3 (AVG V=	0.990 82	20.6 S.D.=	6.54 22.5)	709 (AVG I=	234 276	15.0 S.D.=	51.3 108.6)	28.0	CH4= 0.42 C2H4= 0.00 C2H2= 0.00	ANODE = G-1 REAG. GR. LIME ARC F. STABLE
M-20	31.9	23.3 (AVG V=	0.943 99	11.3 S.D.=	5.11 31.8)	390 (AVG I=	123 127	15.0 S.D.=	0.6 65.0)	1316.0	MISSED	ANODE = G-1 REAG. GR. LIME ARC F. UNSTABLE
M-21	31.0	21.2 (AVG V=	0.883 63	20.7 S.D.=	1.50 5.4)	783 (AVG I=	231 330	15.0 S.D.=	62.3 33.0)	25.5	CH4= 0.24 C2H4= 0.00 C2H2= 0.24	ANODE = G-4 REAG. GR. LIME ARC V. STABLE
M-22	31.9	31.5 (AVG V=	1.276 73	20.9 S.D.=	3.93 11.4)	534 (AVG I=	227 299	15.0 S.D.=	53.6 87.5)	20.2	CH4= 0.76 C2H4= 0.00 C2H2= 0.00	ANODE = G-4 REAG. GR. LIME ARC F. STABLE
M-23	17.2	9.6 (AVG V=	0.721 60	18.2 S.D.=	1.33 4.0)	1525 (AVG I=	367 307	15.0 S.D.=	52.4 31.3)	59.0	CH4= 2.03 C2H4= 0.05 C2H2= 0.22	ANODE = G-1 -325 MESH LIME ARC V. STABLE
M-24	30.0	22.1 (AVG V=	0.951 76	22.0 S.D.=	4.41 23.9)	799 (AVG I=	254 313	15.0 S.D.=	70.7 90.6)	22.8	MISSED	ANODE = G-1 -325 MESH LIME ARC F. STABLE
M-25	31.5	26.4 (AVG V=	1.083 78	17.5 S.D.=	6.13 19.9)	532 (AVG I=	192 244	15.0 S.D.=	29.0 99.1)	37.2	CH4= 0.36 C2H4= 0.00 C2H2= 0.00	ANODE = G-4 REAG. GR. LIME ARC F. STABLE
M-26	32.5	26.4 (AVG V=	1.049 90	19.8 S.D.=	7.98 34.6)	603 (AVG I=	211 266	15.0 S.D.=	49.8 133.0)	24.5	CH4= 0.04 C2H4= 0.00 C2H2= 0.00	ANODE = G-1 REAG. GR. LIME ARC F. STABLE
M-29	30.5	10.3 (AVG V=	0.436 84	16.5 S.D.=	5.35 30.1)	1282 (AVG I=	186 231	15.0 S.D.=	14.4 115.7)	180.3	MISSED	ANODE = G-1 -325 MESH LIME ARC F. STABLE
M-30	30.0	25.0 (AVG V=	1.076 66	22.2 S.D.=	1.44 7.4)	712 (AVG I=	256 340	15.0 S.D.=	66.3 43.7)	21.8	CH4= 0.00 C2H4= 0.00 C2H2= 0.00	ANODE = G-1 -325 MESH LIME ARC V. STABLE
M-31	30.5	25.0 (AVG V=	1.059 63	23.3 S.D.=	1.97 2.6)	749 (AVG I=	264 370	5.0 S.D.=	51.8 34.6)	29.3	CH4= 0.06 C2H4= 0.00 C2H2= 0.20	ANODE = G-1 -325 MESH LIME ARC V. STABLE
M-32	16.7	13.6 (AVG V=	1.052 92	14.7 S.D.=	3.86 24.4)	865 (AVG I=	304 177	15.0 S.D.=	26.0 74.5)	67.4	CH4= 1.05 C2H4= 0.04 C2H2= 0.17	ANODE = G-1 REAG. GR. LIME ARC V. STABLE
M-33	16.7	13.6 (AVG V=	1.052 76	13.8 S.D.=	4.30 15.7)	815 (AVG I=	286 191	15.0 S.D.=	31.2 66.7)	52.9	CH4= 4.86 C2H4= 0.12 C2H2= 0.85	ANODE = G-8 REAG. GR. LIME ARC F. UNSTABLE
M-37	32.1	25.4 (AVG V=	1.022 74	26.1 S.D.=	1.61 3.2)	823 (AVG I=	281 353	5.0 S.D.=	43.5 32.0)	38.3	CH4= 3.53 C2H4= 0.04 C2H2= 0.39	ANODE = G-1 -200 MESH LIME ARC V. STABLE

TABLE 8-1. METHANE SERIES RUNS (CONTINUED)

RUN NO.	METHANE FLOW RATE (L/MIN)	LIME FEED RATE (G/MIN)	ACTUAL/STOI. LIME	AVG P INPUT (KW)	(S.D.)	SOLID ENERGY (KCAL /G MOLE LIME)	GAS ENERGY (KCAL /G ATOM CARBON)	QUENCH DISTANCE (IN.)	CON-VERSION (%)	SER (KW-HR PER LB ACETYLENE)	GASEOUS PRODUCT (VOL.%)	REMARKS
M-38	48.2	38.2 (AVG V=	1.024 92	16.8 S.D.=	10.28 46.2)	353 (AVG I=	121 259	5.0 S.D.=	21.9 194.4)	32.6	MISSED	ANODE = G-1 -200 MESH LIME ARC V. UNSTABLE
M-39	47.3	38.0 (AVG V=	1.038 100	20.4 S.D.=	8.88 46.0)	432 (AVG I=	149 270	5.0 S.D.=	8.6 179.4)	101.7	CH4= 14.90 C2H4= 0.23 C2H2= 0.36	ANODE = G-1 REAG. GR. LIME ARC V. UNSTABLE
M-40	32.0	28.2 (AVG V=	1.138 79	19.0 S.D.=	4.33 27.2)	540 (AVG I=	205 276	5.0 S.D.=	38.0 112.0)	28.8	CH4= 3.68 C2H4= 0.10 C2H2= 0.26	ANODE = G-1 REAG. GR. LIME ARC F. STABLE
M-47	17.3	14.8 (AVG V=	1.105 66	18.0 S.D.=	0.45 3.9)	977 (AVG I=	360 276	15.0 S.D.=	53.1 18.1)	37.3	CH4= 0.00 C2H4= 0.00 C2H2= 0.30	ANODE = G-1 200 MESH LIME ARC V. STABLE
M-48	32.0	24.6 (AVG V=	0.993 94	25.6 S.D.=	4.07 15.3)	835 (AVG I=	277 284	15.0 S.D.=	52.3 78.7)	32.3	CH4= 1.53 C2H4= 0.10 C2H2= 0.20	ANODE = G-1 200 MESH LIME ARC F. STABLE
M-49	17.3	13.2 (AVG V=	0.986 73	22.1 S.D.=	2.65 8.5)	1345 (AVG I=	442 307	15.0 S.D.=	60.0 45.0)	45.4	CH4= 0.09 C2H4= 0.00 C2H2= 0.12	ANODE = G-1 325 MESH LIME ARC F. STABLE
M-50	17.1	13.7 (AVG V=	1.035 63	21.9 S.D.=	1.37 3.4)	1283 (AVG I=	443 348	15.0 S.D.=	82.9 26.9)	31.4	CH4= 0.03 C2H4= 0.02 C2H2= 0.10	ANODE = G-1 325 MESH LIME ARC V. STABLE
M-51	34.5	26.6 (AVG V=	0.996 88	19.0 S.D.=	8.83 29.1)	572 (AVG I=	190 258	15.0 S.D.=	63.5 135.8)	18.2	MISSED	ANODE = G-1 325 MESH LIME ARC F. UNSTABLE
M-52	17.1	15.2 (AVG V=	1.148 64	21.4 S.D.=	0.55 2.7)	1131 (AVG I=	433 337	15.0 S.D.=	71.9 20.5)	31.9	CH4= 0.03 C2H4= 0.00 C2H2= 0.00	ANODE = G-1 200 MESH LIME ARC V. STABLE
M-53	35.8	37.7 (AVG V=	1.360 83	15.7 S.D.=	5.63 27.8)	334 (AVG I=	151 219	15.0 S.D.=	41.5 110.0)	16.3	CH4= 2.20 C2H4= 0.00 C2H2= 0.04	ANODE = G-1 200 MESH LIME ARC V. UNSTABLE
M-54	17.2	12.4 (AVG V=	0.931 67	14.4 S.D.=	0.37 3.0)	930 (AVG I=	289 214	15.0 S.D.=	19.8 12.0)	95.2	CH4= 0.12 C2H4= 0.00 C2H2= 0.15	ANODE = G-1 200 MESH LIME ARC F. STABLE
M-55	17.2	11.0 (AVG V=	0.826 64	19.7 S.D.=	0.49 1.9)	1436 (AVG I=	396 307	15.0 S.D.=	72.6 12.9)	40.1	CH4= 0.03 C2H4= 0.00 C2H2= 0.05	ANODE = G-1 200 MESH LIME ARC V. STABLE
M-56	30.4	19.0 (AVG V=	0.807 114	11.2 S.D.=	6.59 24.8)	473 (AVG I=	127 118	15.0 S.D.=	12.9 110.8)	74.3	CH4= 9.98 C2H4= 0.20 C2H2= 0.88	ANODE = G-1 200 MESH LIME ARC V. UNSTABLE
M-57	30.4	19.0 (AVG V=	0.807 111	13.3 S.D.=	10.50 27.9)	563 (AVG I=	152 148	15.0 S.D.=	18.8 132.5)	60.6	CH4= 4.32 C2H4= 0.09 C2H2= 0.38	ANODE = G-1 200 MESH LIME ARC V. UNSTABLE
M-61	32.0	25.2 (AVG V=	1.017 86	18.7 S.D.=	4.29 27.1)	596 (AVG I=	202 245	5.0 S.D.=	56.6 113.2)	21.3	CH4= 0.85 C2H4= 0.03 C2H2= 0.32	ANODE = G-1 REAG. GR. LIME

TABLE 8-1. METHANE SERIES RUNS (CONTINUED)

RUN NO.	METHANE FLOW RATE (L/MIN)	LIME FEED RATE (G/MIN)	ACTUAL/STOI. LIME	AVG P INPUT (KW)	(S.D.) (S.D.)	SOLID ENERGY (KCAL /G MOLE LIME)	GAS ENERGY (KCAL /G ATOM CARBON)	QUENCH DISTANCE (IN.)	CON-VERSION (%)	SER (KW-HR PER LB ACETYLENE)	GASEOUS PRODUCT (VOL.%)	REMARKS
M-62	44.5	32.0 (AVG V=	0.929 75	20.8 S.D.=	2.90 18.7)	523 (AVG I=	162 292	5.0 S.D.=	35.1 74.9)	30.1	MISSED	ANODE = G-1 REAG. GR. LIME ARC V. UNSTABLE
M-63	16.7	14.9 (AVG V=	1.153 60	21.3 S.D.=	1.47 5.9)	1146 (AVG I=	441 362	5.0 S.D.=	76.7 59.2)	30.3	CH4= 0.09 C2H4= 0.00 C2H2= 0.06	ANODE = G-1 REAG. GR. LIME ARC F. STABLE
M-64	16.7	10.9 (AVG V=	0.843 64	14.8 S.D.=	0.42 7.8)	1089 (AVG I=	306 233	5.0 S.D.=	35.0 26.0)	63.0	MISSED	ANODE = G-1 REAG. GR. LIME ARC F. STABLE
M-65	16.7	10.9 (AVG V=	0.843 108	12.9 S.D.=	0.93 9.6)	947 (AVG I=	266 120	5.0 S.D.=	0.6 7.1)	3199.0	MISSED	ANODE = G-1 REAG. GR. LIME ARC F. STABLE
M-67	16.7	6.5 (AVG V=	0.502 61	14.9 S.D.=	1.14 5.8)	1842 (AVG I=	309 245	15.0 S.D.=	40.0 25.1)	93.2	MISSED	ANODE = G-1 REAG. GR. LIME ARC F. STABLE
M-68	16.7	6.5 (AVG V=	0.502 60	14.9 S.D.=	1.24 5.0)	1834 (AVG I=	307 250	15.0 S.D.=	43.0 16.3)	86.3	MISSED	ANODE = G-8 REAG. GR. LIME ARC F. STABLE
M-69	16.7	11.6 (AVG V=	0.897 64	16.8 S.D.=	1.43 4.8)	1160 (AVG I=	347 264	15.0 S.D.=	69.2 27.1)	33.9	MISSED	ANODE = G-1 REAG. GR. LIME ARC F. STABLE
M-70	16.7	9.6 (AVG V=	0.742 71	16.6 S.D.=	2.60 18.9)	1386 (AVG I=	343 246	15.0 S.D.=	64.0 59.2)	43.9	CH4= 0.01 C2H4= 0.00 C2H2= 0.00	ANODE = G-1 REAG. GR. LIME ARC V. UNSTABLE
M-71	16.7	9.8 (AVG V=	0.758 57	20.0 S.D.=	1.36 4.3)	1638 (AVG I=	414 353	5.0 S.D.=	62.6 10.0)	53.0	CH4= 0.10 C2H4= 0.02 C2H2= 0.48	ANODE = G-1 REAG. GR. LIME ARC F. STABLE
M-73	16.7	13.2 (AVG V=	1.021 63	20.5 S.D.=	0.73 2.6)	1245 (AVG I=	424 324	5.0 S.D.=	79.5 17.0)	31.7	CH4= 0.01 C2H4= 0.00 C2H2= 0.02	ANODE = G-1 -325 MESH LIME ARC V. STABLE
M-74	16.7	12.7 (AVG V=	0.982 112	13.3 S.D.=	1.64 14.6)	841 (AVG I=	276 121	5.0 S.D.=	58.3 24.2)	29.2	CH4= 1.43 C2H4= 0.07 C2H2= 0.54	ANODE = G-1 -325 MESH LIME ARC F. STABLE
M-75	16.7	12.7 (AVG V=	0.982 114	13.2 S.D.=	3.43 20.7)	832 (AVG I=	273 122	5.0 S.D.=	21.7 50.2)	77.7	CH4= 3.35 C2H4= 0.16 C2H2= 0.96	ANODE = G-1 -325 MESH LIME ARC F. UNSTABLE
M-76	16.7	12.6 (AVG V=	0.975 68	23.8 S.D.=	2.83 6.2)	1515 (AVG I=	493 351	5.0 S.D.=	77.0 29.3)	39.8	MISSED	ANODE = G-1 -200 MESH LIME ARC F. STABLE
M-77	16.7	12.6 (AVG V=	0.975 83	13.9 S.D.=	1.39 6.4)	887 (AVG I=	288 169	5.0 S.D.=	73.5 18.6)	24.4	MISSED	ANODE = G-1 -200 MESH LIME ARC F. UNSTABLE
M-79	16.7	12.4 (AVG V=	0.960 109	11.1 S.D.=	4.30 20.7)	720 (AVG I=	230 107	15.0 S.D.=	7.0 45.7)	224.0	MISSED	ANODE = G-1 -325 MESH LIME ARC F. UNSTABLE

TABLE 8-2. METHANE SERIES SPECIAL RUNS

RUN NO.	METHANE FLOW RATE (L/MIN)	LIME FEED RATE (G/MIN)	ACTUAL/STOI. LIME	AVG P INPUT (KW)	(S.D.) (S.D.)	SOLID ENERGY (KCAL /G MOLE LIME)	GAS ENERGY (KCAL /G ATOM CARBON)	QUENCH DISTANCE (IN.)	CON-VERSION (%)	SER (KW-HR PER LB ACETYLENE)	GASEOUS PRODUCT (VOL.%)	REMARKS
SM- 1	16.7	0.0 (AVG V= 72)	72	15.7 S.D.=	1.74 5.6)	(AVG I= 220)	326	5.0 S.D.= 22.9)	0.0		CH4= 0.57 C2H4= 1.15 C2H2= 8.46	ANODE = G-1 NO SOLID FEED ARC V. STABLE
SM- 2	16.7	17.2 (AVG V= 61)	1.330 61	20.5 S.D.=	1.23 5.3)	(AVG I= 340)	1265 425	15.0 S.D.= 20.0)	26.2	97.8	MISSED	ANODE = G-1 HYDRATED LIME
SM- 3	17.1	30.2 (AVG V= 63)	2.282 63	19.6 S.D.=	0.88 4.4)	(AVG I= 313)	928 395	15.0 S.D.= 30.8)	16.7	112.6	CH4= 1.49 C2H4= 0.00 C2H2= 0.11	ANODE = G-1 PPT LIME STONE ARC V. STABLE
SM- 4	34.0	51.6 (AVG V= 103)	1.961 103	18.6 S.D.=	10.84 30.3)	(AVG I= 203)	517 189	15.0 S.D.=132.2)	8.8	119.1	CH4= 6.70 C2H4= 0.07 C2H2= 0.19	ANODE = G-1 PPT LIME STONE ARC V. UNSTABLE

TABLE 8-3. ETHYLENE SERIES RUNS

RUN NO.	C2H4 FLOW RATE (L/MIN)	LIME FEED RATE (G/MIN)	ACTUAL/STOI. LIME	AVG P INPUT (KW)	(S.D.)	SOLID ENERGY (KCAL /G MOLE LIME)	GAS ENERGY (KCAL /G ATOM CARBON)	QUENCH DISTANCE (IN.)	CON- VERSION (%)	SER (KW-HR PER LB ACETYLENE)	GASEOUS PRODUCT (VOL.%)	REMARKS
E- 1	15.8	27.8 (AVG V= 57)	1.136	15.7 S.D.= 18.2)	6.20	454 (AVG I= 294)	172 294	15.0 S.D.=103.5)	50.6	18.2	CH4= 0.06 C2H4= 0.05 C2H2= 0.09	ANODE = G-1 -325 MESH LIME ARC F. UNSTABLE
E- 2	15.8	27.8 (AVG V= 64)	1.136	21.0 S.D.= 19.0)	4.91	608 (AVG I= 343)	230 343	15.0 S.D.= 71.3)	61.5	20.0	CH4= 0.00 C2H4= 0.00 C2H2= 0.00	ANODE = C-0 -325 MESH LIME ARC V. STABLE
E- 3	15.8	29.3 (AVG V= 39)	1.198	13.7 S.D.= 23.8)	7.44	374 (AVG I= 364)	150 364	10.0 S.D.= 32.1)	36.5	20.8	CH4= 0.03 C2H4= 0.05 C2H2= 0.59	ANODE = C-5 -325 MESH LIME ARC F. UNSTABLE
E- 4	15.8	23.3 (AVG V= 62)	0.952	21.1 S.D.= 15.6)	4.70	728 (AVG I= 349)	231 349	10.0 S.D.= 46.7)	52.4	28.1	CH4= 0.04 C2H4= 0.06 C2H2= 0.51	ANODE = C-5 -325 MESH LIME ARC F. STABLE
E- 5	21.9	40.0 (AVG V= 49)	1.180	13.0 S.D.= 20.3)	3.54	261 (AVG I= 289)	103 289	15.0 S.D.= 71.8)	33.0	16.0	CH4= 0.11 C2H4= 0.29 C2H2= 0.15	ANODE = C-0 -325 MESH LIME ARC F. UNSTABLE
E- 6	21.9	40.0 (AVG V= 54)	1.180	17.3 S.D.= 26.6)	7.63	346 (AVG I= 361)	136 361	10.0 S.D.=113.4)	27.1	25.9	CH4= 0.04 C2H4= 0.02 C2H2= 0.49	ANODE = C-5 -325 MESH LIME ARC F. UNSTABLE

TABLE 8-4. COAL SERIES RUNS

RUN NO.	POWDER FEED RATE (G/MIN)	CARBON /LIME MOLAR RATIO	HYDROGEN FLOW RATE (L/MIN)	AVG P INPUT (KW)	(S.D.)	SOLID ENERGY (KCAL /G ATOM CARBON)	GAS ENERGY (KCAL /G MOLE HYDROGEN)	QUENCH DISTANCE (IN.)	CON-VERSION (%)	SER (KW-HR PER LB ACETYLENE)	GASEOUS PRODUCT (VOL.%)	REMARKS
C- 1	20.1	2.034 (AVG V=	29.4 64	18.7 S.D.=	1.69 8.4)	602 (AVG I=	220 298	5.0 S.D.=	61.3 50.7)	40.5	CH4= 0.04 C2H4= 0.00 C2H2= 0.08	ANODE = G-1 ARC F. UNSTABLE C/H RATIO=6.374
C- 2	15.5	2.034 (AVG V=	29.4 82	17.5 S.D.=	6.17 29.7)	731 (AVG I=	206 245	5.0 S.D.=	36.8 122.4)	81.9	CH4= 0.03 C2H4= 0.00 C2H2= 0.12	ANODE = G-1 ARC F. UNSTABLE C/H RATIO=8.002
C- 3	28.2	2.034 (AVG V=	45.6 113	14.7 S.D.=	6.80 25.2)	337 (AVG I=	111 145	5.0 S.D.=	7.3 88.8)	190.4	CH4= 0.22 C2H4= 0.04 C2H2= 0.48	ANODE = C-0 ARC V. UNSTABLE C/H RATIO=6.953
C- 6	26.4	2.034 (AVG V=	26.6 65	18.0 S.D.=	1.77 14.9)	442 (AVG I=	234 286	15.0 S.D.=	38.2 59.7)	47.7	CH4= 0.12 C2H4= 0.00 C2H2= 0.06	ANODE = G-1 ARC F. UNSTABLE C/H RATIO=4.668
C- 8	28.0	2.034 (AVG V=	27.0 75	17.8 S.D.=	7.08 37.0)	412 (AVG I=	228 285	15.0 S.D.=	49.8 119.4)	34.1	CH4= 0.00 C2H4= 0.00 C2H2= 0.00	ANODE = G-1 ARC F. UNSTABLE C/H RATIO=4.505
C- 9	28.0	2.034 (AVG V=	27.0 66	19.7 S.D.=	2.14 7.4)	457 (AVG I=	253 303	15.0 S.D.=	35.5 51.4)	53.1	MISSED	ANODE = G-4 ARC F. STABLE C/H RATIO=4.505
C-10	28.0	2.034 (AVG V=	40.0 74	23.2 S.D.=	4.24 21.2)	536 (AVG I=	200 335	15.0 S.D.=	53.0 93.1)	41.7	CH4= 0.00 C2H4= 0.00 C2H2= 0.40	ANODE = G-4 ARC F. STABLE C/H RATIO=6.246
C-11	28.0	2.034 (AVG V=	30.0 84	18.3 S.D.=	5.70 21.1)	423 (AVG I=	211 245	15.0 S.D.=	24.8 125.0)	70.3	MISSED	ANODE = G-1 ARC F. UNSTABLE C/H RATIO=4.907
C-12	50.8	3.036 (AVG V=	48.4 73	21.2 S.D.=	2.96 19.8)	216 (AVG I=	152 312	5.0 S.D.=	14.7 90.7)	90.6	CH4= 0.16 C2H4= 0.00 C2H2= 0.33	ANODE = G-1 ARC V. UNSTABLE C/H RATIO=3.744
C-13	50.8	3.036 (AVG V=	48.4 81	25.1 S.D.=	3.66 10.7)	256 (AVG I=	179 316	5.0 S.D.=	22.9 70.4)	68.7	CH4= 0.04 C2H4= 0.00 C2H2= 0.07	ANODE = G-4 ARC F. UNSTABLE C/H RATIO=3.744
C-15	41.1	1.017 (AVG V=	46.3 85	18.6 S.D.=	4.67 25.7)	471 (AVG I=	139 243	15.0 S.D.=	11.3 89.4)	85.9	CH4= 0.10 C2H4= 0.00 C2H2= 0.00	ANODE = G-1 ARC V. UNSTABLE C/H RATIO=7.685
C-17	30.2	2.034 (AVG V=	14.6 59	15.5 S.D.=	3.00 7.8)	333 (AVG I=	367 269	15.0 S.D.=	42.7 62.6)	32.1	CH4= 0.00 C2H4= 0.00 C2H2= 0.00	ANODE = C-0 ARC F. STABLE C/H RATIO=2.702
C-19	42.0	2.034 (AVG V=	23.1 75	18.0 S.D.=	16.04 16.0)	278 (AVG I=	270 323	15.0 S.D.=	12.0 73.3)	95.6	MISSED	ANODE = C-0 ARC F. UNSTABLE C/H RATIO=2.952
C-20	51.0	2.034 (AVG V=	28.4 69	10.0 S.D.=	3.47 19.7)	127 (AVG I=	122 146	15.0 S.D.=	3.3 31.0)	159.1	MISSED	ANODE = C-0 ARC F. UNSTABLE C/H RATIO=2.978
C-21	32.4	3.036 (AVG V=	31.1 76	21.0 S.D.=	2.80 9.0)	336 (AVG I=	234 284	15.0 S.D.=	46.6 61.9)	44.4	CH4= 0.14 C2H4= 0.00 C2H2= 0.12	ANODE = C-0 ARC F. UNSTABLE C/H RATIO=3.766

BIBLIOGRAPHY

1. Anderson, L.L., G.R. Hill, E.H. McDonald, and M.J. McIntosh, "Flash Heating and Plasma Processing of Coal," Chemical Engineering Progress Symposium Series, No. 85, Vol. 64, 81 (1968).
2. Anonymous, "Acetylene," in "Chemical Economics Handbook," Stanford Research Institute, Menlo Park, Calif. (1975).
3. Anonymous, "Arc Acetylene Process," Hydrocarbon Processing (June 1971), pp. 133-136.
4. Anonymous, Chemical and Engineering News, Feb. 5, 1968, p. 37.
5. Anonymous, Chemical Engineering, 75(11) (May 20, 1968), p. 71.
6. Anthony, D.B. and J.B. Howard, "Coal Devolatilization and Hydrogasification," AIChE Journal, 22(4) (1976), pp. 625-656.
7. Averitt, P., "Coal Resources in the United States, January, 1974," Geological Survey Bulletin 1412, U.S. Dept. of the Interior, Washington, D.C. (1975), p. 100.
8. Back, M.H., "Mechanism of the Pyrolysis of Acetylene," Canadian Journal of Chemistry, 49 (1971), pp. 2199-2204.
9. _____, "Pyrolysis of Hydrocarbons," in "The Mechanisms of Pyrolysis, Oxidation, and Burning of Organic Materials," Proceedings of the 4th Material Research Symposium, National Bureau of Standards Special Publication 357 (1972), pp. 17-31.
10. Baddour, R.F. and J.L. Blanchet, "Reactions of Carbon Vapor with Hydrogen and with Methane in a High Intensity Arc," I&EC Process Design and Development, 3 (1964), pp. 258-266.
11. Baddour, R.F. and J.M. Iwasyk, "Reactions Between Elemental Carbon and Hydrogen at Temperatures above 2800°K," Ind. Eng. Chem. Process Design Develop., 1 (1962), pp. 169-176.
12. Baddour, R.F. and P.H. Dundas, "Chemical Processing in a Microwave Discharge," in "Microwave Power Engineering," E.C. Okress, ed., Academic Press, Inc., New York (1968), pp. 329-346.

13. Bakardjiev, V. and B.E. Djakov, "Arc Motion in Non-Homogeneous Magnetic Field," 11th International Conference on Phenomena in Ionized Gases, I. Stoll, ed., Prague, Czechoslovakia (1973), p. 252.
14. Barin, I. and O. Knacke, "Thermochemical Properties of Inorganic Substances," Springer-Verlag, Berlin, Germany (1973).
15. Bauer, S.H. and R.E. Duff, "The Equilibrium Composition of the C/H System at Elevated Temperatures," Los Alamos Scientific Laboratory Report LA-2556, Chemistry, TID-4500, 16th Ed., Office of Technical Services, U.S. Dept. of Commerce, Washington, D.C.
16. Blanchet, J.L., "Reactions of Carbon Vapor with Hydrogen and with Methane in a High Intensity Arc," Sc.D. thesis, M.I.T., Cambridge, Mass. (1963).
17. Bond, R.L., I.F. Galbraith, W.R. Lander, and G.I.T. McConnell, "Production of Acetylene from Coal using a Plasma Jet," Nature, 200 (1963), pp. 1313-1314.
18. Bond, R.L., W.R. Lander and G.I.T. McConnell, "Reaction of Coals under Conditions of High Energy Input and High Temperature," Coal Science, R.F. Gould, ed., ACS (1966), pp. 650-665.
19. Bosch, F.M. and I.A. de Vynck, "Essai de Synthese du Carbure et de Nitrure de Bore," Silicates Industriels, 27 (1962), pp. 587-590.
20. Brookes, C., C.E. Gall, and R.R. Hudgins, "A Model for the Formation of Calcium Carbide in Solid Pellets," The Canadian Journal of Chemical Engineering, 53 (1975), pp. 527-535.
21. Capitelli, M., F. Cramarossa, L. Triolo, and E. Molinari, "Decomposition of Al₂O₃ Particles Injected into Argon-Nitrogen Induction Plasmas of 1 Atmosphere," Combustion and Flame, 15 (1970), pp. 23-32.
22. Chen, C.-J., M.H. Back, and R.A. Back, "The Thermal Decomposition of Methane. I. Kinetics of the Primary Decomposition to C₂H₆ + H₂; Rate Constant for the Homogeneous Unimolecular Dissociation of Methane and Its Pressure Dependence," Can. J. Chem., 53 (1975), pp. 3580-3590.
23. Cobine, J.D., "Gaseous Conductors," 2nd ed., Dover Publications, N.Y. (1958).

24. Eisenberg, B. and H. Bliss, "Kinetics of Methane Pyrolysis," Chem. Eng. Prog. Symp. Ser., 63 (1967), pp. 3-17.
25. Fay, J.A. and F.R. Riddell, "Theory of Stagnation Point Heat Transfer in Dissociated Air," Journal of the Aeronautical Sciences, 25 (1958), pp. 73-85.
26. Fey, M.G. and G.A. Kemeny, "Method of Direct Ore Reduction Using a Short Gap Arc Heater," U.S. Pat. 3,765,870, October 16, 1973.
27. Freeman, M.P., "Chemical Research in Streaming Thermal Plasmas," Advan. High-Temp. Chem., 2 (1969), pp. 151-202.
28. Gannon, R.E. and V. Krukonis, "AVCO Arc-Coal Process Development, Final Report," OCR Contract No. 14-01-0001-493, R&D Report No. 34 (1972).
29. Gilles, H.L. and C.W. Clump, "Reduction of Iron Ore with Hydrogen in a Direct Current Plasma Jet," Ind. Eng. Chem. Process Des. Develop., 9 (1970), pp. 194-207.
30. Gladisch, H., "Acetylen-Herstellung im elektrischen Lichtbogen," Chemie-Ing.-Techn., 41(4) (1969), pp. 204-208.
31. Gold, R.G., W.R. Sandall, P.G. Cheplick, and D.R. Mac Rae, "Plasma Reduction of Iron Oxide with Hydrogen and Natural Gas at 100 kw and One Megawatt," Proceedings 1975 International Round Table on Study and Applications of Transport Phenomena in Thermal Plasmas, C. Bonet, ed., International Union of Pure and Applied Chemistry, France (1975).
32. Goldberger, W.M. and C.J. Baroch (The Battelle Development Corp.), "Method of Coating Solid Particles," U.S. Pat. 3,247,014, April 19, 1966.
33. Goulard, R., "On Catalytic Recombination Rates in Hypersonic Stagnation Heat Transfer," Jet Propulsion, 28(11) (1958), pp. 737-745.
34. Graves, R.D., W. Kawa, and R.W. Hiteshue, "Reactions of Coal in a Plasma Jet," Ind. Eng. Chem. Process Design and Development, 5(1) (1966), p. 59.
35. Halliday, D. and R. Resnick, "Physics," Part II, 3rd ed., John Wiley & Sons, Inc., New York (1968), pp. 829-831.

36. Hartig, R., J. Troe, and H.G.G. Wagner, "Thermal Decomposition of Methane behind Reflected Shock Waves," 13th Symposium (International) on Combustion, The Combustion Institute, Pittsburgh (1971), pp. 147-152.
37. Harvey, Richard D., "Petrographic and Mineralogical Characteristics of Carbonate Rocks Related to Sulfur Dioxide Sorption in Flue Gases," Final Report to EPA, Contract No. CPA 22-69-65, Illinois State Geological Survey, Urbana, Ill. (1971).
38. Hirayama, C., M.G. Fey, and F.E. Camp, "Pressure Effects on Products Selectivities in the Pyrolysis of Methane in Arc-Plasma Heater," in "Engineering, Chemistry, and Use of Plasma Reactors," J.E. Flinn, ed., Chemical Engineering Symposium Series, No. 112, Vol. 67, IChE, N.Y., N.Y. (1971), pp. 117-121.
39. Holmen, A., O.A. Rokstad, and A. Solbakken, "High Temperature Pyrolysis of Hydrocarbons, 1. Methane to Acetylene," Ind. Eng. Chem., Process Des. Dev., 15(3) (1976), pp. 439-444.
40. Iwasyk, J.M., "The Carbon-Hydrogen System at Temperatures above 2500°C," Sc.D. thesis, M.I.T., Cambridge, Mass. (1960).
41. Kawana, Y., M. Makino, and T. Kimura, "Formation of Acetylene from Coal by Argon Plasma," Intern. Chem. Eng., 7 (1967), pp. 359-367.
42. Khan, M.S. and B.L. Crynes, "Survey of Recent Methane Pyrolysis Literature," Ind. Eng. Chem., 62(10) (1970), pp. 54-59.
43. Krukonis, V., "AVCO Arc-Coal Process," OCR Contract No. 14-01-0001-493, R&D Report No. 34, AVCO, Lowell, Mass. (1968).
44. Krzemu, B.A., "Studies on Silicon Nitride Obtained in an Arc Discharge Plasma," Roczniki Chemii, 50 (1976), pp. 1453-1454.
45. Lee, .AL., A.L. Feldkirchner, F.C. Schora, and J.J. Henry, "The Heat of Reaction of Hydrogen and Coal," Ind. Eng. Chem. Process Design Develop., 7 (1968), p. 244.
46. Lees, L., "Laminar Heat Transfer over Blunt Nosed Bodies at Hypersonic Flight Speeds," Jet Propulsion, 26 (1956), pp. 259-269.

47. Littlewood, K., "The Direct Production of Acetylene from Coal," Symp. Oils and Chemicals from Coal, Central Research Institute, Bihar (1969).
48. Miller, S.A., "Acetylene; Its Properties, Manufacture and Uses," Vol. I, Academic Press, N.Y., N.Y. (1965).
49. Ibid., p. 168.
50. Ibid., pp. 175-178.
51. Ibid., pp. 371-378.
52. Ibid., pp. 391-415.
53. Moseley, F. and D. Paterson, "Rapid High-Temperature High-Pressure Hydrogenation of Bituminous Coal," J. Inst. Fuel, 40 (1967), p. 523.
54. Mukaibo, T. and Y. Yamanaka, "Calcium Carbides. I. Kinetics of the First Stage of the Reaction Producing Calcium Carbide under Reduced Pressure (2-3 mm Hg)," J. Chem. Soc. Japan, Ind. Chem. Soc., 56(2) (1953), pp. 73-75.
55. Mukaibo T. and Y. Yamanaka, "Calcium Carbide. II. Kinetics of the First Stage of the Reaction Producing Calcium Carbide under Reduced Pressure (2-3 mm Hg)," J. Chem. Soc. Japan, Ind. Chem. Soc., 56(4) (1953), pp. 232-234.
56. Mukaibo, T. and Y. Yamanaka, "Calcium Carbide. III. Effects of Sample Preparation Techniques on the Kinetics of the First Stage of the Reaction Producing Calcium Carbide under Reduced Pressure (2-3 mm Hg)," J. Chem. Soc. Japan, Ind. Chem. Soc., 56(5) (1953), pp. 313-315.
57. Nicholson, R. and K. Littlewood, "Plasma Pyrolysis of Coal," Nature, 236(5347) (1972), pp. 397-400.
58. Norman, P. and I. Fells, "Heat Transfer From Low Current DC Arcs," 11th International Conference on Phenomena in Ionized Gases, I. Stoll, ed., Prague, Czechoslovakia (1973), p. 227.
59. Palmer, H.B., J. Lahaye, and K.C. Hou, "On the Kinetics and Mechanism of the Thermal Decomposition of Methane in a Flow System," J. Phys. Chem., 72(1) (1968), pp. 348-353.
60. Plooster, M.N. and T.B. Reed, "Carbon-Hydrogen-Acetylene Equilibrium at High Temperature," J. Phys. Chem., 31(1) (1959), pp. 66-72.

61. Reed, T.B., "Plasmas for High Temperature Chemistry," Advan. High Temp. Chem., 1 (1967), pp. 259-316.
62. Schulze, R.A., "Du Pont Arc Acetylene Process," Chemistry and Industry, 9 (1968), pp. 1539-1540.
63. Shahin, M.M., "Electrical Discharge Plasmas," in "Reactions under Plasma Conditions," Vol. I, M. Venugopalan, ed., John Wiley & Sons, Inc., New York (1971), pp. 285-328.
64. Skinner, G.B. and E.M. Sokolovski, "Shock-Tube Experiments on the Pyrolysis of Ethylene," J. Phys. Chem., 64 (1960), pp. 1028-1031.
65. Snell, F.D. and L.S. Ettre, eds., "Encyclopedia of Industrial Chemical Analysis," Vol. 8, John Wiley & Sons, New York (1969), pp. 72-114.
66. Stokes, C.S., "Chemical Reactions in Plasma Jets," in "Reactions under Plasma Conditions," Vol. II, M. Venugopalan, ed., John Wiley & Sons, Inc., New York (1971), pp. 259-298.
67. Stokes, C.S. and J.A. Cahill, "Plasma Jet Chemistry, Final Report," Air Force Office of Scientific Research, Grant 775-65, The Research Institute of Temple University, Philadelphia, Pa., December 1965.
68. Stokes, C.S., J.A. Cahill, J.J. Correa, and A.V. Grosse, "Plasma Jet Chemistry, Final Report," Air Force Office of Scientific Research, Grant 62-196, The Research Institute of Temple University, Philadelphia, Pa., December 1964.
69. Tagawa, H. and H. Sugawara, "The Kinetics of the Formation of Calcium Carbide in a Solid-Solid Reaction," Bull. Chem. Soc. Japan, 35(8) (1962), pp. 1276-1279.
70. Tagawa, H., H. Sugawara, and H. Nakajima, "Effects of Burning Conditions on the Chemical Reactivity of Quick Lime Produced from Lime Stone," J. Chem. Soc. Japan, Ind. Chem. Soc. (Kogyo Kagaku Zasshi), 64 (1961), pp. 1741-1759.
71. Torikai, N., T. Sasamoto, and Y. Komine, "The Reactivity of Carbon in the Formation of Calcium Carbide in the Molten Phase," Kogyo Kagaku Zasshi, 70(5) (1967), pp. 633-637.
72. Tylko, J.K., "High Temperature Treatment of Materials," U.S. Pat. 3,783,167, Jan. 1, 1974.

73. Venugopalan, M., "Plasma Chemistry - An Introduction," in "Reactions under Plasma Conditions," Vol. II, M. Venugopalan, ed., John Wiley & Sons, Inc., New York (1971), pp. 1-34.
74. Vursel, F. and L. Polak, "Plasma Chemical Processing," in "Reactions under Plasma Conditions," Vol. II, M. Venugopalan, ed., John Wiley & Sons, Inc., New York (1971), pp. 299-326.
75. Waldie, B., "Review of Recent Work on the Processing of Powders in High Temperature Plasmas: Part I - Processing and Economic Studies," The Chemical Engineer (March 1972), pp. 92-96.
76. Wickens, A.J., "Formation of Boron Carbide in a High-Intensity Arc Plasma," Chemistry and Industry (April 3, 1976), pp. 316-317.